

Evaluating Glial Cell Response to Functional Microelectrode Implants

by

Christopher Tai Yau Tsui

A thesis submitted in partial fulfillment of the requirements for the degree of

Doctor of Philosophy

Department of Biomedical Engineering
University of Alberta

© Christopher Tai Yau Tsui, 2024

Abstract

Neural interfacing devices are designed to interact with the central nervous system to alleviate functional deficits in people with disabilities arising from neurological injuries or diseases. Such devices often involve the use of an invasive microelectrode implant which is designed to acutely target a site of interest in brain or spinal cord tissue for electrical recording and/or stimulation purposes. However, glial cells in the CNS will react to the presence of implanted electrodes and, over weeks to months, form a glial scar that is detrimental to the functionality of the interfacing device. While strides in biomaterials advances have been made in attenuating glial cell reactivity to the electrodes, comparatively little is known about glial cell responses to actual electrical stimulation especially at the electrode-cell interface. To address this gap in the established literature, a high-throughput *in vitro* system was designed and developed to assess glial cell responses to both electrode presence and applied electrical stimulation. Platinum-iridium microelectrodes (75 μm diameter) were fabricated and used in electrical stimulation experiments. Primary mixed glial cell cultures were generated from the brains of postnatal day 2 heterozygous C57BL/6J CX3CR-1^{+EGFP} mice and initially subjected to a biphasic, charge-balanced rectangular stimulation waveform at 0.15 mA and 1.5 mA for 4 h/day over 1, 3, and 7 days. Analysis of immunofluorescence images and scanning electron microscopy images captured the spatiotemporal responses of the glial cells in response to electrical stimulation as well as damage sustained by the electrodes, and validated the feasibility of comparing glial cell responses as a function of different stimulation conditions using the methods employed. Live imaging of EGFP-positive microglia confirmed cell death and formation of a peri-electrode void at close proximity ($r < 50 \mu\text{m}$) to the electrode tip as a result of electrical stimulation. Follow-up experiments focused on modifying various electrical stimulation

paradigm parameters by current, waveform shape, or stimulation frequency reported differential results in glial cell density, biomarker fluorescence intensity and area coverage around the electrode tip after single 4 h rounds of stimulation. Finally, electrochemical testing of the proposed *in vitro* setup revealed influences of different components of the mixed glial cell cultures towards the electrochemical performance of the microelectrodes in terms of cathodic charge storage capacity, impedance, phase angle, and voltage transient excursions. The work presented in this thesis is intended to function as another set of biological testing tools available to neural interfacing device developers. The described methods are also intended to validate the efficacy and safety of proposed iterations of functional microelectrode designs, and complement data generated *in vivo* or in a clinical setting that ultimately results in refined designs that are biocompatible, safe, and longer-lasting in patients.

Preface

This thesis is an original work by Christopher Tsui. The research project, of which this thesis is a part, received research ethics approval from the University of Alberta Animal Care and Use Committee in accordance with Canadian Council for Animal Care guidelines, Project Name “CNS effects of Hypoxia Ischemia”, AUP00000343, 2017-2023.

A portion of the content found in this thesis has been published in the following journal articles. Author contributions to each article are listed after their respective citations:

1. C. Tsui, K. Koss, M.A. Churchward, K.G. Todd, Biomaterials and glia: Progress on designs to modulate neuroinflammation, *Acta Biomaterialia* 83 (2019) 13–28.
<https://doi.org/10.1016/j.actbio.2018.11.008>.

Content found in this paper has been included in chapter 1 of the thesis. CT and KK conducted a survey of the literature, wrote, and edited the manuscript. MC and KT edited and proofread the final manuscript.

2. C.T. Tsui, P. Lal, K.V.R. Fox, M.A. Churchward, K.G. Todd, The effects of electrical stimulation on glial cell behaviour, *BMC Biomed Eng* 4 (2022) 7.
<https://doi.org/10.1186/s42490-022-00064-0>.

Content found in this paper has been included in chapter 1 of the thesis. CT conducted a survey of the literature, wrote, and edited the manuscript. PL conducted a survey of the literature. KF

conducted a survey of the literature and prepared the table in the manuscript. MC and KT edited and proofread the final manuscript.

3. C.T. Tsui, S. Mirkiani, D.A. Roszko, M.A. Churchward, V.K. Mushahwar, K.G. Todd, In vitro biocompatibility evaluation of functional electrically stimulating microelectrodes on primary glia, *Frontiers in Bioengineering and Biotechnology* 12 (2024). <https://www.frontiersin.org/articles/10.3389/fbioe.2024.1351087>.

Content found in this paper has been included in Chapter 2 of the thesis. CT conceptualized the study, designed the experiments, carried out the experiments, collected and processed data, wrote, and edited the manuscript. SM and DR provided technical support with experimental design and fabrication of platinum-iridium microelectrodes, and edited and proofread the manuscript. MC, VM, and KT edited and proofread the final manuscript.

Acknowledgements

I would first and foremost like to thank members of the Todd lab, past and present, for their support and guidance throughout my time at the University of Alberta: Patricia Kent, Stephan Tchir, Lexis Galarneau, Emily Michaud, Preet Lal, Juliana Montoya Sanchez, Josh Tomusiak, and Mutsa Simbi. I wish to give a special acknowledgement to Dr. Kyle Koss, without whose enthusiasm, charisma, and encouragement I may not have even considered a career in research, and to Dr. Matthew Churchward, whose Olympic-level quality of scientific expertise and keen eye for my well-being has propelled me to the end of my PhD program with sanity intact. Many thanks to my supervisor, Dr. Kathryn Todd, for her masterful display of not only scientific prowess, but also core values of what it means to be a public servant. Thank you as well to the members of my supervisory committee, Dr. Karim Fouad and Dr. Anastasia Elias, for their expert input and encouragement throughout the project.

A special thank you is also in order for the students who have directly worked with me over my tenure as a graduate student: Savannah Weber, Katelyn Fox, Anna DeCorby, and Matthew Birtle. It has been the greatest pleasure and honour to work beside each and every one of you. You all have my gratitude, respect, loyalty, and friendship.

I would also like to thank Dr. Somnath Gupta for his friendship and assistance rendered to me, at and outside work, throughout our time together in the Todd lab.

Thank you to the members of the SMART Network (now iSMART) for your technical expertise and support with the project as well as countless interactions replete with fun and

humorous nonsense: Dr. Vivian Mushahwar, Soroush Mirkiani, David Roszko, Carly O’Sullivan, Don Wilson, Avery Nosen, and Neil Tyreman.

Thank you as well to the members of the Neurochemical Research Unit (Department of Psychiatry, University of Alberta) for all the time taken to answer pertinent questions about both science and life in general. Thank you in particular to Dr. Ian Winship, Dr. Allen Chan, Dr. Mischa Bandet, Samantha Ho, Hossein Doosti, and Zijia Yu. I wish to also acknowledge and thank Dr. Glen Baker, C.M., for his excellent support and calming presence that I without fail felt whenever I saw him at work on the 12th floor of the Clinical Sciences Building.

I wish to gratefully acknowledge financial support from the Natural Sciences and Engineering Research Council Postgraduate Scholarship – Doctoral program (NSERC PGS-D), as well as from various funding sources under the University of Alberta’s Faculty of Medicine & Dentistry.

Finally, thank you to numerous friends and family, both within and outside the University, for your time, patience, and care as I worked to complete this degree.

Table of Contents

Abstract	ii
Preface	iv
Acknowledgements	vi
List of Tables	xiv
List of Figures	xv
List of Abbreviations	xviii
1. Chapter 1 – Introduction	1
1.1. Preface	1
1.2. Background	2
1.3. Biomaterials designs for neural electrode implants	4
1.3.1. Microelectrode insulation and coating materials	7
1.3.2. Mechanical properties of microelectrodes	10
1.3.3. Cell grafting onto electrode implants	14
1.3.4. Microelectrode arrays	15
1.3.5. Anti-inflammatory drugs and microelectrode implantation	16
1.3.6. Macrophages vs. Microglia response to electrode implantation	19
1.4. Electrical stimulation considerations for moderating glial cell behaviour	21
1.4.1. Glial cell responses to electrical stimulation	22
1.4.1.1. Non-invasive vs. Invasive electrical stimulation	22

1.4.1.2.	Direct current vs. Alternating current	27
1.4.1.3.	<i>In vitro</i> and <i>in vivo</i> works of note.....	31
1.4.2.	Device development: materials and electrochemistry considerations.....	33
1.5.	Conclusions: considerations for future work	36
1.5.1.	Biomaterials designs for neural implants	36
1.5.2.	Electrical stimulation considerations for modulating glial cell behaviour	37
1.6.	Thesis outline.....	47
1.6.1.	Chapter 2 Synopsis – Design and evaluation of a high-throughput <i>in vitro</i> model for evaluating mixed glial cell responses to functional microelectrode implants	47
1.6.2.	Chapter 3 Synopsis – Microelectrode stimulation parameter modifications elicit differential glial cell responses over a short 4-hour timecourse	49
1.6.3.	Chapter 4 Synopsis – Contributions of mixed glial cell culture components on the <i>in vitro</i> electrochemical performance of platinum-iridium microelectrodes	50
1.6.4.	Chapter 5 Synopsis – Conclusions and Future Directions	52
1.7.	Significance of Thesis.....	53
2.	Chapter 2 – Design and evaluation of a high-throughput <i>in vitro</i> model for evaluating mixed glial cell responses to functional microelectrode implants	54
2.1.	Preface.....	54
2.2.	Abstract.....	54
2.3.	Introduction.....	55

2.4.	Materials and methods	57
2.4.1.	Materials	57
2.4.2.	Cell culture preparation	58
2.4.3.	PDMS ring fabrication	59
2.4.4.	Microelectrode fabrication	60
2.4.5.	Electrode plate setup	60
2.4.6.	Electrical stimulation experiments	62
2.4.7.	Immunofluorescence microscopy	62
2.4.8.	Scanning electron microscopy	64
2.4.9.	Statistical analyses	64
2.5.	Results	65
2.5.1.	Cellular responses at electrode interface	65
2.5.2.	Electrical stimulation-induced electrode damage	73
2.6.	Discussion	81
2.6.1.	Fluorescence imaging analysis	82
2.6.2.	SEM Analysis	87
2.6.3.	EDS Analysis	88
2.6.4.	Charge injection as a damage mechanism	89
2.6.5.	Limitations of study	91
2.7.	Conclusions	92

3. Chapter 3 – Microelectrode stimulation parameter modifications elicit differential glial cell responses over a short 4-hour timecourse	95
3.1. Preface.....	95
3.2. Abstract.....	95
3.3. Introduction.....	97
3.4. Materials and methods	100
3.4.1. Materials	100
3.4.2. Cell culture preparation	101
3.4.3. PDMS ring fabrication	102
3.4.4. Microelectrode fabrication.....	102
3.4.5. Electrode plate setup.....	103
3.4.6. Live imaging electrical stimulation experiments	104
3.4.7. Immunofluorescence microscopy	106
3.4.8. Scanning electron microscopy	108
3.4.9. Statistical analyses	108
3.5. Results	108
3.5.1. Live imaging – signal changes.....	109
3.5.2. Immunofluorescence image analysis.....	111
3.5.3. Electrode damage analysis	127
3.6. Discussion.....	127

3.6.1.	Live imaging analysis.....	129
3.6.2.	Immunofluorescence image analysis.....	131
3.6.3.	Electrode damage analysis.....	135
3.6.4.	Limitations of study.....	136
3.7.	Conclusions.....	138
4.	Chapter 4 – Contributions of mixed glial cell culture components on the <i>in vitro</i> electrochemical performance of platinum-iridium microelectrodes.....	141
4.1.	Preface.....	141
4.2.	Abstract.....	141
4.3.	Introduction.....	142
4.4.	Materials and methods.....	146
4.4.1.	Materials.....	146
4.4.2.	Cell culture preparation.....	146
4.4.3.	PDMS ring fabrication.....	147
4.4.4.	Microelectrode fabrication.....	148
4.4.5.	Electrode plate setup.....	149
4.4.6.	Electrochemistry analyses.....	149
4.4.7.	Scanning electron microscopy.....	150
4.4.8.	Statistical analyses.....	151
4.5.	Results.....	152

4.5.1.	Cyclic voltammetry	152
4.5.2.	Electrical impedance spectroscopy	155
4.5.3.	Voltage transient analysis.....	157
4.6.	Discussion.....	158
4.6.1.	Cyclic voltammetry	159
4.6.2.	Electrical impedance spectroscopy.....	161
4.6.3.	Voltage transient analysis.....	164
4.6.4.	Limitations of study	165
4.7.	Conclusions.....	166
5.	Chapter 5 – Conclusions and Future Directions.....	169
	References	174
	Appendix: Supplemental to Chapter 3	234

List of Tables

Table T-1: Summary of primary studies of electrical stimulation of glia.....	41
Table T-2: Electrical stimulation parameter modification summary	105

List of Figures

Figure 1-1: Summary of invasive neural implant biomaterials advances.....	20
Figure 1-2: CNS electrical stimulation modalities.....	27
Figure 1-3: Summary of biomarker and functional changes to microglia and astrocytes in response to electrical stimulation.....	38
Figure 2-1: Procedure for inserting 75 μm microelectrodes into the sides of PDMS rings.....	61
Figure 2-2: Immunofluorescent images of electrically stimulated mixed glial cell cultures at the electrode interface (4 h/day x 1 day).....	66
Figure 2-3: Immunofluorescent images of electrically stimulated mixed glial cell cultures at the electrode interface (4 h/day x 3 days).	67
Figure 2-4: Immunofluorescent images of electrically stimulated mixed glial cell cultures at the electrode interface (4 h/day x 7 days).	68
Figure 2-5: Quantitative analysis of 1-day stimulation images	70
Figure 2-6: Quantitative analysis of 3-day stimulation images	71
Figure 2-7: Quantitative analysis of 7-day stimulation images	72
Figure 2-8: Scanning electron micrographs of electrodes following 1-day stimulation experiments.....	74
Figure 2-9: Scanning electron micrographs of electrodes following 3-day stimulation experiments.....	75
Figure 2-10: Scanning electron micrographs of electrodes following 7-day stimulation experiments.....	76
Figure 2-11: Energy-dispersive x-ray spectroscopy data (1-day stimulation).....	78

Figure 2-12: Energy-dispersive x-ray spectroscopy data (3-day stimulation).....	79
Figure 2-13: Energy-dispersive x-ray spectroscopy data (7-day stimulation).....	80
Figure 3-1: Experimental workflow of live imaging experiments.....	105
Figure 3-2: Live imaging data summary - current modification.....	113
Figure 3-3: Live imaging data summary - waveform shape modification.....	115
Figure 3-4: Live imaging data summary - frequency modification	117
Figure 3-5: Immunofluorescent images of mixed glia - 4 h stimulation (current modification).....	118
Figure 3-6: Immunofluorescent images of mixed glia - 4 h stimulation (waveform shape modification).....	119
Figure 3-7: Immunofluorescent images of mixed glia - 4 h stimulation (frequency modification)	120
Figure 3-8: Quantitative analysis of current modification images.....	121
Figure 3-9: Quantitative analysis of waveform shape modification images.....	122
Figure 3-10: Quantitative analysis of frequency modification images	123
Figure 3-11: Scanning electron micrographs of electrodes following 4 h current modification experiments	124
Figure 3-12: Scanning electron micrographs of electrodes following 4 h waveform shape modification experiments.....	125
Figure 3-13: Scanning electron micrographs of electrodes following 4 h frequency modification experiments	126
Figure 4-1: Cyclic voltammograms of Pt-Ir microelectrodes immersed in different electrolytes (50 V/s)	153

Figure 4-2: Cyclic voltammograms of Pt-Ir microelectrodes immersed in different electrolytes (50 mV/s)	154
Figure 4-3: EIS Bode plots of Pt-Ir microelectrodes immersed in different electrolytes	155
Figure 4-4: EIS phase angle-frequency plots of Pt-Ir microelectrodes immersed in different electrolytes	156
Figure 4-5: Voltage transient response curves for Pt-Ir microelectrodes immersed in different electrolytes	157
Figure S-1: Time-lapse image series of EGFP-positive microglia (current modification).....	234
Figure S-2: Time-lapse image series of EGFP-positive microglia (waveform shape modification)	235
Figure S-3: Time-lapse image series of EGFP-positive microglia (frequency modification) ...	236

List of Abbreviations

2D - two-dimensional

3D - three-dimensional

AC - alternating current

Akt - protein kinase B

ANOVA - analysis of variance

ATP - adenosine triphosphate

BBB - blood-brain barrier

BDNF - brain-derived neurotrophic factor

BMEP - braided multi-electrode probe

BSA - bovine serum albumin

CD68 - Cluster of Differentiation 68

CNS - central nervous system

CSC_c - cathodic charge storage capacity

CV - cyclic voltammetry

CX3CR-1 - CX3C motif chemokine receptor 1 (fractalkine receptor)

DAMP - damage-associated molecular pattern

DBS - deep brain stimulation

DC - direct current

DMEM - Dulbecco's Modified Eagle Medium

E' - tensile storage modulus

EDS - energy-dispersive x-ray spectroscopy

EDTA - ethylenediaminetetraacetic acid

EES - epidural electrical stimulation

EGFP - enhanced green fluorescent protein

EIS - electrical impedance spectroscopy

E_{mc} - maximum cathodic voltage excursion

ES - Equine serum

FES - functional electrical stimulation

GFAP - glial fibrillary acidic protein

HBSS - Hank's Balanced Salt Solution

HFS - high frequency stimulation

Iba1 - ionized calcium binding adaptor molecule 1

IL-1 β - interleukin-1 beta

IL-6 - interleukin-6

ISMS - intraspinal microstimulation

LIF - leukemia inhibitory factor

MTE - microthread electrodes

NeuN - neuronal nuclei

NSC - neural stem cell

PBS - phosphate buffered saline

PDMS - polydimethyl siloxane

PEDOT - poly(3,4-ethylenedioxythiophene)

PEMGA - poly(ethylene glycol) methacrylate

Pi3 - phosphatidylinositol 3

PIEZO1 - piezo-type mechanosensitive ion channel component 1

PLL - poly-L-lysine

PNS - peripheral nervous system

PS - penicillin-streptomycin

PVAc - poly(vinyl acetate)

ROI - region of interest

ROS - reactive oxygen species

SCI - spinal cord injury

SEM - scanning electron microscopy

tCNC - poly(vinyl acetate)/tunicate cellulose nanocrystal

tDCS - transcranial direct current stimulation

TLR4 - Toll-like receptor 4

TNF α - tumor necrosis factor alpha

TRPA1 - transient receptor potential ankyrin 1

TTX - tetrodotoxin

TX100 - Triton X-100

VT - voltage transient analysis

1. Chapter 1 – Introduction

1.1. Preface

Some contents found in this chapter have been previously published in two papers:

C. Tsui, K. Koss, M.A. Churchward, K.G. Todd, Biomaterials and glia: Progress on designs to modulate neuroinflammation, *Acta Biomaterialia* 83 (2019) 13–28.
<https://doi.org/10.1016/j.actbio.2018.11.008>.

CT and KK conducted a survey of the literature, wrote, and edited the manuscript. MC and KT edited and proofread the final manuscript.

C.T. Tsui, P. Lal, K.V.R. Fox, M.A. Churchward, K.G. Todd, The effects of electrical stimulation on glial cell behaviour, *BMC Biomed Eng* 4 (2022) 7.
<https://doi.org/10.1186/s42490-022-00064-0>.

CT conducted a survey of the literature, wrote, and edited the manuscript. PL conducted a survey of the literature. KF conducted a survey of the literature and prepared the table in the manuscript. MC and KT edited and proofread the final manuscript.

1.2. Background

Neural interfacing is a fast-developing technology that allows external devices to communicate with the nervous system, thereby further closing the gap between man and machine [1–5]. Neural interfacing is often discussed in the context of improving the quality of life of a person with a disability that afflicts the nervous system, restoration of function after injury, or enhancement of function. Successful neural interfacing technologies that have been developed and are currently being used for human patients include cochlear implants, deep brain stimulation (DBS), epidural stimulation, and intraspinal stimulation [6–11]. Electrical activity is measured and/or applied to facilitate communication between an external device and the organ of interest (the brain and/or spinal cord), with the goal of eliciting activity from target sets of neurons and thereby effecting a change in function or behaviour [12–15].

Oftentimes, neural interfacing devices will entail the use of an invasive implant that is designed for insertion into brain/spinal cord tissue and function as a electrical signal recorder and/or stimulator [16,17]. When such implants are inserted into central nervous system (CNS) tissue, they will encounter and interact with different types of cells. Neurons are one major population of cells found in the CNS – the other population are glial cells. Collectively glial cells are vital to the development, growth, and security of the CNS [18–21]. Subtypes of glia, such as microglia, astrocytes, and oligodendrocytes, all have different and numerous roles that enable and enhance neuronal function, fate, and survival [22] leading to crucial impacts on cognition and behaviour.

While glial cells differ substantially from neurons in that they are not classically excitable by electrical stimulation (i.e., they do not produce action potentials), they are highly sensitive to

both the direct effects of electrical stimulation on nervous tissue and to indirect effects on nearby neurons affected by stimulation. Moreover, it has been previously shown [23–28] that there exist voltage-gated ion channels on all glia, and that they are able to communicate with each other through the use of intracellular ion fluxes. Transmembrane movement of ions (e.g., Ca^{2+} , Na^+ , K^+) are commonplace across all cells of the CNS; electrical charge is carried through these ions thus making them responsible for membrane potential changes in the CNS [29].

Neurons are structurally distinct from glia – one of the most obvious differences is that neurons feature dendrites and an axon to facilitate propagation of action potentials from one cell to the next. Neurons and glia communicate with one another via release of soluble molecules and receptor-ligand interactions [30]. Microglia are vital to neuronal development, pruning, and maintaining of homeostasis [31]. They are also constantly surveillant of their environment [32]. Although microglia do not conduct action potentials as neurons do, their functions are similarly affected by membrane potentials and ion channels present on the membrane [33,34]. By regulating the flow of ions such as K^+ , Ca^{2+} , and Cl^- (and therefore membrane potential and intracellular ion concentrations), ion channels are key effectors of cell activities such as migration, proliferation, morphology change, and production of cytokines and reactive oxygen species [33]. Similarly, astrocytes also feature ion channels which are used to regulate flow of ions (e.g., K^+ , Na^+ , Ca^{2+}) between cytosolic and extracellular spaces [35,36]. Transient increases in calcium ion concentrations in astrocytes, for example, have been documented to have an impact at the synapse by influencing phenomena such as plasticity and release of neurotransmitters and gliotransmitters [37,38].

There are many applications of electrical stimulation that target the nervous system. Each application differs from another in terms of the target area, intensity of stimulation, duration of

stimulation, and whether the application requires the use of an invasive implant. When an invasive implant is required, for example in deep brain stimulation (DBS), it offers a more direct and focused interface with target cells and reduces the probability of unwanted diffuse stimulation of areas adjacent to the target site [39]. The major problem with this approach is the phenomenon of glial scarring [40,41]. Microglia and astrocytes cordon off the implant/injury site and segregate it from adjacent healthy tissue. While this normal response to foreign objects can serve to mitigate the spread of damage to adjacent healthy tissue, it also prevents nearby neurons from accessing the interface site. This makes the glial scar a significant contributor to poor signal-to-noise ratios experienced by such implants and failure of the devices altogether over a longer time-course. The stretch goal for many new invasive devices involves improving the biocompatibility of the implants that are inserted into tissue – this is to improve their service life and reduce the need for any troublesome revision surgeries.

The literature review presented in this chapter examines two major topics: a survey of how glial cell behaviour and reactivity have been factored into biomaterial design for invasive neural electrodes as well as how exogenous electrical stimulation affects glial cells.

1.3. Biomaterials designs for neural electrode implants

While much discovery work has focused on promoting axonal regeneration and transplantation of neuronal precursors with the goal of improving a functional deficit that someone may have from an injury or disease that afflicts the CNS, the most clinically successful approaches to date have relied on functional electrical stimulation (FES) to compensate for lost

circuit function. External FES devices are capable of improving motor function through transcutaneous stimulation in cases of stroke and spinal cord injury (SCI) [42,43], while more invasive techniques such as deep brain stimulation (DBS) have been reported to treat tremors and chorea in Huntington's disease, Parkinson's disease, and multiple sclerosis [44–46], and modify pathological behaviours in depression and obsessive compulsive disorder [47–51]. With larger implants, the foreign body response ultimately causes materials to be sequestered by a glial scar comparable to those observed in neuroinflammatory pathology [52].

Given the importance of the inflammatory response, the limited focus on inflammatory cells in biomaterial design leaves much room for growth of the field. Considering that both microglia and astrocytes have recently been demonstrated to be essential in a variety of regenerative roles [53–56], these cells may be key in future design of implants, scaffolds, and drug delivery systems. Biomaterials to be discussed here have been designed for use in neural implant devices (electrodes) for recording and stimulation. Common among all studies presented in this review is their consideration of how biomaterials may interface with different types of glial cells. Frequent challenges that are addressed across virtually every study include reduction of glial scarring, mitigation of pro-inflammatory secretion from immune cells (notably microglia) and the promotion of a regenerative environment at the site of a lesion. Ultimately, glial cells play a significant role in the progression and resolution of an injury to the brain and spinal cord. The goal of this section is to explore the role of these glia and their potential in biomaterial design.

An area of significant focus in the brain-machine interface field is how the electrodes and other components that come into contact with tissue influence neuronal and glial responses. A common theme seen among the surveyed reports, and in general with any type of implant, is the

observation of a foreign body response. Microglia will, in response to the presence of an implant as well as in response to the damage caused by its insertion into tissue, transition to an activated state via retraction of its processes (i.e., assume an amoeboid morphology) [57]. Neuroinflammation is characterized by the migration of activated microglia and astrocytes to the implant site, resulting in the release of pro-inflammatory factors that mitigate recovery events and exacerbate neuronal cell death. A glial scar comprising of microglia and astrocytes will also form an encapsulating layer around an implant, limiting axonal regeneration and promoting restoration of damage done to the blood-brain barrier (BBB) during implantation. Brain-machine interfaces for neural prosthetics have largely focused on the design of microelectrode probes, which aid in the recording and stimulation of neuronal activity. A common and ongoing limitation of neural prosthetics is their inconsistent recording quality and long-term stability due to neuroinflammation altering electrical and chemical activity around any implanted probes. Many strategies have been considered in reducing the effect of neuroinflammation and gliosis due to probe implantation in a bid to improve signal quality and general host response to the implant.

In vivo responses to microelectrode implants have been observed and measured in animal models, but the mechanisms behind chronic electrode signal degradation remains unclear. An *in vitro* 2D culture system presented by Polikov et al. improves upon a widely-used protocol [40]. Cell types known to play a role in neuroinflammation and glial scar formation (i.e., neurons, astrocytes, microglia), are included in the culture. Mechanical injuries and foreign body responses were simulated through scrapes in the culture wells and stainless steel microwire, respectively. Advantages of using such a system include a reduction in resource costs and time, and high-throughput capability, compared to an *in vivo* study. For mechanical scrape injury

models, microglial infiltration to the scrapes was observed in the early stages followed by astrocyte hypertrophy and activation which eventually repopulated the wound. For chronic microwire implant models, glial scars consisting of a microglia core and astrocytes along the periphery were formed after 10 days. Neurons did not respond to either injury model, but were electrically active throughout. Primary glial cell responses observed in this study correlated well with what was typically seen in *in vivo* responses to mechanical insults. This reductionist system can be seen as a useful tool for assessing neuro-electrode biocompatibility and for understanding causes of implant failure. Understanding the role of glial cells in rejection has led to several improvements in design.

1.3.1. Microelectrode insulation and coating materials

As the initiation of rejection occurs at the interface of any implant, many modifications in surface chemistry and insulating coatings have been generated with glial cells and neuroinflammation in mind (Figure 1-1A).

Bioactivity of microelectrode surfaces was emphasized by Leung et al., including examination of microglia interactions (e.g., attachment behaviour, cytokine release profile) with common insulating materials on electrodes (e.g., Epoxylite, parylene-C) [58]. Thin film coatings (e.g., cellulose acetate, Tecoflex) were also studied. Electrodes were implanted into a rat motor cortex for 12 weeks. Low protein-binding materials on electrodes resulted in reduced microglia attachment and activity. Immunostaining was done on electrode surfaces post-implantation to identify attaching cell types. CD11b-positive microglia were present on all materials tested.

Material contact angle measurements suggest that activated microglia attached more readily to hydrophobic surfaces; however, all materials examined readily adsorbed serum proteins, plasma proteins, and extracellular matrix which enabled cell attachment. *In vitro* studies suggested that activated microglia readily attached to commonly used external coatings for neural electrodes, and also secreted pro-inflammatory and neurotoxic cytokines. However, low protein-binding coatings (e.g., BSA, Pluronic F108, sodium alginate) resulted in a reduced number of activated microglia that attach onto an electrode, thus improving their signalling capabilities and biocompatibility.

Kozai et al. proposed a new design for neural microelectrodes that have improved electrical characteristics and a more bioactive surface [59]. Atom transfer radical polymerization allowed for the deposition of a protein-resistant poly(ethylene glycol) methacrylate (PEGMA) layer on the electrode, which has approximately 1/5 the cross-sectional area of a conventional silicon electrode but significantly reduces biofouling and improves in strength and flexibility. Microthread electrodes (MTE) were implanted into rats, and initial studies suggested that they were stable over 5 weeks in the brains without any significant degradation in recorded signals. Tissue response due to implantation stab wounds subsided by 4 weeks; reduced GFAP response in astrocytes, less microglia adjacent to the MTEs, and more neurons reinforced the idea that the addition of the PEGMA layer is an effective “stealth” interface that masks the foreign nature of the electrode. It was suggested that future studies expand on the effect of different probe diameters, bioactive coatings and flexibility compliance levels of various materials.

To promote neuronal growth and activity towards electrode implants as well as improve implant longevity, L1 neural cell adhesion molecules were investigated by Eles et al. as a potential neuroadhesive coating that can be covalently attached to electrode surfaces and reduce

glial scarring [60]. L1 is a transmembrane cell surface glycoprotein that mediates cell recognition and interactions through homophilic interactions with L1 proteins on other cells. It has been reported to improve regenerative conditions in cases of CNS and peripheral nervous system (PNS) injury by facilitating neuronal adhesion, axonal growth, neural migration, differentiation, and survival [61,62]. While *in vivo* studies have also shown L1 to inhibit glial and fibroblast cell attachment [63–66]. NeuroNexus silicon probes were coated with L1 on SiO₂ surfaces and IrO₂ electrode pads, and implanted into transgenic mice. L1 coatings did not affect microglia process extensions towards the probes, but sustainably over 6 hours prevented microglia from covering the surface of the implant. Furthermore, L1 coatings reduced morphological activation of more distant microglia that did not make contact with the probes. It is suggested that while microglia are incapable of L1-L1 homophilic binding interactions, murine microglia express the $\alpha 5\beta 1$ integrin which can interact with L1 and, through a mechanism yet to be described, reduce the number and size of microglial processes covering the coated probes. L1 also features terminal polysialic acid residues, which can bind to microglial SIGLEC-E receptors and suppress phagocytosis. Bioactive peptides related to microglia-neuron and neuron-neuron interactions, such as the sequence reported in Sridar et al.'s work [67], can be considered in such a multi-cellular environment.

Common among studies described herein is the desire to reduce glial cell coverage and inflammation-associated activity. Approaches in achieving this differ as we see surface modifications with the goal of reducing protein adhesion (i.e., impart stealth to the inserted foreign body and prevent detection and attachment by cells), or modifications that promote the growth and attachment of both neurons and glia towards the implant, but by exploiting certain receptor-ligand mechanisms attenuate the undesirable inflammatory responses.

1.3.2. Mechanical properties of microelectrodes

Implants can be designed through a variety of approaches in order to reduce or avoid a foreign body response. For example, materials for CNS implants are often selected for being chemically inert, but other factors must also be considered. Mechanical stimuli are also hypothesized to play a role in such reactions as neural cells are mechanosensitive. Neural implants are usually orders of magnitude stiffer than CNS tissue – such a mismatch in the mechanical properties of both implant and tissue may cause ongoing damage to the CNS and contribute to a foreign body response. As an example, in Moshayedi et al.’s work primary neonatal rat microglia and astrocytes were exposed to materials of varying stiffness but of the same chemical properties [68]. Morphological and inflammatory responses were assessed *in vitro* and *in vivo*. Immunocytochemistry imaging, gene profiling, and protein expression assays suggested that microglia and astrocytes interacting with a biologically foreign surface results in behaviour tantamount to an acute and late chronic inflammatory response, and will act to isolate the surface from the rest of the tissue. These findings reinforce the narrative that mechanical stimuli have a significant impact on cell physiology and pathology, and must be considered in electrode design.

Mechanical properties of microelectrodes were also considered in Kim et al.’s study, which explained that stiff electrodes implanted in tissue are subject to micromotion, which worsens the inflammatory response [69]. They suggested that a biocompatible CNS electrode should have a flexible body (to allow for deformation of local tissue) and a flexible tether (to follow gross CNS tissue motions). The authors proposed the combined use of ultrafine wires, for ease in high density recording, and braiding for better mechanical compliance in spite of the

inevitably large modulus mismatch between tissue and wire material. Implantation of the braided flexible wires would be possible through the use of a temporary, stiff core. A conventional wire currently used for intraspinal recording (Nichrome, 50 μm) was compared against a braided multi-electrode probe (BMEP) design (12.7 or 9.6 μm polyimide insulated Nichrome wires, 12-24 wires). Braids were constructed with different combinations of wires with respect to amount and size. All braid combinations reported a better lateral and axial mechanical compliance than the single Nichrome wire. The number of wires in the braid had a larger impact on compliance than wire diameter. The BMEPs could accurately record single units from frog and rat spinal cords for an extended period of time without becoming dislodged. Future directions include assessing the BMEP design's biocompatibility in implanted tissue as well as further modifying the design of the BMEP by manipulating materials, size, and shape.

To further highlight the importance of a device's mechanical properties and their significance in influencing device rejection, mechanical mismatch between implants and neural tissue was studied as a contributor to the neuroinflammatory response by Nguyen et al [70]. This group developed new 'mechanically-adaptive' nanocomposites which are capable of changing from a rigid to compliant state 5 minutes following implantation. Initial rigidity allows for implant insertion into the brain tissue (tensile storage modulus $E' \sim 5 \text{ MPa}$) – the material will soften upon exposure to physiological conditions ($E' \sim 12 \text{ MPa}$). The nanocomposite used, poly(vinyl acetate)/tunicate cellulose nanocrystal (tCNC), was compared against poly(vinyl acetate) (PVAc), a more rigid and traditional material. A reduced neuroinflammatory response was observed at 16 weeks from using 'mechanically-adaptive' nanocomposites as opposed to stiffer materials. Blood-brain barriers were also more stable with more chronically-implanted and compliant materials. These findings support previous studies on flexible probes suggesting their

ability to better follow tissue movements thus resulting in a less severe tissue response [68,71,72].

Elaborating on this idea, Köhler et al. hypothesized that a combination of improved probe flexibility and embedding probes in gelatin can further limit the astrocyte/microglia response [73]. Probes were designed to be 8000 times more flexible in the lateral direction versus the longitudinal direction, with some embedded in a gelatin matrix. Significant microgliosis and astrocytosis were observed proximal to the probes; flexible probes showed reduced astrogliosis but no change in microgliosis. However, embedding the probe in gelatin further reduced microgliosis when compared with the unembedded flex configuration. Inferences that can be made from these results include the mechanical mismatch caused by rigid implants can exacerbate inflammation. In addition, an implant whose direction of flexibility corresponds to the main direction of movement in the brain (i.e., cortical axis, flex mode) will elicit a smaller astrocytosis reaction, but will not impact microglia activity. Gelatin-embedded probes allowed for higher neuron survival compared to non-embedded probes. These results suggest potential for both reduced microglia response and improved neuronal density near the probe – both important criteria to meet when designing a biocompatible probe.

Thelin et al.'s work focussed on the impact of implant size and fixation mode (tethered vs. untethered electrodes) on CNS tissue response [74]. From a previous study, it was believed the lack of tethering would elicit smaller tissue reactions due to reduced motion between the implant and tissue [75]. Thelin et al.'s study expands on previous reports by monitoring neuronal numbers close to the implants (i.e., 50 μm radius) over long evaluation periods (i.e., 12 weeks) for electrodes that are and are not tethered in a rat model. Round electrodes were used to minimize the extent of anticipated tissue reactions. Tethered implants caused larger tissue

reactions than un-tethered implants, and also induced changes in neuron morphology and organization around the implant. Electrodes with smaller diameters (50 μm) caused less damage to tissue, which correlated with higher neuronal survival. Glial activation persisted at the 12 weeks post-implantation mark with the large diameter/tethered implants; small diameter/untethered implants did not have this issue, suggesting that they elicited the least severe tissue reactions.

Innovative non-*in vivo* approaches have also been taken to account for glial cell responses to mechanical mismatches between electrode implants and surrounding tissue. A 3D *in vitro* primary rat cell model capable of inducing micromotion around an implanted device was developed by Spencer et al. [41]. Axial micromotion was simulated by cyclically displacing borosilicate probes implanted in a collagenous matrix using a custom motion platform. Axial micromotion is representative of respiration and vascular pulsations, and is thought to be the most significant contributor to the phenomenon. Probes were held in place by a fiber chuck and threaded through a polyimide tube which guided the probe towards the collagen gel. Strain field measurements were taken to calculate local displacement of the gel in response to micromotion. Astrocytes were found to be mechanically responsive (e.g., increase cell areas, perimeters) to local strain fields. Using a different approach, Trotier et al.'s study aimed to more accurately account for ways in which electrode micromotion facilitates gliosis using a computation model [76]. Their *in silico* work modelled the peri-electrode region in CNS tissue which saw the creation and enlargement of a void around the electrode as a result of micromotion. This is a more physiologically accurate depiction of mechanical mismatch in comparison to previous studies which assumed side-by-side contact between electrodes and tissue. In their computation model, the solid, liquid, and viscoelastic components were the electrode, fluid-filled peri-

electrode space, and neural tissue, respectively. In follow-up *in vitro* experiments to validate the *in silico* work, rat ventral mesencephalic E14 embryonic cells exposed to fluid shear in a parallel flow chamber exacerbated expression of gliosis-associated proteins piezo-type mechanosensitive ion channel component 1 (PIEZO1) and transient receptor potential ankyrin 1 (TRPA1). PIEZO1 was found to play a role in the facilitation of astrogliosis in the context of electrode micromotion-induced fluid shear stress through the targeting of mitochondrial processes. Results from the works of Spencer et al. and Trotier et al. provide a way to assess the impact and biocompatibility of a neural probe prior to *in vivo* testing.

The reports presented in this section demonstrate major evolutions in the improvement of probe design with respect to mechanical properties (Figure 1-1C). From the initial acknowledgement that material stiffness will impact cell function and inflammatory processes, advances have been made to further characterize the impact of micromotion on glia-mediated inflammation, identify other parameters such as tethering that exacerbate inflammation, develop mechanically adaptive electrodes to reduce inflammation, and design strategies towards improving neuronal survival in the immediate proximity of the implants in addition to reduced glial response.

1.3.3. Cell grafting onto electrode implants

Reports exist of transplanted stem cells participating in a “bystander” effect in the context of tissue damage due to CNS injury [77,78]; specifically, these cells can secrete neuroprotective factors into the surrounding environment and potentially inhibit cytotoxic mechanisms or

biochemical deficits. Purcell et al. designed a novel probe seeded with neural stem cells that promotes a pre-existing biological interface with the goal of improving the biocompatibility of the implant [79]. The probes, made of parylene, feature a hollow well where alginate (a biocompatible polysaccharide) hydrogels with neural stem cells are present. The (untethered) probes were implanted into rats and their inflammatory responses were assessed. Introduction of the neural stem cells in the alginate hydrogel reduced the severity of any early inflammatory responses (within the first week post-implantation). However, neuronal loss and glial encapsulation was more problematic at later stages (6 weeks post-implantation). Purcell et al. suggested that the grafted cells secrete neurotrophic and neuroprotective factors that aid in the healing process early on, but this is eventually followed by cell death and alginate scaffold degradation.

1.3.4. Microelectrode arrays

The use of microelectrode arrays (Figure 1-1D) in *in vitro* and *in vivo* experiments can produce a more clinically relevant host response compared to the insertion of a single electrode. As with studies concerning single electrodes, foreign body response and consequent inflammation are speculated to contribute to device failure; events include activation of microglia, the release of pro-inflammatory cytokines, and BBB rupture. Damage to blood vessels during implantation can also potentially damage adjacent brain tissue. The study of Nolte et al. aimed to better understand implantation injury (e.g., stab wounds) and foreign body response resulting from a more clinically relevant microelectrode array (4x4 Utah Electrode Arrays) being

implanted into young adult rat cortices, and whether foreign body response histology correlates with single unit recording performance changes [80]. Macrophage/microglia accumulation was clearly observed on retrieved electrode arrays. Foreign body responses resulting from the implantation of 4x4 Utah Electrode Arrays are not the same as those caused by devices that create a single penetrating injury likely due to a difference in the degree of vascular damage. The electrode arrays caused a more significant lesion to brain tissue, resulting in a cavity devoid of neuronal elements. Recording performance was affected by BBB 'leakiness', astrogliosis, and tissue loss. This study brings attention to events that result from insertion of a Utah Array and the ways in which they are different compared to insertion of a single shank electrode.

1.3.5. Anti-inflammatory drugs and microelectrode implantation

Microglia are a key part of the neuroinflammatory process that takes place in the CNS as part of the immune response to an injury such as electrode probe insertion. While neuroinflammation is recognized to be a beneficial process in that it helps to clear antigens and cell debris, it is also regarded as double-edged since it also contributes to damage to healthy tissue. Anti-inflammatory drugs (Figure 1-1E), as a result, have been studied by various groups to determine whether it is possible to attenuate the negative aspects of the inflammatory process while still maintaining the pro-recovery aspects.

Retrodialysis of dexamethasone, an anti-inflammatory steroid, was studied by Kozai et al. due to previous reports of it suppressing glial scar formation [81]. This study investigated the extent of the reduction of inflammatory gliosis over time. Transgenic mice expressing green

fluorescent protein in microglia under the CX3CR1 promoter were used. *In vivo* two photon microscopy was used to monitor any changes in microglia morphology/motility around the implanted probe. The probes were under artificial cerebrospinal fluid perfusion with or without dexamethasone. Results reinforced the suggestion that dexamethasone significantly contributed to the reduction of microglia activation in response to electrode insertion.

An alternate approach by Rennaker et al. examined the effects of systemic minocycline when used to treat rats implanted with multichannel neural recording electrodes for up to 4 weeks [82]. Minocycline is a tetracycline antibiotic that has been shown to have anti-inflammatory effects and is neuroprotective in models of ischemic injury and neurodegenerative disease. It was shown to improve the signal-to-noise ratio and longevity of the interface recordings, increased neuronal survival around the implant, decreased inflammation, and reduced microglia and astrocyte activation in treated rats. Improvements were suggested whereby using smaller electrodes can reduce cortical tissue deformation and thus mitigate the strength of the early tissue response [83,84]. Rapid insertion techniques could also reduce any strain on cortical tissue. A longer implant study with minocycline is also warranted given the scope of this study (4 weeks). It was also suggested that a minocycline/dexamethasone co-regimen be explored to see if there are any synergistic benefits to using both drugs at the same time to treat neuroinflammation.

As part of the neuroinflammatory response, activated microglia secrete pro-inflammatory cytokines, chemokines, and reactive oxygen species (ROS) that can enable BBB breakdown and decreased neuronal health [85–87]. ROS, a class of pro-inflammatory molecule, when secreted during inflammation have been shown to impact neuronal health via oxidative stress [87–89]. BBB permeability has been prevented in the past by introducing anti-oxidative enzymes. In the

case of electrode implants, it is hypothesized that reducing ROS accumulation at and near the tissue/implant interface can improve BBB stability and neuronal health. The scope of Potter et al.'s study was on the role of ROS during the initial instability in the biphasic neuroinflammatory response to microelectrodes [74]. Resveratrol, an anti-oxidant derived from grapes, was investigated here for its ability to mitigate inflammatory symptoms following electrode implantation *in vivo*. Resveratrol enabled extended prevention of neurodegeneration following electrode implantation; rats that were systemically administered resveratrol showed higher neuronal cell densities 100 μm from the electrodes 2 weeks after implantation along with improved BBB stability and reduced ROS accumulation. However, no difference in neuron populations, ROS levels, or Toll-like receptor 4 (TLR4) expression in comparison with controls was found at the 4 week mark. Resveratrol-treated rats also showed a higher amount of activated and total microglia/macrophages, but reduced astrogliosis. A subsequent stab wound healing response study produced similar ambiguous results. It was then investigated if chronic administration of anti-oxidants in a rat model could produce a sustained anti-oxidant environment [75]. 'Michigan-style' microelectrodes were inserted into the rat brains, with daily injections of resveratrol for up to 16 weeks following electrode implantation. Classic markers for microglia, astrocytes, NeuN, and BBB stability were examined. Sustained levels of resveratrol were detected around the implanted microelectrodes with reduced amounts of ROS and neuronal cell death. However, increased hemorrhaging was also correlated to this chronic resveratrol regimen along with 'threadlike adhesions' between the liver and diaphragm. Clearly, chronic administration of anti-oxidant resulted in unwanted side effects. An optimized dosing regime would thus be desired to mitigate such drawbacks.

1.3.6. Macrophages vs. Microglia response to electrode implantation

Ravikumar et al. contributed to the broader understanding of the inflammatory process post-device implantation by evaluating and comparing the roles of microglia and blood-borne macrophages infiltrating the CNS due to the rupturing of the BBB [76]. A better understanding of the roles of both types of cells can be exploited when redesigning microelectrodes to account for microglia activity against the electrode, macrophage activity against the electrode, and any interplay between the two cell types. Non-functional, ‘Michigan-style’, silicon microelectrodes were implanted in mice. The results of the study suggest that systemic myeloid cells have an important role in regulating neuronal dieback. Over 60% of an infiltrating cell population consisted of macrophages. A correlation was shown in total infiltrating macrophages (excluding microglia) and neurodegeneration following electrode implantation. From these results, infiltrating macrophages, not microglia, are thought to have more influence in mediation of neurodegeneration.

According to the authors of this study, future studies should aim to study specific receptor-mediated pathways to mediate neuroinflammation and neurodegeneration. Specifically, it was suggested that the use of a bone marrow chimera model with transgenic knock-in or knock-out mice could help clarify differences in inflammatory pathways between cell types and what role they play in neuroinflammation. However, other studies have demonstrated that irradiation utilized in generating such bone marrow chimeras can cause prolonged opening of the BBB, dramatically affecting the function and makeup and distribution of hematopoietic cells in the CNS (i.e., microglia and infiltrating macrophages) and should be interpreted with an

abundance of caution [93]. Ultimately, the results of such studies should lead to the development targeted therapeutics that can result in improved microelectrode performance.

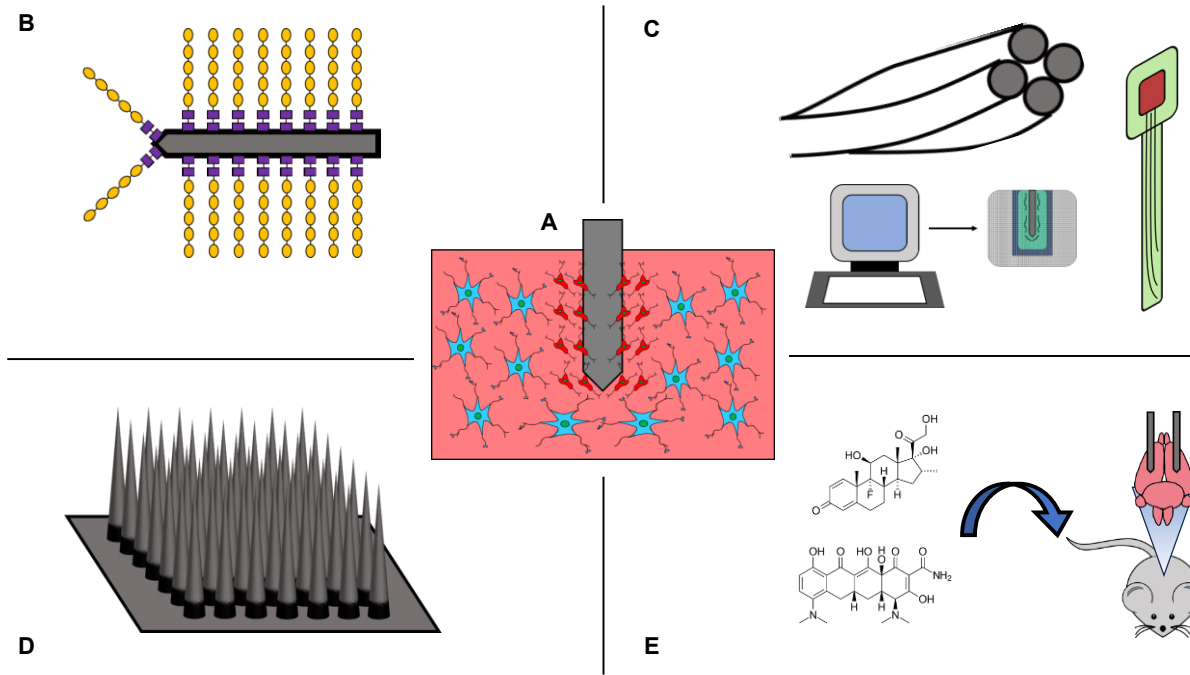


Figure 1-1: Summary of invasive neural implant biomaterials advances

Diverse biomaterials designs have been developed to maximize functionality of devices implanted in CNS tissue and mitigate the extent of glial scarring against electrode implants in CNS tissue – the cells that form the glial scar are microglia (red) and astrocytes (blue) (A). Approaches include conjugation of biomolecules such as cell adhesion molecules onto the surfaces of electrodes (B), the computational modelling and design of more mechanically compliant materials to reduce mechanical mismatch between tissue and devices (C), development of multi-electrode arrays to maximize recording and stimulation capabilities (D),

and systemic administration of anti-inflammatory drugs to counteract neuroinflammation elicited by electrode implantation into CNS tissue (E).

1.4. Electrical stimulation considerations for moderating glial cell behaviour

There remains, however, another question that must be further and more thoroughly addressed when considering the concept of biocompatibility of neural interfacing devices: *how do glial cells respond to electrical stimulation?* In the broader literature, sufficient attention is given to how neurons respond to electrical stimulation patterns and how this translates into modified function and behaviour of the subject organism, but rarely is the response of glial cells to stimulation addressed. As glial cells are the caretakers and defenders of the nervous system, they also have a major role to play in determining the fate of other cells around them following electrical stimulation.

This section of the thesis examines available literature on how exogenous electrical stimulation affects glial cells. Summaries of experiments done *in vitro* and *in vivo* are provided, with consideration of different stimulation paradigms (e.g., direct current vs. alternating current), invasive vs. non-invasive experimental methods, along with discussion of potential cellular mechanisms of the glial response to stimulation.

1.4.1. Glial cell responses to electrical stimulation

1.4.1.1. Non-invasive vs. Invasive electrical stimulation

The glial response to neural interfacing devices has two major elements: the cellular response to electrical stimulation, and the response to the physical presence of an implant. While some stimulation paradigms bypass implanted electrodes (e.g., epidural stimulation, a non-invasive method) the added presence of an invasive implant elicits a foreign body response orchestrated by microglia and astrocytes. This would conceivably exacerbate any tissue response to the device. There have been many studies published which focus on the effect of invasive implants on glial cell reactivity [39,40,94,95], but studies that further integrate electrical stimulation into their experiments are more limited [96]. There are invasive implant studies that focus more extensively on glial cell responses to electrical stimulation and less on responses to the implant itself. Some studies have electrodes that contact cells [97] and apply electrical field stimulation to them, but data pointing towards evidence of a foreign body response is lacking. To our knowledge, it appears that there are few studies published that concurrently detail glial cell responses to both an implant as well as any applied electrical stimulation. Doing such a concurrent assessment would greatly increase the value of a study's appraisal of a novel neural interfacing device.

There also exist invasive studies that offer insight on some fascinating ways in which glial cells respond to electrical stimulation at the cellular level [98]. Electrical stimulation can elicit calcium ion waves in glial cells; whether this includes microglia was of interested and

investigated. Calcium wave generation is made possible through adenosine triphosphate (ATP) release and purinergic receptor activation. Schipke et al.'s experiments showed that both astrocytes and glial precursor cells participated in Ca^{2+} waves. In response to electrical stimulation-induced Ca^{2+} waves, patch clamp recordings also revealed a transient induction of an outward rectifying K^+ current in microglia, though this was only seen in 5 out of 13 microglial cells investigated. ATP was deduced to have been released from glia to serve, in part or in whole, as a carrier for the Ca^{2+} wave. Tetrodotoxin (TTX) and Cd^{2+} were introduced into the brain slices to exclude possible neuronal contributions to the Ca^{2+} wave (e.g., generation of action potentials and synaptic release). Though it has been suggested that ATP coming from astrocytes results in purinergic receptor activation in nearby cells which in turn leads to rising internal calcium levels in those cells [99], it is of interest to determine whether stimulation-induced increases in extracellular ATP levels would be sufficient to act as a damage-associated molecular pattern (DAMP) for microglia thus potentially triggering their activation.

In Roitbak and Fanardjian's study, cat cortices were subjected to electrical stimulation using implanted silver wires [100]. Electrophysiology recordings of glia did not reveal spikes that were indicative of action potentials normally seen in neurons. However, when subjected to stimulation paradigms that were higher in amplitude and frequency, depolarization was observed in affected glia (though membrane voltage decay was extremely rapid). It was suggested that the glia depolarizing was largely due to potassium ion contributions – glial cell movement could be elicited through increases in extracellular concentrations of K^+ .

High frequency stimulation (HFS) is a widely documented form of DBS [38,101] used to suppress tremors associated with Parkinson's disease by targeting structures in the basal ganglia (thalamus, globus pallidus, subthalamic nucleus). Generally, the usage of DBS has been accepted

to be a safe and effective intervention [101]. Chronic effects of stimulation on glia appear to be highly localized at the electrode-tissue interface as exemplified by the 12-month study of DBS on pigs by Orłowski et al. [102]. The effects of HFS on astrocytes have been widely discussed over the past approximately 15 years. They are highly suspected of being involved in the increased release of ATP, its downstream product adenosine, and subsequent A1 receptor activation which result in the reduction of tremors [103]. Astrocytes have also been suspected of being responsible for glutamate release through increased influx of Ca^{2+} into the cell following stimulation [104], as well as mediate extracellular concentrations of K^{+} [105]. In the case of microglia, a study by Vedam-Mai et al. [106] suggests that DBS is helpful in reducing the number of activated microglia at and around the lesion compared to microlesion and sham animals. With regards to its capacity to contribute to the inflammatory response against an implanted electrode, microglia activity at the electrode-tissue interface is also heavily dependent on purinergic signalling. A computational model reported by Silchenko and Tass [107] presents an interesting correlation between the size of a glial scar around an implant and the amount of ATP produced from device implantation and stimulation. As well, an attenuation of fractalkine signalling due to DBS was hypothesized by Chen et al. [108] to contribute to reduced levels of microglia activation. Effects on microglia density and cell size have also been documented in certain parts of the brain as a result of DBS; according to Hadar et al. [109], the introduction of an electrode into the medial prefrontal cortex results in a local increase in microglia density and cell size which was prevented by DBS. They also interestingly found that the same experiments in the nucleus accumbens produced no significant change in microglia density and cell size even after introduction of an electrode and stimulation. The study alludes to how microglia are a

heterogeneous population in the CNS [110], and the way in which they behave are at least in part due to a subject's age, area of the CNS affected, as well as the pathology in question.

Non-invasive implants also require the use of electrodes, but they are applied without penetration of CNS tissue (e.g., transcranial direct current stimulation, tDCS) and thus do not have penetrating contacts within the tissue. An *in vitro* model of such an approach uses bridges made of agar or salt to connect electrolyte solutions to the cultures themselves [111–113]. In a 2015 study, Pelletier et al. cultured murine N2a neuroblastoma cells, BV2 microglial cells, and C8-D1A astrocytic cells that were exposed to direct current fields through the use of agar bridges [112]. Upon being electrically stimulated, morphological changes were noted in the glial cell types – cells either oriented themselves parallel to the electric field (microglia) or were oriented perpendicular to it (astrocytes). Further to these observations, the results suggested that such electric fields were capable of affecting both microglia and astrocytes: cyclooxygenase-2 expression in microglia was upregulated after electrical stimulation and lipopolysaccharide priming, while astrocyte metabolism was increased [114]. These observations suggested an inflammatory and hypertrophic effect, respectively.

Some modalities, such as epidural electrical stimulation (EES), are somewhat intermediate in terms of procedure invasiveness [115,116]. EES requires an implant to be surgically placed at the dorsal surface of the spinal cord, and is necessarily more invasive than applications such as tDCS, yet lacks the target specificity offered by penetrating electrodes as used in procedures such as deep brain stimulation (DBS) and intraspinal microstimulation (ISMS). Baba et al. showed that epidural electrical stimulation of the rat brain had neuroprotective outcomes following ischemic stroke [115]. Electrical stimulation resulted in less apoptotic cells as antiapoptotic cascades were activated (Pi3 kinase/Akt signalling pathway).

Upregulated levels of neurotrophic factors (glial cell line-derived neurotrophic factor, brain-derived neurotrophic factor, vascular endothelial growth factor) were observed. Electrical stimulation also enhanced angiogenesis and suppressed microglia and astrocyte proliferation.

Regardless of whether stimulation utilizes an invasive implant (Figure 1-2), there exists convincing evidence that electrical stimulation paradigms can manipulate glial cells in terms of their morphology and orientation, and elicit intercellular signalling among glia. It is unclear, however, if such observations translate to glia possibly taking on a more pro-inflammatory or anti-inflammatory role and how surrounding cells or tissue would be impacted by this. Further *in vivo* evidence suggests electrical stimulation is capable of therapeutic benefit in part by mitigating inflammation-associated proliferation of glia in the context of stroke – whether such a concept can be applied to other injuries and neurodegenerative contexts warrants further and extensive investigation.

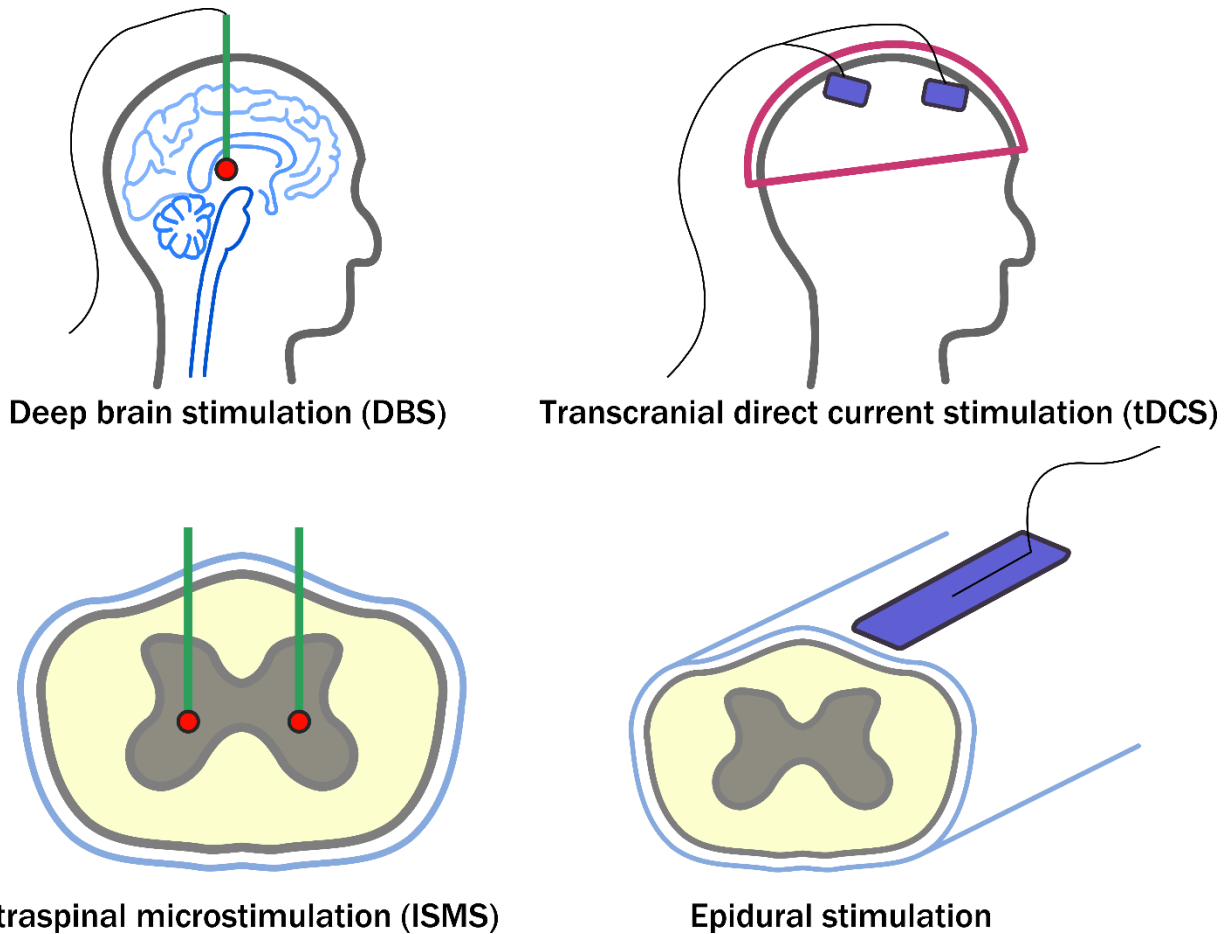


Figure 1-2: CNS electrical stimulation modalities

Different electrical stimulation techniques target different parts of the CNS (brain, spinal cord), and with varying levels of invasiveness.

1.4.1.2. Direct current vs. Alternating current

Application of electrical current to tissues is typically accomplished using either direct current (DC) and alternating current (AC). The choice of which is used for a particular

stimulation paradigm depends on the application. Direct current is often used in applications such as transcranial direct current stimulation (tDCS), which (in the clinical context) makes use of electrodes placed on the outside of the head and is designed to treat disorders such as depression and Parkinson's disease. Latchoumane et al. investigated the molecular pathways underlying the treatment effects of tDCS [117]. Embryonic stem cell-derived neuron-glia co-cultures were subjected to chronic low frequency stimulation and direct current stimulation paradigms in the presence of the excitotoxic mediator L-glutamate to simulate CNS injury. The glia in the cultures, which differentiated into O4-positive oligodendrocytes and GFAP-positive astrocytes, upregulated transcripts for NMDA receptor subunit NR2A, brain derived neurotrophic factor (BDNF), and Ras-related protein RAB3A – collectively suggesting that electrical stimulation can modify neuronal network plasticity. A further summary of key tDCS findings is reviewed elsewhere [118]. It was shown that low intensity brief tDCS increased glucose metabolism in cultured mouse astrocytes [119], and that high intensity anodal and cathodal tDCS activated microglia [120]. In their own experiments, Gellner et al. exposed adult male rats to 20 minutes of anodal tDCS and saw morphological changes in microglia and astrocytes [118]. Their study also suggested that amoeboid microglia may be more susceptible to tDCS due to their higher abundance of voltage-gated ion channels.

Another invasive DC stimulation study utilized monophasic stimulation paradigms on rat C-fibres in the dorsal horn [121] – the mere stimulation of these fibres, even outside of any nerve damage, was sufficient to activate microglia (upregulated Iba1, IL-6, etc.) and sensitize the animal to pain. DC electric fields have also been shown to serve as a helpful, instructive mechanism for neurite extension of dorsal root ganglion neurons, with electrically stimulated Schwann cells contributing heightened levels of neurotrophins [122]. It would be interesting to

know if it would be possible to similarly enable axonal regeneration/neurite extension via electrically stimulated glial cells in the CNS.

In a simpler experiment, Kearns et al. showed how short-term DC stimulation of macrophage cell lines could induce expression of markers that were characteristic of M1 and M2 phenotypes [113]. M1 and M2, alternatively termed the ‘classical’ and ‘alternative’ phenotypes, respectively, describe how macrophages transition between being pro-inflammatory and anti-inflammatory. This terminology has also been applied to microglia [123,124] and has been used in the context of other stimuli. In the context of the CNS, M1 microglia are associated with neurotoxicity and cell death, while M2 microglia are assessed to be acting in a neuroprotective role [125]. Considerable debate over the past several years suggest that microglia (and indeed peripheral macrophages) do not fit nicely into a pro-/anti-inflammatory dichotomy (or even a binary sliding scale). Rather, the way in which microglia would respond to some sort of stimulus is highly contextual; it would depend on where in the CNS the microglia are located, the nature of the stimulus/injury, how far away the microglia of interest are from the injury, and at what point during or after the injury the microglia are being observed. That said, the preceding study suggests the potential for DC stimulation to be applied to modify microglial activity to promote tissue healing.

Electrical stimulation paradigms that utilize AC feature phases of both positive and negative polarities. Such paradigms are often designed with charge balancing in mind – an opposing phase offers a way to cycle electrical charge out from any affected cells or tissue and thus avoid damage. In a recent study, Ishibashi et al. found that astrocytes *promoted* myelination in response to biphasic electrical impulses [126]. The cytokine leukemia inhibitory factor (LIF) was found to be released in larger quantities by astrocytes due to ATP release from firing axons;

LIF was then found to promote myelination by mature oligodendrocytes. In another study, stimulation of C6 glioma cells using a variety of balanced and unbalanced waveforms suggested that the way in which electrical paradigms are designed had an impact on cell oxidative stress and neuroprotective behaviours [127].

Alternating current paradigms were also used to evaluate inflammation and damage in the context of electro-acupuncture stimulation of a rat Parkinson's disease model [128]. Rats with transected medial forebrain bundles were electrically stimulated via stainless steel electrodes inserted into 2 acupuncture points: one at the head (between the ears), and another down at the cervical section of the spinal cord. Whether these electrodes made direct contact with CNS tissue is unclear. In this study, biphasic electrical stimulation protected dopaminergic neurons from microglia-mediated cytotoxic damage. It was found that survival rates of dopaminergic neurons were higher with electrical stimulation than without – this was coupled with observations that the stimulation significantly reduced TNF α and IL-1 β release, and that microglia activation was reduced.

Another application that utilizes charge-balanced biphasic waveforms is intraspinal microstimulation (ISMS) - a functional electrical stimulation technique that uses microwires (tens of μm in diameter) implanted into the spinal cord to elicit movement of the lower limbs following spinal cord injury. The technique has been demonstrated extensively to be effective at eliciting movements following spinal cord transections [129,130]. The effects of ISMS paradigms on glial cells appear to remain limited, however. A study by Bamford et al. provides the only evidence known to the authors on this matter [96]. Microwires were surrounded by reactive astrocytes and CD68-positive cells were found surrounding the microwire – this was indicative of microglia/macrophage recruitment and glial scarring. Recruitment of force was not

altered upon stimulation, which suggests that not enough tissue damage was present to compromise underlying neural networks. Stimulus trains were run for 4 h/day for 30 days; further investigation into glial reactivity and force recruitment over a more chronic timecourse would help determine the maximum lifetime of that implant design in the spinal cord before device failure due to glial scarring.

Differences in cell orientation with respect to the direction of the electric field have been noted as a point of contrast between DC and AC paradigms. While orientation of glia (either parallel or perpendicular to the field) has been documented and is predictable in DC fields [112], AC stimulation had not been shown to direct orientation of migration in a consistent manner [131]. Interestingly, Ariza et al. also found that neural stem/progenitor cells (NSCs) exposed to DC field stimulation favoured differentiation into neurons rather than glia, and that AC stimulation did not favour differentiation into one cell type over another [111]. This observation would have implications in designing strategies for guiding neuronal growth/repair in a damaged nervous system.

1.4.1.3. *In vitro* and *in vivo* works of note

Finally, some attention should be given to the creative ways in which *in vitro* and *in vivo* electrical stimulation experiments have been designed, and the outputs that have been generated from them with respect to glial cell reactivity.

A good summary of *in vitro* experiments explicitly assessing glial cell responses to electrical stimulation has been compiled by Bertucci et al. [132]. Briefly, the collection of experiments characterized glial cell responses in terms of polarization towards the electrodes, cell morphologies, cell protrusion lengths, and cell body sizes. The timecourses of the experiments listed in the review provided for stimulation intervals of up to 24 h, followed by a maximum of 48 h post-stimulation monitoring. With such experiments, it would be of interest to determine glial cell responses past a 24 h time window; what, for example, would be timecourse over which glial scarring/cell death occurs in similar models? How would these phenomena change with repeated (e.g., daily) rounds of electrical stimulation applied? If these questions are addressed, any future *in vitro* experiments studying glial cell reactivity to electrical stimulation would better emulate chronic responses.

Cell culture systems have also been developed to study neuron-glia responses to electrical stimulation. Lee et al. utilized microfluidic systems to create spatially restricted cell cultures which then received electrical stimulation [133]. Their study remarkably showed oligodendrocytes maturing and myelinating neurons more efficiently upon exposure to an electric field. In Xu et al., cortical 3D cultures made of electrospun polypyrrole/polyacrylonitrile nanofibers were electrically stimulated [97]. The formation of cell clumps/clusters was prevented with electrical stimulation, but it did not disperse the clumps that had already formed. Electrical stimulation also increased the degree of glial cell proliferation and accelerated neuron maturation. In another study, a nanocomposite membrane comprising of poly(L-lactic-co-glycolic acid)/graphene oxide was cultured with neural stem cells as a candidate composite material for use in electrically-stimulated nerve repair [134]. The substrate improved neural stem

cell proliferation and differentiation into neurons (at the expense of differentiation into astrocytes), and neurite elongation.

In spinal cord injury (SCI) *in vivo* studies, electrical stimulation of existing glia in the CNS results in increased GFAP expression (i.e., astrocyte hypertrophy increased) 1 week after injury [135,136]. By preconditioning SCI rats with electrical stimulation, astrocytes were activated but secondary symptoms such as edema and necrosis were abated. Brief electrical stimulation has also been found to be beneficial for neuronal regeneration. A leech model was used to examine effects of electrical stimulation on neurons [137]. Different neurons (Retzius and P cells) responded differently to the same electrical stimulation pattern, but regardless of the pattern used more leech microglia were seen around the stimulation electrode each time which implies that neuronal regeneration is at least partly due to microglia distribution and activity.

1.4.2. Device development: materials and electrochemistry considerations

In addition to understanding the effects of electrical stimulation on glial cell behaviour as described in the above sections, acknowledgement must also be given to the engineering and design aspect of neural electrode implants. As far as development of invasive neural electrode implants is concerned, factors to be considered include electrode material selection, stimulation paradigms, and electrode geometry. Detailed documentation of these considerations and more can be found in a comprehensive summary by Merrill et al. [138]. Damage to neural tissue arises from mechanical (tissue/device mismatch and insertion damage) and electrochemical means.

Electrode material selection is important from a safety perspective. It goes without saying that a conducting material should be used; however, other considerations include potential material corrosion, ion leaching, degradation, and byproduct formation from electrochemical reactions. A conductive material that degrades and leaches toxic byproducts into its target environment will inevitably cause implant rejection and exacerbate inflammation and damage at the insertion site.

Common electrode materials include platinum, iridium, gold, and silicon. Carbon-based materials (e.g., graphene, carbon nanotubes) and organic materials (e.g., polyaniline, poly(3,4-ethylenedioxythiophene)) have also been more recently described in the literature [94,139–143]. Such materials are generally understood to be compatible and safe for use in CNS tissue [144]. However, the materials listed above generally will elicit a foreign body response from glial cells – that is, gliosis will ensue and a scar will form that encapsulates the implant. The extent of this response is partly dependent on the stiffness of the material – for stiffer materials such as metals, mechanical mismatch between the implants and tissue are further compounded by micromotion-induced stresses. The materials themselves are generally inert – they do not leach cytotoxic particles into the surrounding tissue by themselves. Whether electrical stimulation results in electrochemical reactions at the interface that produces cytotoxic compounds depends on the material that makes up the implant as well as the parameters of the paradigm itself [138,145]. In the literature, common ways in which glial cell reactivity is assessed include cytokine release/expression [143], cell viability [146], morphological comparisons (e.g., ramified vs. amoeboid morphologies for microglia) [147], and cell area coverage of the probe [67].

Merrill et al. [138] explains and compares different stimulation waveforms in terms of trade-offs between action potential initiation probabilities, tissue damage, and corrosion risk.

Stimulation paradigm design must also take into account the target cell population. As electrode implants are primarily targeting neurons, stimulation parameters at the contact sites must be sensitive to the kinds of tissue in which the electrode is implanted – this will translate into differences in parameters such as charge per phase and pulse width [145].

Probe geometry is important, especially for implant insertion. A probe should be stiff enough to facilitate insertion into tissue, but not too stiff that tissue/device mismatch becomes problematic [148]. Alternatively and interestingly, studies have been done where novel materials such as PEDOT have been successfully polymerized *in situ* to form an integrated network with neural tissue [149] thus effectively blurring the border between device and tissue. The result is an electrically conductive network that is pervasive throughout local extracellular space, to the point where scar tissue can be avoided and healthy neurons can be contacted.

Electrochemical considerations are also tied to device material selection. If an electrical stimulation paradigm results in the oxidation or reduction of a chemical species, especially in a Faradaic reaction where charge is passed between electrode and electrolyte, it is desirable to add an opposing and balancing phase to reverse whatever reactions may have occurred. In addition to redox reactions involving electrode material, other chemical species in the surrounding electrolyte may also be affected by electrical stimulation. A commonly discussed theme is the need to avoid water splitting into constituent species of hydrogen and oxygen gas (i.e., keep voltages within the water window). Gas production can result in local changes in pH near the electrode and adversely affect cells [150]. In the same study, organic compounds are also known to be susceptible to redox reactions (e.g., the oxidation of glucose to gluconic acid, CO_2). Oxygen reduction is also to be expected during stimulation pulses [151]. Reduced oxygen species can be damaging to tissue. There may be further chemical species evolved from electrical stimulation,

with differences seen between *in vitro* (different cell culture media formulations) and *in vivo* (extracellular fluids) [138,150].

1.5. Conclusions: considerations for future work

1.5.1. Biomaterials designs for neural implants

Glia are diverse and multifaceted cells capable of choosing the viable fate of central nervous cells. In biomaterials science, their primary focus has been on their role in implant rejection and use in biocompatibility studies. A large body of research has emerged with the intention of attenuating glial cell accumulation onto microelectrodes and ultimately improving the lifetime of such implants. These electrodes have been modified with scar mitigating coatings, improved flexibility and finer shapes to reduce tissue shearing (individually and in microarrays), and having anti-inflammatory drugs loaded to attenuate acute inflammation.

To date, the biomaterial focus on glia is predominantly shown in studies for biocompatibility and the reduction of acute inflammation. More recently, utilizing microglia and macrophage phagocytosis for targeted drug delivery has emerged. The role of cell types such as microglia in development, regeneration, and neurodegenerative disease has become critical; however, few biomaterials have emerged to explore and exploit these cellular behaviours. For example, microglia are capable of secreting a variety of neurotrophic growth factors, which are essential in repair and restoration after neural injury. It would be tremendously desirable to induce microglia to do so in place of growth factor therapy, a commonly used and

pharmacokinetically poor approach. In addition, it has been determined that microglia and macrophages have different roles in disease pathology. But little thought has been given to developing biomaterials to optimize microglial preventative measures in early stage pathology and macrophage targeted treatments in late stage pathology where the BBB has broken down. As these cells are difficult to distinguish experimentally, their roles are often described interchangeably. Furthermore, phenotypes of microglia are being linked to neurodegenerative disease; however, there is limited capability to identify and target these cells for therapeutics.

The functions of microglia, and their cooperative effects with other glia including astrocytes and oligodendrocytes, has increasingly been shown to be diverse and essential to both neuroprotection and the capacity to regenerate CNS tissue after injury or disease. As such, there is a tremendous unexplored potential in biomaterial and engineered design with respect to modulating glia in the context of neuroinflammation.

1.5.2. Electrical stimulation considerations for modulating glial cell behaviour

Across the literature surveyed in this review, common themes emerge with respect to the outputs explored in the aforementioned studies (Table T-1). While there are several works which suggest that electrical stimulation is foremost an inflammation-inducing action on glia, other studies utilize electrical stimulation with the perspective that it can be harnessed to promote neuroregeneration and tissue healing by using glial cells as a go-between. Caution should be exercised however – the way in which glia respond to an electrical stimulus depends very much

on the nature of the stimulus itself (Figure 1-3), the application, target area within the CNS, and the target cells – the full complexity of which has yet to be explored.

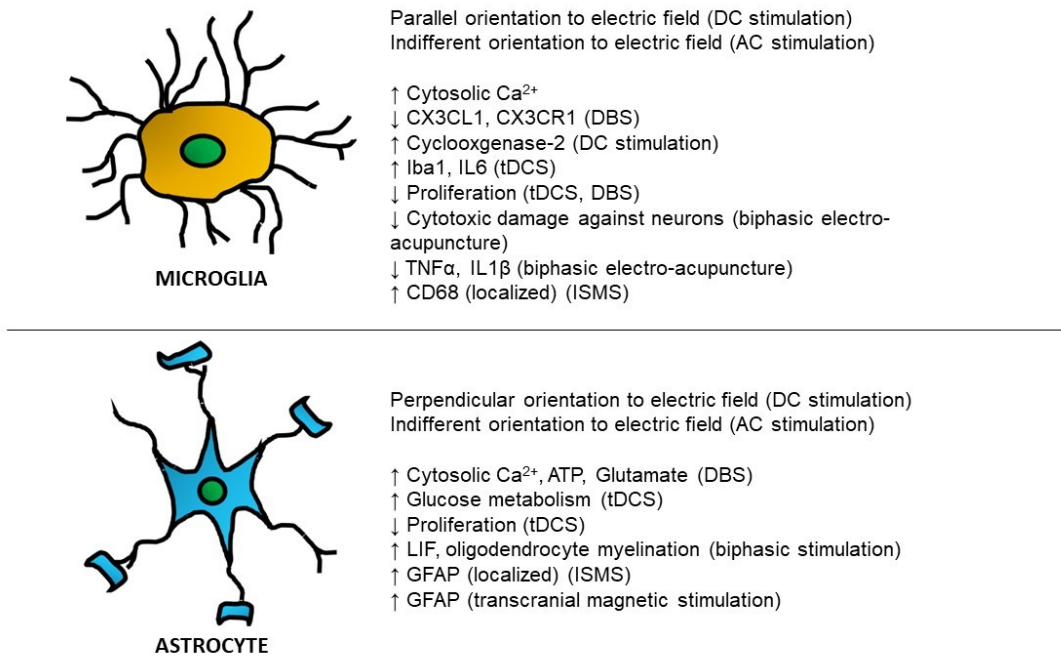


Figure 1-3: Summary of biomarker and functional changes to microglia and astrocytes in response to electrical stimulation

Effects of electrical stimulation differ between microglia and astrocytes, and are further complexed by different modalities and parameters of stimulation. Note: microglia and astrocyte graphics are not to scale.

A great body of literature has emerged and developed over the past approximately 10 years on the biomaterial modification of invasive electrodes into neural tissue. The studies

surveyed have taken a wide breadth of approaches towards mitigating the issue of glial scarring (e.g., mechanical modification of base materials, conjugation of bioactive substrates onto the electrode surface, anti-inflammatory treatments following insertion) [139]. We propose that further advancement of this field of research is required to develop more meaningful devices that could one day see clinical translation – more specifically, studies that take a biomaterials approach to modulating glial scar formation should also eventually integrate electrical stimulation into the proposed experiments. Indeed, the main function of many such devices is to deliver electrical current to tissue. It is therefore of interest to know, for example, if there are any differences in electrochemical activity around the electrode-tissue interface resulting from biomaterial modifications that could negatively impact the biocompatibility of such a device. Furthermore, would frequent electrical stimulation degrade such electrodes and cause them to weaken or fail structurally? Current insight into the range of electrochemical reactions that happen at the electrode-tissue interface is limited, but could potentially be elucidated using methodologies outlined in Cogan’s review on characterization of neural electrodes (e.g., cyclic voltammetry, electrical impedance spectroscopy, voltage transient measurements) [145]. Consider also what the threshold for stimulation-induced damage is as outlined by Shannon’s equation [152], and other aggravating factors in an organism that could contribute to the inflammatory response against an implant: implant tethering to a relatively fixed surface (e.g., skull), electrode wire micromotion, etc.

Any future *in vivo* and *in vitro* electrical stimulation studies would have added value in implementing extended time courses following stimulation (for monitoring of cell responses) and multiple rounds of stimulation into an experiment. It is anticipated that multiple rounds of stimulation will be more reflective of clinical applications where frequent (daily) usage of

exogenous currents is to be expected, and that *in vitro* and *in vivo* models that show this will more accurately recapitulate any chronic cell or tissue response resulting from implant insertion and electrical stimulation.

More work also needs to be done in terms of the effects of different electrical stimulation parameters on CNS cells. As neurons come in different shapes and sizes in the CNS, designing/referencing customized paradigms for stimulating a particular group(s) of neurons in the CNS is an eventuality. What is also of interest are any changes in glial cell reactivity due to differences in stimulation parameters (e.g., AC/DC, different charge-balance schemes, current amplitude, frequency, pulse width, duty cycle, interphase delay, etc.); this is further compounded by evidence of glial cell heterogeneity throughout the CNS [110]. A more thorough understanding of the factors mentioned above will open the door to developing novel electrode and stimulation designs. This will result in reduced glial cell reactivity and translate into a longer lasting (and more effective) implant.

Table T-1: Summary of primary studies of electrical stimulation of glia

Study	Ref.	Invasive/Contact				Current		Glial subtypes	Application/Purpose of study	
		<i>In vitro</i>	<i>In vivo</i>	with cells?		AC	DC			
				Yes	No					
Ariza et al., 2010	[111]	✓			✓		✓	✓	Neural stem/progenitor cells	Engineering of electric fields to control differentiation and growth of transplant cells
Baba et al., 2009	[115]		✓	Semi-invasive (Epidural)				✓	Astrocytes, Microglia	Electrical stimulation as a therapeutic treatment for cerebral ischemia
Bamford et al., 2010	[96]		✓	✓			✓		Astrocytes, Microglia	Intraspinal microstimulation

Chen et al., 2020	[108]		✓	✓			✓	Microglia	DBS suppression of fractalkine signalling in Parkinson's rat model
Cohen et al., 2020	[137]		✓	✓			✓	Microglia	Electrical stimulation mediated neuronal regeneration via microglia (or via differential microglia distribution)
Colmenárez-Raga et al., 2019	[116]		✓	Semi-invasive (Epidural)			✓	Astrocytes, Microglia	Modulation of rat hearing sensitivity via epidural stimulation of auditory cortex
Fu et al.,	[134]	✓		✓			✓	Astrocytes	Electrical stimulation

2019									via a PLGA/graphene oxide substrate for nerve repair
Hadar et al., 2017	[109]		✓	✓			✓	Microglia	DBS suppression of microglia activation from perinatal CNS injury
Hathway et al., 2009	[121]		✓	✓			✓	Microglia	Identifying microglia role in chronic pain/central sensitization in response to C-fibre stimulation
Ishibashi et al., 2006	[126]	✓		✓			✓	Astrocytes, Oligodendrocytes	Electrical stimulation-induced remyelination via

									astrocyte activity
Latchoumane et al., 2018	[117]	✓		✓			✓	Astrocytes, Oligodendrocytes	Investigation into underlying molecular pathways that make tDCS work in context of CNS injury
Lee et al., 2017	[133]	✓		✓			✓	Oligodendrocytes	Model for studying effects of electrical stimulation on oligodendrocyte myelination activity
Liu et al., 2004	[128]		✓	✓			✓	Microglia	Neuroprotective role of electro- acupuncture stimulation against neurodegenerative

									disease
Orlowski et al., 2017	[102]		✓	✓			✓		Astrocytes, Microglia Longitudinal DBS study in Goettingen pigs
Pelletier et al., 2015	[112]	✓				✓		✓	Astrocytes, Microglia Identifying the mechanisms behind the clinical benefits of tDCS
Roitbak and Fanardjian, 1981	[100]		✓	✓				✓	Not specified Characterization of glial cell depolarization
Schipke et al., 2001	[98]		✓	✓			Not specified		Astrocytes, Microglia Proof of Ca ²⁺ wave propagation through microglia using electrophysiological recordings and

									stimulation
Vallejo et al., 2019	[127]	✓			✓	✓	✓	C6 Glioma cells	Electrical stimulation-induced gene expression modulation of glia
Vedam-Mai et al., 2016	[106]		✓	✓		Not specified		Microglia	Assessment of extent of microglia activation following DBS
Xu et al., 2018	[97]	✓		✓			✓	Astrocytes, Ependymal cells	Use of electrical stimulation and nanofibers in neural tissue engineering

1.6. Thesis outline

Considering the review of the above works regarding the effects of electrical stimulation on glial cell behaviour, our literature survey revealed a dearth of information. Although there has been an emergence and substantial advance in biomaterials strategies to modulate glial cell response to electrode implants in CNS tissue over the past two decades, an absence still remains on how glial cells respond to these implants when electrical stimulation is applied. There are limited studies that address how immune cells (not just in the CNS but the body in general) react to electrical stimulation. Other studies utilize immortalized cell lines to study the effects of electrical stimulation. To fill the gap in knowledge that has been identified, the work presented in this thesis centres around recapitulating the glial scarring phenomenon in a 2-dimensional (2D) *in vitro* environment. Such an approach is advantageous in that evaluating glial cell reactivity to stimuli this way has a reduced ethical footprint.

The overarching research objective for the thesis is thus to utilize a high-throughput *in vitro* model to evaluate primary glial cell response to electrical stimulation. The following chapters, outlined in brief below, have been designed to address the research objective:

1.6.1. Chapter 2 Synopsis – Design and evaluation of a high-throughput *in vitro* model for evaluating mixed glial cell responses to functional microelectrode implants

The aim of the study performed in this chapter was to develop the experimental framework used for the electrical stimulation experiments carried out on glial cell cultures in the thesis, and evaluate its feasibility by electrically stimulating cells over multiple days.

Specifically, imaging acquisition and analysis methods were developed to quantify the extent of damage that electrical stimulation inflicted on both glial cells and the microelectrodes themselves. Platinum-iridium microelectrodes (75 μm diameter) were fabricated using a nanosecond laser. These microelectrodes were threaded through custom-made polydimethyl siloxane (PDMS) rings that are designed to fit inside the wells of 12-well cell culture plates. Mixed glial cell cultures were generated using cells harvested from the brains of postnatal day 2 heterozygous CX3CR-1^{+EGFP} mice [153,154]. The cultures were then stimulated 4 h/day over 1 day, 3 days, and 7 days to capture the glial cells' longitudinal response against both the presence of the microelectrode implant as well as applied electrical stimulation. The stimulation paradigms used were biphasic charge-balanced rectangular patterns at 0 mA, 0.15 mA, and 1.5 mA [96]. Glial cell responses were captured in terms of cell density, biomarker (Hoechst, EGFP, GFAP, IL-1 β) fluorescence intensity and area coverage as a function of both current intensity and distance away from the electrode tip [155]. The quantified image data suggest that the glial cell responses examined were localized around the deinsulated tip of the electrodes. These responses were dependent on 1) the level of stimulation current applied, 2) the specific biomarker that was being looked at, and 3) the distances from the electrode tip (i.e., electrical stimulation had a different range of effect for each biomarker). It was also found that glial cell responses did not progressively get worse in a linear manner with increasing time and rounds of stimulation. Specifically, there were no measurable differences in biomarker outputs between stimulation currents at day 1, drastic changes in biomarker area coverage and cell density at day 3, and finally a return to no measurable changes in biomarker outputs at day 7. Further study into the damage that electrical stimulation inflicted onto the electrodes themselves was done via scanning electron microscopy (SEM) and energy-dispersive x-ray spectroscopy (EDS) – those

analyses indicated oxidation of the electrode surfaces at 1.5 mA of stimulation. In comparison, the electrode surfaces at 0 mA and 0.15 mA were still intact and did not oxidize post-experiment. The results generated from this chapter correlate well with the localized glial cell reactivity seen in a similar experimental design that was performed in rat spinal cord tissue [96]. The experimental design and methods described in the chapter were then further built upon and used to evaluate glial cell reactivity to several modified electrical stimulation paradigms (Chapter 3).

1.6.2. Chapter 3 Synopsis – Microelectrode stimulation parameter modifications elicit differential glial cell responses over a short 4-hour timecourse

This chapter builds on the previous chapter – the experimental designs outlined in Chapter 2 were heavily utilized to further explore the effects of different stimulation paradigm parameters on glial cell reactivity [127]. A key finding in the Chapter 2 experiments is that a peri-electrode void forms as a result of electrical stimulation in mixed glial cell cultures – the extent of void formation correlates with the intensity of the stimulation applied. This chapter also asks if these voids are the result of cells in proximity to the electrode dying off and/or migrating away from the electrode. The cells used were harvested from heterozygous CX3CR1^{+EGFP} mice [32,153]. In this specific transgenic strain of mouse, the microglia express enhanced green fluorescent protein (EGFP) under the CX3CR1 promoter gene thus making them imageable under a fluorescence microscope while still alive. This property was leveraged to live-image microglia in the mixed glial cell cultures and observe their response to stimulating microelectrodes using various modified electrical stimulation paradigms. Specifically, EGFP signal changes (biomarker fluorescence intensity and area coverage) were quantified at and

around the electrode for each experimental condition across 4 h of stimulation. Glial cell responses to modifications in current intensity (0.1-0.4 mA) [96,156], waveform shape (rectangular, sinusoidal, ramped) [127,157,158], and frequency (25-55 Hz) [159,160] were assessed. Following these live imaging stimulation experiments, the protocol established in the previous chapter was followed: cells were fixed, immunolabelled, and imaged, and the microelectrodes were extracted for imaging on the SEM and elemental analysis using EDS. Differences in biomarker signal changes were captured for all stimulation modifications over a short 4h experiment. Predictably, greater amounts of biomarker signal losses were seen with increasing stimulation current. Stimulation with rectangular and ramped waveform shapes resulted in greater biomarker signal loss compared to with sinusoidal waveforms. While biomarker signal losses increased with frequency from 25 to 45 Hz, this was not the case when the cells were stimulated at 55 Hz. SEM and EDS analysis following stimulation using any of the modified paradigms did not indicate that the electrodes sustained damage. The work described in this chapter further expands on the work done in the previous chapter by highlighting the impact that multiple electrical stimulation parameters have on glial cell reactivity.

1.6.3. Chapter 4 Synopsis – Contributions of mixed glial cell culture components on the *in vitro* electrochemical performance of platinum-iridium microelectrodes

The goal of this chapter was to describe the contributions of different components in the mixed glial cell culture design on the electrochemical performance of the platinum-iridium microelectrodes. Generating electrochemistry data allows for the gauging of the efficacy and safety of the platinum-iridium electrodes that have been used in the previous chapters’

experiments, as well as the limits to which they can be pushed before the electrodes themselves or the cells around the electrodes become damaged. To address the goal of this chapter, a potentiostat was connected to 12-well plates with embedded electrodes – this allowed for multiple electroanalytical experiments to be conducted. Analyses performed include cyclic voltammetry, electrical impedance spectroscopy, and voltage transient analysis. Cyclic voltammetry assesses the current response of the microelectrodes, at a defined scan rate, within a defined voltage range [161–163]. From the plot generated the reversibility of electron transfer at the electrode-solution interface is determined, and the charge storage capacity is calculated which describes the amount of electrical charge that the platinum-iridium alloy is able to store in the cell culture system. Electrical impedance spectroscopy assesses changes in electrical impedance at the electrode-solution interface as a function of frequency of electrical perturbations applied through the microelectrode [162,164]. Voltage transient analysis is used to calculate the maximum amount of electrical charge that is injectable by a stimulation pulse [145]. Also of importance with this technique is that the maximum cathodic potential is also determined – this metric determines whether or not a given stimulation pulse is safe for cells by comparing the determined potential to the water window. These analyses were conducted with the microelectrodes immersed in various solutions: phosphate buffered saline (PBS), DMEM F12 media, DMEM F12 media + fetal bovine serum (FBS) + penicillin-streptomycin (PS), and DMEM F12 media + FBS + PS + cell culture. Cyclic voltammetry and electrical impedance spectroscopy data suggest that there is less physical surface area available for electrode-electrolyte charge transfer to occur in cell culture media due to presence of large proteins which foul the surface of the electrode, but that this may be rectified in part by mixed glial cell cultures making contact with the electrode and serving as a conductive layer. Voltage transient analysis,

when compared with the threshold for electrolysis of water, suggests that that threshold is not breached until the 200-250 μA mark for mixed glial cell cultures which is in-line with what is considered a safe level of current for *in vivo* microelectrode stimulation. This work was done to determine contributions of different materials to the electrochemical properties of the microelectrodes during a cell culture stimulation experiment.

1.6.4. Chapter 5 Synopsis – Conclusions and Future Directions

In the concluding chapter, a summary of the experiments described in the previous chapters is given. Future directions described include other stimulation parameters (e.g., pulse duration, charge balance, interphase delay, reversed polarity) yet to be tested. These further studies would also be coupled with multi-day studies (1, 3, 7 days, etc.) to test the longitudinal effects that such parameters would have on glial cell reactivity. The thesis focuses strictly on glial cell response as they are a key driver of the fate of all cells in the CNS in many contexts (e.g., injury due to electrode implantation). By integrating neurons into the cell cultures in the future the physiological relevance of this *in vitro* model is improved as the effects of electrical stimulation (and any secondary effects via glial cell reactivity) will also be captured through monitoring neuronal responses. The results generated from this thesis are intended to better inform neural interface device developers of the biocompatibility and safety of invasive neural implants, allowing these devices to last longer and function more effectively in persons experiencing neurological disease or injury.

1.7. Significance of Thesis

With the work completed in the thesis, the data generated expands on knowledge on how electrical stimulation affects actual glial cells – an objective that is effectively addressed by primary cell culture. With the cell culture and analysis methods described in the thesis, the work also serves as a proof-of-concept of a high-throughput strategy for evaluating electrode stimulation designs. Because a core focus of the work done emphasizes modification of electrical stimulation paradigms, optimization of such paradigms is also possible with the goal of improving the biocompatibility and lifetime of an implant in a patient.

2. Chapter 2 – Design and evaluation of a high-throughput *in vitro* model for evaluating mixed glial cell responses to functional microelectrode implants

2.1. Preface

Some contents found in this chapter have been previously published in one paper:

C.T. Tsui, S. Mirkiani, D.A. Roszko, M.A. Churchward, V.K. Mushahwar, K.G. Todd, In vitro biocompatibility evaluation of functional electrically stimulating microelectrodes on primary glia, *Frontiers in Bioengineering and Biotechnology* 12 (2024). <https://www.frontiersin.org/articles/10.3389/fbioe.2024.1351087>.

CT conceptualized the study, designed the experiments, carried out the experiments, collected and processed data, wrote, and edited the manuscript. SM and DR provided technical support with experimental design and fabrication of platinum-iridium microelectrodes, and edited and proofread the manuscript. MC, VM, and KT edited and proofread the final manuscript.

2.2. Abstract

Neural interfacing devices interact with the central nervous system to alleviate functional deficits arising from disease or injury. This often entails the use of invasive microelectrode implants that elicit inflammatory responses from glial cells and leads to loss of device function. Previous work in the literature focused on improving implant biocompatibility by modifying

electrode composition; here, we investigated the direct effects of electrical stimulation on glial cells at the electrode interface. A high-throughput *in vitro* system that assesses primary glial cell response to biphasic stimulation waveforms at 0 mA, 0.15 mA, and 1.5 mA was developed and optimized. Primary mixed glial cell cultures were generated from heterozygous CX3CR-1^{+EGFP} mice, electrically stimulated for 4 h/day over 1, 3, and 7 days using 75 μ m platinum-iridium microelectrodes, and biomarker immunofluorescence was measured. Electrodes were then imaged on a scanning electron microscope to assess sustained electrode damage. Fluorescence and electron microscopy analyses suggest varying degrees of localized responses for each biomarker assayed (Hoechst, EGFP, GFAP, IL-1 β), a result that expands on comparable *in vivo* models. The trends observed from the image data suggest that glial cell responses were non-linear, with no measurable biomarker differences at day 1, drastic changes in outputs such as biomarker area coverage and cell density seen at day 3, and then a repopulation of the peri-electrode void by cells by day 7. Scanning electron microscopy and energy-dispersive x-ray spectroscopy also indicated damage and oxidation of the electrode surfaces at 1.5 mA. This system allows for the comparison of a breadth of electrical stimulation parameters, and opens another avenue through which neural interfacing device developers can improve biocompatibility and longevity of electrodes in tissue.

2.3. Introduction

Neural interfacing devices interact with the central nervous system with the goal of improving a functional deficit from conditions including Parkinson's disease and spinal cord injury [165–168]. Devices used in interventions such as deep brain stimulation (DBS) and

intraspinal microstimulation (ISMS) make use of thin invasive implants sometimes no thicker than a human hair, that are inserted into nervous tissue to physically make contact with and interact with cells [169–173].

Although such an approach is advantageous in that it allows for direct, acute and effective stimulation of neuronal networks [129,174], insertion of material into tissue inevitably elicits a foreign body response. In the case of the central nervous system, the foreign body response is characterized by microglia and astrocytes cordoning off the implant site from the surrounding tissue through the creation of a fibrous glial scar [175–177]. The glial scar is problematic in that it prevents nearby neurons from accessing the implant for recording or stimulation purposes. Glia-driven inflammation persists in the tissue over several weeks to months which can lead to device failure and potential revision surgeries.

Over the past decade, there has been an increased effort to improve upon the biocompatibility of electrodes in the context of neural interfacing [178–180]. The main focus of such efforts has been on improving the material properties of the electrodes such as conductivity and mechanical stiffness [181,182]. Other reports document the conjugation of biomolecules onto the surfaces of the electrodes to mask its foreign signature [60,67]. Antifouling compounds (e.g., zwitterionic polymers, polyethylene glycol) have also been reported in the literature to attenuate acute inflammatory responses elicited against invasive implants [183–187].

Although there have been reports on the effects of direct field electrical stimulation on glial cell lines *in vitro* [112,113,127,157]; there is a paucity of reports documenting the effects of electrical stimulation on primary glial cells and associated cellular responses at the electrode interface. Evidence previously published by our group suggests that any responses from glia

elicited by electrically stimulating electrodes develop acutely and are localized near the device interface [96].

Here, we present a high-throughput and rapid means of assessing glial cell response to microelectrode implants *in vitro* via a hybrid cell biology and engineering approach. We recapitulated cellular responses observed previously *in vivo* – specifically, localized responses observed in tissue in proximity to the electrode in a longitudinal rat study by Bamford et al. [96]. In addition to assessing cellular responses to the presence of the electrode, we also determined cellular responses to different amplitudes of electrical stimulation. Extent of glial cell inflammation and damage was determined by immunofluorescence microscopy of specific biomarkers at and around the electrode. Furthermore, we assessed the extent of damage to the electrode itself through scanning electron microscopy and energy-dispersive x-ray spectroscopy.

2.4. Materials and methods

2.4.1. Materials

Dulbecco's Modified Eagle Medium: Nutrient Mixture F12 (DMEM F12), Hank's Balanced Salt Solution (HBSS), fetal bovine serum (FBS), penicillin streptomycin (PS), 0.25% trypsin-ethylenediaminetetraacetic acid (Trypsin-EDTA), and Equine Serum (ES) were purchased from Gibco (Life Technologies, Burlington, ON, Canada). Poly-L-lysine hydrobromide (PLL) was purchased from Sigma Aldrich (St. Louis, MO, USA). Polystyrene 12-well cell culture plates were purchased from Greiner Bio-One (Frickenhausen, Germany). Cell culture flasks (75 cm²) were purchased from Corning (Corning, NY, USA). Sylgard 184 polydimethyl siloxane (PDMS) kit was purchased from Dow Chemical (Midland, MI, USA).

Rabbit anti-IL-1 β (Invitrogen, Burlington, ON, Canada) and chicken anti-GFAP (Abcam, Toronto, ON, Canada) primary antibodies were used. Donkey anti-rabbit Alexa Fluor 647 (Invitrogen) and goat anti-chicken Alexa Fluor 546 (Invitrogen) secondary antibodies were used. Hoechst 33342, a nuclear stain, was purchased from Molecular Probes (Life Technologies, Burlington, ON, Canada).

Microwires (75 μ m in diameter, Pt-Ir 80%/20% insulated with polyimide) for microelectrode fabrication were purchased from California Fine Wire (Grover Beach, CA, USA). Teflon-insulated, 9-strand stainless steel wires (Cooner AS632) were purchased from Cooner Wire Company (Chatsworth, CA, USA).

2.4.2. Cell culture preparation

Animal protocols were approved by the Animal Care and Use Committee at the University of Alberta and conducted in accordance with the guidelines of the Canadian Council for Animal Care. Mixed glial cell cultures were generated from the brain tissue of postnatal Day 2 C57BL/6J CX3CR-1^{+EGFP} heterozygous transgenic mice [188]. The mice were decapitated and their brains removed using surgical scissors and a metal spatula. Following dissection of the meninges using forceps, the remaining brain tissue was dissociated in 0.25% Trypsin-EDTA at 37 °C for 25 minutes. The Trypsin mixture was then centrifuged twice at 500 *g* for 2 min and triturated in cell culture media (DMEM F12/10% FBS/1% PS) to further dissociate brain tissue and deactivate residual Trypsin-EDTA. The resulting cell suspension was placed in 12-well plates coated with PLL (2 μ g/mL). Cells were incubated for 2 weeks at 37 °C and 5% CO₂, with cell culture media changed twice weekly.

At 2 weeks, mixed glial cells were washed with DMEM F12 and then lifted off from the 12-well plates with a Trypsin-EDTA and DMEM F12 mixture (1:3 ratio) treatment for 25 min [189]. The cells were then collected and subjected to two-fold centrifugation at 500 g for 2 min and trituration in cell culture media. The resulting cell suspension was then passed through a syringe and needle, and plated in a 75 cm² flask at a ratio of 1 plate:1 flask. The flask cultures were then incubated for 1 week at 37 °C and 5% CO₂ prior to another round of isolation and re-seeding onto microelectrodes, with cell culture media changed twice in that week.

2.4.3. PDMS ring fabrication

To stabilize electrode placements in the 12-well plates, custom polydimethyl siloxane (PDMS) rings were created to prevent movement of the wires within the wells (Figure 2-1). PDMS is a silicone-based polymer material that is non-cytotoxic and well-documented for use in various *in vivo* and *in vitro* applications [190–193]. PDMS elastomer base and curing agent were mixed together in a 50 mL tube in a 10:1 ratio, and left to set in the wells of a 12-well plate (2 g/well). Following curing for 2.5 hours in an oven at 70 °C, the resulting PDMS discs were extracted from the wells, hole-punched, and placed in a large 3 L beaker (50% methanol/50% water) under a fume hood overnight to wash out any unreacted monomers leftover from the curing process. Following this, the rings were submerged in water and autoclaved in preparation for use in cell culture.

2.4.4. Microelectrode fabrication

Platinum-iridium microwires (75 μm diameter) were used for fabrication of microelectrodes. Briefly, microwires were cut ~ 15 cm in length. The insulation layer of the microwire tips was removed using nanosecond laser pulses (wavelength = 248 nm, energy = 150 mJ, beam attenuation = 5%, repetition rate = 10 Hz; COMPex 110, Coherent, CA, USA). The deinsulated region of the microwires was cut using a scalpel blade leaving 300-400 μm of bare metal at the tip. The tips of the microwires were then mechanically bevelled using a microelectrode beveler (BV-10, Sutter, CA, USA) to an angle of approximately 15 $^{\circ}$. Microelectrodes were then placed in 15 mL centrifuge tubes (Fisherbrand, Pittsburgh, PA, USA) filled with DI water and Alconox detergent, and treated in an ultrasonic cleaner for 30 minutes to remove the metal debris formed during the mechanical polishing step. The microelectrodes were then sonicated for another 30 minutes in DI water and rinsed with 70% ethanol. Stranded stainless steel wires were manually deinsulated to expose approximately 4-5 cm and were used as the counter electrodes.

2.4.5. Electrode plate setup

Insertion of microelectrodes into the PDMS rings and placement of the rings into the 12-well plates was all done within the aseptic environment of a biosafety cabinet. An 18.5G needle was used to puncture a hole through the side of a ring at a 45 $^{\circ}$ angle. A 10 μL pipette tip was then fitted through the hole, and a microelectrode was threaded through the pipette tip such that the deinsulated end of the wire lay in the inner hole of the PDMS ring (Figure 2-1). The pipette tip was then withdrawn to effectively embed the insulated portion of the microelectrode in the side

of the ring. The ring and microelectrode were then dipped in 70% ethanol, placed in one of the wells of a 12-well plate, and left to dry to form a sterile seal in the well. This also allowed the deinsulated tip of the wire to make contact with the bottom of the well. The insulated portions of the electrodes were then taped down over the edge of the 12-well plate to prevent further movement. Counter electrodes were placed on top of the PDMS rings and held down over the edge of the plate with tape on the day of the experiment.

Cells were isolated from the flask as above using diluted Trypsin-EDTA/DMEM F12, seeded at a density of 70000 cells/well, and left to settle and incubate for 7 days at 37 °C and 5% CO₂ prior to the start of electrical stimulation. Cell culture media (DMEM/10% FBS/1% PS, 2 mL/well) was changed twice during the 7-day incubation period.

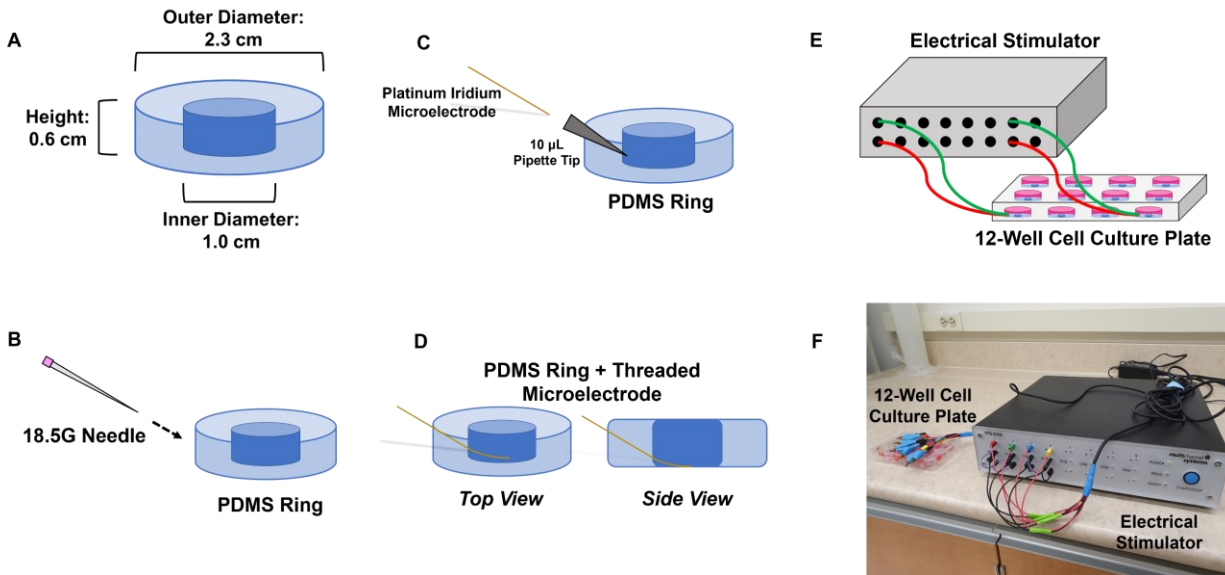


Figure 2-1: Procedure for inserting 75 μm microelectrodes into the sides of PDMS rings

(A) PDMS rings are cured to fit inside the well of a 12-well plate; (B) rings are punctured from the side with an 18.5G needle at a 45° angle; (C) 10 μL pipette tip is fitted inside the punctured hole and the electrode is threaded through the pipette tip; (D) the electrode is threaded through to

the point where its deinsulated tip is able to make contact with the bottom of the well once the ring is inserted. The pipette tip is removed once the electrode is threaded through. Each threaded electrode/PDMS ring assembly is then inserted into a 12-well culture plate that is connected to an electrical stimulator using clamped cables (E, F).

2.4.6. Electrical stimulation experiments

The cells were electrically stimulated for a 4 h duration each day over a total of 1, 3, and 7 days using a paradigm adapted from *in vivo* ISMS work [96]. The experiments were designed to have 4 h of electrical stimulation per day as that is the anticipated amount of usage of electrical stimulation that a patient would require daily in a clinical setting when paired with physical therapy. An STG4008 electrical stimulator (Multi Channel Systems MCS GmbH, Reutlingen, Germany) was used to electrically stimulate the cells, with programming of the stimulation patterns done through the MC_Stimulus II software. Cells were stimulated using a biphasic charge-balanced cathodic-first rectangular waveform, at an amplitude of 0 mA, 0.15 mA or 1.5 mA, 200 μ s pulse duration, and 25 Hz. The charge injected per phase at 0 mA, 0.15 mA and 1.5 mA was 0 nC, 30 nC, and 300 nC, respectively.

2.4.7. Immunofluorescence microscopy

Following electrical stimulation experiments, glial cells were fixed with 5% formalin at 37 °C for 10 min and washed three times with PBS. Cells were permeabilized with 0.1% Triton X-100 (TX100) in PBS and 10% Equine Serum (ES) for 2 h. Following this, the cells were

incubated overnight at 4 °C with rabbit anti-IL-1 β (1:1000) and chicken anti-GFAP (1:5000) primary antibodies plus 1% ES. The cells were then washed three times with PBS, and incubated for 2 h at room temperature with goat anti-chicken Alexa Fluor 546 (1:200) and donkey anti-rabbit Alexa Fluor 647 (1:200) secondary antibodies plus Hoechst 33342 (1:1000) and 1% ES. The cells were then washed three times with PBS. Fluorescence microscopy was carried out on a Leica TCS SPE confocal microscope (Wetzlar, Germany). Components labelled included Hoechst for cell nuclei, enhanced green fluorescent protein (EGFP) expressed from transgenic microglia, glial fibrillary acidic protein (GFAP) for astrocytes, and interleukin-1 beta (IL-1 β) as a pro-inflammatory biomarker. Analysis of fluorescence microscopy images was carried out with ImageJ (National Institutes of Health, Bethesda, MD, USA) using a custom macro measuring for fluorescence intensity and area coverage of biomarkers. Area coverage measured the total geometric surface generated by each biomarker from the cells in the image's field of view. Fluorescence intensity was calculated by dividing the image-wide sum of each pixel intensity value for a biomarker divided by the area coverage of that biomarker in that image. Cell density was calculated by counting the number of nuclei found in each image. These metrics (fluorescence intensity, area coverage, cell density) were expressed as fold change against control wells with no wire. Zonal analysis (i.e., how outputs change as a function of distance from the electrode tip) was carried out at prescribed circular radii from the electrode tip ($r = 50 \mu\text{m}$, $100 \mu\text{m}$, $250 \mu\text{m}$) [155]. This was compared to data analyzed from the full frame of the image ($734.05 \mu\text{m} \times 734.05 \mu\text{m}$).

2.4.8. Scanning electron microscopy

Qualitative assessment of damage to electrodes was carried out using a ThermoFisher Phenom XL Desktop scanning electron microscope (SEM) (Waltham, MA, USA). Images were acquired using backscattered electron detection at 610x and 4000x magnification. Elemental makeup of the electrode surfaces was quantified using the energy-dispersive x-ray spectroscopy (EDS) add-on to the SEM, at 4000x magnification.

2.4.9. Statistical analyses

All experiments were analyzed with a sample size of six ($n = 6$) with 2 internal replicates for each independent experiment. For statistical analysis of fluorescence intensity and area coverage of biomarkers and cell density, a two-way analysis of variance (two-way ANOVA) with Bonferroni's *post hoc* test was performed. The independent variables analyzed were electrical stimulation amplitude and distance away from the tip of the electrode. For statistical analysis of EDS data, a one-way analysis of variance (one-way ANOVA) with Tukey's *post hoc* test was performed using GraphPad Prism 10 (San Diego, CA, USA) with electrical stimulation amplitude being the main effect analyzed.

2.5. Results

2.5.1. Cellular responses at electrode interface

Mixed glial cell cultures were electrically stimulated using a biphasic charge-balanced rectangular waveform paradigm for 4 hours daily over a short timecourse of 1, 3, and 7 days. The cells were then fixed, immunolabelled and imaged on a confocal fluorescence microscope. Images were acquired across all stimulation amplitudes tested (0 mA, 0.15 mA, 1.5 mA) (Figures 2-2, 2-3, 2-4).

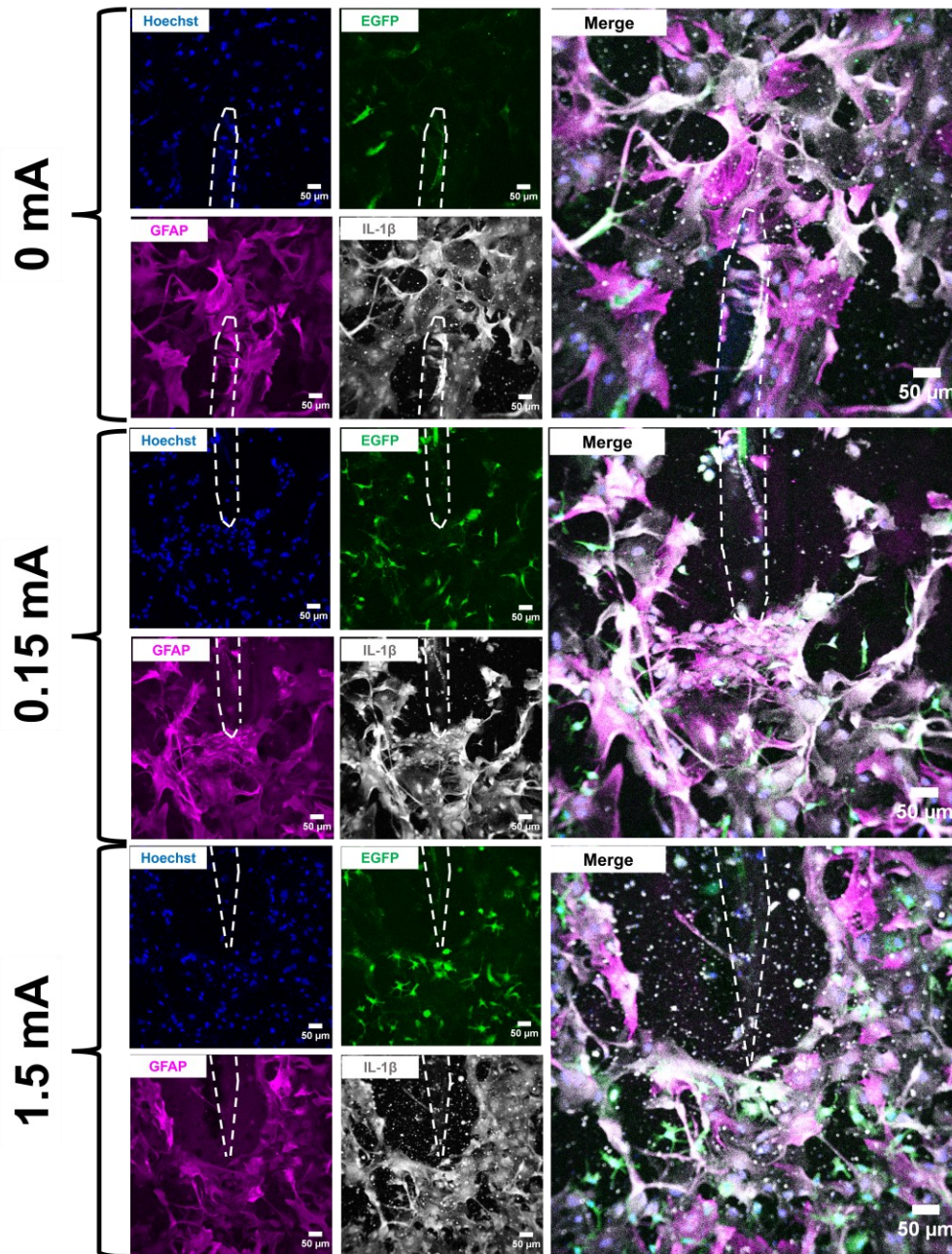


Figure 2-2: Immunofluorescent images of electrically stimulated mixed glial cell cultures at the electrode interface (4 h/day x 1 day).

Electrodes are marked by the white dashed outline in each image. Cell cultures were labelled with Hoechst 33342 (blue), EGFP (green), GFAP (magenta), and IL-1 β (grey). An enlarged merged channel overlay of each condition is shown on the far right. Scale bars: 50 μ m.

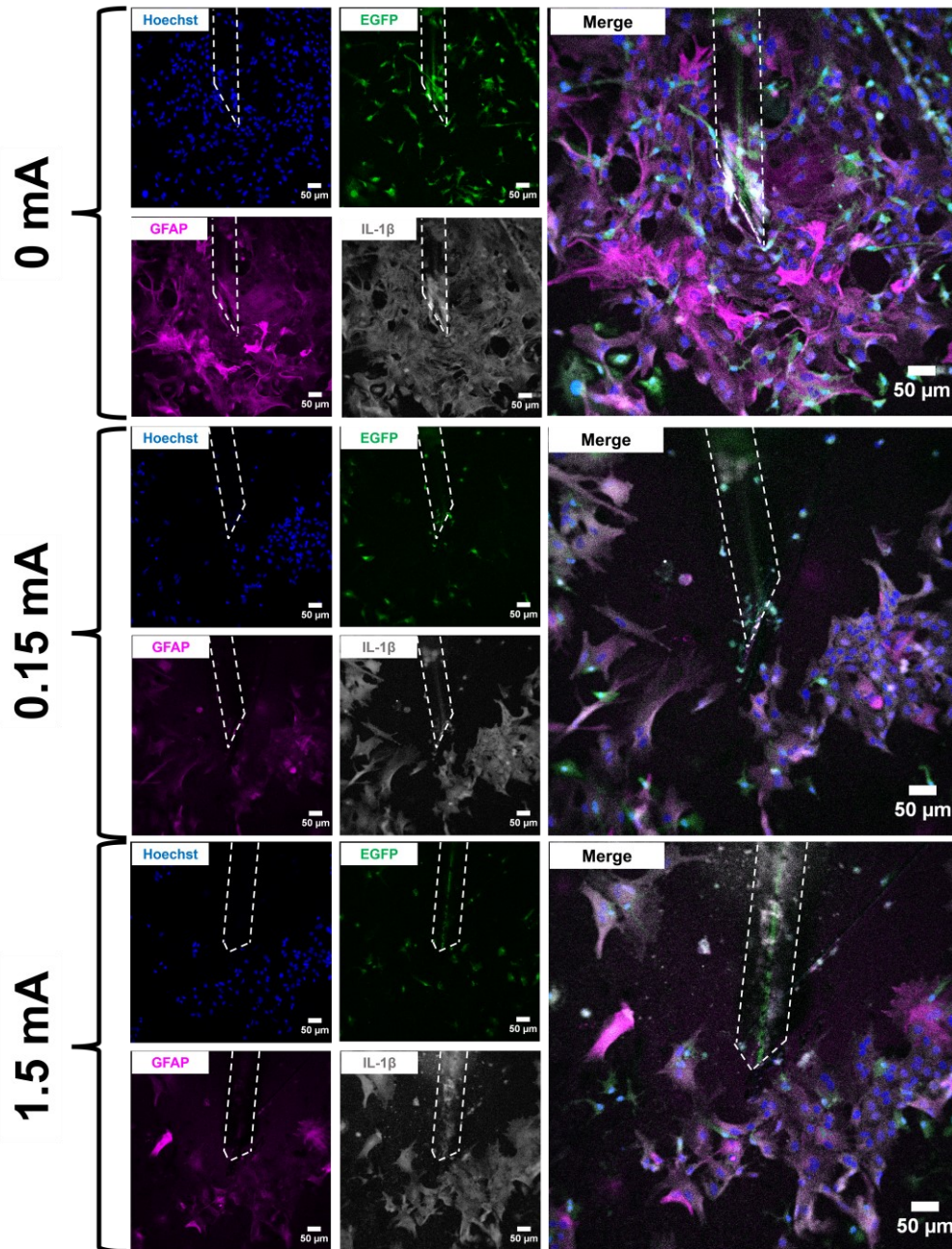


Figure 2-3: Immunofluorescent images of electrically stimulated mixed glial cell cultures at the electrode interface (4 h/day x 3 days).

Electrodes are marked by the white dashed outline in each image. Cell cultures were labelled with Hoechst 33342 (blue), EGFP (green), GFAP (magenta), and IL-1 β (grey). An enlarged merged channel overlay of each condition is shown on the far right. Scale bars: 50 μ m.

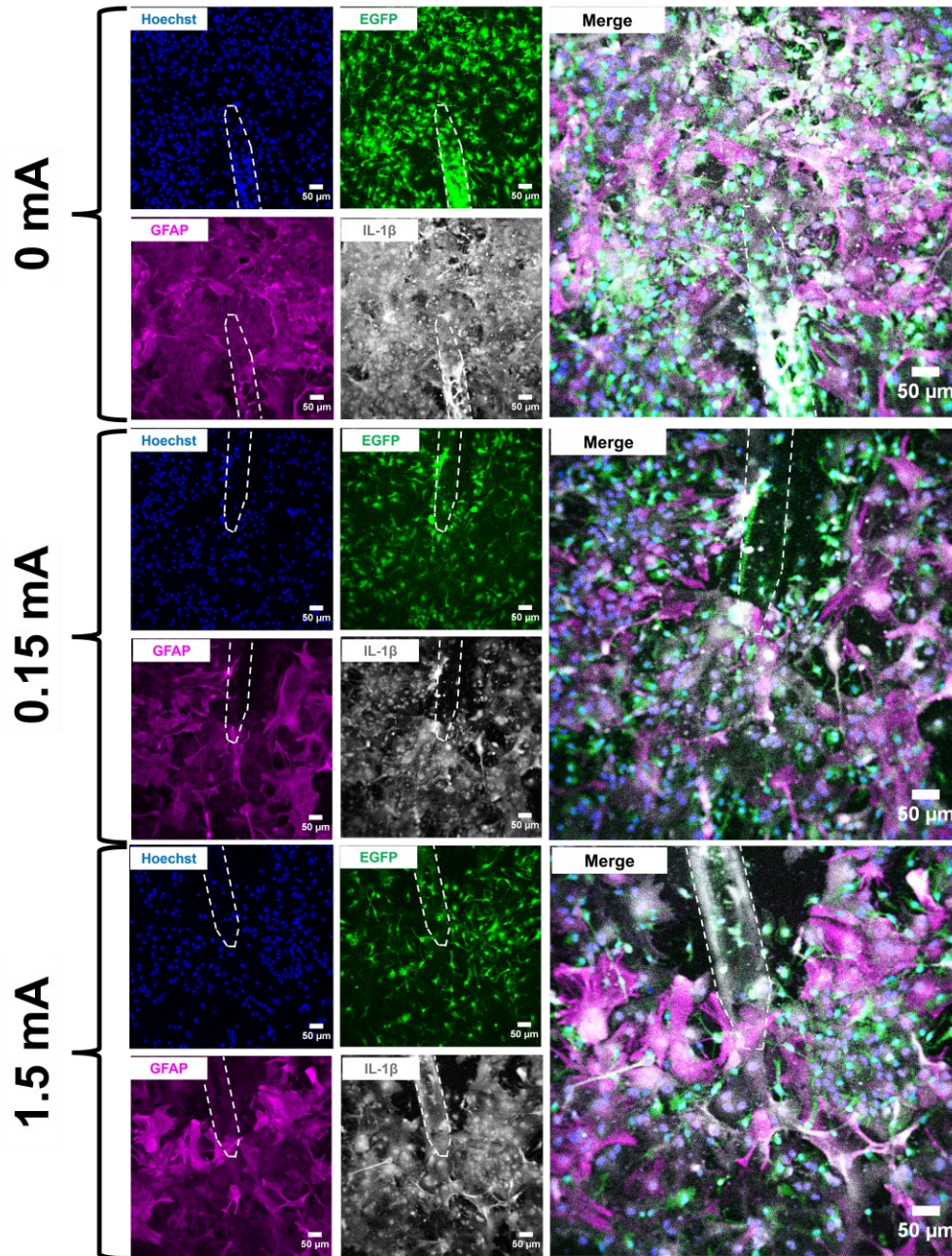


Figure 2-4: Immunofluorescent images of electrically stimulated mixed glial cell cultures at the electrode interface (4 h/day x 7 days).

Electrodes are marked by the white dashed outline in each image. Cell cultures were labelled with Hoechst 33342 (blue), EGFP (green), GFAP (magenta), and IL-1 β (grey). An enlarged merged channel overlay of each condition is shown on the far right. Scale bars: 50 μ m.

Fluorescence intensity, area coverage, and cell density analyses are shown in Figures 2-5, 2-6, and 2-7. At 1 day, a statistically significant effect was detected for IL-1 β area coverage (Figure 2-5). At 3 days, significant main effects were detected across all biomarkers with the exception of GFAP fluorescence intensity and EGFP area coverage. *Post hoc* analyses revealed significant differences between different distances from the electrode tip and stimulation amplitudes in Hoechst fluorescence intensity, IL-1 β fluorescence intensity, Hoechst area coverage, Hoechst cell density, GFAP area coverage, and IL-1 β area coverage (Figure 2-6). At 7 days, a main effect was detected for Hoechst fluorescence intensity, EGFP fluorescence intensity, and area coverage for all biomarkers analyzed. *Post hoc* analyses revealed significant differences for Hoechst fluorescence intensity and EGFP area coverage (Figure 2-7).

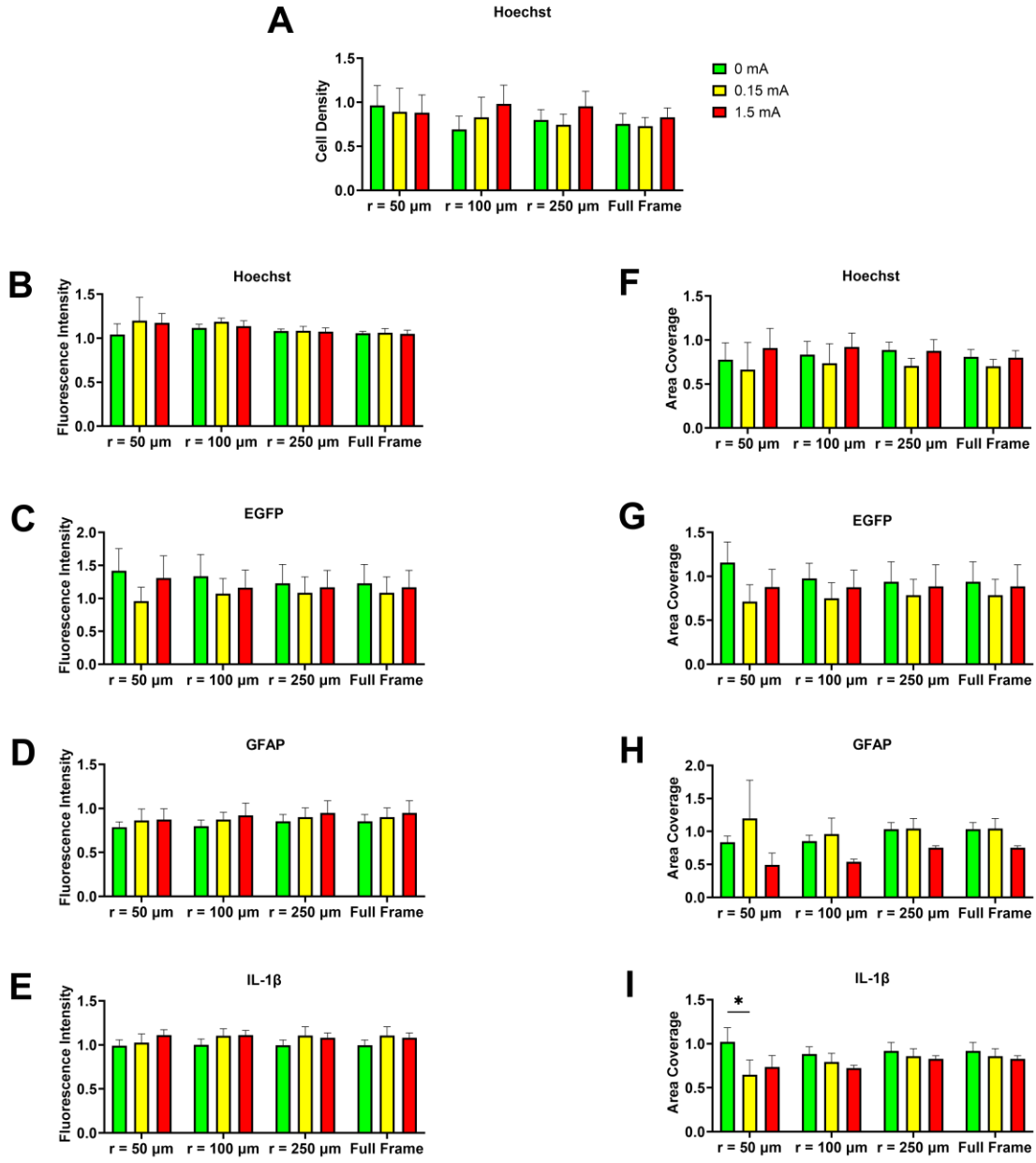


Figure 2-5: Quantitative analysis of 1-day stimulation images

(A) Cell density, (B, C, D, E) fluorescence intensity, and (F, G, H, I) area coverage profiles of immunofluorescent images as a function of electrical stimulation (4 h/day x 1 day) current and distance from the electrode tip. Values are expressed as fold change versus no-wire control cell cultures ($n = 6$, two-way ANOVA with Bonferroni *post hoc* test). * $p < 0.05$; Data = means \pm SEM.

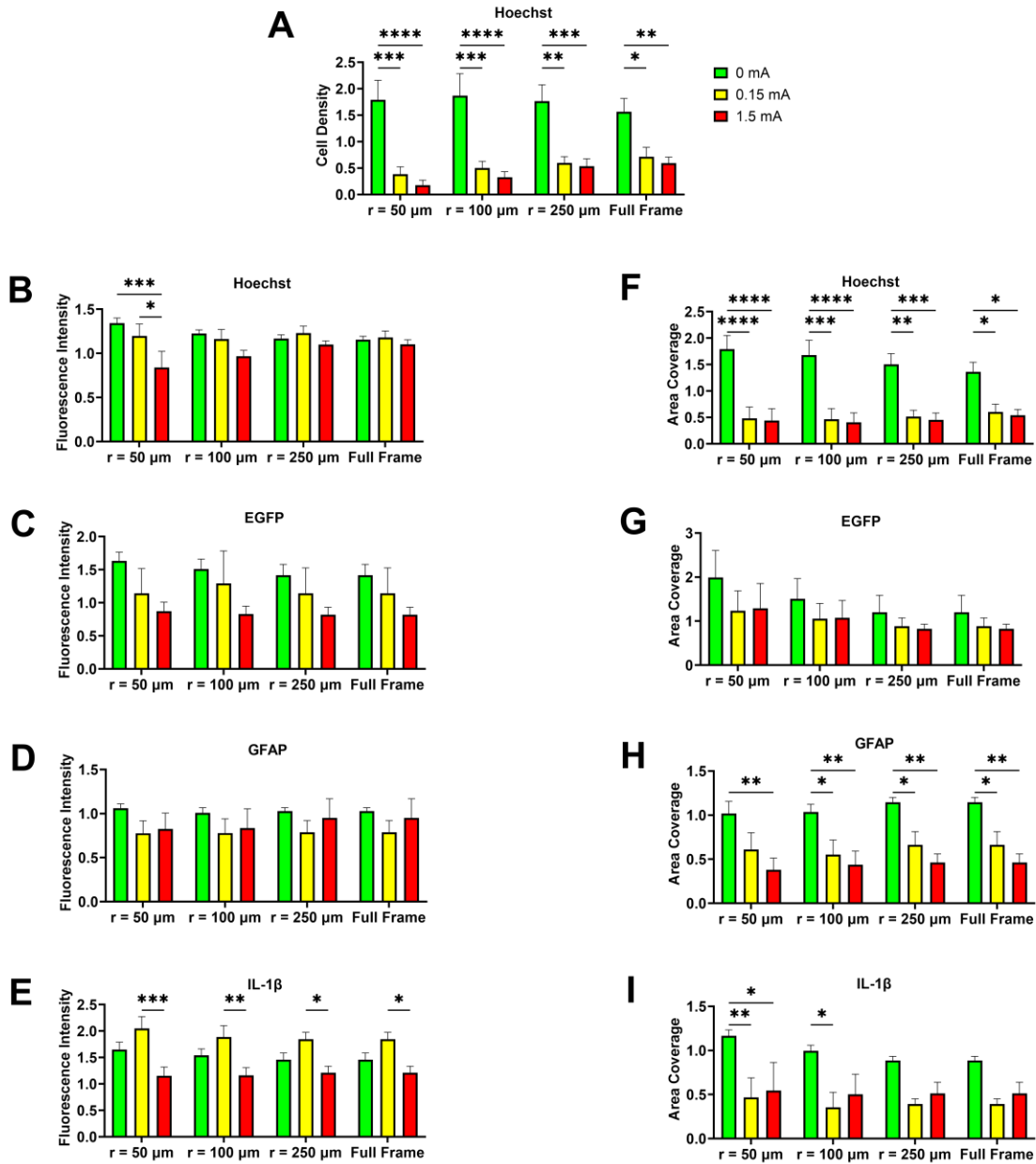


Figure 2-6: Quantitative analysis of 3-day stimulation images

(A) Cell density, (B, C, D, E) fluorescence intensity, and (F, G, H, I) area coverage profiles of immunofluorescent images as a function of electrical stimulation (4 h/day x 3 days) current and distance from the electrode tip. Values are expressed as fold change versus no-wire control cell cultures ($n = 6$, two-way ANOVA with Bonferroni *post hoc* test). * $p < 0.05$, ** $p < 0.01$, *** $p < 0.001$, **** $p < 0.0001$; Data = means \pm SEM.

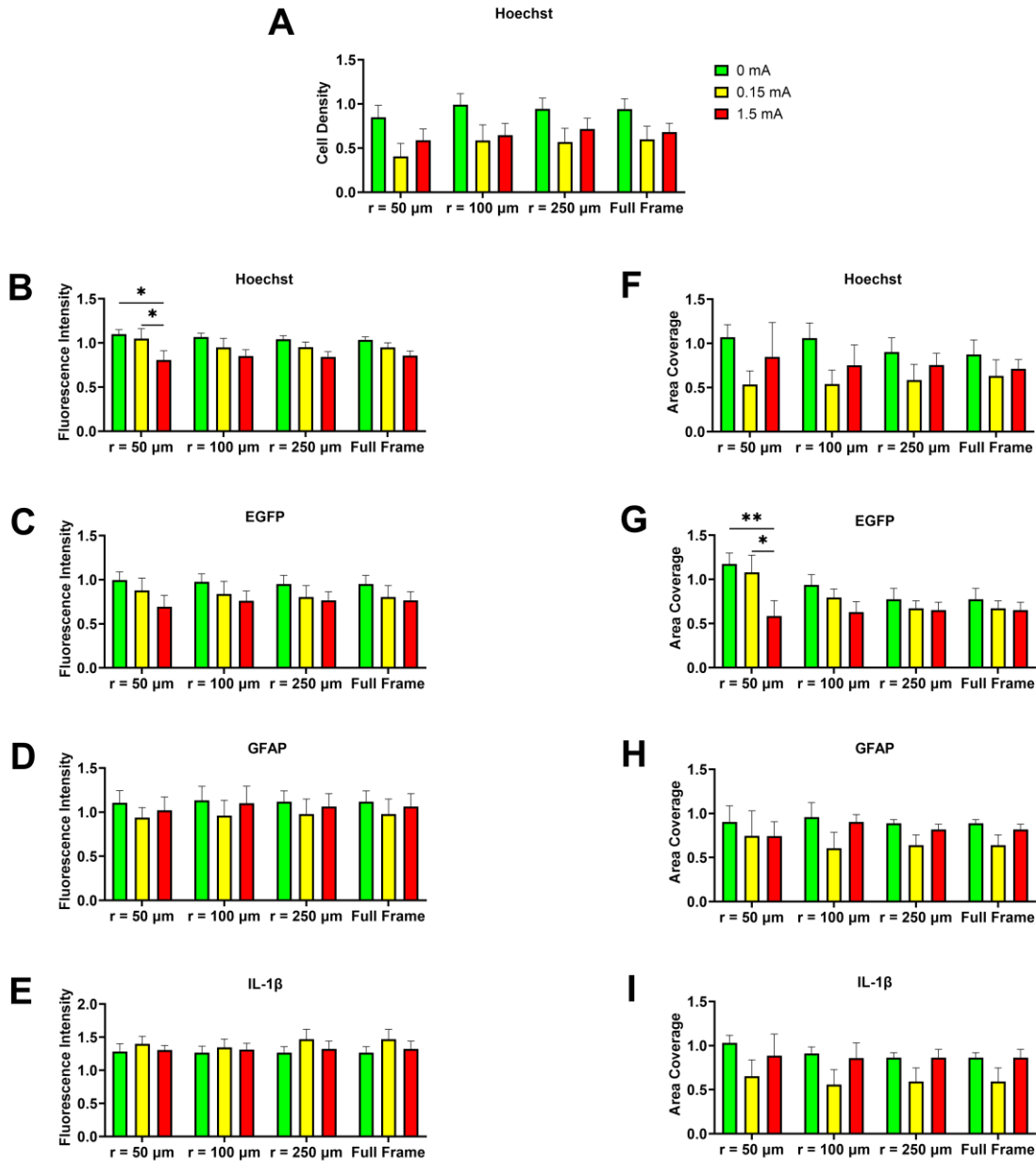


Figure 2-7: Quantitative analysis of 7-day stimulation images

(A) Cell density, (B, C, D, E) fluorescence intensity, and (F, G, H, I) area coverage profiles of immunofluorescent images as a function of electrical stimulation (4 h/day x 7 days) current and distance from the electrode tip. Values are expressed as fold change versus no-wire control cell cultures ($n = 6$, two-way ANOVA with Bonferroni *post hoc* test). * $p < 0.05$; Data = means \pm SEM.

2.5.2. Electrical stimulation-induced electrode damage

Following immunolabelling and confocal fluorescence microscopy, the electrodes were extracted from the cell culture wells and imaged on an SEM to qualitatively assess damage caused by the stimulation experiments (Figures 2-8, 2-9, 2-10). The SEM images at for the 0 mA electrodes (Figures 2-8A, 2-8D, 2-9A, 2-9D, 2-10A, 2-10D) are best described as having large amounts of non-conductive deposits on their surfaces. In the 0.15 mA electrodes (Figures 2-8B, 2-8E, 2-9B, 2-9E, 2-10B, 2-10E), lesser amounts of such deposits were seen, but the overall shape of the electrode was intact. At 1.5 mA, however, deformation of the entire deinsulated tip of the electrode was apparent with the surface appearing warped and crateriform (Figures 2-8C, 2-8F, 2-9C, 2-9F, 2-10C, 2-10F).

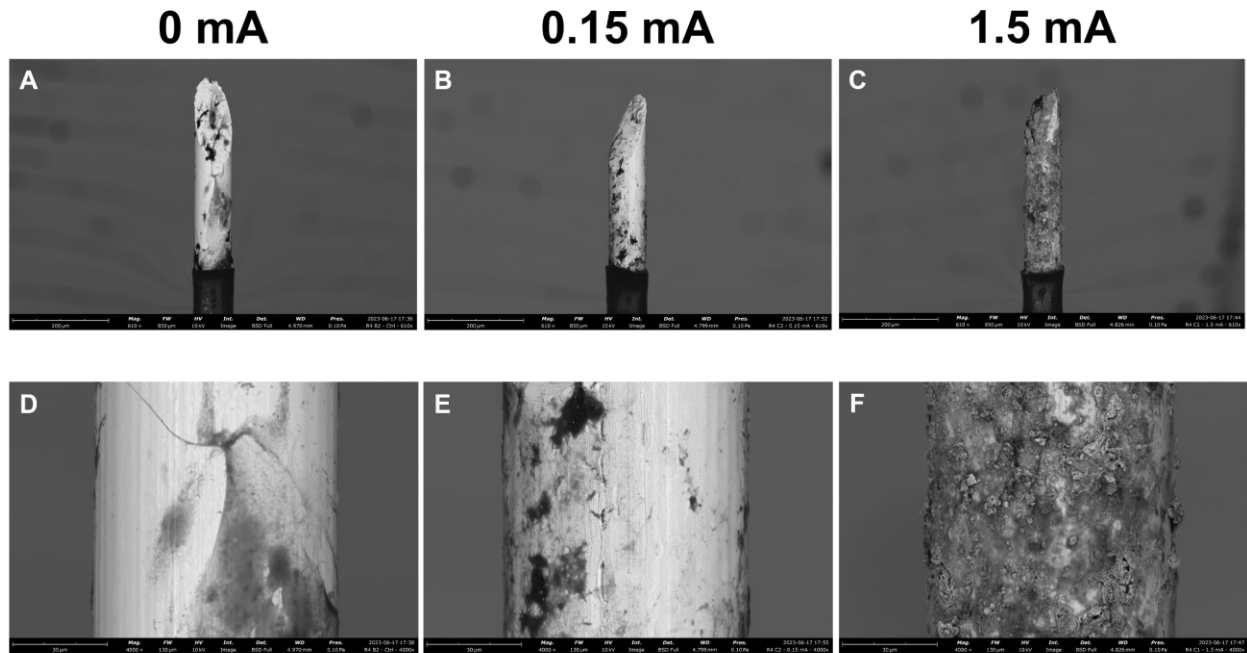


Figure 2-8: Scanning electron micrographs of electrodes following 1-day stimulation experiments

Stimulation amplitudes through the electrodes were 0 mA, 0.15 mA, and 1.5 mA. Images were acquired at 610x (A, B, C) and 4000x (D, E, F) magnification. Scale bars: 200 μm (610x), 30 μm (4000x).

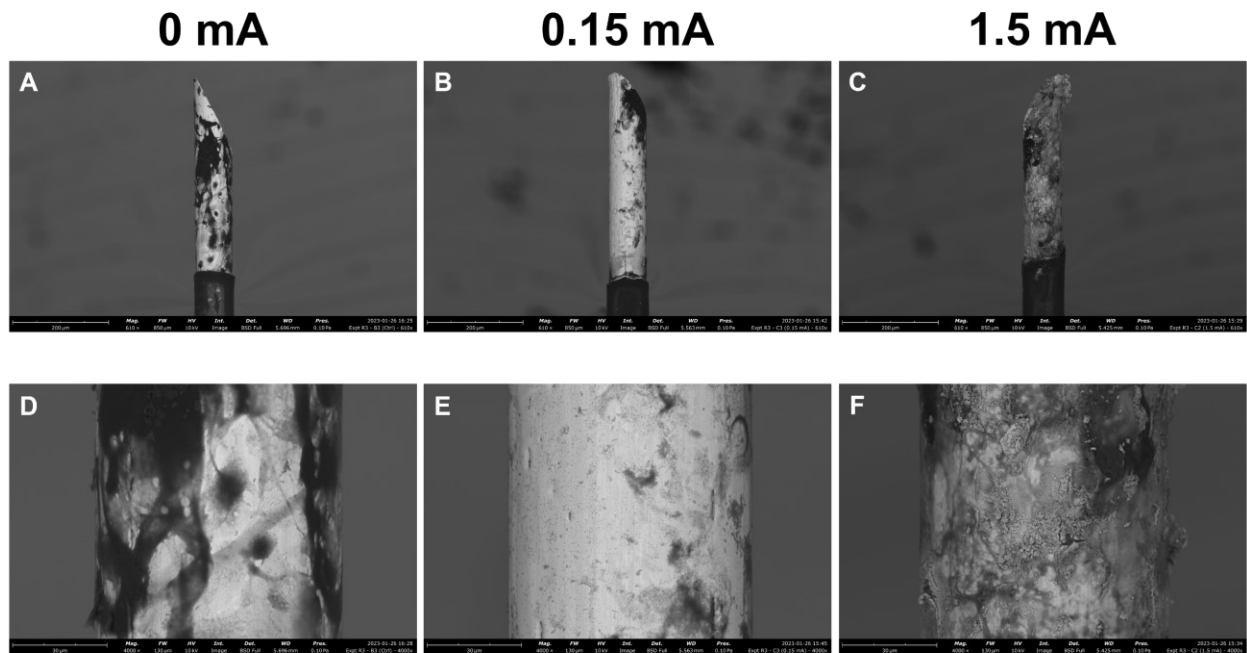


Figure 2-9: Scanning electron micrographs of electrodes following 3-day stimulation experiments

Stimulation amplitudes through the electrodes were 0 mA, 0.15 mA, and 1.5 mA. Images were acquired at 610x (A, B, C) and 4000x (D, E, F) magnification. Scale bars: 200 μm (610x), 30 μm (4000x).

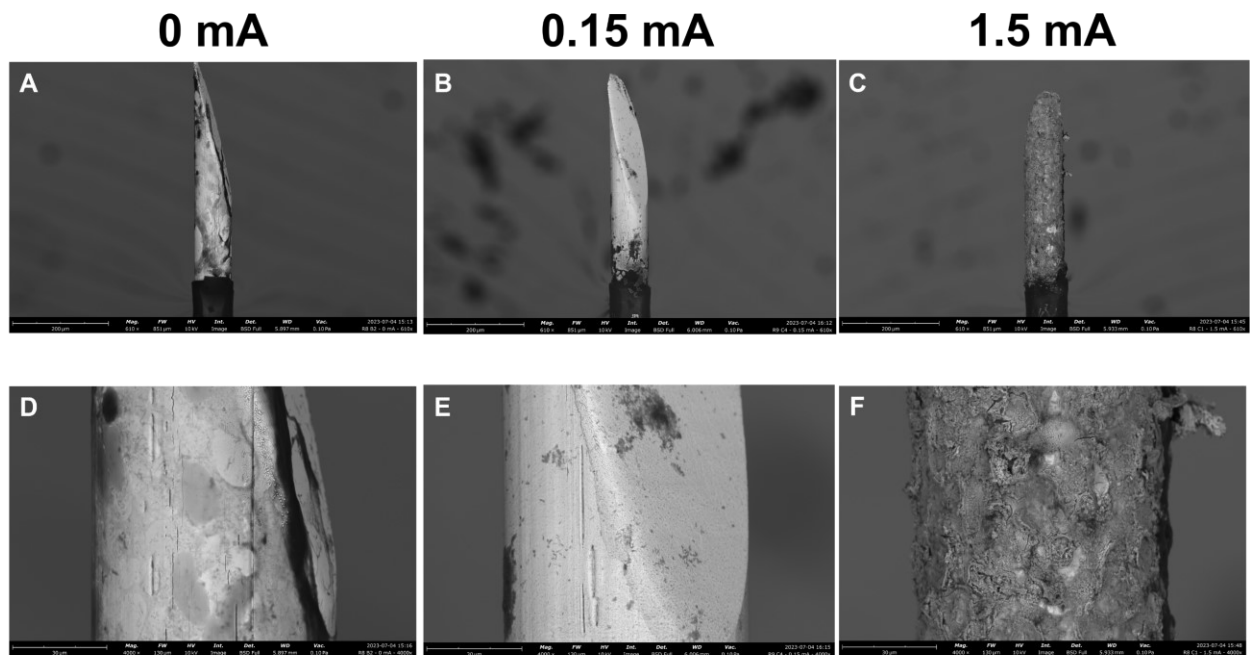


Figure 2-10: Scanning electron micrographs of electrodes following 7-day stimulation experiments

Stimulation amplitudes through the electrodes were 0 mA, 0.15 mA, and 1.5 mA. Images were acquired at 610x (A, B, C) and 4000x (D, E, F) magnification. Scale bars: 200 μm (610x), 30 μm (4000x).

In addition to SEM, EDS was used to quantify the elemental composition of the surfaces of the electrodes across the different experimental conditions (Figures 2-11, 2-12, 2-13). The most notable differences in composition were between the 0.15 mA and 1.5 mA conditions. At 1 day, a main effect was detected only for oxygen and platinum, with Tukey *post hoc* analysis calculating a significant difference as well for those elements (Figures 2-11A, 2-11G). Specifically, there was a significant difference detected between the 0 mA and 1.5 mA group for oxygen and between 0.15 mA and 1.5 mA for platinum. At 3 days, electrodes subjected to 1.5 mA of current had a much lower proportion of platinum at their surfaces compared to at 0.15 mA (Figure 2-12A). No significant differences were found across stimulation conditions for iridium (Figure 2-12B). Atomic concentrations of carbon across all conditions were similar (Figure 2-12E). No significant main effects were detected in the nitrogen group across the different stimulation conditions (Figure 2-12F). There was a statistically significant finding with oxygen (Figure 2-12G), with higher concentrations detected in the 1.5 mA condition versus the 0.15 mA condition. At 7 days, statistically significant differences were found for all elements examined except for chlorine. Specifically, differences were detected for platinum (Figure 2-13A, across all stimulation conditions), iridium (Figure 2-13B, 0.15 mA vs. 1.5 mA), sodium (Figure 2-13C, 0 mA vs. 1.5 mA), carbon (Figure 2-13E, 0 mA vs. 1.5 mA), nitrogen (Figure 2-13F, 0.15 mA vs. 1.5 mA), and oxygen (Figure 2-13G, 0 mA vs. 1.5 mA, 0.15 mA vs. 1.5 mA). Trace amounts of elemental sodium and chlorine found on the electrode samples were likely from the use of PBS, an aqueous salt solution, while the fixed cell cultures were in storage.

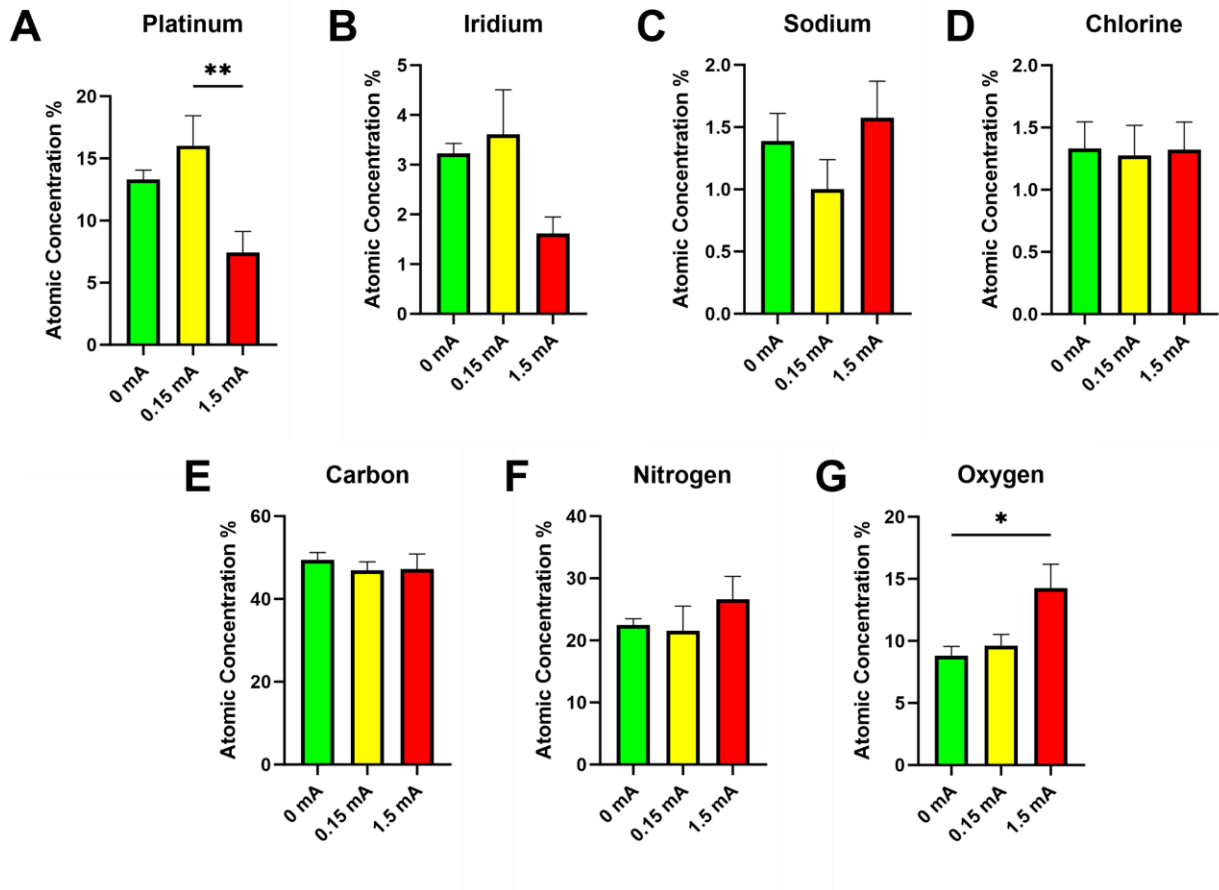


Figure 2-11: Energy-dispersive x-ray spectroscopy data (1-day stimulation)

Atomic concentrations of (A) platinum, (B) iridium, (C) sodium, (D) chlorine, (E) carbon, (F) nitrogen, and (G) oxygen on the surfaces of electrodes (n = 6, one-way ANOVA with Tukey's *post hoc* test). *p < 0.05, **p < 0.01; Data = means ± SEM.

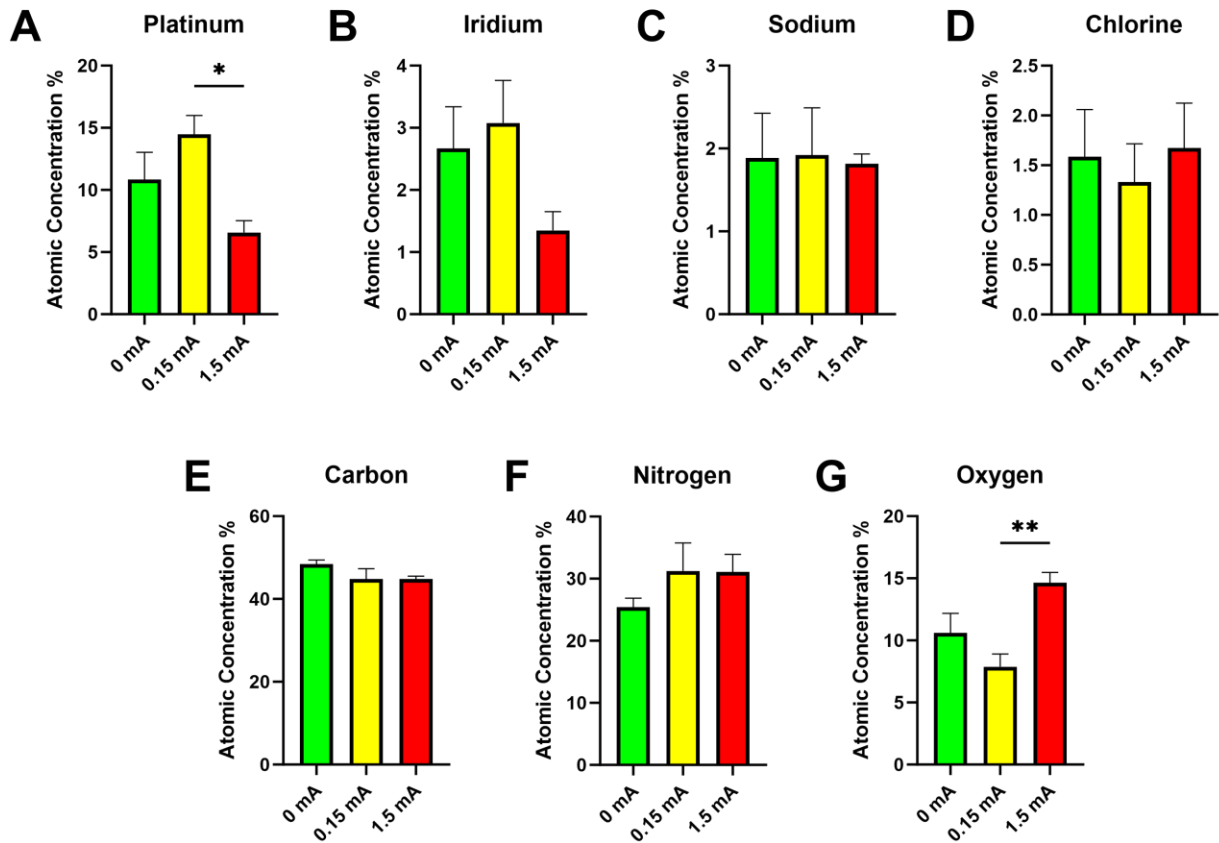


Figure 2-12: Energy-dispersive x-ray spectroscopy data (3-day stimulation)

Atomic concentrations of (A) platinum, (B) iridium, (C) sodium, (D) chlorine, (E) carbon, (F) nitrogen, and (G) oxygen on the surfaces of electrodes ($n = 6$, one-way ANOVA with Tukey's *post hoc* test). * $p < 0.05$, ** $p < 0.01$; Data = means \pm SEM.

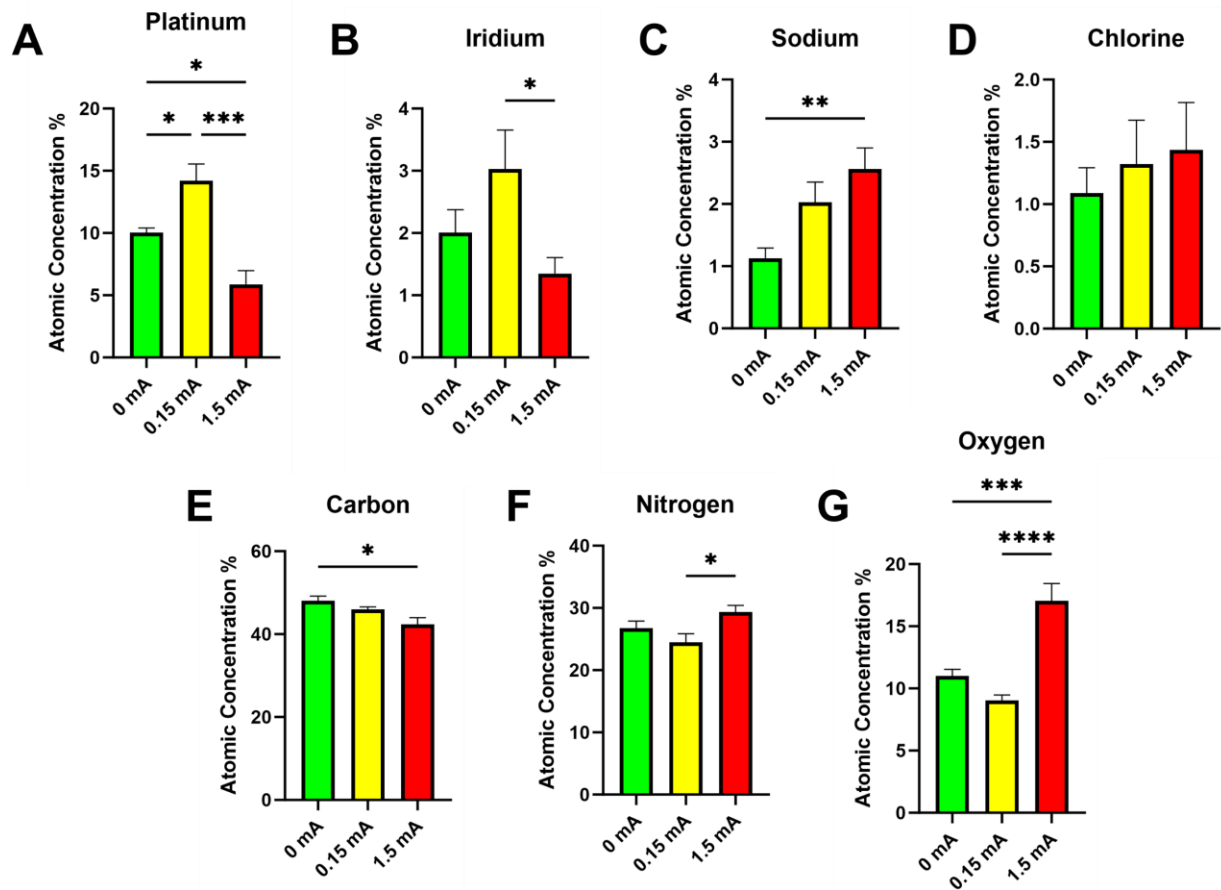


Figure 2-13: Energy-dispersive x-ray spectroscopy data (7-day stimulation)

Atomic concentrations of (A) platinum, (B) iridium, (C) sodium, (D) chlorine, (E) carbon, (F) nitrogen, and (G) oxygen on the surfaces of electrodes (n = 6, one-way ANOVA with Tukey's *post hoc* test). *p < 0.05, **p < 0.01, ***p < 0.001, ****p < 0.0001; Data = means ± SEM.

2.6. Discussion

The goal of this work was to examine the effects of electrical stimulation on mixed glial cell cultures at the interface of a microelectrode designed for invasive stimulation of central nervous tissue using imaging-based methods. We also aimed to replicate *in vitro* the foreign body response that is orchestrated by microglia and astrocytes – namely, the formation of a glial scar that has been observed *in vivo* [39,96,194,195]. Previous studies successfully used *in vitro* methods to demonstrate the glial cell response [40]. We present a refined system with the integration of electrical stimulation into the experimental model as well as a hybrid cell biology-engineering approach to assessing damage to both physiologically relevant primary cells and electrodes.

In our experiments, stimulation paradigms of differing currents (0.15 mA vs. 1.5 mA) were compared while keeping other factors, such as cell culture composition and microelectrode material and geometry, constant. In other words, the variable manipulated was the amount of electrical charge delivered through the electrode interface with every pulse. Biphasic electrical pulse paradigms are pervasive in invasive implants as they are designed to mitigate tissue damage by cycling electrical charge out of tissue through the use of a second phase of opposite polarity [196]. The low current of 0.15 mA was selected for this experiment as it is considered a safe, physiologically relevant current in *in vivo* experiments; it has been shown in previously published ISMS work, for example, that currents near or at this magnitude passed by microelectrodes of similar design to the ones in our study are capable of activating interneurons at the lumbar enlargement and eliciting load-bearing movements or other effective functions in animals [129,130,197–199]. In contrast, a current of 1.5 mA would not be appropriate for *in vivo* work using such microelectrodes. That amount of current would risk not only excessive

activation of the stimulated limbs, but also substantial damage to the stimulated tissue. The 1.5 mA amplitude was selected for this study as a means of inducing maximum damage to the cell cultures (i.e., a worst-case scenario).

Although the stimulation paradigms used in our experiments are adapted from previous *in vivo* ISMS work, the experimental platform and workflow presented have a wider reach. They can accommodate testing of additional stimulation parameters (e.g., pulse width, frequency, waveform shape) as well as different electrode materials, sizes, and geometries. Although such parameters can also be tested *in vivo*, an *in vitro* approach allows us to conduct these experiments with relatively higher throughput and with a reduced ethical footprint. Invasive electrical stimulation of nervous tissue has applications in treating a large breadth of diseases and injuries [200–202]; assessing electrical stimulation-induced damage on glial cells and finding ways in which to modulate glial cell response by modifying both implant and stimulation paradigm designs are thus valuable research goals for stimulation targets in the brain or spinal cord.

2.6.1. Fluorescence imaging analysis

In these experiments, it was of interest to determine glial cell reactivity through various image-based metrics including fluorescence intensity. Fluorescence intensity, a measure of the image-wide sum of the pixel intensity values for a biomarker divided by the area coverage of that biomarker, was calculated for each immunofluorescence image. As the method is dependent on labelling of molecules of interest in cells using fluorescent tags, the data acquired gives insight into whether certain biomarkers are upregulated or downregulated when exposed to stimuli.

Significant differences with Hoechst were detected up to 50 μm from the electrode at the 3-day and 7-day mark. These differences were not seen when analyzing Hoechst using the larger ROIs thus suggesting that electrical stimulation does have a localized effect on Hoechst expression in mixed glia (Figure 2-6B, 2-7B). No significant differences were detected in the EGFP and GFAP fluorescence intensity data as a function of either stimulation current or distance from the electrode across the timepoints measured (Figures 2-5C, 2-5D, 2-6C, 2-6D, 2-7C, 2-7D). However, the IL-1 β fluorescence intensity data at 3 days (Figure 2-6E) suggest that not only does electrical stimulation significantly downregulate IL-1 β production but that also this observation is detectable even when measuring the full image as opposed to a subset of it. Interestingly, this finding contrasts with the data from the 1-day and 7-day sets which saw no significant changes in IL-1 β production across different stimulation conditions and radii from the electrode tip. *In vivo* findings revealed that electrical stimulation did not lead to additional upregulation in inflammatory biomarkers in electrically stimulated animals compared to unstimulated animals [96]. However, it is worth noting that the levels of IL-1 β seen in 0 mA, 0.15 mA, and 1.5 mA seen are all above that of a control that we used where there was no wire. This suggests that the mere presence of the microelectrode in the cells is capable of eliciting upregulation of inflammatory biomarkers such as IL-1 β [203–206], but that additional stimulus in the form of electrical current does not induce further significant biomarker upregulation even at the interface. Such observations were also made in Bamford et al.'s study [96]. In that study, the encapsulation responses by reactive GFAP-positive astrocytes as well as inflammatory responses were attributed in large part to the insertion of the wires and not to subsequent repeated electrical stimulation. The current study draws inspiration from the stimulation paradigm and microelectrodes used in Bamford et al.'s study. IL-1 β is a documented pro-inflammatory

biomarker associated with neuroinflammation and is expressed by both microglia and astrocytes. Our study revealed differences in IL-1 β fluorescence intensity as a function of stimulation current up to the full size of the images measured – this supports evidence suggesting that IL-1 β is upregulated in astrocytes and microglia in a wide range of diseases and injuries [207–209]. The highest IL-1 β signals were seen in the 0.15 mA condition compared to the 1.5 mA condition – peri-electrode void formation at 1.5 mA likely explains the lower IL-1 β signal at that current. GFAP is a biomarker associated with the cytoskeleton of astrocytes; its upregulation is associated with astrocyte response to injury or disease [210–213]. However, in the current study, analyses of GFAP fluorescence intensity showed no significant differences between the different stimulation conditions and across the different distances from the electrode tip.

Immunofluorescence images were also acquired and measured for area coverage – the total geometric size of a biomarker’s signal across all cells present in the image’s field of view. From the images acquired of the cell cultures interacting with the electrodes (Figures 2-2, 2-3, 2-4), a large mass of both microglia and astrocytes were observed at and around the electrodes. More specifically, microglia in the 0 mA images have been seen in very close proximity to the surface of the electrode while larger concentrations of astrocytes were seen further afield from the electrode. This is in line with established knowledge on how glial scar formation occurs; specifically, microglia are known to migrate to a lesion or foreign body first and facilitate migration of astrocytes to the site of interest [214–219]. The two cell types then work together to cordon off the site from any nearby healthy tissue. *In vivo*, glial scarring takes place over the course of several weeks [220,221]. Given our experimental design and timecourse, we are only able to model an early response that is consistent with the glial scarring process and not the glial scar itself. When electrical stimulation is used, however, our image data suggest a localized

disruption of the aggregation of cell bodies around the electrode. The Hoechst area coverage data trends observed in this study vary across the different time points that were sampled. At 1 day, Hoechst expression did not change across stimulation conditions or distance from the electrode tip (Figure 2-5F). However, the data at 3 days suggest that electrical stimulation, even at a low current of 0.15 mA, significantly reduces mixed glia area coverage compared to the 0 mA condition even when the entirety of each image (734.05 μm x 734.05 μm) was measured (Figure 2-6F). The trend observed from this holds true even when calculating cell density from the Hoechst image data (Figure 2-6A). Although differences in Hoechst area coverage between stimulation conditions were also detected at 7 days (Figure 2-7F), such a difference was only found up to 50 μm from the electrode tip. Although no differences were detected in the EGFP area coverage data with respect to stimulation conditions or distance from electrode until the 7-day mark (Figure 2-7G), GFAP area coverage data suggests reduced area coverage with 0.15 mA and 1.5 mA conditions vs 0 mA even when the full frame of the image was measured (Figure 2-6H). This contrasts with the data presented for 1 day and 7 days (Figure 2-5H, 2-7H), which saw no differences in GFAP area coverage between any of the conditions analyzed. The IL-1 β area coverage data at 1 day and 3 days (Figure 2-5I, 2-6I) suggests a more localized effect, with significant differences between stimulation conditions detected up to a distance of 100 μm from the electrode tip – at 7 days, however, any differences seen between stimulation conditions disappear (Figure 2-7I). The gap devoid of cells (plus evidence of autofluorescent debris) observed from the immunofluorescent images was expected for the 1.5 mA stimulation amplitude as it was an extremely high current for the size of electrode that was used; however, it was not expected that this gap would also be present in the 0.15 mA case as this is a safer and more physiologically relevant stimulation amplitude that has been tolerated *in vivo* [96,199]. The

data suggest a trendwise decrease in area coverage with the 0.15 mA and 1.5 mA stimulation conditions compared to 0 mA – we believe the formation of the voids around the electrodes as a result of stimulation is reflected in this drop in area coverage. The observation that electrical stimulation reduces cell coverage at the interface presents two possible scenarios as to the fate of the cells that otherwise would have been at the interface: 1) the cells at the interface had died as a result of the electrical stimulation, or 2) the cells at the interface had migrated away from the interface as a result of the stimulation. While the methods described in this study do not allow us to determine if one or the other scenario occurred, follow-up live cell imaging experiments that take advantage of transgenic EGFP expression in the microglia will enable us to track cell movements and behaviour over a 4-hour stimulation time course at the electrode interface.

The temporal changes seen in the immunofluorescence data for this study are similar to what has been seen in *in vivo* work. In other injury models, microglia activation and astrocyte responses have been observed within hours and days of injury, with the scarring process unfolding over the course of many weeks. A neuroinflammation study by Xie et al. demonstrated that, *in vivo*, the scarring process can span upwards of 6 weeks, with GFAP expression diminishing over time in areas further away from a flexible polyimide microelectrode assembly implanted into cortical tissue [222]. In that study, Iba1-positive cells were not observed to have proliferated over the duration of the experiments. Additional surveys of the literature indeed suggest the glial encapsulation phenomenon to be a process that spans upwards of 12 weeks in the context of implanted neural electrodes [223]. In other contexts, such as stroke, it has been shown that GFAP expression in brain tissue exposed to intracerebral hemorrhage was elevated 7 days post-injury followed by a diminished signal at 21 days post-injury [224]. In another murine stroke model, temporal evaluation of IL-1 β expression in brain tissue showed that expression

was significantly higher than controls at 3 h post-injury, a decreased expression at 48 h post-injury, and again increased expression at 1 week post-injury [225]. In the context of SCI, microglia are activated and rapidly advance to the site of injury within hours to days. The glial scar in this context has been reported to consist of a high density of glial cells and extracellular matrix material at the 2-week mark following injury [226]. Other reports suggest that, in the acute phase of SCI, reactive astrocytes migrate to the site of injury around 7 to 14 days post-injury and facilitate a substantial secretion of scar-related extracellular matrix material (e.g., chondroitin sulfate proteoglycans - CSPGs) [227]. Although spatial and temporal dynamics of glial cell reactivity and scar formation differ depending on the context of injury (stroke, SCI, neural implant insertion, etc.), a common feature of all these injuries is the ability of glial cells to mobilize to the site of injury and undergo actions such as cytokine release. Such activities may exacerbate, attenuate, or oscillate over the course of a few days as shown *in vivo* – the immunofluorescence analysis of the biomarkers in the current study have also demonstrated primary glial cells' capacity to respond in such manners, within days, to electrically stimulating microelectrodes in an *in vitro* environment.

2.6.2. SEM Analysis

In addition to assessing and quantifying damage to the mixed glial cell cultures as a result of electrical stimulation, we sought to assess electrical stimulation-induced damage to the electrodes themselves. This was done using scanning electron microscopy, which enables close inspection of a material's microstructure. The non-conductive deposits seen in abundance on the 0 mA electrodes (Figures 2-8A, 2-8D, 2-9A, 2-9D, 2-10A, 2-10D) are likely residual organic

matter (i.e., cells) that were attached to the surfaces of these electrodes. The images for this condition support the findings from the immunofluorescence images of the 0 mA condition, and reinforce the idea that the glial cells congregate at and around the electrode as part of a foreign body response [40,228,229]. Electrical stimulation at 0.15 mA (Figures 2-8B, 2-8E, 2-9B, 2-9E, 2-10B, 2-10E) resulted in less of these organic deposits covering the surface of the electrode, but the current was otherwise not intense enough to cause deformation and warping of the material at the surface. Applying an extreme current of 1.5 mA, on the other hand, caused visible deformation and corrosion of the electrodes (Figures 2-8C, 2-8F, 2-9C, 2-9F, 2-10C, 2-10F). With this comes a change in the surface material composition and geometric surface area of the electrodes [138,145,150,230–232] – such a change at even just 4 hours of usage would of course suggest that 1.5 mA is an inappropriate level of current to be passed through these microelectrodes.

2.6.3. EDS Analysis

In assessing electrical stimulation-induced damage to the electrodes following experiments, energy-dispersive x-ray spectroscopy was also available for use on the scanning electron microscope. This was done alongside the SEM work outlined in the preceding section. The EDS, which measures elemental composition of the surface of the material, provides information regarding the types of deposits on the surface of the electrode as well as potential reaction byproducts arising from electrochemical reactions. A higher proportion of oxygen (and lower proportion of platinum) seen for the 1.5 mA electrodes across all time points was likely due to an increase in irreversible oxidation induced by such a high current (Figures 2-11A, 2-

11G, 2-12A, 2-12G, 2-13A, 2-13G) [138]. No differences in levels of these elements were detected between the 0 mA and 0.15 mA conditions until the 7-day mark, thus suggesting that any redox reactions that occurred at the interface were reversible and that continued, repeated, usage of the electrodes eventually would result in a higher susceptibility to oxidation. Iridium followed a similar trend compared to platinum (Figures 2-11B, 2-12B, 2-13B); however, a statistically significant drop in atomic concentration was not detected until the 7-day mark. A higher proportion of carbon was expected from the 0 mA electrodes compared to the other conditions as suggested by the non-conductive organic deposits seen from the SEM images. Cells and extracellular matrices are primarily comprised of carbon compounds hence our hypothesis that the 0 mA electrodes would have a higher carbon content [233,234]. The high atomic carbon readings across all conditions tested (Figures 2-11E, 2-12E) were thus contrary to what we had expected. However, the high readings of carbon across all electrodes examined was possibly the result of the cell cultures, electrodes included, being subjected to the same types and concentrations of organic compounds in the fixation and immunolabelling processes (e.g., formalin, ES, antibodies) – to preserve the integrity of the cell cultures following experiments, our electrodes were extracted only after the immunolabelling and fluorescence microscopy steps.

2.6.4. Charge injection as a damage mechanism

Also of interest to us are the potential mechanisms of damage inflicted upon cells as a result of electrical stimulation. Irreversible redox reactions, as previously mentioned, could potentially lead to leaching of cytotoxic byproducts into the cell culture media and have an adverse effect on nearby glial cells [138]. The amount of electrical charge delivered in a pulse is

a function of stimulation amplitude and pulse width, and would also have an effect on cellular response. The charge injection capacity for Pt-Ir electrodes has previously been quoted to be in the range of 50–150 $\mu\text{C}\cdot\text{cm}^{-2}\cdot\text{ph}^{-1}$ [235]. Factoring in the geometric surface area of the deinsulated portion of our Pt-Ir microelectrodes (approximately 89 000 μm^2) suggests that supplying a current of 1.5 mA will far exceed this charge injection capacity range, while a current of 0.15 mA (approximately 33.7 $\mu\text{C}\cdot\text{cm}^{-2}\cdot\text{ph}^{-1}$) will not. Charge density is an important parameter to calculate when designing neural electrodes as the size and material of electrodes affect design safety limits [138,236,237]. Other previous reports document using stimulating electrodes at varying charge densities across different materials (e.g., platinum, iridium oxide, platinum-iridium, stainless steel, PEDOT/polypyrrole nanotubes) [238–242] – comparisons made in these works highlight the significance of material selection in electrode design as well as the differences seen in terms of charge injection, development of toxic byproducts, and tissue damage. In McCreery et al.’s work, circular platinum disk electrodes of varying sizes (0.01 – 0.1 cm^2) were subjected to charge injection of 1 μC (i.e., charge densities ranging between 10 - 100 $\mu\text{C}\cdot\text{cm}^{-2}\cdot\text{ph}^{-1}$) with the goal of confirming and studying the effects of electrode size and charge density on neuronal injury [236]. In the same study, penetrating microelectrodes ($6.5 \pm 3 \times 10^5$ cm^2) were injected with current resulting in a geometric charge density of 800 $\mu\text{C}\cdot\text{cm}^{-2}\cdot\text{ph}^{-1}$ – although this was beyond the referenced safe range quoted in Rose and Robblee, it was also mentioned in the study that the microelectrodes were subjected to potentiodynamic cycling to increase charge capacity and reduce electrode dissolution [236]. Charge injection into tissue, or in this case cell cultures, is intended to elicit action potentials in neurons. In the case of glia, it is possible that even biphasic charge injection can cause charge imbalances along the membranes of cells. This in turn may trigger activation of glial ion channels, voltage-gated or otherwise, in

an effort to restore perturbed membrane potentials back to their resting values [23,243]. Doing so may also cause cells to become damaged through changes in tonicity [244]. Characterizing the microelectrode's capabilities with regards to impedance, charge storage capacity, and charge injection limit are important to better understanding some of the mechanisms behind the sorts of electrochemical phenomena that take place at the electrode-cell culture interface as well as the limits to which the electrodes can be stimulated before corrosion occurs [138,145].

2.6.5. Limitations of study

The current study uses primary mixed glial cell cultures as a way of exclusively studying glial cell response to electrode presence and electrical stimulation. This reductionist approach to controlling for variability brought on by other factors also means that there is a limit to how much this *in vitro* model is representative of *in vivo* physiology. Although neurons were not included in the cell culture model, Bamford et al. did note that a local (but statistically insignificant) increase in NeuN in their electrically stimulated animals [96]. Other structures, such as the blood-brain barrier, were also not modelled in the current study. *In vitro* cell density is also less compared to *in vivo*. In our experimental design, routine refreshes of cell culture media and a finite space for cell cultures to grow in prevented us from examining longer term (e.g., 30 day) effects that could otherwise be done in animals or other cell culture models [245–247]. A seeding density of 70000 cells/well was selected to provide a confluent amount of cells in the centre of each cell culture well at the time of the start of the experiment. The space in each well that was available for cell culture (0.79 cm²) was much smaller than the total surface area of the well itself (4.15 cm²) due to the presence of the PDMS ring (Figure 2-1). In our design there

was therefore limited space available for cell culture in each well thus limiting potential culture time prior to passaging or fixation. Furthermore, the electrodes were inserted into the plates first before cell seeding took place (i.e., a stab wound scenario was not captured in the experiments). When inserting the PDMS rings and electrodes into the 12-well plates, they were first sterilized in 70% ethanol as such work takes place in a biosafety cabinet. Previous trial work we conducted saw cell death from potential residual ethanol as well as the PDMS rings sitting on top of cells that would have already been seeded in the plate. For this reason we elected to embed the PDMS rings and electrodes in the plates first before cell seeding.

Despite the limitations of conducting *in vitro* studies as described above, the *in vitro* results reported herein agree well with results reported from previous *in vivo* studies - although inflammatory responses were observed in response to the presence of the electrodes themselves, applied electrical stimulation does not induce additional upregulation of biomarkers associated with a pro-inflammatory state. Specifically, in Bamford et al.'s study consistent applied electrical stimulation (48 nC/phase, 25 pulses per second) over a 30 day timespan induced no further damage in rat spinal cords than was found in unstimulated rats. This may also mean that astrocytes are more responsive to other cells' reactions to electrical stimulation than react directly to the electrical stimulation itself [248,249].

2.7. Conclusions

The experiments in the present work investigated the effects of electrical stimulation on mixed glial cell populations at the interface of Pt-Ir microelectrodes. An *in vitro* setup was used to evaluate the responses of primary mouse glial cells in a high-throughput setup that is designed

to inform the design of *in vivo* experiments. The cellular responses to both the presence of the electrodes as well as applied electrical stimulation were captured.

The data presented herein suggest a large aggregation of microglia and astrocytes at the electrode interface, which is reminiscent of a foreign body response observed *in vivo*. When electrical stimulation is factored in, a lower density of cells at and around the electrode interface was observed. A previous *in vivo* study reported comparable findings in rats - although inflammatory biomarkers were upregulated in electrically stimulated animals, this was attributed to the initial insertion of the electrodes into tissue and cell reactivity to the electrode itself as opposed to reactivity from consistently applied stimulation over a maximum of 30 days [96]. Analysis of the fluorescence image data collected revealed differences in biomarker fluorescence intensity and area coverage as a function of both stimulation current intensity as well as distance from the electrode tip – taken together, this suggests that electrical stimulation of mixed glia induces localized responses around the electrode tip to varying degrees. *In vitro*, the microglia and astrocytes may be either dying as a result of electrical stimulation or retreating away from the vicinity of the electrode. Live cell imaging using transgenic cells expressing EGFP can determine the fate of glial cells at the electrode interface as a result of different electrical stimulation paradigms in future experiments.

Varying stimulation parameters such as current, pulse width, frequency, and waveform pattern (e.g., rectangular, sinusoidal, ramped) can be readily investigated using the experimental approach developed in this work (Chapter 3). Furthermore, additional data analysis such as microglia-astrocyte ratio changes, up- or down-regulation of other cytokines, etc. would greatly benefit from these proposed experiments examining the impact of various parameters. The types of electrochemical reactions at the interface as a result of varying stimulation parameters and

factors such as electrode material composition, electrode geometry, and cell culture media, can also be determined (Chapter 4).

The results generated from this work are intended to better inform device developers of neural interfaces of the biocompatibility and safety of invasive neural implants, allowing these devices to last longer and function more effectively in persons experiencing neurological disease or injury.

3. Chapter 3 – Microelectrode stimulation parameter modifications elicit differential glial cell responses over a short 4-hour timecourse

3.1. Preface

The work presented in this chapter would not have been possible without the assistance of Anna DeCorby (BSc. Hons. Neuroscience Student 2020-21), and Matthew Birtle (BSc. Hons. Neuroscience Student 2022-23). AD had contributed to the development of the live-imaging protocol used for the EGFP-positive microglia in this study, and also generated preliminary live-imaging data (current modification between 0.5 and 1.5 mA) as part of her NEURO 498 thesis project. MB had further contributed to the lab's live-imaging program by generating preliminary data for the waveform modification work as part of his NEURO 498 thesis project. No data gathered by either AD or MB were used in any of the figures presented in this chapter. Christopher Tsui designed and performed the experiments described in this chapter, generated ImageJ code to process and compile the live-imaging and immunolabeled image data, and wrote the contents of this chapter in its entirety.

3.2. Abstract

In the previous chapter, a cell culture model to assess glial cell responses to electrically stimulating microelectrodes was developed. Using that model, glial cell responses to functional stimulating platinum-iridium microelectrodes were captured and quantified. The experiments described in Chapter 3 measure glial cell responses to various modified stimulation paradigms,

and further highlight the importance of electrical stimulation considerations when designing a biocompatible neural interfacing device. The formation of peri-electrode voids around the immediate vicinity of stimulating 75 μm diameter platinum-iridium microelectrodes also prompted an investigation into the fate of cells that would have once populated that area. Live imaging experiments were designed where EGFP-positive microglia from heterozygous CX3CR-1^{+EGFP} mice were imaged over a 4-hour timecourse. The resulting live-imaging animations showed necrotic microglial cell death around the electrodes as a result of biphasic, charge-balanced, cathodic-first stimulation. The degree to which this was occurring was further analyzed by electrically stimulating mixed glia for 4 hours with modified parameters by current (0.1-0.4 mA), waveform shape (rectangular vs. sinusoidal vs. ramped), and frequency (25-55 Hz); live imaging was performed in addition to post-fixation immunolabelling to draw conclusions for each modification study. Current modification experiments predictably suggested that higher currents resulted in more biomarker signal loss around the electrode interface and thus cell death. Waveform shape modifications suggested that sinusoidal waveforms resulted in less cell death than the other waveform shapes tested. Frequency modifications suggested that, although increasing frequency from 25 Hz to 45 Hz resulted in more signal loss/cell death, the lesser amount of signal loss seen at 55 Hz does not follow this trend. Scanning electron microscopy and energy-dispersive x-ray spectroscopy of the electrode surfaces post-stimulation did not reveal any significant damage or changes to surface elemental composition. The results presented in this study highlight the impact that electrical stimulation parameters have on glial cell fate at the electrode-cell culture interface, and provide data towards potential refinement of stimulation paradigms used in functional electrical stimulation applications.

3.3. Introduction

Neural interfacing devices are designed to treat neurological injuries or disease, often through the use of an invasive implant (e.g., microelectrodes) [250–255]. The use of microelectrodes, while effective in acutely targeting a site of interest, also elicits a foreign body response from glial cells. Glia are the group of cells in the central nervous system that regulates its overall function, homeostasis, and fate [256–259]. The established literature extensively documents the foreign body response against electrode implants; microglia and astrocytes work together to cordon off the site of the implant from the surrounding tissue to limit the spread of cell death and damage caused by both insertion and otherwise presence of the implant in the tissue [68,194,260,261]. This is done through the formation of a glial scar, a fibrous assembly made primarily of microglia and astrocytes that encapsulates the implant. However, this is disadvantageous in that the fibrous scar prevents effective communication between the electrode implant and any nearby neurons – as neural electrodes are designed to send or receive electrical signal from nearby neurons, instances of glial scar formation left unchecked risk device failure over weeks to months [195].

The risk that glial scarring poses to the overall functionality and efficacy of neural electrode implants has thus motivated researchers to devise strategies to mitigate the effects of glial scarring (and by extension glial cell reactivity) with the overall goal to facilitate effective communication between electrodes and nearby neurons. Many innovative tissue engineering strategies have emerged, especially over the past decade, to attenuate glial cell reactivity to microelectrode implants. Many reports suggest using bioactive molecules conjugated onto the surface of the microelectrodes to ‘mask’ its foreign signature [262–267], the use of anti-

inflammatory compounds to mitigate neuroinflammation [268–272], and more mechanically compliant materials to reduce the stiffness mismatch between electrodes and much softer CNS tissue [273–278]. The vast majority of the reports focus on glial cell reactivity against the microelectrodes themselves – however, there exists a gap in the literature regarding the effects of electrical stimulation paradigms on glial cell behaviour. There are limited reports on the effects of electrical field modulation on the behaviour of glial cell lines [112,113,127]. By investigating such effects, neural interface device developers will be better informed of more of the factors at play that influence the biocompatibility and longevity of electrode devices.

The previous chapter addressed the motivation for investigating the influence of electrical stimulation on glial cell by describing a high-throughput *in vitro* cell culture system that models the early onset of glial scarring as it pertains to functional microelectrode implants. Microelectrodes (75 μm diameter) were fabricated, threaded through custom-made PDMS rings, and placed in 12-well culture plates that were then connected to a stimulator. Mixed glial cell cultures harvested from P2 heterozygous CX3CR-1^{+EGFP} mice were stimulated over 1, 3, and 7 days with currents of 0 mA, 0.15 mA, and 1.5 mA to demonstrate the fundamental feasibility of comparing glial cell response using the methods employed in the study, namely primary cell culture, immunofluorescent image analysis, scanning electron microscopy, and energy-dispersive x-ray spectroscopy. The data collected in the previous chapter suggest a significant difference in glial cell responses through biomarker (Hoechst, EGFP, GFAP, IL-1 β) expression. Statistically significant differences were found in biomarker expression profiles in response to the different current amplitudes applied across the different timepoints. Furthermore, biomarkers were analyzed according to fluorescence intensity, cell count, and geometric area coverage at

prescribed distances from the deinsulated tip of the microelectrodes – zonal analysis revealed that with the stimulation currents used there were different areas of effect on each biomarker.

A key observation made from the results of the previous chapter is that a peri-electrode void was formed from electrically stimulating the cell cultures – this was most prominent in the 1.5 mA condition. It was then of interest to determine whether the glial cells that had once occupied the spaces closer to the electrode interface had died, or had retreated away from the interface when stimulation current was applied. To further investigate the fate of these cells, we leveraged the transgenic mouse species that were used in the previous chapter – specifically, C57BL/6J mice that have been genetically modified to express enhanced green fluorescent protein (EGFP) under the CX3CR1 promoter gene [153]. This allows for the live imaging of microglia in the cell cultures without the use of immunolabelling procedures. By imaging the microglia situated at the electrode interface and applying electrical stimulation, the question of the fate of the cells near the electrode when stimulation is applied is answered.

In addition to determining the fate of the microglia through live cell imaging, another goal of the work presented in this chapter was to further build on the foundation that the work in the previous chapter laid out by exploring the effects of other electrical stimulation parameters on glial cell behaviour and reactivity. It is therefore of interest to more closely explore the effects of lower, more physiologically relevant stimulation current [279–283], stimulation waveform shape [143,157,284], and stimulation frequency [285,286]. By employing the methods used in the previous chapter as well as live imaging of EGFP-positive microglia, a more acute examination of the fate of the glial cells at the interface can be undertaken.

3.4. Materials and methods

3.4.1. Materials

Dulbecco's Modified Eagle Medium: Nutrient Mixture F12 (DMEM F12), Hank's Balanced Salt Solution (HBSS), fetal bovine serum (FBS), penicillin streptomycin (PS), 0.25% trypsin-ethylenediaminetetraacetic acid (Trypsin-EDTA), and Equine Serum (ES) were purchased from Gibco (Life Technologies, Burlington, ON, Canada). Poly-L-lysine hydrobromide (PLL) was purchased from Sigma Aldrich (St. Louis, MO, USA). Polystyrene 12-well cell culture plates were purchased from Greiner Bio-One (Frickenhausen, Germany). Cell culture flasks (75 cm²) were purchased from Corning (Corning, NY, USA). Sylgard 184 polydimethyl siloxane (PDMS) kit was purchased from Dow Chemical (Midland, MI, USA).

Rabbit anti-IL-1 β (Invitrogen, Burlington, ON, Canada) and chicken anti-GFAP (Abcam, Toronto, ON, Canada) primary antibodies were used. Donkey anti-rabbit Alexa Fluor 647 (Invitrogen) and goat anti-chicken Alexa Fluor 546 (Invitrogen) secondary antibodies were used. Hoechst 33342, a nuclear stain, was purchased from Molecular Probes (Life Technologies, Burlington, ON, Canada).

Microwires (75 μ m in diameter, Pt-Ir 80%/20% insulated with polyimide) for microelectrode fabrication were purchased from California Fine Wire (Grover Beach, CA, USA). Teflon-insulated, 9-strand stainless steel wires (Cooner AS632) were purchased from Cooner Wire Company (Chatsworth, CA, USA).

3.4.2. Cell culture preparation

Animal protocols were approved by the Animal Care and Use Committee at the University of Alberta and conducted in accordance with the guidelines of the Canadian Council for Animal Care. Mixed glial cell cultures were generated from the brain tissue of postnatal Day 2 C57BL/6J CX3CR-1^{+EGFP} heterozygous transgenic mice [188]. The mice were decapitated and their brains removed using surgical scissors and a metal spatula. Following dissection of the meninges using forceps, the remaining brain tissue was dissociated in 0.25% Trypsin-EDTA at 37 °C for 25 minutes. The Trypsin mixture was then centrifuged twice at 500 g for 2 min and triturated in cell culture media (DMEM F12/10% FBS/1% PS) to further dissociate brain tissue and deactivate residual Trypsin-EDTA. The resulting cell suspension was placed in 12-well plates coated with PLL (2 µg/mL). Cells were incubated for 2 weeks at 37 °C and 5% CO₂, with cell culture media changed twice weekly.

At 2 weeks, mixed glial cells were washed with DMEM F12 and then lifted off from the 12 well plates with a Trypsin-EDTA and DMEM F12 mixture (1:3 ratio) treatment for 25 min [189]. The cells were then collected and subjected to two-fold centrifugation at 500 g for 2 min and trituration in cell culture media. The resulting cell suspension was then passed through a syringe and needle, and plated in a 75 cm² flask at a ratio of 1 plate:1 flask. The flask cultures were then incubated for 1 week at 37 °C and 5% CO₂ prior to another round of isolation and re-seeding onto microelectrodes, with cell culture media changed twice in that week.

3.4.3. PDMS ring fabrication

To stabilize electrode placements in the 12-well plates, custom polydimethyl siloxane (PDMS) rings were created to prevent movement of the wires within the wells. PDMS elastomer base and curing agent were mixed together in a 50 mL tube in a 10:1 ratio, and left to set in the wells of a 12-well plate (2 g/well). Following curing for 2.5 hours in an oven at 70 °C, the resulting PDMS discs were extracted from the wells, hole-punched, and placed in a large 3 L beaker (50% methanol/50% water) under a fume hood overnight to wash out any unreacted monomers leftover from the curing process. Following this, the rings were submerged in water and autoclaved in preparation for use in cell culture.

3.4.4. Microelectrode fabrication

Platinum-iridium microwires (75 µm diameter) were used for fabrication of microelectrodes. Briefly, microwires were cut ~15 cm in length. The insulation layer of the microwire tips was removed using nanosecond laser pulses (wavelength = 248 nm, energy = 150 mJ, beam attenuation = 5%, repetition rate = 10 Hz; COMPex 110, Coherent, CA, USA). The deinsulated region of the microwires was cut using a scalpel blade leaving 300-400 µm of bare metal at the tip. The tips of the microwires were then mechanically bevelled using a microelectrode beveler (BV-10, Sutter, CA, USA) to an angle of approximately 15°. Microelectrodes were then placed in 15 mL centrifuge tubes (Fisherbrand, Pittsburgh, PA, USA) filled with DI water and Alconox detergent, and treated in an ultrasonic cleaner for 30 minutes to remove the metal debris formed during the mechanical polishing step. The microelectrodes were

then sonicated for another 30 minutes in DI water and rinsed with 70% ethanol. Stranded stainless steel wires were manually deinsulated to expose approximately 4-5 cm and were used as the counter electrodes.

3.4.5. Electrode plate setup

Insertion of microelectrodes into the PDMS rings and placement of the rings into the 12-well plates was all done within the aseptic environment of a biosafety cabinet. An 18.5G needle was used to puncture a hole through the side of a ring at a 45° angle. A 10 µL pipette tip was then fitted through the hole, and a microelectrode was threaded through the pipette tip such that the deinsulated end of the wire lay in the inner hole of the PDMS ring. The pipette tip was then withdrawn to effectively embed the insulated portion of the microelectrode in the side of the ring. The ring and microelectrode were then dipped in 70% ethanol, placed in one of the wells of a 12-well plate, and left to dry to form a sterile seal in the well. This also allowed the deinsulated tip of the wire to make contact with the bottom of the well. Tape was then used to hold down the insulated portion of the electrodes over the edge of the 12-well plate to prevent further movement. Counter electrodes were placed on top of the PDMS rings and taped down over the edge of the plate on the day of the experiment.

Cells were isolated from the flask as above using diluted Trypsin-EDTA/DMEM F12, seeded at a density of 70000 cells/well, and left to settle and incubate for 7 days at 37 °C and 5% CO₂ prior to the start of electrical stimulation. Cell culture media (DMEM/10% FBS/1% PS, 2 mL/well) was changed twice during the 7-day incubation period.

3.4.6. Live imaging electrical stimulation experiments

The cells were electrically stimulated for a 4 h duration using stimulation paradigms adapted from previously reported *in vivo* ISMS work [96]. An STG4008 electrical stimulator (Multi Channel Systems MCS GmbH, Reutlingen, Germany) was used to electrically stimulate the cells, with programming of the stimulation patterns done through the MC_Stimulus II software. To confirm that current was running through the cell cultures (and to rule out any short-circuits in the setup), a Tektronix MDO3014 Oscilloscope was used to assess electrical signal in each stimulating well at the start of each experiment. A summary of each live imaging study, along with parameters tested, is presented in Table T-2. Each study used a 200 μ s pulse duration and a biphasic charge-balanced cathodic-first waveform.

Study	Waveform	Current	Frequency	Charge/phase
Current mod.	Rectangular	0 mA	25 Hz	0 nC
		0.1 mA		20 nC
		0.2 mA		40 nC
		0.3 mA		60 nC
		0.4 mA		80 nC
Waveform mod.	Rectangular	0.15 mA	25 Hz	30 nC
	Sinusoidal			23.56 nC
	Ramped			15 nC
Frequency mod.	Rectangular	0.15 mA	25 Hz	30 nC
			35 Hz	
			45 Hz	
			55 Hz	

Table T-2: Electrical stimulation parameter modification summary

A summary of the different stimulation modification studies described in this study (current modification, waveform shape modification, frequency modification) and their associated stimulation parameters (waveform shape, current, frequency, charge per phase).

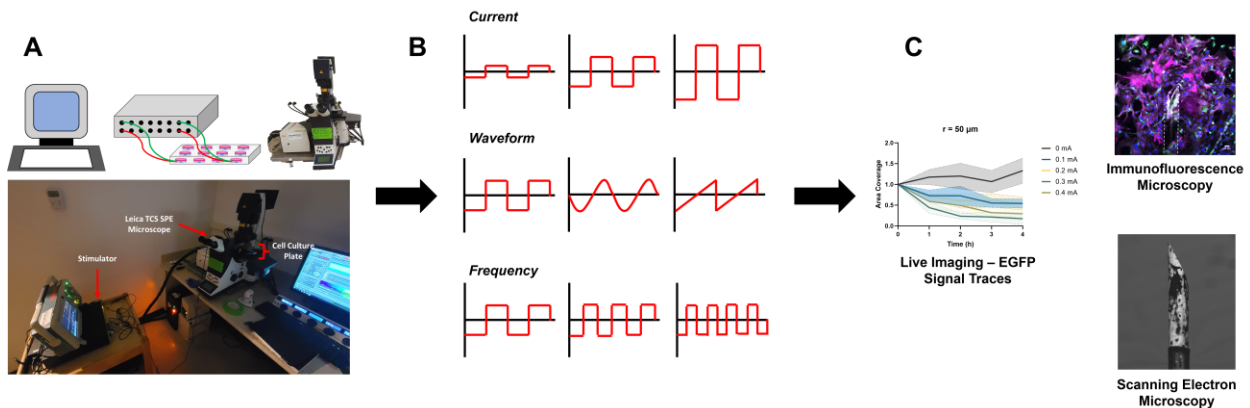


Figure 3-1: Experimental workflow of live imaging experiments

Mixed glial cell cultures are generated, embedded with microelectrodes, and placed on a confocal microscope for live cell imaging (A). Stimulation paradigm modifications performed were based on current, waveform shape, and frequency (B). Live imaging produced EGFP signal traces; cells were then fixed, immunolabeled, and imaged. Electrodes were extracted after and imaged on a scanning electron microscope (C).

Live imaging was done on a Leica TCS SPE confocal microscope (Figure 3-1) (Wetzlar, Germany). The detection channel was set up to capture EGFP signal from the microglia in the otherwise mixed glial cell cultures. The live imaging time-lapse series were captured in stacks of

125 frames per 4 h experiment. A 5-frame baseline was captured at the beginning of each experiment, followed by 4 h of electrical stimulation over the next 120 frames (i.e., approximately 2 minutes between frames in each series). Following stimulation, glial cells were fixed and immunolabeled according to the protocol outlined in the following subsection (3.4.7. Immunofluorescence microscopy).

Analysis of the time-lapse series was performed on ImageJ (National Institutes of Health, Bethesda, MD, USA) using a custom macro that calculates temporal change in EGFP fluorescence intensity as well as geometric area coverage in the field of view of the image. This is expressed as a fold-change versus the first frame in the series, and normalized to control wells that received neither electrical stimulation nor electrode insertion. These data were further analyzed by zone (i.e., how EGFP metrics change as a function of distance from the electrode tip) by restricting mean pixel intensity and area coverage measurements to prescribed circular radii from the electrode tip ($r = 50 \mu\text{m}$, $100 \mu\text{m}$, $250 \mu\text{m}$) [155]. This was compared to data analyzed from the full frame of the image ($734.05 \mu\text{m} \times 734.05 \mu\text{m}$). Image animations were prepared using the ImageJ StackReg plugin (Rigid Body option) [287]. Multi-colour overlays showing net changes in cell movement over the 4 h experiments were generated using the ImageJ Time-Lapse Colour Coder tool.

3.4.7. Immunofluorescence microscopy

Following 3 days of stimulation, glial cells were fixed with 5% formalin at 37°C for 10 min and washed three times with PBS. Cells were permeabilized with 0.1% Triton X-100

(TX100) in PBS and 10% Equine Serum (ES) for 2 h. Following this, the cells were incubated overnight at 4 °C with rabbit anti-IL-1 β (1:1000) and chicken anti-GFAP (1:5000) primary antibodies plus 1% ES. The cells were then washed three times with PBS, and incubated for 2 h at room temperature with goat anti-chicken Alexa Fluor 546 (1:200) and donkey anti-rabbit Alexa Fluor 647 (1:200) secondary antibodies plus Hoechst 33342 (1:1000) and 1% ES. The cells were then washed three times with PBS. Fluorescence microscopy was carried out on a Leica TCS SPE confocal microscope. Components labelled included Hoechst for cell nuclei, enhanced green fluorescent protein (EGFP) expressed from transgenic microglia, glial fibrillary acidic protein (GFAP) for astrocytes, and interleukin-1 beta (IL-1 β) as a pro-inflammatory biomarker. Analysis of fluorescence microscopy images was carried out with ImageJ using a custom macro measuring for fluorescence intensity and area coverage of biomarkers. Area coverage measured the total geometric surface generated by each biomarker from the cells in the image's field of view. Fluorescence intensity was calculated by dividing the image-wide sum of each pixel intensity value for a biomarker divided by the area coverage of that biomarker in that image. Cell density was calculated by counting the number of nuclei found in each image. These metrics (fluorescence intensity, area coverage, cell density) were expressed as fold change against control wells with no wire. Zonal analysis (i.e., how outputs change as a function of distance from the electrode tip) was carried out at prescribed circular radii from the electrode tip ($r = 50 \mu\text{m}$, $100 \mu\text{m}$, $250 \mu\text{m}$) [155]. This was compared to data analyzed from the full frame of the image ($734.05 \mu\text{m} \times 734.05 \mu\text{m}$).

3.4.8. Scanning electron microscopy

Qualitative assessment of damage to electrodes was carried out using a ThermoFisher Phenom XL Desktop scanning electron microscope (SEM) (Waltham, MA, USA). Images were acquired using backscattered electron detection at 610x and 4000x magnification. Elemental makeup of the electrode surfaces was quantified using the energy-dispersive x-ray spectroscopy (EDS) add-on to the SEM, at 4000x magnification.

3.4.9. Statistical analyses

For statistical analysis of fluorescence intensity and area coverage of biomarkers and cell density, a two-way analysis of variance (two-way ANOVA) with Bonferroni's *post hoc* test was performed. The independent variables analyzed were electrical stimulation amplitude and distance away from the tip of the electrode. For statistical analysis of EDS data, a one-way analysis of variance (one-way ANOVA) with Tukey's *post hoc* test was performed. The statistical analyses stated were performed using GraphPad Prism 10 (San Diego, CA, USA).

3.5. Results

In the present study, two goals were addressed: 1) ascertain how different parameters of electrical stimulation impact glial cell behaviour at the electrode interface, and 2) determine the cause of the formation of the peri-electrode void seen in the results generated in the previous

chapter (and by doing so determine the fates of the cells that would have otherwise populated that void). To address these research aims in detail, live imaging was used to monitor microglia dynamics over a 4 h stimulation timecourse – this was possible as the microglia used in the cultures were harvested from transgenic C57BL/6 mice that expressed EGFP under the CX3CR1 promoter gene. Primary mixed glial cell cultures were electrically stimulated using paradigms modified in terms of stimulation current, waveform shape, and frequency – this was done in a 4 h window while the microglia were live-imaged on a confocal fluorescence microscope (Figures S-1, S-2, S-3). The acquired EGFP fluorescence intensity and area coverage signal traces and colour-coded maps showing net movement of cells at the electrode interface are shown in Figures 3-2, 3-3, and 3-4. The cells were then fixed, immunolabelled and imaged on a confocal fluorescence microscope (Figures 3-5, 3-6, 3-7).

3.5.1. Live imaging – signal changes

Live imaging animations were captured for each experimental condition, collapsed into colour-coded images showing net movement over an entire 4 h stimulation experiment (Figures 3-2A, 3-3A, 3-4A) and quantified in terms of signal (fluorescence intensity and area coverage) changes over the duration of the experiment at different ROIs (Figures 3-2B, 3-3B, 3-4B). In all signal traces captured, the changes in EGFP fluorescence intensity and area coverage were most readily seen within the smallest ROI ($r < 50 \mu\text{m}$); as the ROI increases in size, it becomes more difficult to observe any differences in EGFP signal that the electrical stimulation paradigms elicit compared to baseline controls thus highlighting the localized effects of the stimulation.

Net EGFP signal changes over the course of each 4 h live imaging experiment are shown in Figures 3-2C, 3-2D, 3-3C, 3-3D, 3-4C, and 3-4D. For the current modification study, statistically significant differences in EGFP area coverage were found between the different currents used within distances of 50 μm , 100 μm , and 250 μm away from the electrode tips. Loss in area coverage increased with current. For the waveform modification study, a statistically significant difference was found in EGFP fluorescence intensity between the rectangular and sinusoidal waveform conditions at 50 μm away from the electrode tip. For the frequency modification study, significant differences were found in EGFP fluorescence intensity and area coverage between the frequencies used at 50 μm away from the electrode tip. Although greater losses in EGFP fluorescence intensity and area coverage were observed with increasing stimulation frequency from 25 to 45 Hz, the comparatively smaller decrease in EGFP area coverage and increase in fluorescence intensity seen at 55 Hz did not conform with this trend.

3.5.2. Immunofluorescence image analysis

Fluorescence intensity, area coverage, and cell density analyses are shown in Figures 3-8, 3-9, and 3-10. For the current modification study (Figure 3-8), statistically significant differences in cell density, Hoechst area coverage, and EGFP area coverage were detected between the different currents used at 50 μm and 100 μm away from the electrode tip; statistically significant differences were also detected for IL-1 β area coverage for all ROIs examined. For the waveform modification study (Figure 3-9), statistically significant differences were detected for cell density, Hoechst area coverage, EGFP area coverage, IL-1 β area coverage, and IL-1 β fluorescence intensity between the different waveform shapes employed up to 100 μm away from the electrode tip. For the frequency modification study (Figure 3-10), significant differences were found in cell density and EGFP area coverage between the stimulation frequencies used within 50 μm from the electrode tip.

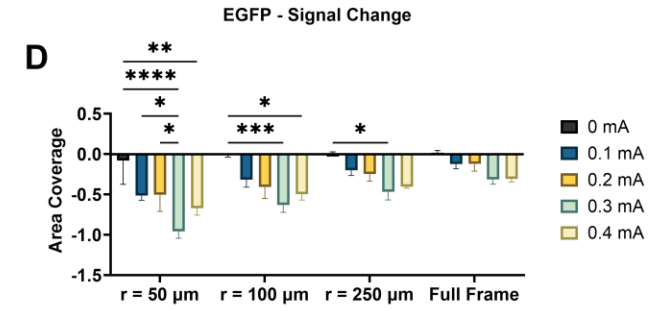
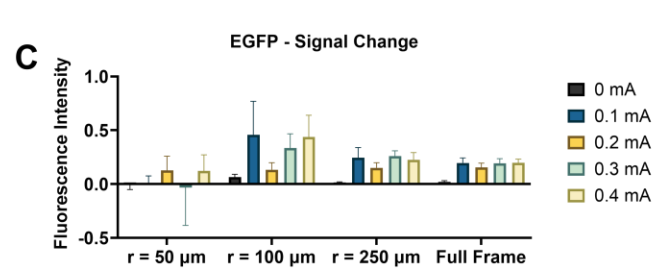
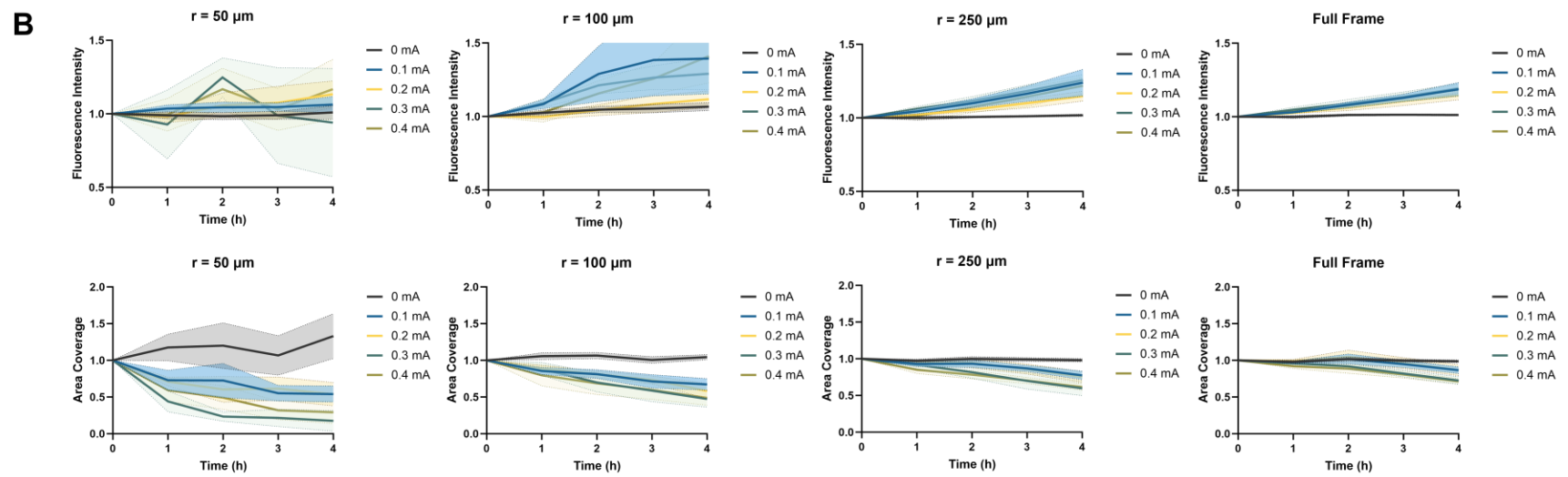
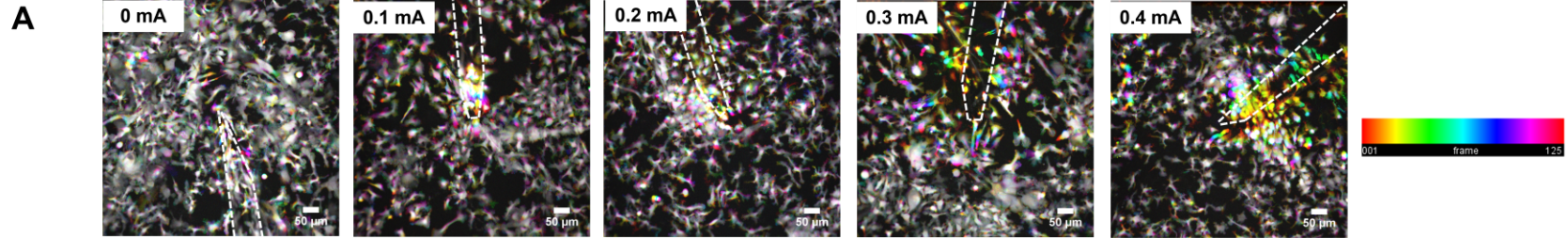


Figure 3-2: Live imaging data summary - current modification

Primary glial cell cultures were electrically stimulated using modified levels of current. Microglia in the cultures were live imaged on a confocal fluorescence microscope over 4 h – the resulting image stacks for each condition were then collapsed into colour-coded overlays which is a visual representation of net movement of microglia in the fields of view over the course of the stimulation experiment (A). Scale bars: 50 μm . EGFP signal traces were calculated in terms of fluorescence intensity and area coverage over 4 h (B). Net EGFP signal changes over 4 h were also calculated in terms of fluorescence intensity (C) and area coverage (D). EGFP signal change values are expressed as fold change versus the first frame in the live imaging set, and normalized to no-wire control cell cultures ($n = 5$, two-way ANOVA with Bonferroni *post hoc* test). * $p < 0.05$, ** $p < 0.01$, *** $p < 0.001$, **** $p < 0.0001$; Data = means \pm SEM.

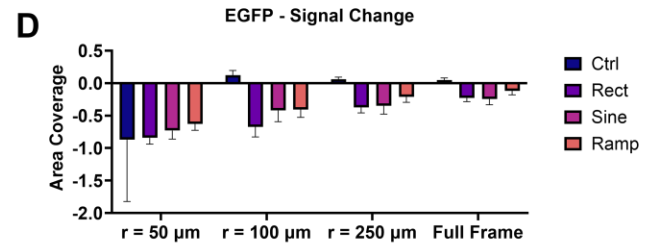
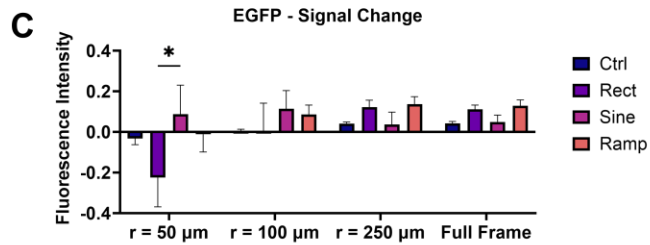
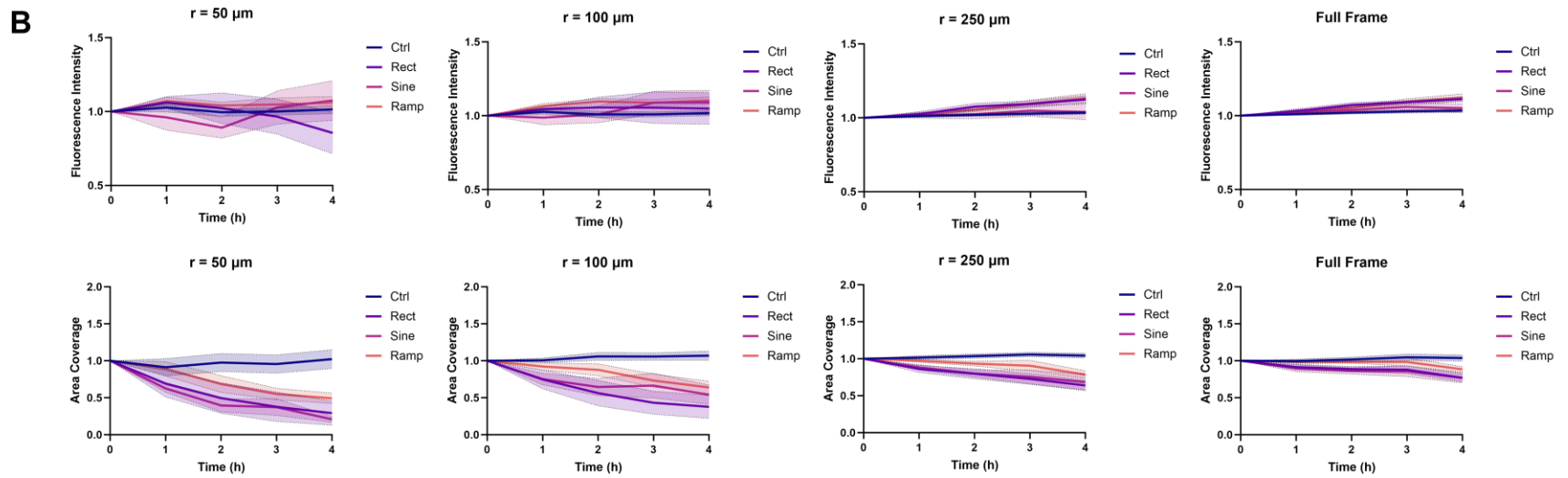
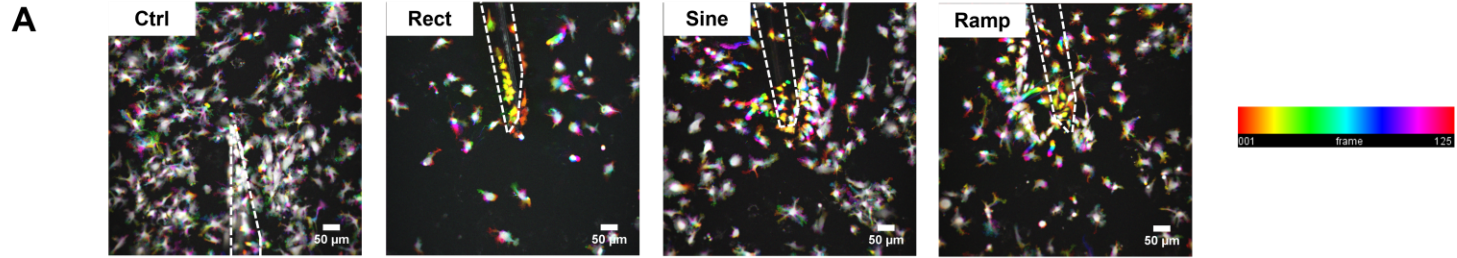


Figure 3-3: Live imaging data summary - waveform shape modification

Primary glial cell cultures were electrically stimulated using modified waveform shapes. Microglia in the cultures were live imaged on a confocal fluorescence microscope over 4 h – the resulting image stacks for each condition were then collapsed into colour-coded overlays which is a visual representation of net movement of microglia in the fields of view over the course of the stimulation experiment (A). Scale bars: 50 μm . EGFP signal traces were calculated in terms of fluorescence intensity and area coverage over 4 h (B). Net EGFP signal changes over 4 h were also calculated in terms of fluorescence intensity (C) and area coverage (D). EGFP signal change values are expressed as fold change versus the first frame in the live imaging set, and normalized to no-wire control cell cultures (n = 6, two-way ANOVA with Bonferroni *post hoc* test). *p < 0.05; Data = means \pm SEM.

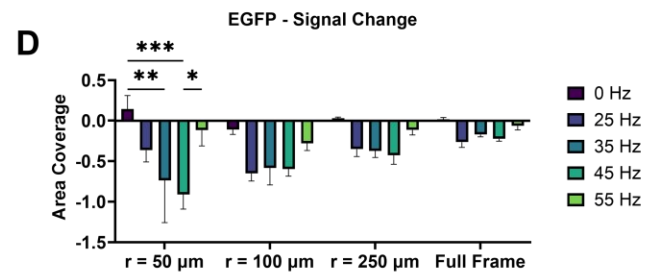
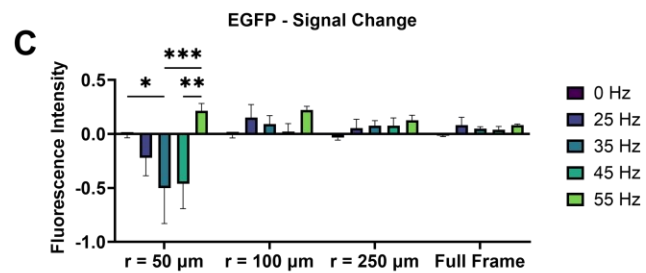
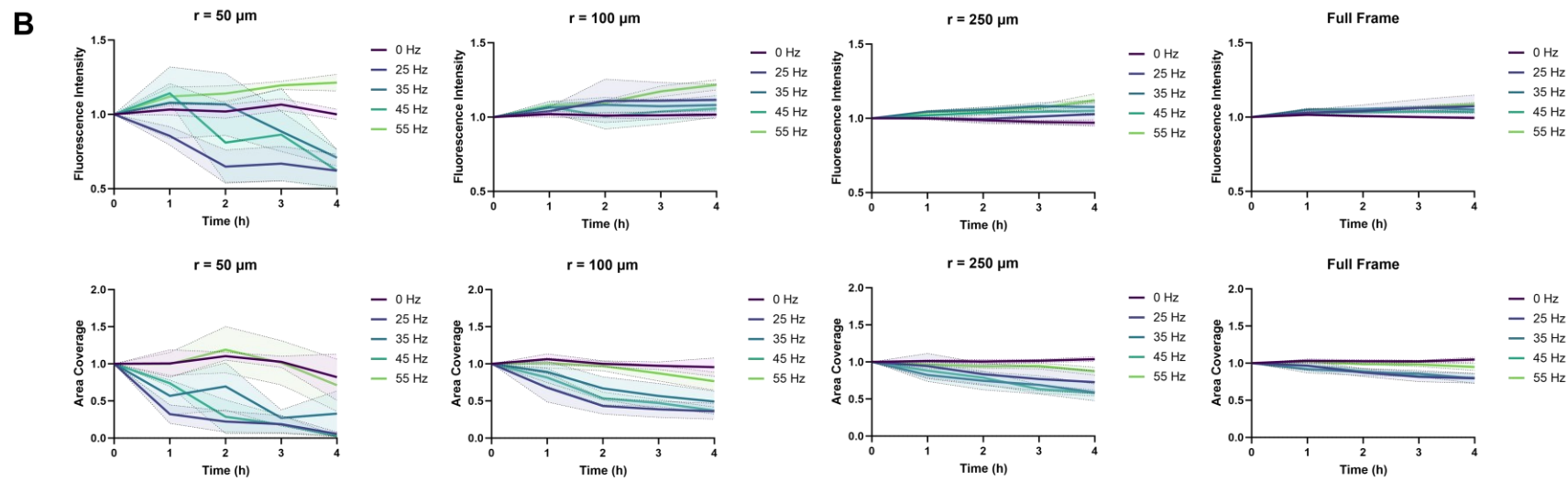
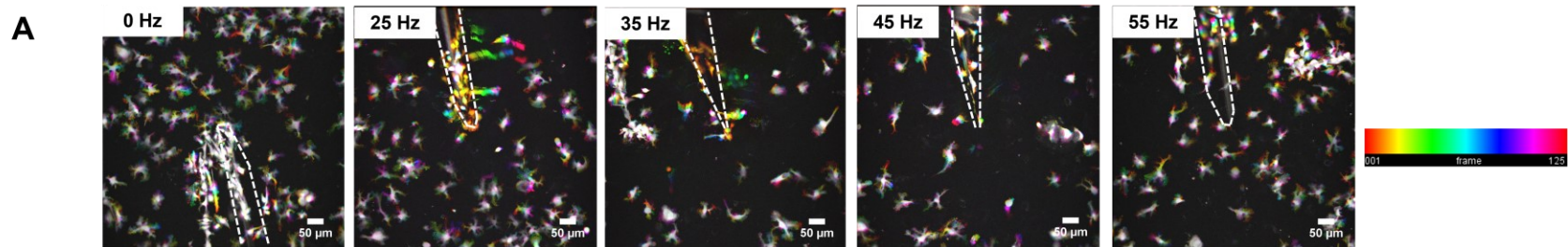


Figure 3-4: Live imaging data summary - frequency modification

Primary glial cell cultures were electrically stimulated using modified frequencies. Microglia in the cultures were live imaged on a confocal fluorescence microscope over 4 h – the resulting image stacks for each condition were then collapsed into colour-coded overlays which is a visual representation of net movement of microglia in the fields of view over the course of the stimulation experiment (A). Scale bars: 50 μm . EGFP signal traces were calculated in terms of fluorescence intensity and area coverage over 4 h (B). Net EGFP signal changes over 4 h were also calculated in terms of fluorescence intensity (C) and area coverage (D). EGFP signal change values are expressed as fold change versus the first frame in the live imaging set, and normalized to no-wire control cell cultures ($n = 3$, two-way ANOVA with Bonferroni *post hoc* test). * $p < 0.05$, ** $p < 0.01$, *** $p < 0.001$; Data = means \pm SEM.

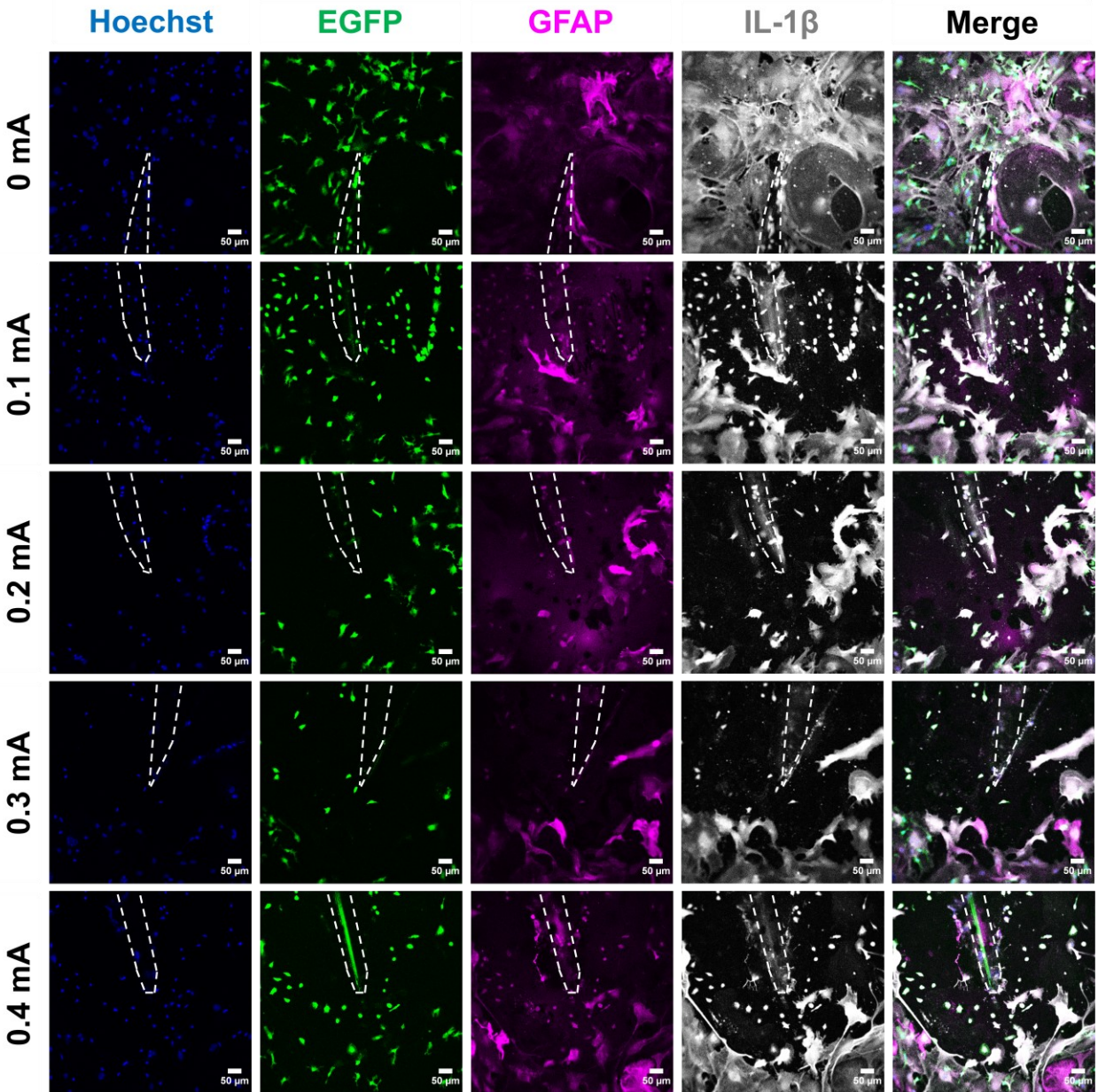


Figure 3-5: Immunofluorescent images of mixed glia - 4 h stimulation (current modification)

Electrodes are marked by the white dashed outline in each image. Cell cultures were labelled with Hoechst 33342 (blue), EGFP (green), GFAP (magenta), and IL-1 β (grey). A merged channel overlay of each condition is shown on the far right. Scale bars: 50 μ m.

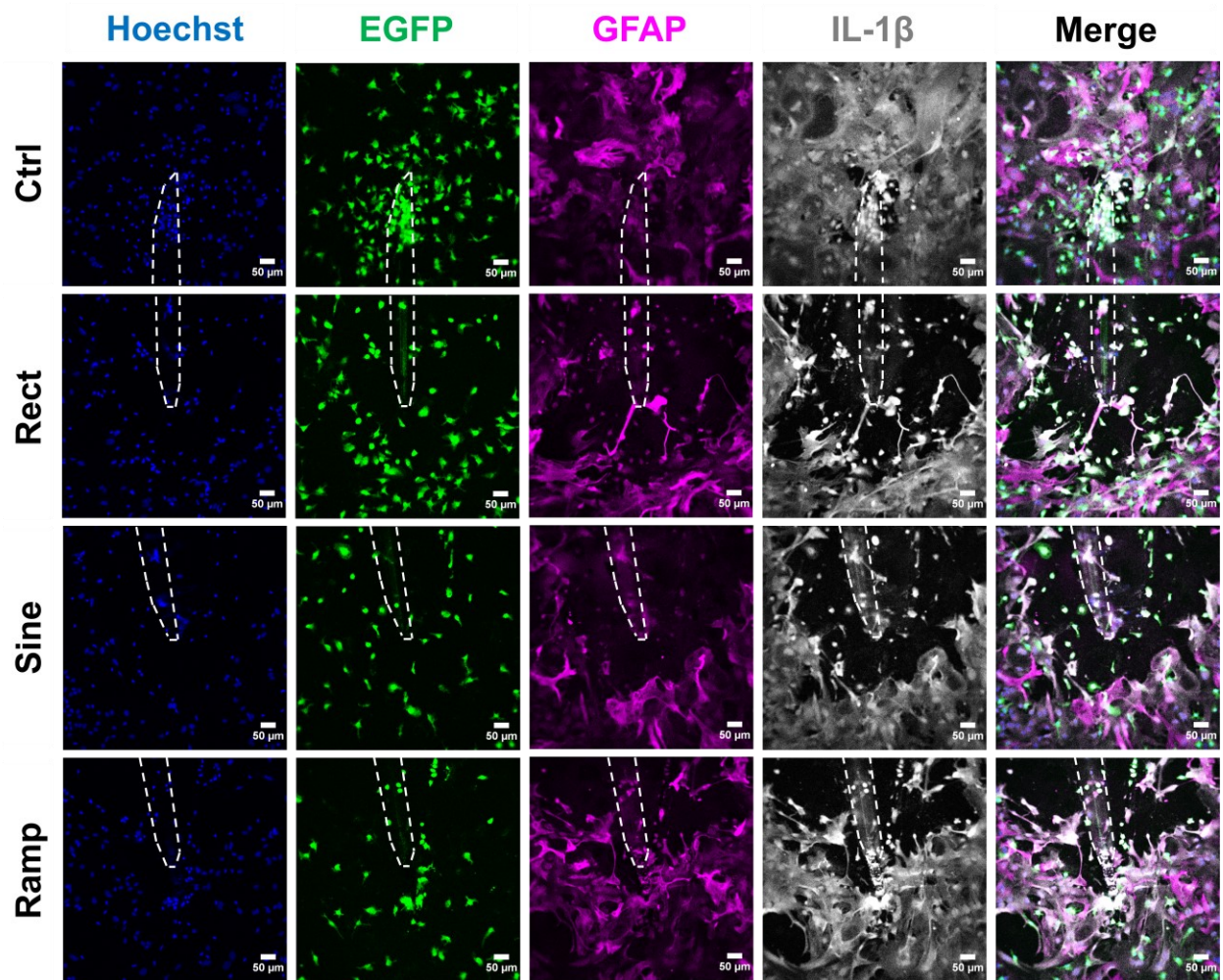


Figure 3-6: Immunofluorescent images of mixed glia - 4 h stimulation (waveform shape modification)

Electrodes are marked by the white dashed outline in each image. Cell cultures were labelled with Hoechst 33342 (blue), EGFP (green), GFAP (magenta), and IL-1 β (grey). A merged channel overlay of each condition is shown on the far right. Scale bars: 50 μ m.

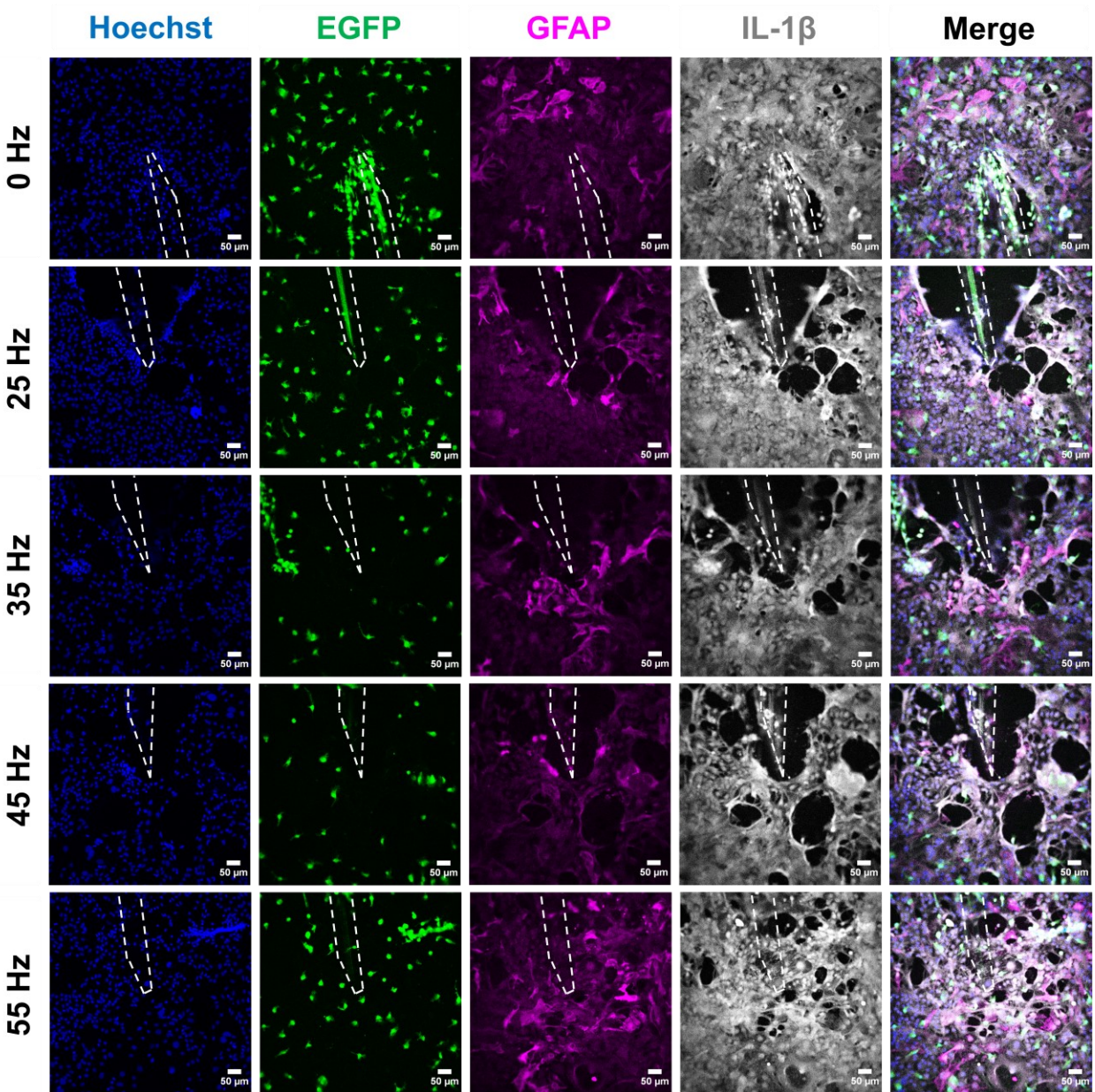


Figure 3-7: Immunofluorescent images of mixed glia - 4 h stimulation (frequency modification)

Electrodes are marked by the white dashed outline in each image. Cell cultures were labelled with Hoechst 33342 (blue), EGFP (green), GFAP (magenta), and IL-1 β (grey). A merged channel overlay of each condition is shown on the far right. Scale bars: 50 μ m.

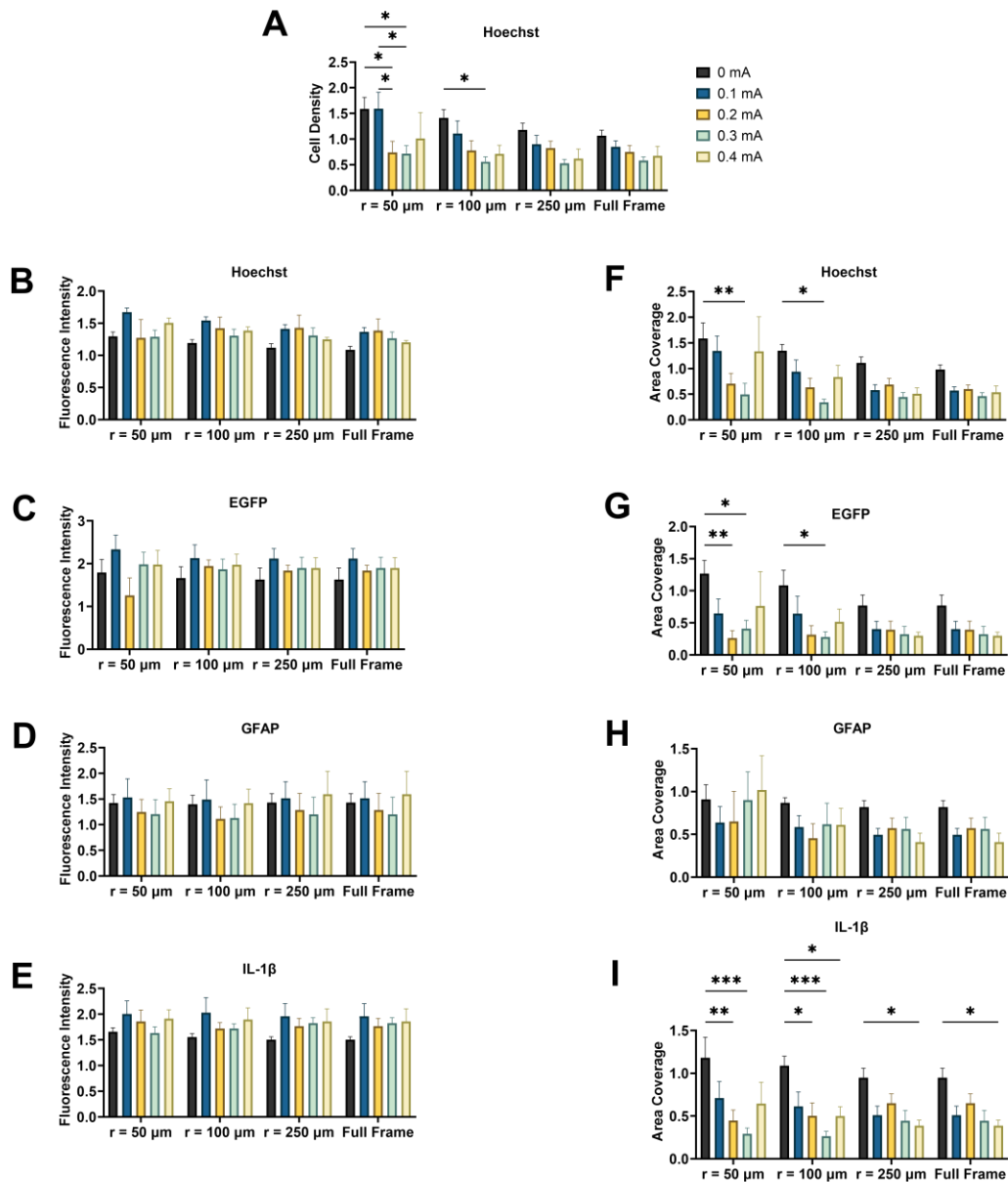


Figure 3-8: Quantitative analysis of current modification images

(A) Cell density, (B, C, D, E) fluorescence intensity, and (F, G, H, I) area coverage profiles of immunofluorescent images as a function of electrical stimulation (4 h) current and distance from the electrode tip. Values are expressed as fold change versus no-wire control cell cultures ($n = 6$, two-way ANOVA with Bonferroni *post hoc* test). * $p < 0.05$, ** $p < 0.01$, *** $p < 0.001$; Data = means \pm SEM.

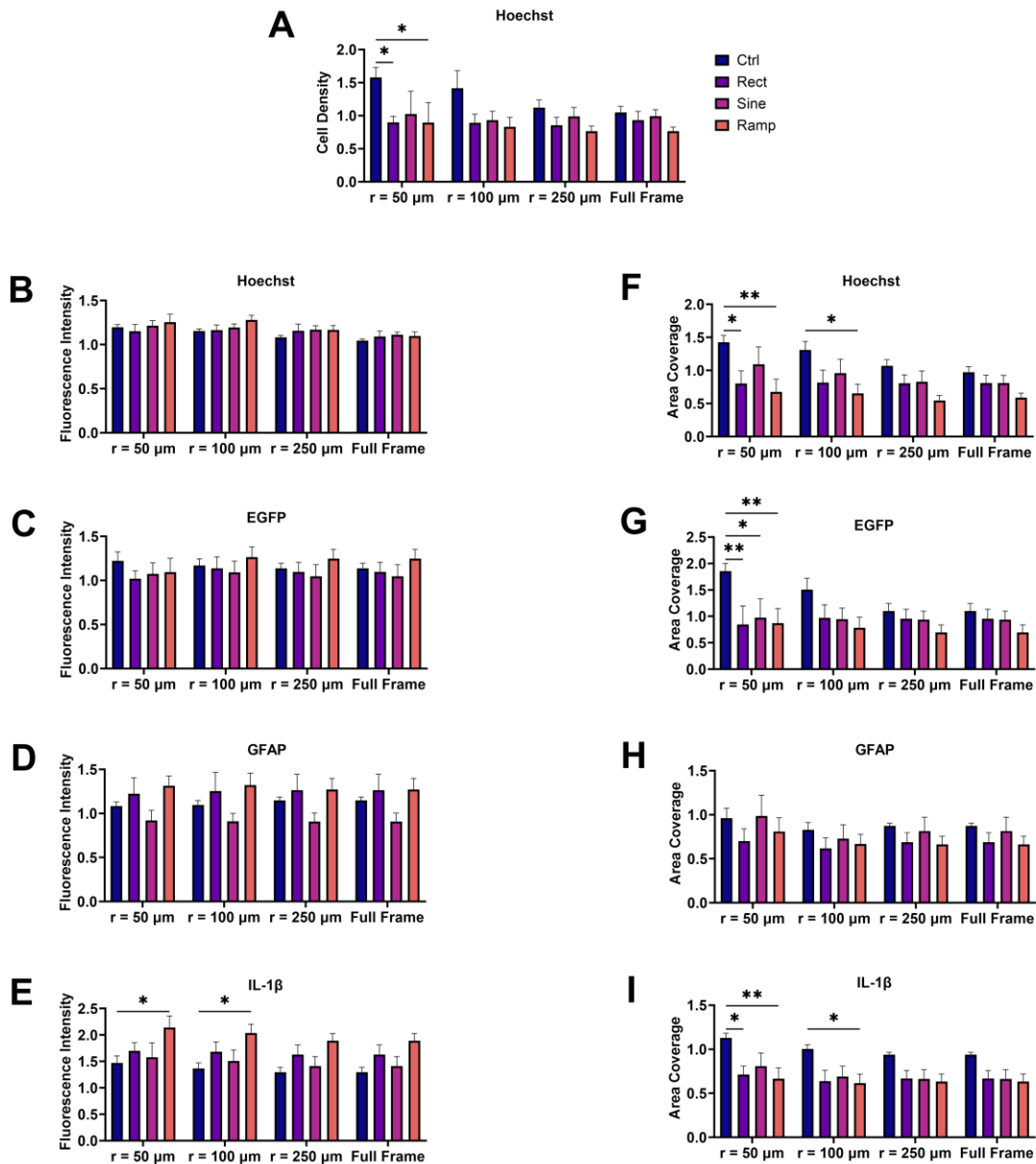


Figure 3-9: Quantitative analysis of waveform shape modification images

(A) Cell density, (B, C, D, E) fluorescence intensity, and (F, G, H, I) area coverage profiles of immunofluorescent images as a function of electrical stimulation (4 h) waveform shape and distance from the electrode tip. Values are expressed as fold change versus no-wire control cell cultures ($n = 7$, two-way ANOVA with Bonferroni *post hoc* test). * $p < 0.05$, ** $p < 0.01$, *** $p < 0.001$; Data = means \pm SEM.

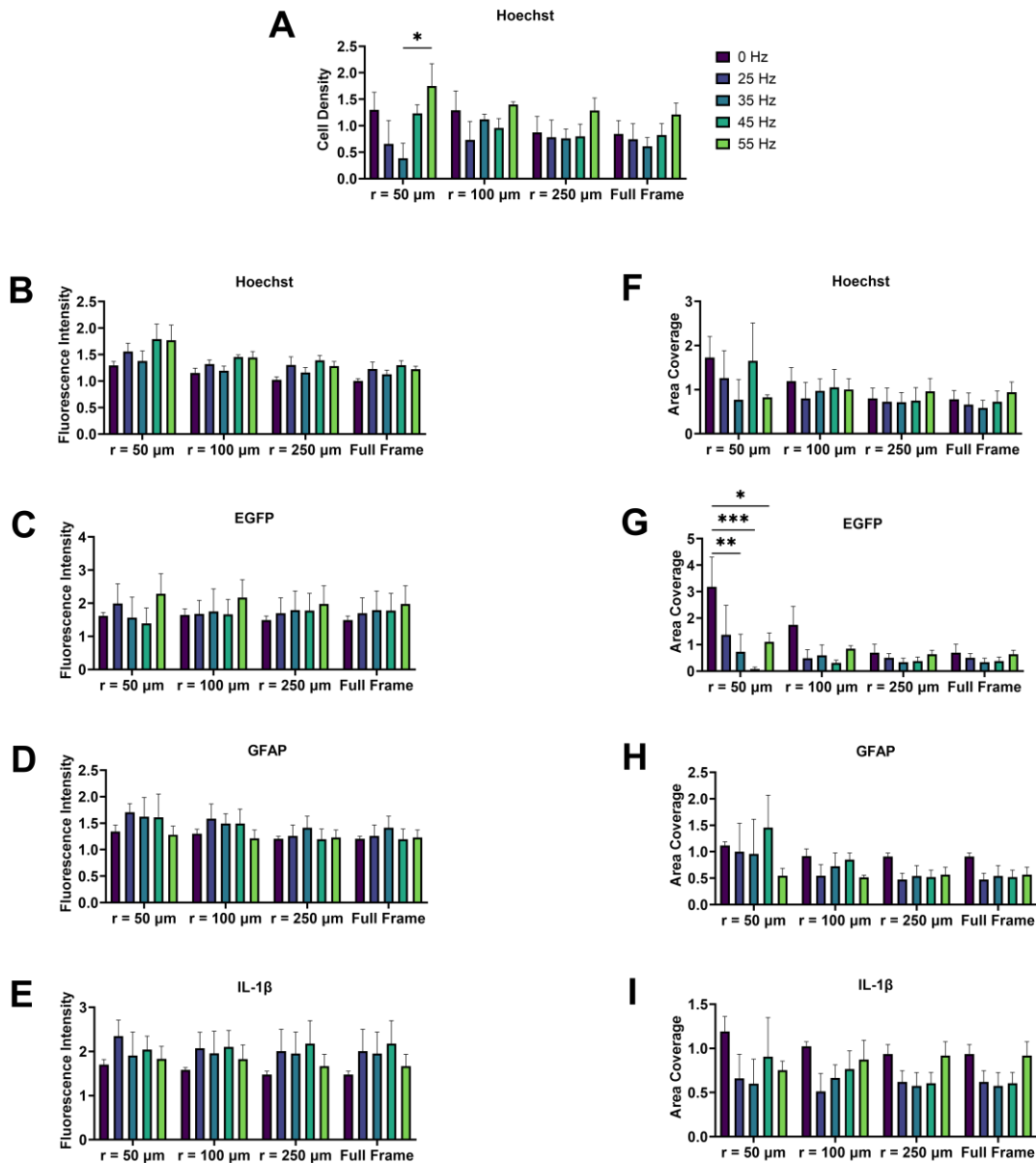


Figure 3-10: Quantitative analysis of frequency modification images

(A) Cell density, (B, C, D, E) fluorescence intensity, and (F, G, H, I) area coverage profiles of immunofluorescent images as a function of electrical stimulation (4 h) frequency and distance from the electrode tip. Values are expressed as fold change versus no-wire control cell cultures ($n = 3$, two-way ANOVA with Bonferroni *post hoc* test). * $p < 0.05$, ** $p < 0.01$, *** $p < 0.001$; Data = means \pm SEM.

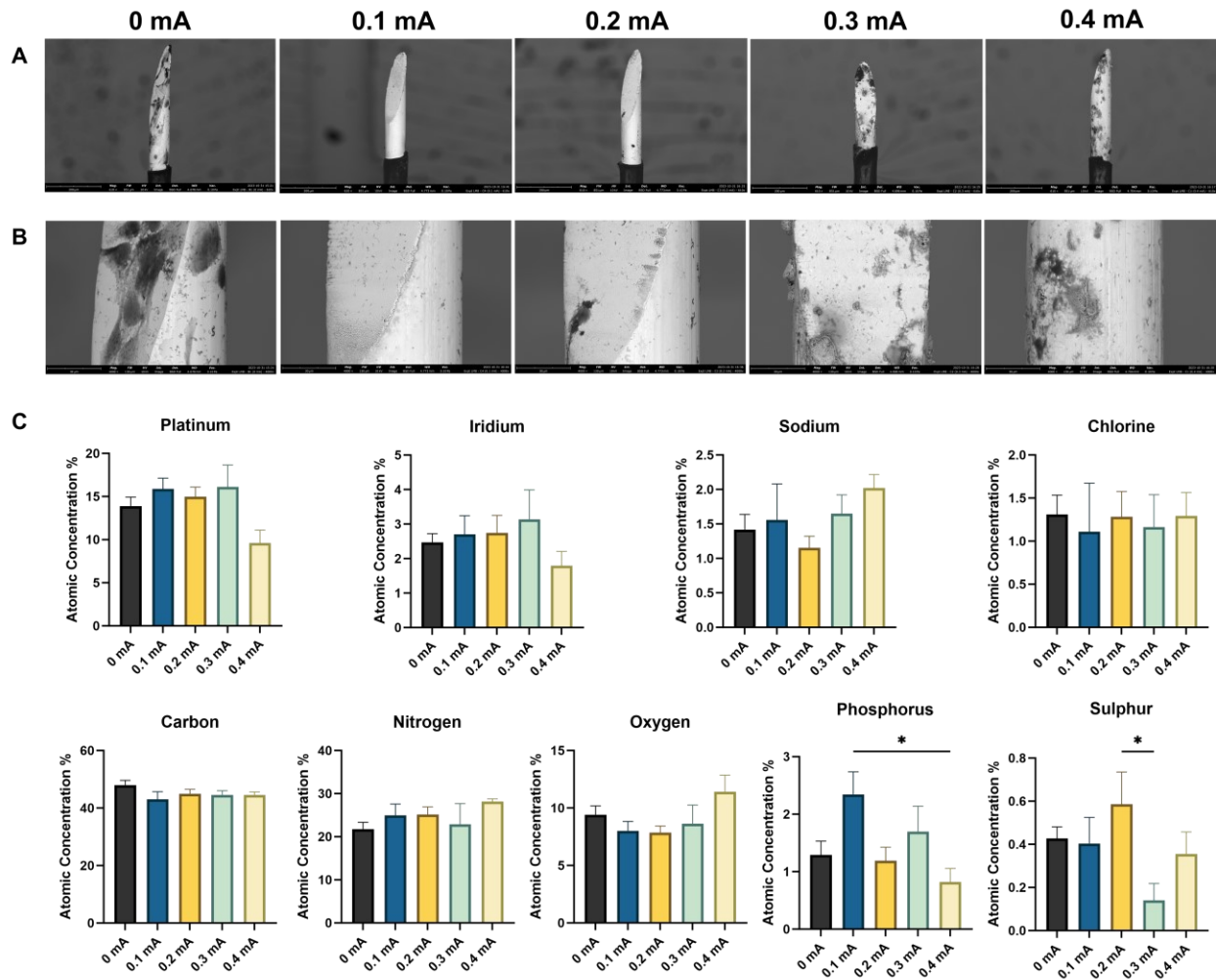


Figure 3-11: Scanning electron micrographs of electrodes following 4 h current modification experiments

Images were acquired at 610x (A) and 4000x (B) magnification. Scale bars: 200 μm (610x), 30 μm (4000x). Energy-dispersive x-ray spectroscopy data showing atomic concentrations (C) of platinum, iridium, sodium, chlorine, carbon, nitrogen, oxygen, phosphorus, and sulphur on the surfaces of electrodes following stimulation experiments ($n = 6$, one-way ANOVA with Tukey's *post hoc* test). * $p < 0.05$; Data = means \pm SEM.

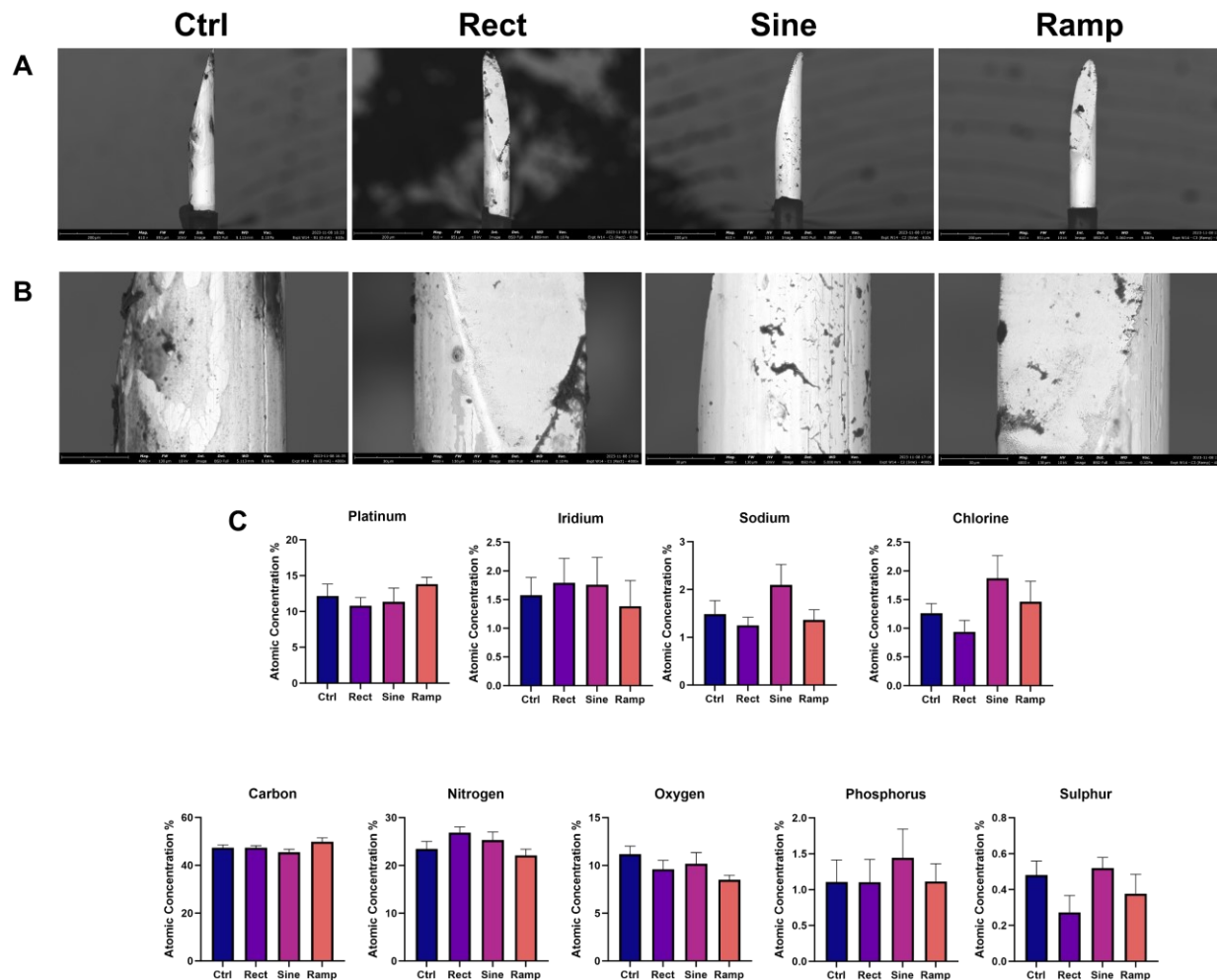


Figure 3-12: Scanning electron micrographs of electrodes following 4 h waveform shape modification experiments

Images were acquired at 610x (A) and 4000x (B) magnification. Scale bars: 200 μm (610x), 30 μm (4000x). Energy-dispersive x-ray spectroscopy data showing atomic concentrations (C) of platinum, iridium, sodium, chlorine, carbon, nitrogen, oxygen, phosphorus, and sulphur on the surfaces of electrodes following stimulation experiments ($n = 7$, one-way ANOVA with Tukey's *post hoc* test). * $p < 0.05$; Data = means \pm SEM.

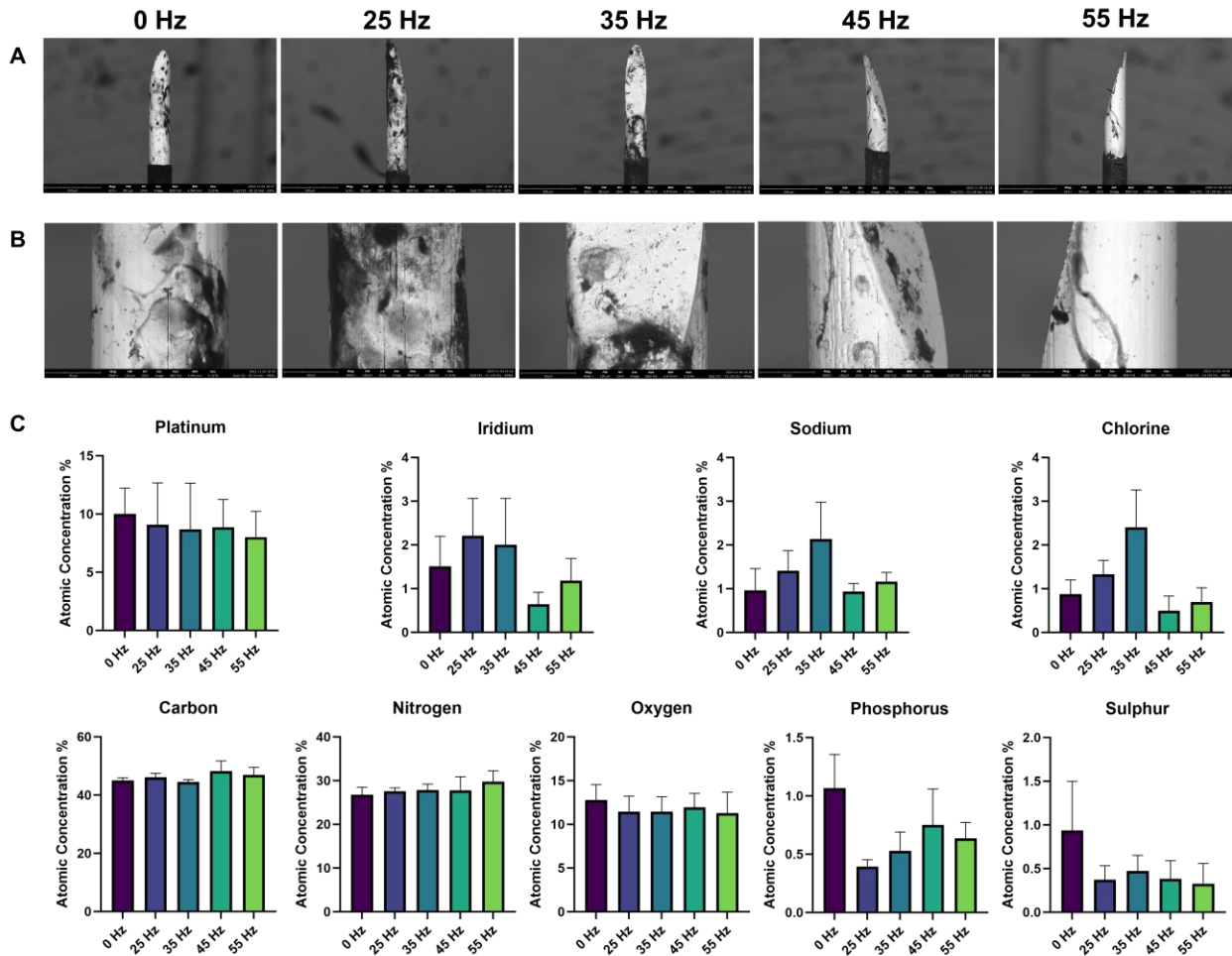


Figure 3-13: Scanning electron micrographs of electrodes following 4 h frequency modification experiments

Images were acquired at 610x (A) and 4000x (B) magnification. Scale bars: 200 μm (610x), 30 μm (4000x). Energy-dispersive x-ray spectroscopy data showing atomic concentrations (C) of platinum, iridium, sodium, chlorine, carbon, nitrogen, oxygen, phosphorus, and sulphur on the surfaces of electrodes following stimulation experiments ($n = 3$, one-way ANOVA with Tukey's *post hoc* test). * $p < 0.05$; Data = means \pm SEM.

3.5.3. Electrode damage analysis

Following immunolabelling and confocal fluorescence microscopy, the electrodes were extracted from the cell culture wells and imaged on an SEM to qualitatively assess damage caused by the stimulation experiments (Figures 3-11A, 3-11B, 3-12A, 3-12B, 3-13A, 3-13B), with images taken of the entire deinsulated tip of the electrode as well as a close-up view of the tip's microstructure.

In addition to SEM, EDS was used to quantify the elemental composition of the surfaces of the electrodes across the different experimental conditions (Figures 3-11C, 3-12C, 3-13C). Across all of the experimental conditions tested, *post hoc* tests revealed statistically significant differences only in phosphorous (0.1 mA vs 0.4 mA) and sulphur atomic concentrations (0.2 mA vs 0.3 mA) for the stimulation current modification study. No significant differences were observed in the other elements across any of the stimulation parameters tested.

3.6. Discussion

The main goal of the work described in this chapter was to use the cell culture model established in the previous chapter to further investigate glial cell reactivity to various electrical stimulation parameter modifications (current, waveform shape, and frequency). Secondary to this main goal was the need to assess the feasibility of analyzing live transgenic EGFP signal from microglia – this was done to determine the fate of the microglia around the electrode interface and shed light on the origins of the peri-electrode void described in Chapter 2. From the time-lapse animations acquired from the live imaging experiments, microglia near the electrodes were

seen exploding – in other words, cells were dying as a result of electrical stimulation. The animations show a sudden rupturing of microglial cell membranes over the duration of the 4-hour stimulation experiments – this specifically suggests that necrotic cell death is occurring. Previous literature also suggests transient openings in cell membranes when electrical stimulation is applied thus allowing for influx of water into the cell or efflux of cellular contents [288]. This is in contrast to apoptotic cell death, which is a more ordered process and may take up to several days to occur [289,290]. This also outweighs evidence for the other hypothesis which postulated that cells were retreating away from the electrode interface when electrical stimulation was being applied – the time-lapse animations and compiled colour-coded images showing net movement of microglia over the course of a 4-hour experiment showed that cells were either dying near the interface, or were otherwise stationary if placed further afield.

Although the live imaging animations contrast with evidence of glial cells migrating in the presence of an electric field [291,292], the context of other studies differs from the work presented in this thesis in that attention is being placed on glial cells that are at or near a microelectrode implant rather than looking at how glial cells generally behave in the presence of an electric field. As glial cell reactivity and the scarring process are detrimental events to the long-term functionality of invasive microelectrode implants into CNS tissue, there is merit in assessing if there are ways in which to modify various electrical stimulation parameters with the goal of reducing glial cell reactivity and thus improve the biocompatibility of an implant design.

3.6.1. Live imaging analysis

Live imaging is a technique that allows for the observation of dynamic changes in cell movement and behaviour – its advantage over immunolabelling is that cells are being imaged while they are still alive. Previously published works take great advantage of the same transgenic strain utilized in this chapter to image microglia in a wide variety of contexts [32,293–296]. The experiments described in this chapter allowed for the collection of time-lapse image data which was then used to calculate EGFP signal change from microglia over a 4 h experiment in terms of fluorescence intensity and area coverage. Fluorescence intensity is a measure of the image-wide sum of the pixel intensity values for a biomarker divided by the area coverage of that biomarker, and area coverage is the total geometric size of a biomarker’s signal across all cells present in the image’s field of view. The time-lapse image data suggests that the majority of microglia in the field of view around the deinsulated electrode tip do not move much – this is best shown by the color-coded maps representing net microglia movement over the 4 h time span of each experiment (Figures 3-2A, 3-3A, 3-4A) where stationary objects are shown in white. Traces of fluorescence intensity and area coverage signal for each time-lapse image series are shown (Figures 3-2B, 3-3B, 3-4B), with the most drastic differences in how the signal traces behave for each experimental condition seen in the region of interest (ROI) closest to the electrode tip ($r = 50 \mu\text{m}$). The data gathered from the live imaging experiments present a look into the fate of the cells present at the electrode interface when stimulation is applied. The data suggest that, although cells die to varying degrees as a result of differing stimulation parameters, the effects seen are highly restricted to the immediate vicinity of the electrode interface and do not suggest more widespread cell damage or death. This further builds on the results reported in the previous chapter as well as previous work [96] that any glial cell reaction towards the electrodes and

applied electrical stimulation are likely to be highly localized. The signal traces seen for the current, waveform shape, and frequency modification data are similar in that any differences in stimulation conditions are best highlighted within the $r = 50 \mu\text{m}$ ROI; this is in comparison to the other ROIs presented ($r = 100 \mu\text{m}$, $r = 250 \mu\text{m}$, full frame) where not much of a deviation is seen in signal traces from the various experimental conditions versus the baseline control traces.

When calculating net signal change over a 4 h experiment, a few observations were drawn from each of the studies performed. EGFP fluorescence intensity generally increased as a result of electrical stimulation regardless of change in current, waveform shape, or frequency as seen in the larger ROIs. The most drastic changes seen, however, were mostly confined to within $50 \mu\text{m}$ away from the electrode tip as exemplified with changes in stimulation frequency (Figure 3-4C). Increases in EGFP signal over time may suggest activation of microglia as a result of electrical stimulation. Statistically significant increases in EGFP fluorescence intensity in the live imaging data were seen for the waveform shape modification data and frequency modification data within the $r = 50 \mu\text{m}$ ROI (Figures 3-3C, 3-4C) – at this ROI, increases in fluorescence intensity over 4 h were seen when sinusoidal stimulation or stimulation at 55 Hz was used.

EGFP area coverage signal, on the other hand, diminished over the course of 4 h of stimulation regardless of modifications applied to electrical stimulation paradigms. Statistically significant differences between different experimental groups were found in the current modification and frequency modification data to varying degrees ($250 \mu\text{m}$ and $50 \mu\text{m}$, respectively). The current modification data (Figure 3-2D) suggest that as the stimulation current increases, the greater the EGFP area coverage drop thus implying a greater loss of microglia around the electrode interface at 0.3 mA and 0.4 mA compared to 0 mA. Similar trends are also seen in the frequency modification data (Figure 3-4D). Although increasing frequency up to 45

Hz resulted in a greater loss in area coverage signal as shown at $r = 50 \mu\text{m}$, remarkably this trend does not continue at 55 Hz. At 55 Hz, EGFP area coverage change is comparable to 0 Hz thus suggesting that less microglia are lost at the interface when stimulating at that frequency compared to stimulation at 25, 35, or 45 Hz. In contrast to the other modification studies, however, waveform modification did not result in any significant change in EGFP area coverage over the course of a 4 h stimulation experiment (Figure 3-3D). These observations, along with no statistically significant findings in the waveform shape modification data, suggest that different stimulation parameters have differing degrees of impact on microglial presence at the electrode interface.

3.6.2. Immunofluorescence image analysis

Following live imaging experiments, cell cultures were fixed, immunolabelled, and imaged to further assess responses of other relevant biomarkers. The immunofluorescent images acquired across the different studies undertaken suggest that modification of parameters such as current, waveform shape, and frequency to the degree that has been described in these experiments is capable of creating the peri-electrode space that has been previously described in Chapter 2 and earlier in the current chapter. Analysis of the immunolabelled images revealed differences in glial cell reactivity in terms of cell density, biomarker fluorescence intensity and biomarker area coverage as a function of differences in stimulation parameters as well as the range to which those differences are seen from the tip of the electrode.

In the current modification study, there was a higher cell density in the 0 mA and 0.1 mA conditions compared to the higher currents as shown within the $r = 50 \mu\text{m}$ ROI of Figure 3-8A. This conforms to the hypothesis made that applying a higher current would result in a lower number of cells near the electrode even after 4 h of stimulation. This finding is corroborated by the Hoechst and EGFP area coverage data (Figures 3-8F, 3-8G), but not the GFAP area coverage data which may suggest that modification of exogenous stimulation current in the range defined in this work (0 mA – 0.4 mA) is more impactful on microglia at the interface than astrocytes. Expression of IL-1 β , a pro-inflammatory cytokine that has been reported in the literature to be produced by activated microglia and astrocytes [297–301], was also found in the analysis to be widespread in the images acquired. Although there was more IL-1 β signal coverage in the 0 mA groups compared to 0.4 mA even when the full frame of the images ($734.05 \mu\text{m} \times 734.05 \mu\text{m}$) was analyzed (Figure 3-8I), this did not necessarily translate to there being statistically significant differences in IL-1 β fluorescence intensity among the different experimental groups involved (Figure 3-8E). No differences among the different experimental groups were found in terms of fluorescence intensity for the other biomarkers examined (Figures 3-8B, 3-8C, 3-8D) either. The current modification data generated suggests that, even at a physiologically appropriate range and level of electrical stimulation [302], increasing electrical current is capable of decreasing biomarker area coverage but not fluorescence intensity.

In the waveform modification study, the data suggest that the rectangular and ramped waveforms produced the strongest glial cell response compared to the control condition. A statistically significant decrease in cell density versus control was found for these two waveform shapes within $50 \mu\text{m}$ from the electrode tip (Figure 3-9A). Hoechst, EGFP, and IL-1 β area coverage also suggest localized (up to $100 \mu\text{m}$ from the electrode tip) decreases in biomarker

area coverage compared to control when using a rectangular or ramped waveform (Figures 3-9F, 3-9G, 3-9I). Like with the current modification data, stimulating glial cells using modified waveform shapes has a more pronounced impact on microglia than astrocytes as far as biomarker area coverage is concerned. The only significant differences seen in the biomarker fluorescence intensity data was for IL-1 β , which showed ramped waveforms inducing a higher degree of IL-1 β expression compared to control at a range of within 100 μ m from the tip of the electrode. The findings of this study on varying waveform modifications contrasts with a recent report by Lennikov et al. which found a diminished level of microglia activation when exposed to an electrical field of a ramped waveform [157]. However, several key differences exist which may explain the contrasting results between that study and the data reported herein including the usage of BV-2 cell lines and the application of an electrical field across the generated cell cultures as opposed to examining the cells at the electrode-cell culture interface. Furthermore, the data presented in Figure 3-9 contrast with the hypothesis that the ramped waveform would be the least damaging paradigm in the experiment given that it delivered a smaller amount of electrical charge per phase (15 nC/ph) compared to the rectangular (30 nC/ph) and sinusoidal (23.56 nC/ph) waveforms. Aside from the total amount of charge that is delivered per phase, the rate at which charge is being delivered to the cells may also influence the way in which they respond. The rate of charge delivery is more gradual for sinusoidal stimulation compared to rectangular and ramped stimulation, which feature sudden and steeper increases in charge delivery, respectively. The data presented here suggest that, of the three waveform shapes examined, a sinusoidal waveform would be the least detrimental in terms of either ablating cells away from the electrode interface or otherwise upregulating pro-inflammatory cytokines in the cells that do remain.

The frequency modification study varied stimulation frequencies between 25 Hz and 55 Hz. It has been reported in the literature that different groups of neurons in various parts of the CNS are best activated using specific frequencies [303–307]. However, the effects of varying stimulation frequency on glial cell behaviour remain not well understood. The range of frequencies selected for the experiments performed in this chapter are considered within the low-frequency range of CNS electrical stimulation modalities [308,309]. Functional electrical stimulation following spinal cord injury, which is the application from which the stimulation paradigm used in this chapter was adapted, typically uses stimulation frequencies of 20-30 Hz for efficient activation of motor neurons [96,310]. From the immunofluorescence data analyzed, a higher stimulation frequency (55 Hz) resulted in a higher cell density compared to a lower frequency of 35 Hz – this difference was seen closer to the tip of the electrode at $r = 50 \mu\text{m}$ (Figure 3-10A). This observation correlates with the EGFP area coverage signal traces in the live imaging work (Figure 3-4D) – there, at $r = 50 \mu\text{m}$, decreases in microglia coverage were much greater at lower frequencies compared to at 55 Hz which suggests that stimulating at that frequency is less detrimental to microglia at the interface compared to stimulation at 25, 35, and 45 Hz. This is contrary to the hypothesis that a higher frequency would result in a higher degree of cell reactivity or cell death since a higher stimulation frequency entails more charge cycling in a given period of time, thus resulting in more stress placed on the cells. Resonance, which describes how an external stimulus at certain frequencies can cause an object to vibrate more intensely, may play a role in causing a greater amount of cell death to occur when going from 25 to 45 Hz. At that range of frequencies for electrical stimulation, the cells may be more susceptible to having their membranes ruptured. Because the glial cells used in the experiment come from whole mouse brains, resonance frequencies may vary depending on the region of the

CNS being examined due to heterogeneity in glial cell characteristics [311]. There also exists literature describing electrical stimulation of various locations in the CNS (e.g., hippocampus, subthalamic nucleus, spinal cord) using frequencies of >100 Hz thus suggesting efficacy in using higher frequencies without adverse long-term effects [312–317]. In the immunolabelled image data, no other statistically significant differences were found in terms of biomarker fluorescence intensity and area coverage between the different frequencies tested, across different distances from the electrode tip (Figures 3-10B-E, F, H, I). Taken together, the data produced in the frequency modification study suggest that frequency, for the most part, neither exacerbates nor attenuates glial cell activity compared to a no stimulation (0 Hz) condition.

3.6.3. Electrode damage analysis

Following stimulation experiments, it was also of interest to assess any damage that the platinum-iridium electrodes had sustained as a result of modifying electrical stimulation parameters. SEM allows for inspection of the deinsulated tip for any damage or deposits as a result of the cell culture experiments performed. Similar to the 0 mA and 0.15 mA electrodes from the previous chapter, evidence of organic deposits were seen on the electrodes employed in each of the modification studies described in this chapter. The 0 mA wires (current modification study, Figure 3-11A), control wires (waveform shape study, Figure 3-12A), and 0 Hz wires (frequency study, Figure 3-13A), all qualitatively had larger amounts of organic deposits on the deinsulated tips compared to the other experimental groups in their respective studies. The SEM images acquired already suggest that electrical stimulation, regardless of the modification

applied to the stimulation paradigm, is capable of reducing the amount of organic matter on the deinsulated surface of the electrode without visually damaging or corroding the electrode itself.

In addition to SEM, EDS allows for the measurement of the elemental composition of the surface of a sample. From the EDS scans performed, no significant differences were found across the vast majority of the elements surveyed (Pt, Ir, Na, Cl, C, N, O, P, S). The selection of elements scanned was adapted from the experimental design of the previous study – in the current chapter, however, phosphorous and sulphur were also scanned to account for the presence of additional biomolecule residue (nucleic acids) that may be on the surfaces of the electrodes. Across the three modification studies performed, no statistically significant differences were found among any of the stimulation parameters tested (Figures 3-11C, 3-12C, 3-13C). The exceptions to this finding were for phosphorus and sulphur in the current modification study – larger amounts of phosphorus were found at 0.1 mA compared to 0.4 mA, and larger amounts of sulphur were found at 0.2 mA compared to 0.3 mA. Taken together, the SEM and EDS data generated across the different experiments performed suggest that modification of stimulation parameters (current, waveform shape, frequency), to the extent defined in the experiments in this chapter do not result in damage to the electrode following 4 h of stimulation.

3.6.4. Limitations of study

The study described in this chapter is a high-throughput *in vitro* setup designed to assess glial cell reactivity and electrode damage to various electrical stimulation parameters before

potential *in vivo* or clinical work. As it is a continuation of the work described in the previous chapter, it also inherits its shortcomings (e.g., limited space for growth in each cell culture well, lack of stab injury replication). The mixed glial cell cultures generated used cells taken from the entire postnatal day 2 mouse brains – although it allows for the ‘global averaging’ of the glial cell response in response to stimuli in an *in vitro* environment, for future work it may be advantageous to further tease out the heterogeneity of responses of glial cells depending on which region of the CNS they originate from [311]. Because of the way in which the work described in this chapter was carried out, namely live imaging over a 4 h timecourse, the results produced from the experiments in this chapter paint a very limited window in the temporal response of the glial cell cultures in response to the parameter modifications used. Because live imaging entails removal of cell culture plates from the incubator for several hours to an imaging space that is at room temperature, results generated in this chapter cannot necessarily be compared 1-to-1 to data generated in the previous chapter. Additional live imaging sessions of the same cultures, for example over several days, would be able to provide additional information on how factors such as EGFP signal, biomarker responses and electrode damage play out as the acute phase of the glial scarring process unfolds. Live imaging was also done only on microglia in this work given the nature of the transgenic mouse breed that was employed in the experimental design. Although comparisons of microglia versus astrocyte response were inferred from the immunofluorescence data, it would also be worthwhile to capture live astrocyte responses to electrical stimulation by, for example, employing a murine strain that expresses a fluorescent protein under the GFAP reporter gene [318–321]. For the SEM/EDS analysis, the high carbon readings taken from all of the electrodes across the different studies can, like in the previous chapter, be attributed to the fixation and immunolabelling process applied to each cell

culture plate following an electrical stimulation experiment – electrodes were extracted only after immunolabelling and fluorescence microscopy of each well was completed. Additionally, it would be of interest to determine whether the statistically significant differences in phosphorus and sulphur concentrations found in the current modification study, as well as atomic concentrations of other non-metallic elements, can be attributed to differing amounts of biomolecules present on the surfaces of the electrodes, or whether they are from residue from storage in PBS or immunolabeling material – follow-up work with mass spectrometry, for example, may be able to answer this question [322–325].

3.7. Conclusions

This chapter builds on the work described in the previous chapter and other *in vitro* works described in the literature by assessing glial cell responses to both the presence of the electrode as well as any applied electrical stimulation. The experiments in this chapter were designed to address how glial cells respond to electrical stimulation paradigms modified in terms of current, waveform shape, and frequency. In the pursuit of this objective, a secondary objective was also defined to determine the fate of glial cells located at or near the electrode interface from electrical stimulation using live cell imaging. EGFP signal traces showing microglial responses at the electrode interface during 4 h live imaging experiments were also calculated. Finally, SEM/EDS data generated allowed for the comparison of any damage sustained by electrodes as a result of the stimulation paradigms tested.

Localized responses to the live imaging and immunofluorescence metrics defined were found to varying degrees. EGFP signalling traces from the live imaging data suggest that increasing stimulation current up to 0.4 mA does decrease microglial area coverage by the electrode interface, and that this effect diminishes when farther away from the electrode interface. EGFP signal traces did not differ statistically between different waveform shapes tested. When stimulation frequency was tested, however, a lesser degree of microglia loss was observed at the electrode interface with a 55 Hz paradigm compared to lower frequencies used. The finding of lesser microglia loss at 55 Hz was also corroborated with the cell density data from immunofluorescent image analysis. In addition, immunofluorescent image analysis determined that increasing current reduced biomarker area coverage in cells but did not influence biomarker fluorescence intensity. Analysis of immunolabeled cell cultures stimulated using different waveform shapes suggests that sinusoidal waveform stimulation results in a lesser amount of cell loss and changes in biomarker fluorescence intensity and area coverage when compared to rectangular and ramped waveforms. Finally, SEM and EDS analyses of the electrodes for potential damage and surface composition change as a result of modifying waveform parameters did not turn up any significant changes in elemental compositions for Pt, Ir, Na, Cl, C, N, O, P, S nor was there any evidence of surface degradation/corrosion on the deinsulated tips. A more detailed appreciation for the electrochemical performance of the electrodes resulting from stimulation, however, would be best acquired with follow-up experiments (Chapter 4) – in other words, it would be of interest to learn about the phenomena taking place at the electrode-cell culture interface that may be causing the cells to react the way they do.

By continuing to expand on the work done in this chapter (e.g., increase timecourse of experiments to several days, test more stimulation parameters – pulse width, interpulse delay, charge balancing, anodic-first stimulation), a more fulsome picture of how glial cells respond to varying stimulation parameters over time in the context of mounting an inflammatory response against a functional microelectrode implant and glial scarring can be captured. The main advantage of carrying out such work in an *in vitro* environment is that a substantial amount of high-throughput work can be done at a reduced cost in terms of animal lives. By creating this additional methodology/platform with which neuroscientists and device developers can test varying designs of neural interface devices before potential translation to *in vivo* applications and beyond, time and resources can be more efficiently devoted to further refining more promising design iterations that are biocompatible, safe, and longer-lasting in patients.

4. Chapter 4 – Contributions of mixed glial cell culture components on the *in vitro* electrochemical performance of platinum-iridium microelectrodes

4.1. Preface

The work presented in this chapter would not have been possible without the assistance of Soroush Mirkiani, who provided technical assistance with the experimental setup and data collection described in the chapter. SM supplied the MATLAB code which was used to analyze raw data in this chapter. Christopher Tsui designed the experiments, performed the experiments, collected and analyzed data, and wrote the contents of the chapter in its entirety.

4.2. Abstract

Electrically-stimulating microelectrodes in a biological setting are capable of causing damage to nearby cells. Repeated rounds of stimulation over long time courses may result in unintended changes to the local environment around an invasive microelectrode implant and have implications on the biocompatibility and longevity of a neural interfacing device. A description of the phenomena that are taking place at the electrode-cell culture interface is thus required for the 75 μm diameter platinum-iridium microelectrodes with the goal of providing context into why and how electrical stimulation occurs in mixed glial cell cultures. Specifically, the potential contributions that certain parts of the cell cultures have on the electrochemical performance of the platinum-iridium microelectrodes are of interest. Using cyclic voltammetry,

electrical impedance spectroscopy, and voltage transient analysis, microelectrode performance in various electrolytes (PBS, DMEM F12, DMEM F12 + FBS + PS, live cell cultures) was assessed. Cyclic voltammetry measurements yielded cathodic charge storage capacity values that were lower in magnitude in cell culture media ($-1356 \mu\text{C}/\text{cm}^2 \pm 221 \mu\text{C}/\text{cm}^2$, 50 mV/s) compared to PBS ($-2982 \mu\text{C}/\text{cm}^2 \pm 404 \mu\text{C}/\text{cm}^2$, 50 mV/s) – a result that is likely attributed to amino acids and larger proteins present in cell culture media fouling the surfaces of the microelectrodes and making less physical area available on the electrode for electrode-electrolyte charge transfer. Impedance ($7838 \Omega \pm 1264 \Omega$, 1 kHz) and phase angle measurements ($-62.68^\circ \pm 3.81^\circ$, 1 kHz) for cell culture media also support the observations made in cyclic voltammetry. However, integrating live glial cells with the cell culture media suggests that they serve as a conductive layer (i.e., reduce impedance and improve charge storage capacity). Voltage transient analysis showed that the threshold for electrolysis of water is reached sooner for cell culture media at lower currents when compared to PBS. The presence of cells, however, acts as a voltage buffer thus making electrical stimulation at higher currents possible ($\sim 200\text{-}250 \mu\text{A}$) without breaching the water window as soon compared with just cell culture media ($\sim 100\text{-}150 \mu\text{A}$). The methods described in this chapter are well-suited for describing the impact that electrical stimulation has at the electrode-electrolyte interface for platinum-iridium microelectrodes in cell culture, and pave the way for further predictive testing into the potential service life of microelectrodes.

4.3. Introduction

Electrical stimulation of the brain and spinal cord using devices designed to interface with the central nervous system (CNS) is an established field of study, with many examples

existing of neural interfacing devices successfully alleviating functional deficits arising from a person's neurological injury or disease [326–329]. Invasive neural interfacing devices which make use of electrodes designed to penetrate into CNS tissue are advantageous in that they allow for acute, specific activation of target neurons [185,260,330].

Although invasive neural implants have the advantage of high stimulation target specificity, their physical proximity to the target tissue is also their drawback. Such implants are subject to neuroinflammation and the foreign body response that is brought on by glia, the regulatory cells of the CNS [331–333]. These events will eventually lead to the formation of a glial scar around an implanted electrode over the course of many weeks [222,334,335]. The presence of the glial scar acts as a double-edged sword – while it serves as a physicochemical barrier around an implant to prevent further cell death that would have been initially caused by insertion into tissue (i.e., a stab wound), it also is detrimental in that it prevents nearby neurons from accessing the implant for either recording or stimulating purposes.

Because of this issue that glial scarring presents to electrode implants in CNS tissue, it is important to devise ways in which to mitigate the glial scarring phenomenon and attenuate glial cell reactivity to the presence of the electrode implants [277,336]. The literature on improving biocompatibility of invasive neural electrode implants into CNS tissue has largely focused on modifying glial cell responses to the implant itself. However, to more accurately appreciate and gauge the responses of glia to these implants it is also important to assess their responses to electrical stimulation. Electrical stimulation, along with neuronal signal recording, are possible features of such implants. The field of literature that examines the effects of electrical stimulation as they relate to glial cell reactivity is limited [112,127,157]; therefore, there exists an opportunity to expand on this field of study and generate information on glial cell reactivity to

functional electrode implants that will aid device development and engineering efforts to improve on their biocompatibility and longevity in humans.

In the previous chapter, primary mixed glial cell cultures were used to explore the effects of electrical stimulation parameter modifications (current, waveform shape, frequency) on glial cell reactivity. Live cell imaging of EGFP-positive microglia revealed that cells at close proximity to the deinsulated electrode tip ($< 50 \mu\text{m}$) died as a result of 4 h of electrical stimulation. Follow-up post-fixation immunolabelling of the cell cultures suggests that increasing stimulation current results in a greater amount of cell death near the electrode. Of the three waveform shapes investigated (rectangular, sinusoidal, ramped), the sinusoidal waveform was inferred to have caused the least amount of cell death at the electrode interface. When stimulation frequency was modified, it was found that electrically stimulating glial cells at 55 Hz resulted in less cell death compared to stimulation at lower frequencies (25 Hz, 35 Hz, 45 Hz). Taken together, the data presented in the previous chapter demonstrate the significant impact that stimulation parameter modification has on the reactivity and fate of cells at an electrode interface.

In Chapters 2 and 3, attention was also paid in part to the effect that the electrical stimulation experiments had on the $75 \mu\text{m}$ platinum-iridium microwires themselves. In Chapter 2, for example, stimulating at a very high current of 1.5 mA resulted in a highly deformed surface of the deinsulated tip of the microwires. This, coupled with statistically higher readings of oxygen versus a lower current condition of 0.15 mA, suggests that a sufficiently high current is able to irreversibly oxidize the surface of the microelectrode's platinum-iridium alloy. In Chapter 3, none of the stimulation parameter modifications tested resulted in corrosion of the electrode tips nor did it result in higher concentrations of oxygen on the surfaces of the

electrodes. Platinum and iridium are considered to be noble metals, meaning that they are not expected to oxidize unless in cases of high current. However, cells were still observed to have died at the interface from the stimulation paradigms applied.

It is therefore of interest to further investigate the capabilities of the platinum-iridium microwires in their current design and dimensions, and ascertain the limits to which they can be pushed before irreversible oxidation occurs. It is also of interest to identify the electrochemical reactions that are occurring at the interface – this will allow for the identification of compounds that may be produced at the interface as a result of electrical stimulation, and whether or not such compounds are cytotoxic or otherwise detrimental to cell health. To investigate these objectives using the *in vitro* cell culture model presented thus far in the thesis, electrochemical analyses were performed on 75 μm microelectrodes embedded in 12-well cell culture plates. By using well-established electrochemistry methods for evaluating neural electrodes [145,162,164,337–339], the contributions of components of the cell culture (e.g., glial cells, cell culture media ingredients) to the electrochemical properties of the microelectrodes can also be ascertained. Understanding the electrochemical mechanisms underlying electrical stimulation in cell culture using these microelectrodes will provide additional information as to their safety and efficacy prior to potential insertion into tissue for *in vivo* work or clinical trials.

4.4. Materials and methods

4.4.1. Materials

Dulbecco's Modified Eagle Medium: Nutrient Mixture F12 (DMEM F12), Hank's Balanced Salt Solution (HBSS), fetal bovine serum (FBS), penicillin streptomycin (PS), 0.25% trypsin-ethylenediaminetetraacetic acid (Trypsin-EDTA), and Equine Serum (ES) were purchased from Gibco (Life Technologies, Burlington, ON, Canada). Poly-L-lysine hydrobromide (PLL) was purchased from Sigma Aldrich (St. Louis, MO, USA). Polystyrene 12-well cell culture plates were purchased from Greiner Bio-One (Frickenhausen, Germany). Cell culture flasks (75 cm²) were purchased from Corning (Corning, NY, USA). Sylgard 184 polydimethyl siloxane (PDMS) kit was purchased from Dow Chemical (Midland, MI, USA). Phosphate buffered saline tablets were purchased from BioShop (Burlington, ON, Canada).

Microwires (75 μm diameter, Pt-Ir 80%/20% insulated with polyimide) for microelectrode fabrication were purchased from California Fine Wire (Grover Beach, CA, USA). Teflon-insulated, 9-strand stainless steel wires (304.8 μm diameter) (Cooner AS632) were purchased from Cooner Wire Company (Chatsworth, CA, USA).

4.4.2. Cell culture preparation

Animal protocols were approved by the Animal Care and Use Committee at the University of Alberta and conducted in accordance with the guidelines of the Canadian Council for Animal Care. Mixed glial cell cultures were generated from the brain tissue of postnatal Day

2 C57BL/6J CX3CR-1^{+EGFP} heterozygous transgenic mice [188]. The mice were decapitated and their brains removed using surgical scissors and a metal spatula. Following dissection of the meninges using forceps, the remaining brain tissue was dissociated in 0.25% Trypsin-EDTA at 37 °C for 25 minutes. The Trypsin mixture was then centrifuged twice at 500 g for 2 min and triturated in cell culture media (DMEM F12/10% FBS/1% PS) to further dissociate brain tissue and deactivate residual Trypsin-EDTA. The resulting cell suspension was placed in 12-well plates coated with PLL (2 µg/mL). Cells were incubated for 2 weeks at 37 °C and 5% CO₂, with cell culture media changed twice weekly.

At 2 weeks, mixed glial cells were washed with DMEM F12 and then lifted off from the 12 well plates with a Trypsin-EDTA and DMEM F12 mixture (1:3 ratio) treatment for 25 min [189]. The cells were then collected and subjected to two-fold centrifugation at 500 g for 2 min and trituration in cell culture media. The resulting cell suspension was then passed through a syringe and needle, and plated in a 75 cm² flask at a ratio of 1 plate:1 flask. The flask cultures were then incubated for 1 week at 37 °C and 5% CO₂ prior to another round of isolation and re-seeding onto microelectrodes, with cell culture media changed twice in that week.

4.4.3. PDMS ring fabrication

To stabilize electrode placements in the 12-well plates, custom polydimethyl siloxane (PDMS) rings were created to prevent movement of the wires within the wells. PDMS elastomer base and curing agent were mixed together in a 50 mL tube in a 10:1 ratio, and left to set in the wells of a 12-well plate (2 g/well). Following curing for 2.5 hours in an oven at 70 °C, the

resulting PDMS discs were extracted from the wells, hole-punched, and placed in a large 3 L beaker (50% methanol/50% water) under a fume hood overnight to wash out any unreacted monomers leftover from the curing process. Following this, the rings were submerged in water and autoclaved in preparation for use in cell culture.

4.4.4. Microelectrode fabrication

Platinum-iridium microwires (75 μm diameter) were used for fabrication of microelectrodes. Briefly, microwires were cut ~ 15 cm in length. The insulation layer of the microwire tips was removed using nanosecond laser pulses (wavelength = 248 nm, energy = 150 mJ, beam attenuation = 5%, repetition rate = 10 Hz; COMPex 110, Coherent, CA, USA). The deinsulated region of the microwires was cut using a scalpel blade leaving 300-400 μm of bare metal at the tip. The tips of the microwires were then mechanically bevelled using a microelectrode beveler (BV-10, Sutter, CA, USA) to an angle of approximately 15° . Microelectrodes were then placed in 15 mL centrifuge tubes (Fisherbrand, Pittsburgh, PA, USA) filled with DI water and Alconox detergent, and treated in an ultrasonic cleaner for 30 minutes to remove the metal debris formed during the mechanical polishing step. The microelectrodes were then sonicated for another 30 minutes in DI water and rinsed with 70% ethanol. Stranded stainless steel wires were manually deinsulated to expose approximately 4-5 cm and were used as the counter electrodes.

4.4.5. Electrode plate setup

Insertion of microelectrodes into the PDMS rings and placement of the rings into the 12-well plates was all done within the aseptic environment of a biosafety cabinet. An 18.5G needle was used to puncture a hole through the side of a ring at a 45° angle. A 10 µL pipette tip was then fitted through the hole, and a microelectrode was threaded through the pipette tip such that the deinsulated end of the wire lay in the inner hole of the PDMS ring. The pipette tip was then withdrawn to effectively embed the insulated portion of the microelectrode in the side of the ring. The ring and microelectrode were then dipped in 70% ethanol, placed in one of the wells of a 12-well plate, and left to dry to form a sterile seal in the well. This also allowed the deinsulated tip of the wire to make contact with the bottom of the well. Tape was then used to hold down the insulated portion of the electrodes over the edge of the 12-well plate to prevent further movement. Counter electrodes were placed on top of the PDMS rings and taped down over the edge of the plate on the day of the experiment.

Cells were isolated from the flask as above using diluted Trypsin-EDTA/DMEM F12, seeded at a density of 70000 cells/well, and left to settle and incubate for 7 days at 37 °C and 5% CO₂ prior to the start of electrical stimulation. Cell culture media (DMEM/10% FBS/1% PS, 2 mL/well) was changed twice during the 7-day incubation period.

4.4.6. Electrochemistry analyses

Electrochemistry experiments were conducted using a MET16 Electrode Analyzer potentiostat (Sigenics, Chicago, IL, USA). 12-Well plates with microelectrodes (and without

cells) were prepared and filled with 2 mL/well of PBS, DMEM F12 (Plain DMEM), or cell culture media (DMEM F12/10% FBS/1% PS). Live cell culture plates with microelectrodes and cell culture media (2 mL/well) were also prepared as described above (4.4.5. Electrode plate setup).

Cyclic voltammetry (CV) experiments were carried out using a fast ramp rate (50 V/sec) and slow ramp rate (50 mV/sec) between -0.6 V and +0.8 V versus an Ag|AgCl reference electrode. A total of 10 CV cycles were recorded at both ramp rates with a dwell time of 2 seconds. Cathodic charge storage capacity (CSC_c) values were calculated by integrating the area under the resulting current-voltage loops at < 0 A. Electrical impedance spectroscopy (EIS) was conducted at a frequency range of 1-10000 Hz, with values for impedance and phase angle reported at 1000 Hz. Voltage transient analysis (VT) was conducted using cathodic-first biphasic rectangular pulses ranging between 50-250 μ A, with a cathodic pulse duration of 200 μ s, interphase duration of 100 μ s and prepulse duration of 400 μ s. Raw data from all analyses were processed through custom MATLAB (Mathworks, Natick, MA, USA) coding scripts for calculating cathodic charge storage capacity for CV, impedance and phase angle at 1000 Hz for EIS, and maximum cathodic voltage excursions for VT.

4.4.7. Scanning electron microscopy

Qualitative assessment of damage to electrodes was carried out using a ThermoFisher Phenom XL Desktop scanning electron microscope (SEM) (Waltham, MA, USA). Images were acquired using backscattered electron detection at 610x and 4000x magnification. Dimensions of

each individual microelectrode tested was measured for the purpose of calculating surface area and charge density.

4.4.8. Statistical analyses

All experiments were analyzed with a sample size of six ($n = 6$). Statistical analyses for cyclic voltammetry and electrical impedance spectroscopy consisted of a one-way analysis of variance (one-way ANOVA) with Tukey's *post hoc* test comparing data means by electrolyte used. Voltage transient analysis data was further compared by stimulation current using a two-way analysis of variance (two-way ANOVA) with Bonferroni's *post hoc* test. These analyses were performed using GraphPad Prism 10 (San Diego, CA, USA).

4.5. Results

Platinum-iridium microelectrodes (75 μm diameter) were fabricated, inserted into cell culture wells, and underwent electrochemical testing to determine their behaviour in different *in vitro* electrolytes (PBS, plain DMEM, DMEM + FBS + PS, and cell culture).

4.5.1. Cyclic voltammetry

Cyclic voltammetry data was generated using a fast voltage ramp rate (50 V/s, Figure 4-1) and a slow voltage ramp rate (50 mV/s, Figure 4-2). The deinsulated tips of the electrodes used were determined to have a surface area of $95792 \mu\text{m}^2 \pm 9759 \mu\text{m}^2$ ($n = 24$) using the formula for surface area of a cylinder with an angular cut at the top:

$$SA = \pi r(r + a + h_1 + h_2)$$

where r is the cylindrical radius, h_1 is the short height of the cylinder, h_2 is the long height of the cylinder and a is the semi-minor axis at the angular top-cut that is further defined by the following formula:

$$a = \sqrt{r^2 + \left(\frac{h_2 - h_1}{2}\right)^2}$$

CSC_c values for both fast and slow scan data were normalized to the surface area of the deinsulated tips of each electrode fabricated, and were calculated to be approximately an order of magnitude in difference. In the fast scan data, a one-way ANOVA did not compute any

statistically significant differences between the different electrolytes analyzed. However, in the slow scan data, a one-way ANOVA did detect a statistically significant difference, with *post hoc* analysis revealing significant differences between PBS and plain DMEM, and PBS and DMEM + FBS + PS.

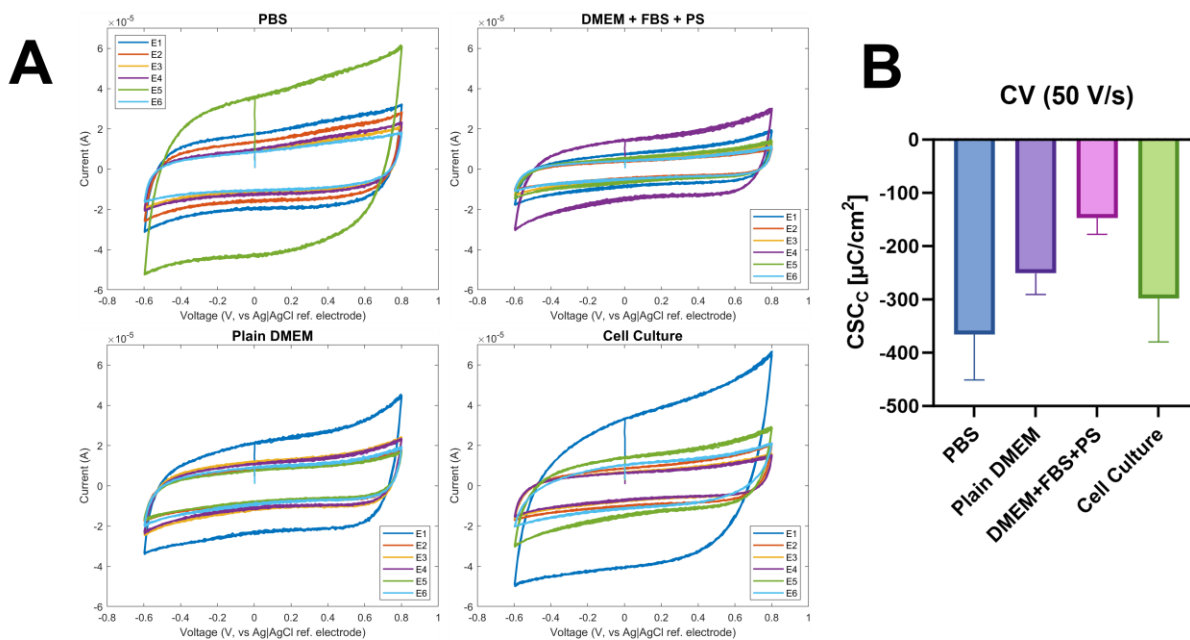


Figure 4-1: Cyclic voltammograms of Pt-Ir microelectrodes immersed in different electrolytes (50 V/s)

(A) Each curve seen on the cyclic voltammograms corresponds to one of six electrodes tested in that specific electrolyte. (B) Cathodic charge storage capacity (CSC_c) values were calculated for each electrolyte ($n = 6$, one-way ANOVA with Tukey's *post hoc* test). * $p < 0.05$; Data = means \pm SEM.

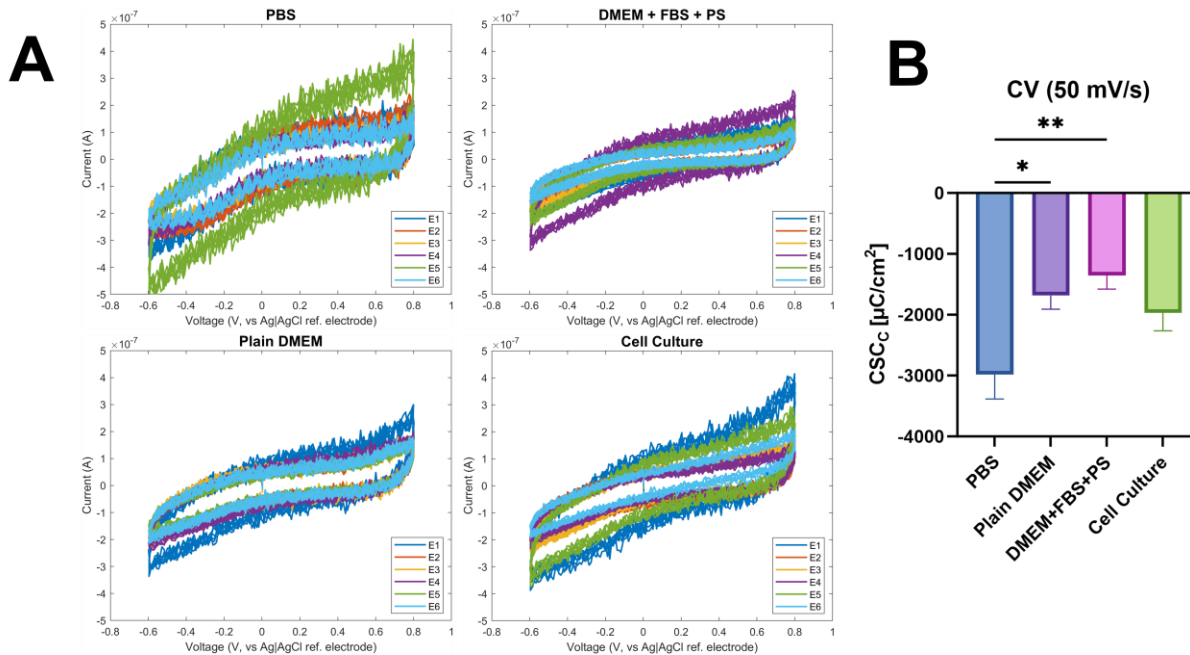


Figure 4-2: Cyclic voltammograms of Pt-Ir microelectrodes immersed in different electrolytes (50 mV/s)

(A) Each curve seen on the cyclic voltammograms corresponds to one of six electrodes tested in that specific electrolyte. (B) Cathodic charge storage capacity (CSC_c) values were calculated for each electrolyte ($n = 6$, one-way ANOVA with Tukey's *post hoc* test). * $p < 0.05$, ** $p < 0.01$; Data = means \pm SEM.

4.5.2. Electrical impedance spectroscopy

EIS scans computed for impedance (Figure 4-3) and phase angle (Figure 4-4) at a frequency of 1000 Hz. For impedance, statistically significant differences were observed between PBS and DMEM + FBS + PS, and between plain DMEM and DMEM + FBS + PS. For phase angle, *post hoc* analysis revealed statistically significant differences between the PBS and DMEM + FBS + PS group.

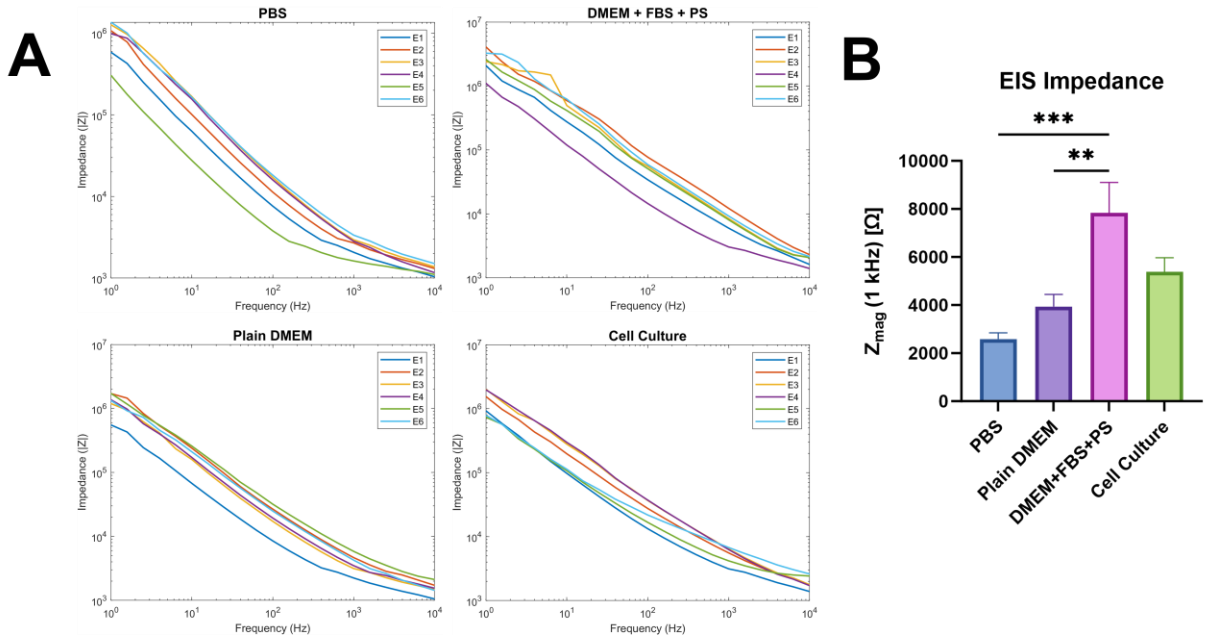


Figure 4-3: EIS Bode plots of Pt-Ir microelectrodes immersed in different electrolytes

(A) Each curve seen on the Bode plots corresponds to one of six electrodes tested in that specific electrolyte. (B) Impedance at 1 kHz was recorded (n = 6, one-way ANOVA with Tukey's *post hoc* test). *p < 0.05, **p < 0.01, ***p < 0.001; Data = means ± SEM.

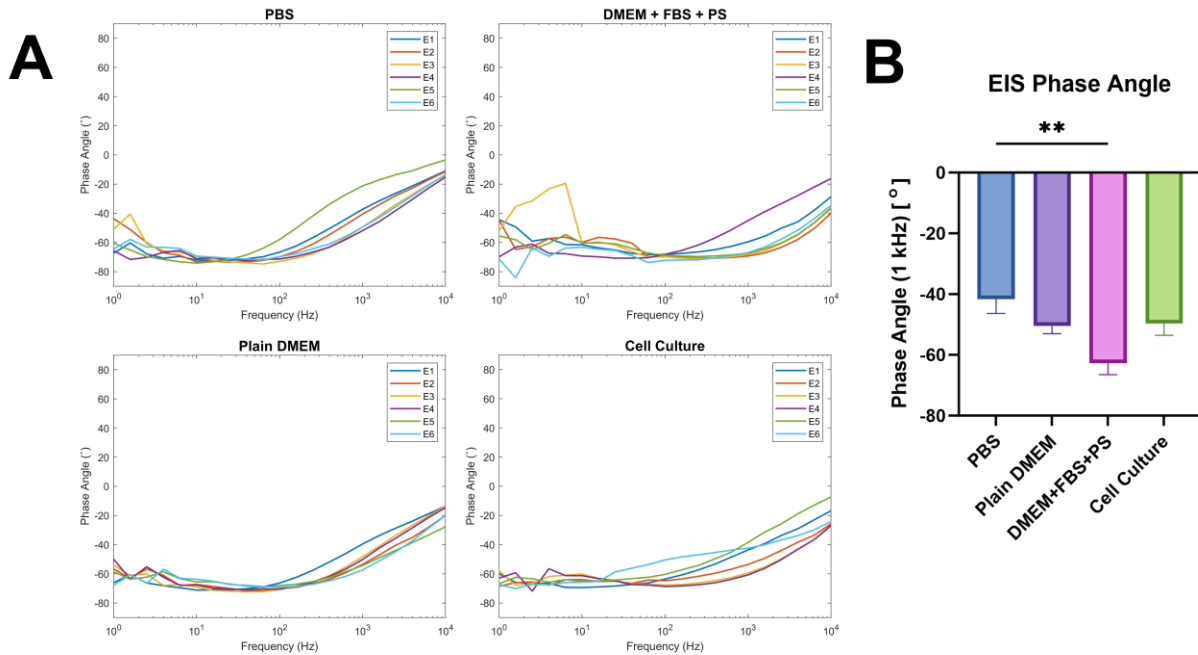


Figure 4-4: EIS phase angle-frequency plots of Pt-Ir microelectrodes immersed in different electrolytes

(A) Each curve seen on the phase angle-frequency plots corresponds to one of six electrodes tested in that specific electrolyte. (B) Phase angle at 1 kHz was recorded ($n = 6$, one-way ANOVA with Tukey's *post hoc* test). * $p < 0.05$, ** $p < 0.01$; Data = means \pm SEM.

4.5.3. Voltage transient analysis

Electrode plates were also subjected to voltage transient analysis whereby biphasic rectangular pulses of varying currents were injected into the electrode-electrolyte setups and the resulting voltage-time responses recorded. The maximum cathodic voltage excursion (E_{mc}) was then calculated for each voltage-time curve (Figure 4-5) and compared against the lower limit of the water window (-0.6 V vs. Ag|AgCl). Following a two-way ANOVA and *post hoc* analysis, where the independent variables analyzed were pulse current and electrolyte type, statistically significant differences were found between PBS and DMEM + FBS + PS for all pulse currents examined, as well as additional significant differences between PBS and cell cultures at 200 μA and 250 μA .

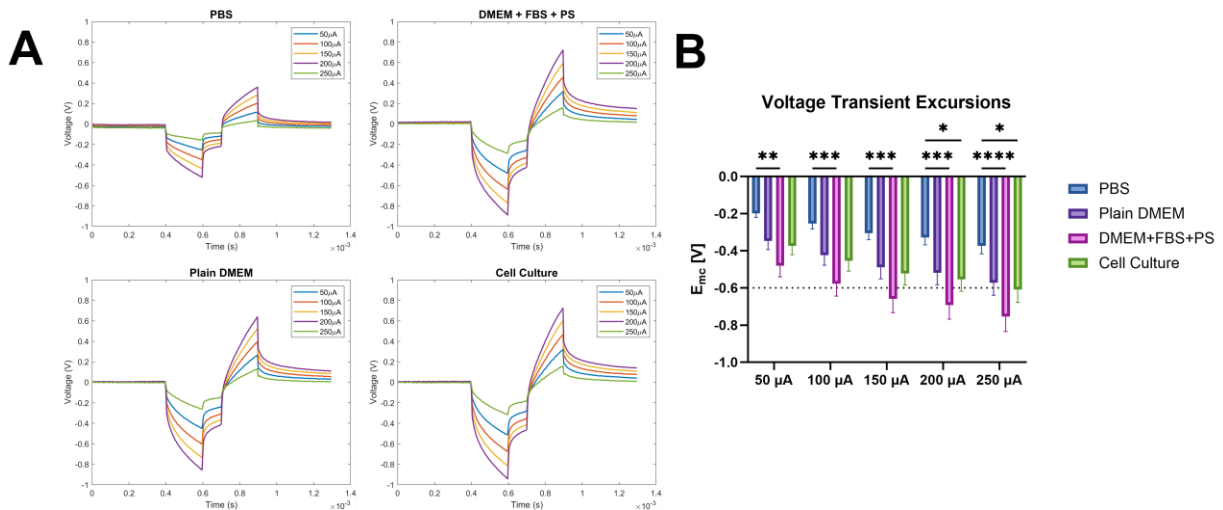


Figure 4-5: Voltage transient response curves for Pt-Ir microelectrodes immersed in different electrolytes

Pulses applied ranged from 50 μA to 250 μA . From each curve (A), the maximum cathodic voltage excursion (E_{mc}) was calculated (B) ($n = 6$, two-way ANOVA with Bonferroni *post hoc* test). * $p < 0.05$, ** $p < 0.01$, *** $p < 0.001$, **** $p < 0.0001$; Data = means \pm SEM. Voltage transient curves shown are from one representative electrode in each electrolyte tested. The lower limit of the water window (-0.6 V) is depicted as a horizontal dotted line on the bar graph for reference.

4.6. Discussion

The purpose of the study defined in this chapter was to describe the electrochemical mechanisms through which 75 μm platinum-iridium microelectrodes behave *in vitro* when being used in the electrode cell culture setups mentioned thus far in the thesis. Electrochemical performance of the electrodes in the electrolytes presented in the chapter was assessed via cyclic voltammetry (CV), electrical impedance spectroscopy (EIS), and voltage transient analysis (VT). By comparing how responses in CV, EIS, and VT differ in the presence of the electrolytes tested, one can determine the contributions of key components of live cell cultures towards the electrochemical performance of the microelectrodes.

Platinum and iridium are commonly-used materials for neural electrode applications [340–344]. The counter electrodes used in the thesis are made of stainless steel and are much larger compared to the platinum-iridium microelectrodes (308.4 $\mu\text{m} > 75.0 \mu\text{m}$ diameter). When the surface area of the counter electrode is much larger than that of the microelectrode as is the case in the experimental designs presented in this work, the capacitance of the counter electrodes is

also much greater than that of the microelectrodes. This, in turn, also means that the counter electrodes' contribution to impedance in the system is comparably negligible versus that of the microelectrodes which is important for the purposes of EIS.

In the work presented throughout the thesis, mixed glial cell cultures were used as the basis for a high-throughput *in vitro* system designed to rapidly test various functional electrode designs and model the acute phase of the glial scarring phenomenon. For culturing primary mixed glial cells, DMEM F12 media is used; this is a media formulation that has been used extensively for a wide range of primary mammalian cell and cell line cultures [345–348]. Additional supplementation in the form of fetal bovine serum (FBS) is also common for culturing of glial cells as a nutritional and growth factor supplement that would otherwise not be present in DMEM F12 on its own [349–352]. In the case of the mixed glial cell cultures used in this work, DMEM F12 is supplemented with 10% FBS and 1% of penicillin-streptomycin (PS), an antibiotic additive to prevent bacterial contamination of the cultures.

4.6.1. Cyclic voltammetry

Cyclic voltammetry is an established electrochemical analysis technique that measures voltage-current responses based on reduction and oxidation reactions that take place at an electrode-electrolyte interface [353]. Voltage is swept in a linear fashion and current is allowed to flow between the electrode of interest (in this case, the Pt-Ir microelectrode) and the stainless steel counter electrode. Plotting voltage-current responses from CV measurements gives insight

into the presence of any electrochemical reactions happening at the interface, the stability of the electrode material, and its capability to store electrical charge [145].

Charge storage capacity refers to the total amount of electrical charge available per unit surface area on an electrode for injection into a stimulation pulse [145]. In the context of the work that is being done, cathodic charge storage capacity (CSC_c) specifically refers to the Pt-Ir microelectrode as it is the electrode of interest. CSC_c is mathematically calculated by integrating the area under a CV voltage-current curve for currents below 0 A. The CSC_c values calculated from the CV data suggest the extent to which the microelectrode is able to hold electrical charge when immersed in a specific electrolyte. CSC_c values calculated were done so in CV data ranging between -0.6 V to +0.8 V versus an Ag|AgCl reference electrode as that is the voltage range at which water will not electrolyze (i.e., the water window) [354].

When a fast voltage ramp rate is applied in CV (50 V/s), the resulting voltage-current plots and calculated CSC_c values reflect the amount of exposed (deinsulated) tip for the Pt-Ir microelectrodes. From the 50 V/s CV data shown in Figure 4-1, no statistically significant differences were found in the CSC_c values shown between any of the electrolytes tested. Trend-wise, however, PBS was shown to have a larger CSC_c compared to plain DMEM and DMEM + FBS + PS. When cells were included in with DMEM + FBS + PS, however, CSC_c increased in magnitude compared to without cells. The trend shown with the 50 V/s ramp rate is almost identical to the CV data acquired with the slower ramp rate of 50 mV/s (Figure 4-2). When a slow voltage ramp rate is applied (50 mV/s), electrolyte seepage into some of the insulated Pt-Ir metal adjacent to the exposed tip is also factored into the resulting CV plot. In addition, at 50 mV/s the electrodes would have been injecting current for longer compared to at 50 V/s. These factors result in a higher CSC_c as reflected in the 50 mV/s values being an order of magnitude

higher than the 50 V/s values. Furthermore, a statistically significant difference was found in the 50 mV/s data suggesting that the Pt-Ir microelectrodes are capable of holding more charge for stimulation in PBS compared to plain DMEM or DMEM + FBS + PS. This may be linked to ingredients found in the electrolytes. PBS is an isotonic aqueous solution whose pH (7.4) and ionic concentrations (137 mM NaCl, 10 mM NaH₂PO₄·2H₂O, 2.7 mM KCl) are similar to what is found in extracellular fluid *in vivo* [355–358]. DMEM F12 is a far more complex aqueous mixture in comparison, with vitamins, amino acids, inorganic salts, and other compounds included [351,359,360]. FBS, a product derived from cow fetuses, is itself also comprised of a complex combination of proteins (e.g., growth factors, hormones, enzymes), lipids, vitamins, sugars, and pH-buffering compounds [361–363]. Factors such as amino acids in plain DMEM may cover the surface of the electrodes thus making less exposed area available for faradaic charge transfer to occur. This may also be further exacerbated by including larger, more complex proteins found in FBS resulting in a decrease in CSC_c magnitude. Protein fouling of electrode surfaces has been previously reported to impact such electrochemical properties of electrodes [364].

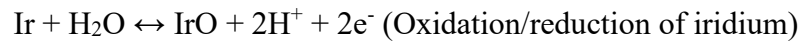
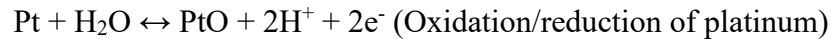
4.6.2. Electrical impedance spectroscopy

Electrical impedance spectroscopy measures the response of an electrode to minor electrical perturbations supplied by the potentiostat over a range of frequencies. Impedance, the measure of opposition to flow of current in a circuit, is calculated from linear current-voltage relationships obtained at each frequency applied in EIS. From the EIS data collected, the impedance measurements recorded from the electrolytes used (Figure 4-3) correlate well to the

CSC_c trends presented in Figures 4-1 and 4-2. Specifically, statistically higher impedances were found in plain DMEM and DMEM + FBS + PS compared to PBS. As previously mentioned in Section 4.6.1., impedance in this case may have increased with the addition of amino acids and proteins found in the cell culture media mixtures. However, impedance did not further increase when live cells were included with cell culture media thus suggesting that mixed glial cell populations form a conductive layer that allows for charge transfer to take place more easily in cell culture media when using Pt-Ir microelectrodes. Mixed glial cell populations comprise of multiple cell types including microglia, astrocytes, and oligodendrocytes. Evidence from the literature supports the notion that glial cells, especially oligodendrocytes, are electrically conductive [365] in nature given their role in facilitating action potential propagation along axons via saltatory conduction [366]. Voltage-gated ion channels also exist on the membranes of glial cells [243] which further reinforces the idea that there exist mechanisms through which they can respond to electrical perturbations in tissue.

Phase angle measurements are also obtained from EIS experiments. Mathematically, phase angle represents the degree to which current lags in relation to voltage; practically, calculating this value allows one to determine whether a circuit behaves more in a capacitive (phase shift towards -90°) or resistive (phase shift towards 0°) manner [367]. Phase angle measurements from the EIS scans performed (Figure 4-4) report a more negative phase angle for DMEM + FBS + PS compared to PBS – this suggests that, in cell culture media, a circuit involving a platinum-iridium microelectrode behaves in a more capacitive manner compared to in PBS.

When Pt-Ir electrodes are stimulated, the following reduction and oxidation reactions have been reported to occur in aqueous solutions [138]:



In the case of Pt-Ir electrodes, it is known that there exist faradaic and non-faradaic (i.e., capacitive) mechanisms at play at the electrode interface [358]. A double-layered structure, called the Helmholtz layer, develops at the phase boundary between the electrode and electrolyte [368,369]. The Helmholtz layer consists of an assembly of water-soluble ions such as H^+ or OH^- that may be produced from faradaic reactions that occur at the interface. Such a layer acts as a capacitive feature, and would be supplanted with the inclusion of other molecules in the electrolyte that come from things such as FBS and DMEM. Adsorbed amino acids and larger proteins act as a dielectric material between electrodes [370–373], would reduce the amount of physical space available on the electrode surface for interactions between the electrode and electrolyte ions, and result in a more capacitive system that is supported by the phase angle result reported for cell culture media.

4.6.3. Voltage transient analysis

Voltage transient analysis is used to estimate the maximum amount of charge that is injectable by a stimulation pulse [145,374]. The data obtained from VT experiments are also compared to established limits such as the water window to determine whether a given stimulation pulse would be safe for use in a biological setting. Maximum cathodic voltage excursion (E_{mc}) values were determined from the voltage-time plots shown in Figure 4-5 [375], and compared across different electrolytes presented in this study. Mathematically, E_{mc} is calculated by subtracting the access voltage from the maximum negative voltage obtained in the transient curve [145,338]. The results obtained predictably suggest that, as stimulation current increases, E_{mc} also increases in magnitude. Notably, beginning at 150 μA , E_{mc} for Pt-Ir microelectrodes immersed in DMEM + FBS + PS cross -0.6 V vs. Ag|AgCl (the lower limit for the water window). However, when mixed glial cell cultures were added into the wells E_{mc} was comparatively further away from the -0.6 V threshold. Although there was no statistically significant difference between these two groups, the trend observed from the data may suggest that the presence of the cells acts as a voltage buffer to make *in vitro* electrical stimulation using higher currents possible without breaching the water window. The data presented here suggest that this may only be possible *in vitro* up to a maximum of 250 μA – more chronic stimulation using higher currents may then result in degradation and corrosion of the Pt-Ir microelectrode.

4.6.4. Limitations of study

The electrochemistry experiments conducted in this chapter are intended to further contextualize the electrical stimulation experiments in the previous chapters. However, caution must be taken in the translatability of these results to an *in vivo* environment [145,376]. *In vitro* testing of the electrochemical performance of electrodes is done in a controlled environment where factors such as electrolyte composition can be carefully monitored. *In vivo*, however, the electrochemical performance of an electrode may differ depending on the stimulation target in the CNS – tissue is highly anisotropic with conductivities depending on its cellular and extracellular composition [377–380].

In the presented experimental design, the deinsulated tips of the electrodes made contact with the bottom of each well due to the need to make direct contact with any glial cells that are seeded in the well. The side of the electrode tip that makes contact with the bottom of the well may not contribute in equal measure to the electrochemical outputs described in the chapter as it would have been difficult for that part of the electrode to form a charge-transfer layer as with the parts of the electrode tips that were more exposed to the electrolyte.

The study presented in this chapter focused on comparing electrochemical performance of the Pt-Ir microelectrodes in the presence of different electrolytes – specifically, the goal was to determine the potential contributions of different components of the mixed glial cell cultures on parameters such as charge storage capacity, impedance, and voltage excursions. The study, however, did not address long-term performance of the microelectrodes. A topic of interest to further explore in future experiments would be to determine how the electrochemical properties explored through CV, EIS, and VT would change after repeated usage of the same electrodes in

more chronic stimulation experiments (e.g., comparison of electrode performance at various timepoints). Gradual electrode degradation is possible even when stimulating with a charge-balanced paradigm which, in theory, assumes total reversibility of reduction and oxidation reactions at the electrode-electrolyte interface [358]. Conducting a longitudinal study into this would add further insight into the rate of degradation that such electrodes would experience and help drive ways in which to prolong their service life once implanted into tissue.

4.7. Conclusions

Platinum-iridium microelectrodes have been used in neural interfacing applications for both stimulation and recording purposes. They are designed to penetrate into CNS tissue and therefore be in direct contact with cells – these include glial cells, which are the primary drivers behind the neuroinflammatory response and glial scar formation. Designing and constructing a high-throughput *in vitro* setup for testing primary mixed glial cell responses to electrical stimulation paradigms necessitates follow-up electrochemistry experiments to describe the mechanisms by which electrical stimulation occurs. By conducting potentiostat measurements to gauge their electrochemical performance in an *in vitro* setting, additional information is made available regarding the contributions of different components of the cell culture media to things such as electrode charge storage capabilities, electrode impedance, and voltage excursion properties.

Cyclic voltammetry experiments were conducted – CSC_c values calculated from voltage-current loop plots for each electrolyte suggest that, with cell culture media (DMEM + FBS +

PS), there is less electrical charge available per unit surface area of deinsulated electrode for charge injection compared to PBS. However, CSC_c may be improved with the inclusion of mixed glial cell cultures which could act as a conductive layer at the electrode interface. Impedance and phase angle measurements also support the trends observed from the CV data. Finally, voltage transient analysis logically confirmed that, *in vitro*, stimulation pulses of larger current eventually exceed the negative voltage threshold for the electrolysis of water – breaching of this threshold is most readily seen with microelectrodes immersed in cell culture media. However, the amount of current required to breach this threshold is increased when mixed glia are factored in thus suggesting their capacity in acting as a voltage buffer.

Future electrochemistry experiments should aim to further contextualize the capabilities of the Pt-Ir microelectrodes in a mixed glial cell culture environment. As the main goal of such cell culture work is to characterize glial cell reactivity and scarring dynamics in response to both the presence of the electrode and any electrical stimulation applied through it, the stability of the electrode itself as it sustains persistent cellular responses and rounds of electrical stimulation becomes a concern. Therefore, more longitudinal testing of the same electrodes in stimulation experiments over several days to weeks becomes warranted. Since microelectrodes, by virtue of their small surface areas, face issues with higher impedances, improving their performance using conductive materials such as PEDOT [381–383] and polypyrrole [384,385] may also warrant consideration. Patterning microelectrodes by altering deinsulated areas using laser, for example, is also an option for increasing their electroactive surface area [386]. Voltage transient analysis of stimulation pulses using different waveform shapes (e.g., sinusoidal, ramped) would also provide useful information as to the charge injection limits associated with those parameter changes.

Electrochemical measurements of electrodes offer insight into their capabilities and limits while operating in certain environments. Capturing information as to their performance in the presence of factors such as cell culture media, proteins, and cells themselves enable researchers to describe the manners in which electrical stimulation is occurring at the electrode-cell culture interface, and suggest ways in which electrode performance can be improved in terms of augmented charge storage, reduced impedance, etc. while avoiding electrode dissolution and potential damage to any nearby cells.

5. Chapter 5 – Conclusions and Future Directions

Glial cell reactivity to implanted microelectrode devices for amelioration of functional deficits from neurological disease or injury is a well-highlighted and discussed issue in the field of neuroengineering [39]. When an electrode implant is inserted into delicate tissue either in the brain or the spinal cord, a foreign body response naturally follows with glial scar formation resulting from the cellular (namely microglia and astrocyte) interactions with the implant over the course of several weeks to months. Although much focus has been given to potential biomaterial modifications to the electrodes themselves with the goal of mitigating glial cell reactivity and scar formation [60,387,388], comparatively less attention has been paid towards studying glial cell responses to applied electrical stimulation through the electrode interface.

A model capturing both glial cell responses to the presence of electrodes as well as applied electrical stimulation was therefore designed (Chapter 2). This was done with cell culture in mind as an *in vitro* approach offers high-throughput analysis of various parameters in a short amount of time while having a small ethical footprint in terms of animal lives used. Custom PDMS molds were designed to fit in the wells of 12-well cell culture plates, with fabricated platinum-iridium microwires (75 μm diameter) threaded through the molds to secure the deinsulated tips down at the bottom of the wells. Mixed murine glial cell cultures were prepared in these culture plates and electrically stimulated using a charge-balanced, cathodic-first rectangular pulse of either 0.15 mA (low current) or 1.5 mA (high current) for 4 h/day over 1, 3, and 7 days. Glial cell responses were thus captured over a short longitudinal time course. Biomarkers analyzed (Hoechst, EGFP, GFAP, IL-1 β) suggest a non-linear temporal response to applied electrical stimulation at either current used. At 1 day, electrical stimulation was observed

to have a negligible effect on glial cell density, biomarker fluorescence intensity, and area coverage. This changed at 3 days where the formation of a peri-electrode void around the electrode interface was most prominent as reflected in the area coverage data. At 7 days, however, such differences in biomarker signal across different currents and distances around the electrode tip disappeared thus suggesting a gradual repopulation of the peri-electrode void by cells. Importantly, scanning electron microscopy and follow-up energy-dispersive x-ray spectroscopy also predictably revealed severe oxidation damage to the electrode itself when stimulating at 1.5 mA. The goal of the chapter was to evaluate the feasibility of evaluating damage to both glial cells and microelectrodes over a short time course using the proposed *in vitro* design presented.

Following the feasibility study of the *in vitro* setup proposed, it was decided to further explore glial cell reactivity to electrical stimulation at the electrode interface by modifying stimulation paradigm parameters (Chapter 3). Specifically, modifications to stimulation current (at more clinically relevant levels), waveform shape, and stimulation frequency were made. It was also of interest to investigate the cause behind the formation of the peri-electrode voids – live imaging of EGFP-positive microglia from the transgenic cell cultures used showed that, indeed, cells close to the electrode were dying as a result of electrical stimulation and not migrating away from the electrode. Live imaging analyses further support published results [96] suggesting that changes in microglia behaviour are mostly observed in a very localized manner (within 50 μm of the electrode tip) regardless of stimulation parameter modifications. Follow-up analyses of immunolabelled cell cultures further suggest that, predictably, a greater loss of biomarker area coverage correlated with larger amounts of current being applied (0.1 mA – 0.4 mA). With regards to waveform shape modification, a sinusoidal waveform resulted in the least

amount of biomarker signal loss compared to the rectangular and ramped waveform shapes. Frequency modification experiments suggest that, although increasing frequency from 25 to 45 Hz resulted in increasing biomarker area coverage loss, stimulating at 55 Hz did not follow this trend in signal loss. None of the stimulation parameter modifications applied caused damage or degradation to the microelectrodes based on the SEM and EDS data acquired. The focus of this chapter was on further extending the capabilities of the proposed *in vitro* electrical stimulation cell culture setup by measuring, and confirming, differential responses in mixed glial cell responses to stimulation parameter modifications with just 4 hours of electrical stimulation.

Finally, it was of interest to describe the electrochemical mechanisms behind how the Pt-Ir microelectrodes behaved while interacting with the mixed glial cell cultures (Chapter 4). Electrochemical measurements were carried out on various electrolytes (PBS, DMEM F12, cell culture media, cell culture media + live cells) to determine potential contributions of individual components of the glial cell cultures to the electrochemical performance of the microelectrodes. Cyclic voltammetry measurements allowed for the calculation of charge storage capacity values for the microelectrodes, which suggested that CSC_c was smaller in cell culture media compared to in PBS. This was likely due to protein adsorption on the surface of the electrodes – analysis with electrical impedance spectroscopy for impedance and phase angle values support this idea. Voltage transient analysis also provided insight into the maximum charge injection limits of the microelectrodes prior to water electrolysis – the data suggest that the microelectrodes reach the water window threshold sooner at lower currents in cell culture media compared to other electrolytes tested. Interestingly, when mixed glial cells were factored into the voltage transient measurements their addition suggested that they may act as a sort of voltage buffer in the *in vitro* setup, and that stimulation at higher amounts of current would be possible before the resulting

maximum cathodic voltage excursions exceed the water window threshold. The data gathered and analyzed in this chapter provided further insight into the measurable contributions of components in the cell culture (e.g., media proteins, mixed glial cells) and how they impact the electrochemical performance of platinum-iridium microelectrodes in a biological setting.

Further experiments can still be conducted using the *in vitro* setup with the goal of better understanding glial cell reactivity to electrical stimulation paradigms at the electrode interface. Using the methods described herein, it would be beneficial to conduct more longitudinal experiments spanning several days to weeks to better capture more of the timeline associated with glial scar formation around an electrode. In addition, conducting follow-up experiments on the temporal response of glial cells to stimulation parameter modifications (such as the ones mentioned in Chapter 2) would yield more relevant information on their longer-term impact. Modifying other parameters such as charge balancing, interpulse delay, and pulse duration may also influence glial cell reactivity over longer time courses [127]. Such work would ideally also integrate neurons into the experimental designs as electrical stimulation is designed primarily to target and stimulate neurons in CNS tissue. Live imaging of other glial subtypes such as astrocytes and oligodendrocytes would provide additional context as to the fate of these cells at the electrode interface when exposed to diverse electrical stimulation paradigms [319,389]. Electrical stimulation experiments may also elicit heterogeneous responses depending on the part of the CNS that is being stimulated – stimulation of glial cell cultures exclusively generated from different tissues in the brain or spinal cord is therefore warranted [311]. Finally, these cell culture experiments would have to be paired with additional electrochemistry experiments that focus on electrode stability and how the electrodes might degrade over time after repeated usage of modified stimulation waveforms. The methods used in the thesis, namely CV, EIS, and VT, are

well-suited to calculating and tracking how electrochemical performance of electrodes changes over time.

Research on neural interface devices has progressed over the span of many decades [390,391], with technologies existing today that are already approved for use in people with disabilities [202,392–394]. The research presented in this thesis is intended to provide an additional experimental platform for biological testing and validation of functional microelectrode designs alongside work *in vivo* or in a clinical setting. Importantly, the data generated from the thesis also serve to fill a gap in the broader knowledge about how electrical stimulation directly affects glial cell behaviour in the context of an invasive electrode implant; this is often overlooked in favour of focusing on neuronal or overall functional responses to electrical stimulation designs. The information gleaned from the methodological tools described herein will better inform device developers of the efficacy and potential drawbacks of certain electrode and stimulation designs prior to further, more costly investment in animal testing. It is meant to supplement findings that would otherwise be made *in vivo* or clinically, and streamline engineering and device development efforts in designing a biocompatible, safe, effective, and longer-lasting implant in patients with functional impairments.

References

- [1] J.P. Donoghue, Bridging the Brain to the World: A Perspective on Neural Interface Systems, *Neuron* 60 (2008) 511–521. <https://doi.org/10.1016/j.neuron.2008.10.037>.
- [2] N.G. Hatsopoulos, J.P. Donoghue, The Science of Neural Interface Systems, *Annu. Rev. Neurosci.* 32 (2009) 249–266. <https://doi.org/10.1146/annurev.neuro.051508.135241>.
- [3] S. Kim, R. Bhandari, M. Klein, S. Negi, L. Rieth, P. Tathireddy, M. Toepper, H. Oppermann, F. Solzbacher, Integrated wireless neural interface based on the Utah electrode array, *Biomed Microdevices* 11 (2009) 453–466. <https://doi.org/10.1007/s10544-008-9251-y>.
- [4] R.A. Normann, E. Fernandez, Clinical applications of penetrating neural interfaces and Utah Electrode Array technologies, *J. Neural Eng.* 13 (2016) 061003. <https://doi.org/10.1088/1741-2560/13/6/061003>.
- [5] A.E. Rochford, A. Carnicer-Lombarte, V.F. Curto, G.G. Malliaras, D.G. Barone, When Bio Meets Technology: Biohybrid Neural Interfaces, *Advanced Materials* 32 (2020) 1903182. <https://doi.org/10.1002/adma.201903182>.
- [6] H. Ulsan, S. Chamanian, O. Zorlu, A. Muhtaroglu, H. Kulah, Neural stimulation interface with ultra-low power signal conditioning circuit for fully-implantable cochlear implants, in: 2017 IEEE Biomedical Circuits and Systems Conference (BioCAS), IEEE, Torino, Italy, 2017: pp. 1–4. <https://doi.org/10.1109/BIOCAS.2017.8325060>.
- [7] J.K. Krauss, N. Lipsman, T. Aziz, A. Boutet, P. Brown, J.W. Chang, B. Davidson, W.M. Grill, M.I. Hariz, A. Horn, M. Schulder, A. Mammis, P.A. Tass, J. Volkmann, A.M.

- Lozano, Technology of deep brain stimulation: current status and future directions, *Nat Rev Neurol* 17 (2021) 75–87. <https://doi.org/10.1038/s41582-020-00426-z>.
- [8] C.C. McIntyre, A. Chaturvedi, R.R. Shamir, S.F. Lempka, Engineering the Next Generation of Clinical Deep Brain Stimulation Technology, *Brain Stimulation* 8 (2015) 21–26. <https://doi.org/10.1016/j.brs.2014.07.039>.
- [9] A. Jackson, J.B. Zimmermann, Neural interfaces for the brain and spinal cord—restoring motor function, *Nat Rev Neurol* 8 (2012) 690–699. <https://doi.org/10.1038/nrneurol.2012.219>.
- [10] G. Schiavone, F. Wagner, F. Fallegger, X. Kang, N. Vachicouras, B. Barra, M. Capogrosso, J. Bloch, G. Courtine, S.P. Lacour, Long-term functionality of a soft electrode array for epidural spinal cord stimulation in a minipig model, in: 2018 40th Annual International Conference of the IEEE Engineering in Medicine and Biology Society (EMBC), 2018: pp. 1432–1435. <https://doi.org/10.1109/EMBC.2018.8512584>.
- [11] M.A.Y. Heravi, K. Maghooli, F. Nowshiravan Rahatabad, R. Rezaee, Application of a neural interface for restoration of leg movements: Intra-spinal stimulation using the brain electrical activity in spinally injured rabbits, *J Appl Biomed* 18 (2020) 33–40. <https://doi.org/10.32725/jab.2020.009>.
- [12] A.R. Kent, W.M. Grill, Analysis of deep brain stimulation electrode characteristics for neural recording, *J. Neural Eng.* 11 (2014) 046010. <https://doi.org/10.1088/1741-2560/11/4/046010>.
- [13] G. Hong, C.M. Lieber, Novel electrode technologies for neural recordings, *Nat Rev Neurosci* 20 (2019) 330–345. <https://doi.org/10.1038/s41583-019-0140-6>.

- [14] M. David-Pur, L. Bareket-Keren, G. Beit-Yaakov, D. Raz-Prag, Y. Hanein, All-carbon-nanotube flexible multi-electrode array for neuronal recording and stimulation, *Biomed Microdevices* 16 (2014) 43–53. <https://doi.org/10.1007/s10544-013-9804-6>.
- [15] J.B. Fallon, P.M. Carter, Principles of Recording from and Electrical Stimulation of Neural Tissue, in: *Neurobionics: The Biomedical Engineering of Neural Prostheses*, John Wiley & Sons, Ltd, 2016: pp. 89–120. <https://doi.org/10.1002/9781118816028.ch4>.
- [16] C.M. Hales, J.D. Rolston, S.M. Potter, How to Culture, Record and Stimulate Neuronal Networks on Micro-electrode Arrays (MEAs), *JoVE (Journal of Visualized Experiments)* (2010) e2056. <https://doi.org/10.3791/2056>.
- [17] J.-H. Kim, G. Kang, Y. Nam, Y.-K. Choi, Surface-modified microelectrode array with flake nanostructure for neural recording and stimulation, *Nanotechnology* 21 (2010) 085303. <https://doi.org/10.1088/0957-4484/21/8/085303>.
- [18] D.R. Cotter, C.M. Pariante, I.P. Everall, Glial cell abnormalities in major psychiatric disorders: the evidence and implications, *Brain Research Bulletin* 55 (2001) 585–595. [https://doi.org/10.1016/S0361-9230\(01\)00527-5](https://doi.org/10.1016/S0361-9230(01)00527-5).
- [19] M.C. Geloso, V. Corvino, E. Marchese, A. Serrano, F. Michetti, N. D'Ambrosi, The Dual Role of Microglia in ALS: Mechanisms and Therapeutic Approaches, *Front. Aging Neurosci.* 9 (2017) 242. <https://doi.org/10.3389/fnagi.2017.00242>.
- [20] D.M. Angelova, D.R. Brown, Microglia and the aging brain: are senescent microglia the key to neurodegeneration?, *J. Neurochem.* 151 (2019) 676–688. <https://doi.org/10.1111/jnc.14860>.

- [21] A.-L. Hemonnot, J. Hua, L. Ulmann, H. Hirbec, Microglia in Alzheimer Disease: Well-Known Targets and New Opportunities, *Front. Aging Neurosci.* 11 (2019) 233. <https://doi.org/10.3389/fnagi.2019.00233>.
- [22] G.R. John, S.C. Lee, C.F. Brosnan, Cytokines: Powerful Regulators of Glial Cell Activation, *Neuroscientist* 9 (2003) 10–22. <https://doi.org/10.1177/1073858402239587>.
- [23] L. Nowak, P. Ascher, Y. Berwald-Netter, Ionic channels in mouse astrocytes in culture, *J. Neurosci.* 7 (1987) 101–109. <https://doi.org/10.1523/JNEUROSCI.07-01-00101.1987>.
- [24] B.A. Barres, Glial ion channels, *Current Opinion in Neurobiology* 1 (1991) 354–359. [https://doi.org/10.1016/0959-4388\(91\)90052-9](https://doi.org/10.1016/0959-4388(91)90052-9).
- [25] S. Bevan, S.Y. Chiu, P.T.A. Gray, J.M. Ritchie, The Presence of Voltage-Gated Sodium, Potassium and Chloride Channels in Rat Cultured Astrocytes, *Proceedings of the Royal Society of London. Series B, Biological Sciences* 225 (1985) 299–313.
- [26] S. Gautron, G. Dos Santos, D. Pinto-Henrique, A. Koulakoff, F. Gros, Y. Berwald-Netter, The glial voltage-gated sodium channel: cell- and tissue-specific mRNA expression., *Proceedings of the National Academy of Sciences* 89 (1992) 7272–7276. <https://doi.org/10.1073/pnas.89.15.7272>.
- [27] H. Sontheimer, E. Fernandez-Marques, N. Ullrich, C. Pappas, S. Waxman, Astrocyte Na⁺ channels are required for maintenance of Na⁺/K⁽⁺⁾-ATPase activity, *J. Neurosci.* 14 (1994) 2464–2475. <https://doi.org/10.1523/JNEUROSCI.14-05-02464.1994>.
- [28] H. Sontheimer, J.A. Black, S.G. Waxman, Voltage-gated Na⁺ channels in glia: properties and possible functions, *Trends in Neurosciences* 19 (1996) 325–331. [https://doi.org/10.1016/0166-2236\(96\)10039-4](https://doi.org/10.1016/0166-2236(96)10039-4).

- [29] F.A. Henn, H. Haljamaäe, A. Hamberger, Glial cell function: Active control of extracellular K⁺ concentration, *Brain Research* 43 (1972) 437–443. [https://doi.org/10.1016/0006-8993\(72\)90399-X](https://doi.org/10.1016/0006-8993(72)90399-X).
- [30] Z. Szepesi, O. Manouchehrian, S. Bachiller, T. Deierborg, Bidirectional Microglia–Neuron Communication in Health and Disease, *Front. Cell. Neurosci.* 12 (2018) 323. <https://doi.org/10.3389/fncel.2018.00323>.
- [31] B.T. Casali, E.G. Reed-Geaghan, Microglial Function and Regulation during Development, Homeostasis and Alzheimer’s Disease, *Cells* 10 (2021) 957. <https://doi.org/10.3390/cells10040957>.
- [32] A. Nimmerjahn, F. Kirchhoff, F. Helmchen, Resting Microglial Cells Are Highly Dynamic Surveillants of Brain Parenchyma in Vivo, 308 (2005) 6.
- [33] C. Eder, Regulation of microglial behavior by ion channel activity, *J. Neurosci. Res.* 81 (2005) 314–321. <https://doi.org/10.1002/jnr.20476>.
- [34] P. Izquierdo, D. Attwell, C. Madry, Ion Channels and Receptors as Determinants of Microglial Function, *Trends in Neurosciences* 42 (2019) 278–292. <https://doi.org/10.1016/j.tins.2018.12.007>.
- [35] M.L. Olsen, B.S. Khakh, S.N. Skatchkov, M. Zhou, C.J. Lee, N. Rouach, New Insights on Astrocyte Ion Channels: Critical for Homeostasis and Neuron-Glia Signaling, *Journal of Neuroscience* 35 (2015) 13827–13835. <https://doi.org/10.1523/JNEUROSCI.2603-15.2015>.
- [36] J. McNeill, C. Rudyk, M.E. Hildebrand, N. Salmaso, Ion Channels and Electrophysiological Properties of Astrocytes: Implications for Emergent Stimulation

- Technologies, *Front. Cell. Neurosci.* 15 (2021) 644126.
<https://doi.org/10.3389/fncel.2021.644126>.
- [37] S. Guerra-Gomes, N. Sousa, L. Pinto, J.F. Oliveira, Functional Roles of Astrocyte Calcium Elevations: From Synapses to Behavior, *Front. Cell. Neurosci.* 11 (2018) 427.
<https://doi.org/10.3389/fncel.2017.00427>.
- [38] V. Vedam-Mai, E.Y. van Battum, W. Kamphuis, M.G.P. Feenstra, D. Denys, B.A. Reynolds, M.S. Okun, E.M. Hol, Deep brain stimulation and the role of astrocytes, *Mol Psychiatry* 17 (2012) 124–131. <https://doi.org/10.1038/mp.2011.61>.
- [39] J.W. Salatino, K.A. Ludwig, T.D.Y. Kozai, E.K. Purcell, Glial responses to implanted electrodes in the brain, *Nat Biomed Eng* 1 (2017) 862–877.
<https://doi.org/10.1038/s41551-017-0154-1>.
- [40] V.S. Polikov, M.L. Block, J.-M. Fellous, J.-S. Hong, W.M. Reichert, In vitro model of glial scarring around neuroelectrodes chronically implanted in the CNS, *Biomaterials* 27 (2006) 5368–5376. <https://doi.org/10.1016/j.biomaterials.2006.06.018>.
- [41] K.C. Spencer, J.C. Sy, R. Falcón-Banchs, M.J. Cima, A three dimensional in vitro glial scar model to investigate the local strain effects from micromotion around neural implants, *Lab Chip* 17 (2017) 795–804. <https://doi.org/10.1039/C6LC01411A>.
- [42] C.H. Ho, R.J. Triolo, A.L. Elias, K.L. Kilgore, A.F. DiMarco, K. Bogie, A.H. Vette, M. Audu, R. Kobetic, S.R. Chang, K.M. Chan, S. Dukelow, D.J. Bourbeau, S.W. Brose, K.J. Gustafson, Z. Kiss, V.K. Mushahwar, Functional Electrical Stimulation and Spinal Cord Injury, *Physical Medicine and Rehabilitation Clinics of North America* 25 (2014) 631–ix.
<https://doi.org/10.1016/j.pmr.2014.05.001>.

- [43] J. Eraifej, W. Clark, B. France, S. Desando, D. Moore, Effectiveness of upper limb functional electrical stimulation after stroke for the improvement of activities of daily living and motor function: a systematic review and meta-analysis, *Systematic Reviews* 6 (2017). <https://doi.org/10.1186/s13643-017-0435-5>.
- [44] L. Wojtecki, S.J. Groiss, C.J. Hartmann, S. Elben, S. Omlor, A. Schnitzler, J. Vesper, Deep Brain Stimulation in Huntington's Disease—Preliminary Evidence on Pathophysiology, Efficacy and Safety, *Brain Sciences* 6 (2016). <https://doi.org/10.3390/brainsci6030038>.
- [45] H. Wishart, D. Roberts, R. Roth, B. McDonald, D. Coffey, A. Mamourian, C. Hartley, L. Flashman, C. Fadul, A. Saykin, Chronic deep brain stimulation for the treatment of tremor in multiple sclerosis: review and case reports, *Journal of Neurology, Neurosurgery, and Psychiatry* 74 (2003) 1392–1397. <https://doi.org/10.1136/jnnp.74.10.1392>.
- [46] J. Mathers, C. Rick, C. Jenkinson, R. Garside, H. Pall, R. Mitchell, S. Bayliss, L.L. Jones, Patients' experiences of deep brain stimulation for Parkinson's disease: a qualitative systematic review and synthesis, *BMJ Open* 6 (2016) e011525. <https://doi.org/10.1136/bmjopen-2016-011525>.
- [47] P. Alonso, D. Cuadras, L. Gabriëls, D. Denys, W. Goodman, B.D. Greenberg, F. Jimenez-Ponce, J. Kuhn, D. Lenartz, L. Mallet, B. Nuttin, E. Real, C. Segalas, R. Schuurman, S.T. Du Montcel, J.M. Menchon, Deep brain stimulation for obsessive-compulsive disorder: A meta-analysis of treatment outcome and predictors of response, *PLoS ONE* 10 (2015) 1–17. <https://doi.org/10.1371/journal.pone.0133591>.
- [48] E.F. Chang, L.E. Schrock, P.A. Starr, J.L. Ostrem, Long-Term Benefit Sustained after Bilateral Pallidal Deep Brain Stimulation in Patients with Refractory Tardive Dystonia, *Stereotactic and Functional Neurosurgery* 88 (2010) 304–310.

- [49] I. Graat, M. Figeo, D. Denys, The application of deep brain stimulation in the treatment of psychiatric disorders, *International Review of Psychiatry* 29 (2017) 178–190. <https://doi.org/10.1080/09540261.2017.1282439>.
- [50] P.E. Holtzheimer, M.E. Kelley, R.E. Gross, M.M. Filkowski, S.J. Garlow, A. Barrocas, D. Wint, M.C. Craighead, J. Kozarsky, R. Chismar, J.L. Moreines, K. Mewes, P. Riva Posse, D.A. Gutman, H.S. Mayberg, Subcallosal cingulate deep brain stimulation for treatment-resistant unipolar and bipolar depression, *Archives of General Psychiatry* 69 (2012) 150–158. <https://doi.org/10.1001/archgenpsychiatry.2011.1456>.
- [51] N.R. Williams, T.R. Hopkins, E.B. Short, G.L. Sahlem, J. Snipes, G.J. Revuelta, M.S. George, I. Takacs, Reward circuit DBS improves Parkinson’s gait along with severe depression and OCD, *Neurocase* 22 (2016) 201–204. <https://doi.org/10.1080/13554794.2015.1112019>.
- [52] V.S. Polikov, P.A. Tresco, W.M. Reichert, Response of brain tissue to chronically implanted neural electrodes, *Journal of Neuroscience Methods* 148 (2005) 1–18. <https://doi.org/10.1016/j.jneumeth.2005.08.015>.
- [53] X. Hu, R.K. Leak, Y. Shi, J. Suenaga, Y. Gao, P. Zheng, J. Chen, Microglial and macrophage polarization—new prospects for brain repair, *Nature Reviews Neurology* 11 (2015) 56. <https://doi.org/10.1038/nrneurol.2014.207>.
- [54] V.E. Miron, A. Boyd, J.-W. Zhao, T.J. Yuen, J.M. Ruckh, J.L. Shadrach, P. van Wijngaarden, A.J. Wagers, A. Williams, R.J.M. Franklin, C. ffrench-Constant, M2 microglia and macrophages drive oligodendrocyte differentiation during CNS remyelination, *Nature Neuroscience* 16 (2013) 1211. <https://doi.org/10.1038/nn.3469>.

- [55] M.A. Anderson, J.E. Burda, Y. Ren, Y. Ao, T.M. O'Shea, R. Kawaguchi, G. Coppola, B.S. Khakh, T.J. Deming, M. V. Sofroniew, Astrocyte scar formation aids central nervous system axon regeneration, *Nature* 532 (2016) 195–200. <https://doi.org/10.1038/nature17623>.
- [56] A.R. Filous, J.H. Miller, Y.M. Coulson-Thomas, K.P. Horn, W.J. Alilain, J. Silver, Immature astrocytes promote CNS axonal regeneration when combined with chondroitinase ABC, *Developmental Neurobiology* 70 (2010) 826–841. <https://doi.org/10.1002/dneu.20820>.
- [57] T.D.Y. Kozai, A.L. Vazquez, C.L. Weaver, S.-G. Kim, X.T. Cui, In vivo two-photon microscopy reveals immediate microglial reaction to implantation of microelectrode through extension of processes, *J. Neural Eng.* 9 (2012) 066001. <https://doi.org/10.1088/1741-2560/9/6/066001>.
- [58] B.K. Leung, R. Biran, C.J. Underwood, P.A. Tresco, Characterization of microglial attachment and cytokine release on biomaterials of differing surface chemistry, *Biomaterials* 29 (2008) 3289–3297. <https://doi.org/10.1016/j.biomaterials.2008.03.045>.
- [59] T.D.Y. Kozai, N.B. Langhals, P.R. Patel, X. Deng, H. Zhang, K.L. Smith, J. Lahann, N.A. Kotov, D.R. Kipke, Ultrasmall implantable composite microelectrodes with bioactive surfaces for chronic neural interfaces., *Nature Materials* 11 (2012) 1065–73. <https://doi.org/10.1038/nmat3468>.
- [60] J.R. Eles, A.L. Vazquez, N.R. Snyder, C. Lagenaur, M.C. Murphy, T.D.Y. Kozai, X.T. Cui, Neuroadhesive L1 coating attenuates acute microglial attachment to neural electrodes as revealed by live two-photon microscopy, *Biomaterials* 113 (2017) 279–292. <https://doi.org/10.1016/j.biomaterials.2016.10.054>.

- [61] H. Kamiguchi, V. Lemmon, Neural cell adhesion molecule L1: signaling pathways and growth cone motility, *Journal of Neuroscience Research* 49 (1997) 1–8.
- [62] K. Thelen, V. Kedar, A.K. Panicker, R.-S. Schmid, B.R. Midkiff, P.F. Maness, The neural cell adhesion molecule L1 potentiates integrin-dependent cell migration to extracellular matrix proteins, *The Journal of Neuroscience: The Official Journal of the Society for Neuroscience* 22 (2002) 4918–4931.
- [63] K. Webb, E. Budko, T.J. Neuberger, S. Chen, M. Schachner, P.A. Tresco, Substrate-bound human recombinant L1 selectively promotes neuronal attachment and outgrowth in the presence of astrocytes and fibroblasts, *Biomaterials* 22 (2001) 1017–1028.
- [64] E. Azemi, W.R. Stauffer, M.S. Gostock, C.F. Lagenaur, X.T. Cui, Surface immobilization of neural adhesion molecule L1 for improving the biocompatibility of chronic neural probes: In vitro characterization, *Acta Biomaterialia* 4 (2008) 1208–1217. <https://doi.org/10.1016/j.actbio.2008.02.028>.
- [65] J.C.M. Vega L., M.K. Lee, J.H. Jeong, C.E. Smith, K.Y. Lee, H.J. Chung, D.E. Leckband, H. Kong, Recapitulating Cell–Cell Adhesion Using N-Cadherin Biologically Tethered to Substrates, *Biomacromolecules* 15 (2014) 2172–2179. <https://doi.org/10.1021/bm500335w>.
- [66] J.E. Collazos-Castro, G.R. Hernández-Labrado, J.L. Polo, C. García-Rama, N-Cadherin- and L1-functionalised conducting polymers for synergistic stimulation and guidance of neural cell growth, *Biomaterials* 34 (2013) 3603–3617. <https://doi.org/10.1016/j.biomaterials.2013.01.097>.
- [67] S. Sridar, M.A. Churchward, V.K. Mushahwar, K.G. Todd, A.L. Elias, Peptide modification of polyimide-insulated microwires: Towards improved biocompatibility

- through reduced glial scarring, *Acta Biomaterialia* 60 (2017) 154–166. <https://doi.org/10.1016/j.actbio.2017.07.026>.
- [68] P. Moshayedi, G. Ng, J.C.F. Kwok, G.S.H. Yeo, C.E. Bryant, J.W. Fawcett, K. Franze, J. Guck, The relationship between glial cell mechanosensitivity and foreign body reactions in the central nervous system, *Biomaterials* 35 (2014) 3919–3925. <https://doi.org/10.1016/j.biomaterials.2014.01.038>.
- [69] T. Kim, A. Branner, T. Gulati, S.F. Giszter, Braided multi-electrode probes: mechanical compliance characteristics and recordings from spinal cords, *J Neural Eng* 10 (2013) 45001. <https://doi.org/10.1088/1741-2560/10/4/045001>.
- [70] J.K. Nguyen, D.J. Park, J.L. Skousen, A.E. Hess-Dunning, D.J. Tyler, S.J. Rowan, C. Weder, J.R. Capadona, Mechanically-compliant intracortical implants reduce the neuroinflammatory response., *Journal of Neural Engineering* 11 (2014) 056014. <https://doi.org/10.1088/1741-2560/11/5/056014>.
- [71] D.K. Cullen, C.M. Simon, M.C. LaPlaca, Strain rate-dependent induction of reactive astrogliosis and cell death in three-dimensional neuronal–astrocytic co-cultures, *Brain Research* 1158 (2007) 103–115. <https://doi.org/10.1016/j.brainres.2007.04.070>.
- [72] A. Sridharan, S.D. Rajan, J. Muthuswamy, Long-term changes in the material properties of brain tissue at the implant–tissue interface, *Journal of Neural Engineering* 10 (2013) 066001. <https://doi.org/10.1088/1741-2560/10/6/066001>.
- [73] P. Köhler, A. Wolff, F. Ejserholm, L. Wallman, J. Schouenborg, C.E. Linsmeier, Influence of probe flexibility and gelatin embedding on neuronal density and glial responses to brain implants, *PLoS ONE* 10 (2015) 1–13. <https://doi.org/10.1371/journal.pone.0119340>.

- [74] J. Thelin, H. Jörntell, E. Psouni, M. Garwicz, J. Schouenborg, N. Danielsen, C.E. Linsmeier, Implant size and fixation mode strongly influence tissue reactions in the CNS, *PLoS ONE* 6 (2011). <https://doi.org/10.1371/journal.pone.0016267>.
- [75] R. Biran, D.C. Martin, P.A. Tresco, The brain tissue response to implanted silicon microelectrode arrays is increased when the device is tethered to the skull, *Journal of Biomedical Materials Research Part A* 82A (2007) 169–178. <https://doi.org/10.1002/jbm.a.31138>.
- [76] A. Trotier, E. Bagnoli, T. Walski, J. Evers, E. Pugliese, M. Lowery, M. Kilcoyne, U. Fitzgerald, M. Biggs, Micromotion Derived Fluid Shear Stress Mediates Peri-Electrode Gliosis through Mechanosensitive Ion Channels, *Advanced Science* 10 (2023) 2301352. <https://doi.org/10.1002/advs.202301352>.
- [77] A. Gaillard, L. Prestoz, B. Dumartin, A. Cantereau, F. Morel, M. Roger, M. Jaber, Reestablishment of damaged adult motor pathways by grafted embryonic cortical neurons, *Nature Neuroscience* 10 (2007) 1294.
- [78] O. Lindvall, Z. Kokaia, A. Martinez-Serrano, Stem cell therapy for human neurodegenerative disorders—how to make it work, *Nature Medicine* 10 (2004) S42.
- [79] E.K. Purcell, J.P. Seymour, S. Yandamuri, D.R. Kipke, In vivo evaluation of a neural stem cell-seeded prosthesis., *Journal of Neural Engineering* 6 (2009) 026005. <https://doi.org/10.1088/1741-2560/6/2/026005>.
- [80] N.F. Nolta, M.B. Christensen, P.D. Crane, J.L. Skousen, P.A. Tresco, BBB leakage, astrogliosis, and tissue loss correlate with silicon microelectrode array recording performance, *Biomaterials* 53 (2015) 753–762. <https://doi.org/10.1016/j.biomaterials.2015.02.081>.

- [81] T.D.Y. Kozai, A.S. Jaquins-Gerstl, A.L. Vazquez, A.C. Michael, X.T. Cui, Dexamethasone retrodialysis attenuates microglial response to implanted probes in vivo, *Biomaterials* 87 (2016) 157–169. <https://doi.org/10.1016/j.biomaterials.2016.02.013>.
- [82] R.L. Rennaker, J. Miller, H. Tang, D.A. Wilson, Minocycline increases quality and longevity of chronic neural recordings., *Journal of Neural Engineering* 4 (2007) L1-5. <https://doi.org/10.1088/1741-2560/4/2/L01>.
- [83] D.H. Szarowski, M.D. Andersen, S. Retterer, A.J. Spence, M. Isaacson, H.G. Craighead, J.N. Turner, W. Shain, Brain responses to micro-machined silicon devices, *Brain Research* 983 (2003) 23–35. [https://doi.org/10.1016/S0006-8993\(03\)03023-3](https://doi.org/10.1016/S0006-8993(03)03023-3).
- [84] D.J. Edell, V. V Toi, V.M. McNeil, L.D. Clark, Factors influencing the biocompatibility of insertable silicon microshafts in cerebral cortex, *IEEE Transactions on Biomedical Engineering* 39 (1992) 635–643. <https://doi.org/10.1109/10.141202>.
- [85] M.B. Graeber, W. Li, M.L. Rodriguez, Role of microglia in CNS inflammation, *FEBS Letters* 585 (2011) 3798–3805. <https://doi.org/10.1016/J.FEBSLET.2011.08.033>.
- [86] H. Uwe-Karsten, Microglia as a source and target of cytokines, *Glia* 40 (2002) 140–155. <https://doi.org/10.1002/glia.10161>.
- [87] M.L. Block, L. Zecca, J.-S. Hong, Microglia-mediated neurotoxicity: uncovering the molecular mechanisms, *Nature Reviews Neuroscience* 8 (2007) 57.
- [88] W. Tongguang, Q. Liya, L. Bin, L. Yuxin, W. Belinda, E.T. E., L. Robert, T. Seijiro, H. Jau-Shyong, Role of reactive oxygen species in LPS-induced production of prostaglandin E2 in microglia, *Journal of Neurochemistry* 88 (2004) 939–947. <https://doi.org/10.1046/j.1471-4159.2003.02242.x>.

- [89] Y. Quan, C. Jiang, B. Xue, S. Zhu, X. Wang, High glucose stimulates TNF α and MCP-1 expression in rat microglia via ROS and NF- κ B pathways, *Acta Pharmacologica Sinica* 32 (2011) 188.
- [90] K.A. Potter, A.C. Buck, W.K. Self, M.E. Callanan, S. Sunil, J.R. Capadona, The effect of resveratrol on neurodegeneration and blood brain barrier stability surrounding intracortical microelectrodes, *Biomaterials* 34 (2013) 7001–7015. <https://doi.org/10.1016/j.biomaterials.2013.05.035>.
- [91] K.A. Potter-Baker, W.G. Stewart, W.H. Tomaszewski, C.T. Wong, W.D. Meador, N.P. Ziats, J.R. Capadona, Implications of chronic daily anti-oxidant administration on the inflammatory response to intracortical microelectrodes, *Journal of Neural Engineering* 12 (2015) 046002. <https://doi.org/10.1088/1741-2560/12/4/046002>.
- [92] M. Ravikumar, S. Sunil, J. Black, D.S. Barkauskas, A.Y. Haung, R.H. Miller, S.M. Selkirk, J.R. Capadona, The roles of blood-derived macrophages and resident microglia in the neuroinflammatory response to implanted Intracortical microelectrodes, *Biomaterials* 35 (2014) 8049–8064. <https://doi.org/10.1016/j.biomaterials.2014.05.084>.
- [93] B. Ajami, J.L. Bennett, C. Krieger, W. Tetzlaff, F.M. V Rossi, Local self-renewal can sustain CNS microglia maintenance and function throughout adult life, *Nature Neuroscience* 10 (2007) 1538.
- [94] R.W. Griffith, D.R. Humphrey, Long-term gliosis around chronically implanted platinum electrodes in the Rhesus macaque motor cortex, *Neuroscience Letters* 406 (2006) 81–86. <https://doi.org/10.1016/j.neulet.2006.07.018>.
- [95] J.P. Harris, J.R. Capadona, R.H. Miller, B.C. Healy, K. Shanmuganathan, S.J. Rowan, C. Weder, D.J. Tyler, Mechanically adaptive intracortical implants improve the proximity of

- neuronal cell bodies, *J. Neural Eng.* 8 (2011) 066011. <https://doi.org/10.1088/1741-2560/8/6/066011>.
- [96] J.A. Bamford, K.G. Todd, V.K. Mushahwar, The effects of intraspinal microstimulation on spinal cord tissue in the rat, *Biomaterials* 31 (2010) 5552–5563. <https://doi.org/10.1016/j.biomaterials.2010.03.051>.
- [97] Q. Xu, L. Jin, C. Li, S. Kuddannayai, Y. Zhang, The effect of electrical stimulation on cortical cells in 3D nanofibrous scaffolds, *RSC Adv.* 8 (2018) 11027–11035. <https://doi.org/10.1039/C8RA01323C>.
- [98] C.G. Schipke, C. Boucsein, C. Ohlemeyer, F. Kirchhoff, H. Kettenmann, Astrocyte Ca²⁺ waves trigger responses in microglial cells in brain slices, *FASEB j.* 16 (2002) 1–16. <https://doi.org/10.1096/fj.01-0514fje>.
- [99] M.L. Cotrina, J.H.-C. Lin, J.C. López-García, C.C.G. Naus, M. Nedergaard, ATP-Mediated Glia Signaling, *J. Neurosci.* 20 (2000) 2835–2844. <https://doi.org/10.1523/JNEUROSCI.20-08-02835.2000>.
- [100] A.I. Roitbak, V.V. Fanardjian, Depolarization of cortical glial cells in response to electrical stimulation of the cortical surface, *Neuroscience* 6 (1981) 2529–2537. [https://doi.org/10.1016/0306-4522\(81\)90098-1](https://doi.org/10.1016/0306-4522(81)90098-1).
- [101] Z. Blumenfeld, H. Brontë-Stewart, High Frequency Deep Brain Stimulation and Neural Rhythms in Parkinson's Disease, *Neuropsychol Rev* 25 (2015) 384–397. <https://doi.org/10.1007/s11065-015-9308-7>.
- [102] D. Orłowski, A. Michalis, A.N. Glud, A.R. Korshøj, L.M. Fitting, T.W. Mikkelsen, A. Mercanzini, A. Jordan, A. Dransart, J.C.H. Sørensen, Brain Tissue Reaction to Deep Brain

- Stimulation—A Longitudinal Study of DBS in the Goettingen Minipig, *Neuromodulation: Technology at the Neural Interface* 20 (2017) 417–423. <https://doi.org/10.1111/ner.12576>.
- [103] L. Bekar, W. Libionka, G.-F. Tian, Q. Xu, A. Torres, X. Wang, D. Lovatt, E. Williams, T. Takano, J. Schnermann, R. Bakos, M. Nedergaard, Adenosine is crucial for deep brain stimulation-mediated attenuation of tremor, *Nat Med* 14 (2008) 75–80. <https://doi.org/10.1038/nm1693>.
- [104] F. Agnesi, C.D. Blaha, J. Lin, K.H. Lee, Local glutamate release in the rat ventral lateral thalamus evoked by high-frequency stimulation, *J. Neural Eng.* 7 (2010) 026009. <https://doi.org/10.1088/1741-2560/7/2/026009>.
- [105] A. Etiévant, G. Lucas, O. Dkhissi-Benyahya, N. Haddjeri, The Role of Astroglia in the Antidepressant Action of Deep Brain Stimulation, *Front. Cell. Neurosci.* 9 (2016). <https://doi.org/10.3389/fncel.2015.00509>.
- [106] V. Vedam-Mai, M. Baradaran-Shoraka, B.A. Reynolds, M.S. Okun, Tissue Response to Deep Brain Stimulation and Microlesion: A Comparative Study, *Neuromodulation: Technology at the Neural Interface* 19 (2016) 451–458. <https://doi.org/10.1111/ner.12406>.
- [107] A.N. Silchenko, P.A. Tass, Computational modeling of chemotactic signaling and aggregation of microglia around implantation site during deep brain stimulation, *Eur. Phys. J. Spec. Top.* 222 (2013) 2647–2653. <https://doi.org/10.1140/epjst/e2013-02044-5>.
- [108] Y. Chen, G. Zhu, D. Liu, X. Zhang, Y. Liu, T. Yuan, T. Du, J. Zhang, Subthalamic nucleus deep brain stimulation suppresses neuroinflammation by Fractalkine pathway in Parkinson's disease rat model, *Brain, Behavior, and Immunity* 90 (2020) 16–25. <https://doi.org/10.1016/j.bbi.2020.07.035>.

- [109] R. Hadar, L. Dong, L. del-Valle-Anton, D. Guneykaya, M. Voget, H. Edemann-Callesen, R. Schweibold, A. Djodari-Irani, T. Goetz, S. Ewing, H. Kettenmann, S.A. Wolf, C. Winter, Deep brain stimulation during early adolescence prevents microglial alterations in a model of maternal immune activation, *Brain, Behavior, and Immunity* 63 (2017) 71–80. <https://doi.org/10.1016/j.bbi.2016.12.003>.
- [110] V. Stratoulis, J.L. Venero, M. Tremblay, B. Joseph, Microglial subtypes: diversity within the microglial community, *EMBO J* 38 (2019). <https://doi.org/10.15252/emboj.2019101997>.
- [111] C.A. Ariza, A.T. Fleury, C.J. Tormos, V. Petruk, S. Chawla, J. Oh, D.S. Sakaguchi, S.K. Mallapragada, The Influence of Electric Fields on Hippocampal Neural Progenitor Cells, *Stem Cell Rev and Rep* 6 (2010) 585–600. <https://doi.org/10.1007/s12015-010-9171-0>.
- [112] S.J. Pelletier, M. Lagace, I. St-Amour, D. Arsenault, G. Cisbani, A. Chabrat, S. Fecteau, M. Levesque, F. Cicchetti, The Morphological and Molecular Changes of Brain Cells Exposed to Direct Current Electric Field Stimulation, *International Journal of Neuropsychopharmacology* 18 (2015) pyu090–pyu090. <https://doi.org/10.1093/ijnp/pyu090>.
- [113] K.R. Kearns, D.M. Thompson, Macrophage response to electrical stimulation, in: 2015 41st Annual Northeast Biomedical Engineering Conference (NEBEC), IEEE, Troy, NY, USA, 2015: pp. 1–2. <https://doi.org/10.1109/NEBEC.2015.7117101>.
- [114] S.J. Pelletier, F. Cicchetti, Cellular and Molecular Mechanisms of Action of Transcranial Direct Current Stimulation: Evidence from In Vitro and In Vivo Models, *International Journal of Neuropsychopharmacology* 18 (2015) pyu047–pyu047. <https://doi.org/10.1093/ijnp/pyu047>.

- [115] T. Baba, M. Kameda, T. Yasuhara, T. Morimoto, A. Kondo, T. Shingo, N. Tajiri, F. Wang, Y. Miyoshi, C.V. Borlongan, M. Matsumae, I. Date, Electrical Stimulation of the Cerebral Cortex Exerts Antiapoptotic, Angiogenic, and Anti-Inflammatory Effects in Ischemic Stroke Rats Through Phosphoinositide 3-Kinase/Akt Signaling Pathway, *Stroke* 40 (2009). <https://doi.org/10.1161/STROKEAHA.109.563627>.
- [116] A.C. Colmenárez-Raga, I. Díaz, M. Pernia, D. Pérez-González, J.M. Delgado-García, J. Carro, I. Plaza, M.A. Merchán, Reversible Functional Changes Evoked by Anodal Epidural Direct Current Electrical Stimulation of the Rat Auditory Cortex, *Front. Neurosci.* 13 (2019) 356. <https://doi.org/10.3389/fnins.2019.00356>.
- [117] C.-F.V. Latchoumane, L. Jackson, M.S.E. Sendi, K.F. Tehrani, L.J. Mortensen, S.L. Stice, M. Ghovanloo, L. Karumbaiah, Chronic Electrical Stimulation Promotes the Excitability and Plasticity of ESC-derived Neurons following Glutamate-induced Inhibition In vitro, *Sci Rep* 8 (2018) 10957. <https://doi.org/10.1038/s41598-018-29069-3>.
- [118] A.-K. Gellner, J. Reis, B. Fritsch, Glia: A Neglected Player in Non-invasive Direct Current Brain Stimulation, *Front. Cell. Neurosci.* 10 (2016). <https://doi.org/10.3389/fncel.2016.00188>.
- [119] R. Huang, L. Peng, L. Hertz, Effects of a low-voltage static electric field on energy metabolism in astrocytes, *Bioelectromagnetics* 18 (1997) 77–80. [https://doi.org/10.1002/\(SICI\)1521-186X\(1997\)18:1<77::AID-BEM11>3.0.CO;2-N](https://doi.org/10.1002/(SICI)1521-186X(1997)18:1<77::AID-BEM11>3.0.CO;2-N).
- [120] M.A. Rueger, M.H. Keuters, M. Walberer, R. Braun, R. Klein, R. Sparing, G.R. Fink, R. Graf, M. Schroeter, Multi-Session Transcranial Direct Current Stimulation (tDCS) Elicits Inflammatory and Regenerative Processes in the Rat Brain, *PLoS ONE* 7 (2012) e43776. <https://doi.org/10.1371/journal.pone.0043776>.

- [121] G.J. Hathway, D. Vega-Avelaira, A. Moss, R. Ingram, M. Fitzgerald, Brief, low frequency stimulation of rat peripheral C-fibres evokes prolonged microglial-induced central sensitization in adults but not in neonates, *Pain* 144 (2009) 110–118. <https://doi.org/10.1016/j.pain.2009.03.022>.
- [122] A.N. Koppes, N.W. Zaccor, C.J. Rivet, L.A. Williams, J.M. Piselli, R.J. Gilbert, D.M. Thompson, Neurite outgrowth on electrospun PLLA fibers is enhanced by exogenous electrical stimulation, *J. Neural Eng.* 11 (2014) 046002. <https://doi.org/10.1088/1741-2560/11/4/046002>.
- [123] F.O. Martinez, S. Gordon, The M1 and M2 paradigm of macrophage activation: time for reassessment, *F1000Prime Rep* 6 (2014). <https://doi.org/10.12703/P6-13>.
- [124] R.M. Ransohoff, A polarizing question: do M1 and M2 microglia exist?, *Nat Neurosci* 19 (2016) 987–991. <https://doi.org/10.1038/nn.4338>.
- [125] S. Guo, H. Wang, Y. Yin, Microglia Polarization From M1 to M2 in Neurodegenerative Diseases, *Front. Aging Neurosci.* 14 (2022) 815347. <https://doi.org/10.3389/fnagi.2022.815347>.
- [126] T. Ishibashi, K.A. Dakin, B. Stevens, P.R. Lee, S.V. Kozlov, C.L. Stewart, R.D. Fields, Astrocytes Promote Myelination in Response to Electrical Impulses, *Neuron* 49 (2006) 823–832. <https://doi.org/10.1016/j.neuron.2006.02.006>.
- [127] R. Vallejo, D.C. Platt, J.A. Rink, M.A. Jones, C.A. Kelley, A. Gupta, C.L. Cass, K. Eichenberg, A. Vallejo, W.J. Smith, R. Benyamin, D.L. Cedeño, Electrical Stimulation of C6 Glia-Precursor Cells In Vitro Differentially Modulates Gene Expression Related to Chronic Pain Pathways, *Brain Sciences* 9 (2019) 303. <https://doi.org/10.3390/brainsci9110303>.

- [128] X.-Y. Liu, H.-F. Zhou, Y.-L. Pan, X.-B. Liang, D.-B. Niu, B. Xue, F.-Q. Li, Q.-H. He, X.-H. Wang, X.-M. Wang, Electro-acupuncture stimulation protects dopaminergic neurons from inflammation-mediated damage in medial forebrain bundle-transected rats, *Experimental Neurology* 189 (2004) 189–196. <https://doi.org/10.1016/j.expneurol.2004.05.028>.
- [129] J.A. Bamford, V.K. Mushahwar, Intraspinal microstimulation for the recovery of function following spinal cord injury, in: *Progress in Brain Research*, Elsevier, 2011: pp. 227–239. <https://doi.org/10.1016/B978-0-444-53815-4.00004-2>.
- [130] B.J. Holinski, K.A. Mazurek, D.G. Everaert, A. Toossi, A.M. Lucas-Osma, P. Troyk, R. Etienne-Cummings, R.B. Stein, V.K. Mushahwar, Intraspinal microstimulation produces over-ground walking in anesthetized cats, *J. Neural Eng.* 13 (2016) 056016. <https://doi.org/10.1088/1741-2560/13/5/056016>.
- [131] C.N.M. Ryan, M.N. Doulgkeroglou, D.I. Zeugolis, Electric field stimulation for tissue engineering applications, *BMC Biomed Eng* 3 (2021) 1. <https://doi.org/10.1186/s42490-020-00046-0>.
- [132] C. Bertucci, R. Koppes, C. Dumont, A. Koppes, Neural responses to electrical stimulation in 2D and 3D in vitro environments, *Brain Research Bulletin* 152 (2019) 265–284. <https://doi.org/10.1016/j.brainresbull.2019.07.016>.
- [133] H.U. Lee, A. Blasiak, D.R. Agrawal, D.T.B. Loong, N.V. Thakor, A.H. All, J.S. Ho, I.H. Yang, Subcellular electrical stimulation of neurons enhances the myelination of axons by oligodendrocytes, *PLoS ONE* 12 (2017) e0179642. <https://doi.org/10.1371/journal.pone.0179642>.

- [134] C. Fu, S. Pan, Y. Ma, W. Kong, Z. Qi, X. Yang, Effect of electrical stimulation combined with graphene-oxide-based membranes on neural stem cell proliferation and differentiation, *Artificial Cells, Nanomedicine, and Biotechnology* 47 (2019) 1867–1876. <https://doi.org/10.1080/21691401.2019.1613422>.
- [135] M. Fujiki, H. Kobayashi, R. Inoue, M. Goda, Electrical Preconditioning Attenuates Progressive Necrosis and Cavitation following Spinal Cord Injury, *Journal of Neurotrauma* 21 (2004) 459–470. <https://doi.org/10.1089/089771504323004601>.
- [136] A.S. Jack, C. Hurd, J. Martin, K. Fouad, Electrical Stimulation as a Tool to Promote Plasticity of the Injured Spinal Cord, *Journal of Neurotrauma* 37 (2020) 1933–1953. <https://doi.org/10.1089/neu.2020.7033>.
- [137] S. Cohen, A. Richter-Levin, O. Shefi, Brief Electrical Stimulation Triggers an Effective Regeneration of Leech CNS, *eNeuro* 7 (2020) ENEURO.0030-19.2020. <https://doi.org/10.1523/ENEURO.0030-19.2020>.
- [138] D.R. Merrill, M. Bikson, J.G.R. Jefferys, Electrical stimulation of excitable tissue: design of efficacious and safe protocols, *Journal of Neuroscience Methods* 141 (2005) 171–198. <https://doi.org/10.1016/j.jneumeth.2004.10.020>.
- [139] C. Tsui, K. Koss, M.A. Churchward, K.G. Todd, Biomaterials and glia: Progress on designs to modulate neuroinflammation, *Acta Biomaterialia* 83 (2019) 13–28. <https://doi.org/10.1016/j.actbio.2018.11.008>.
- [140] C.A.R. Chapman, H. Chen, M. Stamou, J. Biener, M.M. Biener, P.J. Lein, E. Seker, Nanoporous Gold as a Neural Interface Coating: Effects of Topography, Surface Chemistry, and Feature Size, *ACS Appl. Mater. Interfaces* 7 (2015) 7093–7100. <https://doi.org/10.1021/acsami.5b00410>.

- [141] R. Biran, D.C. Martin, P.A. Tresco, The brain tissue response to implanted silicon microelectrode arrays is increased when the device is tethered to the skull, *J. Biomed. Mater. Res.* 82A (2007) 169–178. <https://doi.org/10.1002/jbm.a.31138>.
- [142] E. Saracino, S. Zuppolini, V. Guarino, V. Benfenati, A. Borriello, R. Zamboni, L. Ambrosio, Polyaniline nano-needles into electrospun bio active fibres support *in vitro* astrocyte response, *RSC Adv.* 11 (2021) 11347–11355. <https://doi.org/10.1039/D1RA00596K>.
- [143] C. Vallejo-Giraldo, K. Krukiewicz, I. Calaresu, J. Zhu, M. Palma, M. Fernandez-Yague, BenjaminW. McDowell, N. Peixoto, N. Farid, G. O'Connor, L. Ballerini, A. Pandit, M.J.P. Biggs, Attenuated Glial Reactivity on Topographically Functionalized Poly(3,4-Ethylenedioxythiophene):P-Toluene Sulfonate (PEDOT:PTS) Neuroelectrodes Fabricated by Microimprint Lithography, *Small* 14 (2018) 1800863. <https://doi.org/10.1002/sml.201800863>.
- [144] W. Yang, Y. Gong, W. Li, A Review: Electrode and Packaging Materials for Neurophysiology Recording Implants, *Front. Bioeng. Biotechnol.* 8 (2021) 622923. <https://doi.org/10.3389/fbioe.2020.622923>.
- [145] S.F. Cogan, Neural Stimulation and Recording Electrodes, *Annu. Rev. Biomed. Eng.* 10 (2008) 275–309. <https://doi.org/10.1146/annurev.bioeng.10.061807.160518>.
- [146] A. Bendali, C. Agnès, S. Meffert, V. Forster, A. Bongrain, J.-C. Arnault, J.-A. Sahel, A. Offenhäusser, P. Bergonzo, S. Picaud, Distinctive Glial and Neuronal Interfacing on Nanocrystalline Diamond, *PLoS ONE* 9 (2014) e92562. <https://doi.org/10.1371/journal.pone.0092562>.

- [147] W. He, G.C. McConnell, R.V. Bellamkonda, Nanoscale laminin coating modulates cortical scarring response around implanted silicon microelectrode arrays, *J. Neural Eng.* 3 (2006) 316–326. <https://doi.org/10.1088/1741-2560/3/4/009>.
- [148] M. Polanco, H. Yoon, S. Bawab, Micromotion-induced dynamic effects from a neural probe and brain tissue interface, *J. Micro/Nanolith. MEMS MOEMS* 13 (2014) 023009. <https://doi.org/10.1117/1.JMM.13.2.023009>.
- [149] S.M. Richardson-Burns, J.L. Hendricks, D.C. Martin, Electrochemical polymerization of conducting polymers in living neural tissue, *J. Neural Eng.* 4 (2007) L6. <https://doi.org/10.1088/1741-2560/4/2/L02>.
- [150] S.B. Brummer, M.J. Turner, Electrochemical Considerations for Safe Electrical Stimulation of the Nervous System with Platinum Electrodes, *IEEE Trans. Biomed. Eng.* BME-24 (1977) 59–63. <https://doi.org/10.1109/TBME.1977.326218>.
- [151] S.L. Morton, M.L. Daroux, J.T. Mortimer, The Role of Oxygen Reduction in Electrical Stimulation of Neural Tissue, *Journal of The Electrochemical Society* 141 (1994) 122–130.
- [152] S.F. Cogan, K.A. Ludwig, C.G. Welle, P. Takmakov, Tissue damage thresholds during therapeutic electrical stimulation, *J. Neural Eng.* 13 (2016) 021001. <https://doi.org/10.1088/1741-2560/13/2/021001>.
- [153] S. Jung, J. Aliberti, P. Graemmel, M.J. Sunshine, G.W. Kreutzberg, A. Sher, D.R. Littman, Analysis of Fractalkine Receptor CX₃CR1 Function by Targeted Deletion and Green Fluorescent Protein Reporter Gene Insertion, *Molecular and Cellular Biology* 20 (2000) 4106–4114. <https://doi.org/10.1128/MCB.20.11.4106-4114.2000>.

- [154] S. Sellner, R. Paricio-Montesinos, A. Spieß, A. Masuch, D. Erny, L.A. Harsan, D.V. Elverfeldt, M. Schwabenland, K. Biber, O. Staszewski, S. Lira, S. Jung, M. Prinz, T. Blank, Microglial CX3CR1 promotes adult neurogenesis by inhibiting Sirt 1/p65 signaling independent of CX3CL1, *Acta Neuropathol Commun* 4 (2016) 102. <https://doi.org/10.1186/s40478-016-0374-8>.
- [155] M. Mohammed, J. Thelin, L. Gällentoft, P.T. Thorbergsson, L.S. Kumosa, J. Schouenborg, L.M.E. Pettersson, Ice coating –A new method of brain device insertion to mitigate acute injuries, *Journal of Neuroscience Methods* 343 (2020) 108842. <https://doi.org/10.1016/j.jneumeth.2020.108842>.
- [156] I. Kin, T. Sasaki, T. Yasuhara, M. Kameda, T. Agari, M. Okazaki, K. Hosomoto, Y. Okazaki, S. Yabuno, S. Kawauchi, K. Kuwahara, J. Morimoto, K. Kin, M. Umakoshi, Y. Tomita, N. Tajiri, C. Borlongan, I. Date, Vagus Nerve Stimulation with Mild Stimulation Intensity Exerts Anti-Inflammatory and Neuroprotective Effects in Parkinson’s Disease Model Rats, *Biomedicines* 9 (2021) 789. <https://doi.org/10.3390/biomedicines9070789>.
- [157] A. Lennikov, M. Yang, K. Chang, L. Pan, M.S. Saddala, C. Lee, A. Ashok, K.-S. Cho, T.P. Utheim, D.F. Chen, Direct modulation of microglial function by electrical field, *Front. Cell Dev. Biol.* 10 (2022) 980775. <https://doi.org/10.3389/fcell.2022.980775>.
- [158] Z.-X. Wang, Z.-Y. Feng, L.-P. Zheng, Y. Yuan, Sinusoidal stimulation on afferent fibers modulates the firing pattern of downstream neurons in rat hippocampus, *Journal of Integrative Neuroscience* 19 (2020) 413. <https://doi.org/10.31083/j.jin.2020.03.207>.
- [159] Y. Wang, T.P. Burghardt, G.A. Worrell, H.-L. Wang, The frequency-dependent effect of electrical fields on the mobility of intracellular vesicles in astrocytes, *Biochemical and*

<https://doi.org/10.1016/j.bbrc.2020.11.064>.

- [160] K.M. Garza, L. Zhang, B. Borron, L.B. Wood, A.C. Singer, Gamma Visual Stimulation Induces a Neuroimmune Signaling Profile Distinct from Acute Neuroinflammation, *J. Neurosci.* 40 (2020) 1211–1225. <https://doi.org/10.1523/JNEUROSCI.1511-19.2019>.
- [161] R.M. Mayall, V.I. Birss, The Chalkboard: Relating Cyclic Voltammetry and Electrochemical Impedance Spectroscopy in a Mass Transport Controlled System, *Electrochem. Soc. Interface* 26 (2017) 53–56. <https://doi.org/10.1149/2.F03174if>.
- [162] S. Dave, J. Das, S. Dave, P. Mohanty, G.M. Priya, P. Jagtap, R. Pawar, Contribution of Cyclic Voltammetry and Electrochemical Impedance Spectroscopy in Deciphering the Electron Transport System in Biofilm, in: M. Nag, D. Lahiri (Eds.), *Analytical Methodologies for Biofilm Research*, Springer US, New York, NY, 2021: pp. 129–152. https://doi.org/10.1007/978-1-0716-1378-8_6.
- [163] J. Lipus, K. Krukiewicz, Challenges and limitations of using charge storage capacity to assess capacitance of biomedical electrodes, *Measurement* 191 (2022) 110822. <https://doi.org/10.1016/j.measurement.2022.110822>.
- [164] H.S. Magar, R.Y.A. Hassan, A. Mulchandani, Electrochemical Impedance Spectroscopy (EIS): Principles, Construction, and Biosensing Applications, *Sensors* 21 (2021) 6578. <https://doi.org/10.3390/s21196578>.
- [165] S.J. Groiss, L. Wojtecki, M. Südmeyer, A. Schnitzler, Review: Deep brain stimulation in Parkinson's disease, *Ther Adv Neurol Disord* 2 (2009) 379–391. <https://doi.org/10.1177/1756285609339382>.

- [166] I. Lavrov, P.E. Musienko, V.A. Selionov, S. Zdunowski, R.R. Roy, V. Reggie Edgerton, Y. Gerasimenko, Activation of spinal locomotor circuits in the decerebrated cat by spinal epidural and/or intraspinal electrical stimulation, *Brain Research* 1600 (2015) 84–92. <https://doi.org/10.1016/j.brainres.2014.11.003>.
- [167] V. Píkov, D.B. McCreery, M. Han, Intraspinal stimulation with a silicon-based 3D chronic microelectrode array for bladder voiding in cats, *J. Neural Eng.* (2020). <https://doi.org/10.1088/1741-2552/abca13>.
- [168] J. Volkmann, E. Moro, R. Pahwa, Basic algorithms for the programming of deep brain stimulation in Parkinson’s disease, *Mov Disord.* 21 (2006) S284–S289. <https://doi.org/10.1002/mds.20961>.
- [169] S. Arcot Desai, C.-A. Gutekunst, S.M. Potter, R.E. Gross, Deep brain stimulation macroelectrodes compared to multiple microelectrodes in rat hippocampus, *Front. Neuroeng.* 7 (2014). <https://doi.org/10.3389/fneng.2014.00016>.
- [170] J.A. Bamford, R. Marc Lebel, K. Parseyan, V.K. Mushahwar, The Fabrication, Implantation, and Stability of Intraspinal Microwire Arrays in the Spinal Cord of Cat and Rat, *IEEE Trans. Neural Syst. Rehabil. Eng.* 25 (2017) 287–296. <https://doi.org/10.1109/TNSRE.2016.2555959>.
- [171] S. Eick, Iridium oxide microelectrode arrays for in-vitro stimulation of individual rat neurons from dissociated cultures, *Front. Neuroeng* 2 (2009). <https://doi.org/10.3389/neuro.16.016.2009>.
- [172] T.M. Herrington, J.J. Cheng, E.N. Eskandar, Mechanisms of deep brain stimulation, *Journal of Neurophysiology* 115 (2016) 19–38. <https://doi.org/10.1152/jn.00281.2015>.

- [173] M.D. Sunshine, F.S. Cho, D.R. Lockwood, A.S. Fechko, M.R. Kasten, C.T. Moritz, Cervical intraspinal microstimulation evokes robust forelimb movements before and after injury, *J. Neural Eng.* 10 (2013) 036001. <https://doi.org/10.1088/1741-2560/10/3/036001>.
- [174] L. Guevremont, C.G. Renzi, J.A. Norton, J. Kowalczewski, R. Saigal, V.K. Mushahwar, Locomotor-Related Networks in the Lumbosacral Enlargement of the Adult Spinal Cat: Activation Through Intraspinal Microstimulation, *IEEE Trans. Neural Syst. Rehabil. Eng.* 14 (2006) 266–272. <https://doi.org/10.1109/TNSRE.2006.881592>.
- [175] Z. Bérces, K. Tóth, G. Márton, I. Pál, B. Kováts-Megyesi, Z. Fekete, I. Ulbert, A. Pongrácz, Neurobiochemical changes in the vicinity of a nanostructured neural implant, *Sci Rep* 6 (2016) 35944. <https://doi.org/10.1038/srep35944>.
- [176] C. Keogh, Optimizing the neuron-electrode interface for chronic bioelectronic interfacing, *Neurosurgical Focus* 49 (2020) E7. <https://doi.org/10.3171/2020.4.FOCUS20178>.
- [177] S.M. Wellman, T.D.Y. Kozai, Understanding the Inflammatory Tissue Reaction to Brain Implants To Improve Neurochemical Sensing Performance, *ACS Chem. Neurosci.* 8 (2017) 2578–2582. <https://doi.org/10.1021/acchemneuro.7b00403>.
- [178] J. Frenzel, A. Kupferer, M. Zink, S.G. Mayr, Laminin Adsorption and Adhesion of Neurons and Glial Cells on Carbon Implanted Titania Nanotube Scaffolds for Neural Implant Applications, *Nanomaterials* 12 (2022) 3858. <https://doi.org/10.3390/nano12213858>.
- [179] L. Luan, X. Wei, Z. Zhao, J.J. Siegel, O. Potnis, C.A. Tuppen, S. Lin, S. Kazmi, R.A. Fowler, S. Holloway, A.K. Dunn, R.A. Chitwood, C. Xie, Ultraflexible nanoelectronic probes form reliable, glial scar-free neural integration, *Sci. Adv.* 3 (2017) e1601966. <https://doi.org/10.1126/sciadv.1601966>.

- [180] E. Redolfi Riva, S. Micera, Progress and challenges of implantable neural interfaces based on nature-derived materials, *Bioelectron Med* 7 (2021) 6. <https://doi.org/10.1186/s42234-021-00067-7>.
- [181] E. Dauton, A.E. Mansour, M.R. Niazi, R. Munir, D.-M. Smilgies, X. Sallenave, C. Plesse, F. Goubard, A. Amassian, Conducting and Stretchable PEDOT:PSS Electrodes: Role of Additives on Self-Assembly, Morphology, and Transport, *ACS Appl. Mater. Interfaces* 11 (2019) 17570–17582. <https://doi.org/10.1021/acsami.9b00934>.
- [182] Y. Shi, R. Liu, L. He, H. Feng, Y. Li, Z. Li, Recent development of implantable and flexible nerve electrodes, *Smart Materials in Medicine* 1 (2020) 131–147. <https://doi.org/10.1016/j.smaim.2020.08.002>.
- [183] A. Golabchi, B. Wu, B. Cao, C.J. Bettinger, X.T. Cui, Zwitterionic polymer/polydopamine coating reduce acute inflammatory tissue responses to neural implants, *Biomaterials* 225 (2019) 119519. <https://doi.org/10.1016/j.biomaterials.2019.119519>.
- [184] Q. Yang, B. Wu, J.R. Eles, A.L. Vazquez, T.D.Y. Kozai, X.T. Cui, Zwitterionic Polymer Coating Suppresses Microglial Encapsulation to Neural Implants In Vitro and In Vivo, *Advanced Biosystems* 4 (2020) 1900287. <https://doi.org/10.1002/adbi.201900287>.
- [185] M. Gori, G. Vadalà, S.M. Giannitelli, V. Denaro, G. Di Pino, Biomedical and Tissue Engineering Strategies to Control Foreign Body Reaction to Invasive Neural Electrodes, *Frontiers in Bioengineering and Biotechnology* 9 (2021). <https://www.frontiersin.org/articles/10.3389/fbioe.2021.659033> (accessed December 31, 2023).
- [186] Y. Cho, Y. Choi, H. Seong, Nanoscale surface coatings and topographies for neural interfaces, *Acta Biomaterialia* (2023). <https://doi.org/10.1016/j.actbio.2023.12.025>.

- [187] B. Wu, E. Castagnola, X.T. Cui, Zwitterionic Polymer Coated and Aptamer Functionalized Flexible Micro-Electrode Arrays for In Vivo Cocaine Sensing and Electrophysiology, *Micromachines* 14 (2023) 323. <https://doi.org/10.3390/mi14020323>.
- [188] S. Jung, J. Aliberti, P. Graemmel, M.J. Sunshine, G.W. Kreutzberg, A. Sher, D.R. Littman, Analysis of Fractalkine Receptor CX₃CR1 Function by Targeted Deletion and Green Fluorescent Protein Reporter Gene Insertion, *Mol Cell Biol* 20 (2000) 4106–4114. <https://doi.org/10.1128/MCB.20.11.4106-4114.2000>.
- [189] L. Lin, R. Desai, X. Wang, E.H. Lo, C. Xing, Characteristics of primary rat microglia isolated from mixed cultures using two different methods, *J Neuroinflammation* 14 (2017) 101. <https://doi.org/10.1186/s12974-017-0877-7>.
- [190] J. Park, H. Koito, J. Li, A. Han, A Multi-compartment CNS Neuron-glia Co-culture Microfluidic Platform, *JoVE (Journal of Visualized Experiments)* (2009) e1399. <https://doi.org/10.3791/1399>.
- [191] I.R. Mineev, P. Moshayedi, J.W. Fawcett, S.P. Lacour, Interaction of glia with a compliant, microstructured silicone surface, *Acta Biomaterialia* 9 (2013) 6936–6942. <https://doi.org/10.1016/j.actbio.2013.02.048>.
- [192] S. Kuddannaya, J. Bao, Y. Zhang, Enhanced In Vitro Biocompatibility of Chemically Modified Poly(dimethylsiloxane) Surfaces for Stable Adhesion and Long-term Investigation of Brain Cerebral Cortex Cells, *ACS Appl. Mater. Interfaces* 7 (2015) 25529–25538. <https://doi.org/10.1021/acsami.5b09032>.
- [193] S. Girardin, S.J. Ihle, A. Menghini, M. Krubner, L. Tognola, J. Duru, I. Fruh, M. Müller, T. Ruff, J. Vörös, Engineering circuits of human iPSC-derived neurons and rat primary glia, *Front. Neurosci.* 17 (2023) 1103437. <https://doi.org/10.3389/fnins.2023.1103437>.

- [194] M. Gulino, D. Kim, S. Pané, S.D. Santos, A.P. Pêgo, Tissue Response to Neural Implants: The Use of Model Systems Toward New Design Solutions of Implantable Microelectrodes, *Front. Neurosci.* 13 (2019) 689. <https://doi.org/10.3389/fnins.2019.00689>.
- [195] E. Otte, A. Vlachos, M. Asplund, Engineering strategies towards overcoming bleeding and glial scar formation around neural probes, *Cell Tissue Res* 387 (2022) 461–477. <https://doi.org/10.1007/s00441-021-03567-9>.
- [196] A.C. Weitz, M.R. Behrend, A.K. Ahuja, P. Christopher, J. Wei, V. Wuyyuru, U. Patel, R.J. Greenberg, M.S. Humayun, R.H. Chow, J.D. Weiland, Interphase gap as a means to reduce electrical stimulation thresholds for epiretinal prostheses, *J. Neural Eng.* 11 (2014) 016007. <https://doi.org/10.1088/1741-2560/11/1/016007>.
- [197] A.N. Dalrymple, D.G. Everaert, D.S. Hu, V.K. Mushahwar, A speed-adaptive intraspinal microstimulation controller to restore weight-bearing stepping in a spinal cord hemisection model, *J. Neural Eng.* 15 (2018) 056023. <https://doi.org/10.1088/1741-2552/aad872>.
- [198] A.N. Dalrymple, D.A. Roszko, R.S. Sutton, V.K. Mushahwar, Pavlovian control of intraspinal microstimulation to produce over-ground walking, *J. Neural Eng.* 17 (2020) 036002. <https://doi.org/10.1088/1741-2552/ab8e8e>.
- [199] L.M. Mercier, E.J. Gonzalez-Rothi, K.A. Streeter, S.S. Posgai, A.S. Poirier, D.D. Fuller, P.J. Reier, D.M. Baekey, Intraspinal microstimulation and diaphragm activation after cervical spinal cord injury, *Journal of Neurophysiology* 117 (2017) 767–776. <https://doi.org/10.1152/jn.00721.2016>.

- [200] D.R. Dolbow, A.S. Gorgey, T.W. Sutor, V. Bochkezanian, K. Musselman, Invasive and Non-Invasive Approaches of Electrical Stimulation to Improve Physical Functioning after Spinal Cord Injury, *JCM* 10 (2021) 5356. <https://doi.org/10.3390/jcm10225356>.
- [201] J.T. Hachmann, J.H. Jeong, P.J. Grahn, G.W. Mallory, L.Q. Evertz, A.J. Bieber, D.A. Lobel, K.E. Bennet, K.H. Lee, J.L. Lujan, Large Animal Model for Development of Functional Restoration Paradigms Using Epidural and Intraspinal Stimulation, *PLoS ONE* 8 (2013) e81443. <https://doi.org/10.1371/journal.pone.0081443>.
- [202] S. Miocinovic, S. Somayajula, S. Chitnis, J.L. Vitek, History, Applications, and Mechanisms of Deep Brain Stimulation, *JAMA Neurol* 70 (2013) 163. <https://doi.org/10.1001/2013.jamaneurol.45>.
- [203] H.F. Green, Y.M. Nolan, GSK-3 mediates the release of IL-1 β , TNF- α and IL-10 from cortical glia, *Neurochemistry International* 61 (2012) 666–671. <https://doi.org/10.1016/j.neuint.2012.07.003>.
- [204] M.M. Iravani, M. Sadeghian, C.C.M. Leung, P. Jenner, S. Rose, Lipopolysaccharide-induced nigral inflammation leads to increased IL-1 β tissue content and expression of astrocytic glial cell line-derived neurotrophic factor, *Neuroscience Letters* 510 (2012) 138–142. <https://doi.org/10.1016/j.neulet.2012.01.022>.
- [205] A.M. Minogue, J.P. Barrett, M.A. Lynch, LPS-induced release of IL-6 from glia modulates production of IL-1 β in a JAK2-dependent manner, *J Neuroinflammation* 9 (2012) 629. <https://doi.org/10.1186/1742-2094-9-126>.
- [206] D. Srinivasan, J.-H. Yen, D.J. Joseph, W. Friedman, Cell Type-Specific Interleukin-1 β Signaling in the CNS, *J. Neurosci.* 24 (2004) 6482–6488. <https://doi.org/10.1523/JNEUROSCI.5712-03.2004>.

- [207] X. Liu, N. Quan, Microglia and CNS Interleukin-1: Beyond Immunological Concepts, *Front. Neurol.* 9 (2018) 8. <https://doi.org/10.3389/fneur.2018.00008>.
- [208] A.S. Mendiola, A.E. Cardona, The IL-1 β phenomena in neuroinflammatory diseases, *J Neural Transm* 125 (2018) 781–795. <https://doi.org/10.1007/s00702-017-1732-9>.
- [209] S.S. Shaftel, W.S.T. Griffin, M.K. O'Banion, The role of interleukin-1 in neuroinflammation and Alzheimer disease: an evolving perspective, *J Neuroinflammation* 5 (2008) 7. <https://doi.org/10.1186/1742-2094-5-7>.
- [210] L. Ben Haim, M.-A. Carrillo-de Sauvage, K. Ceyzériat, C. Escartin, Elusive roles for reactive astrocytes in neurodegenerative diseases, *Front. Cell. Neurosci.* 9 (2015). <https://doi.org/10.3389/fncel.2015.00278>.
- [211] S. Brahmachari, Y.K. Fung, K. Pahan, Induction of Glial Fibrillary Acidic Protein Expression in Astrocytes by Nitric Oxide, *J. Neurosci.* 26 (2006) 4930–4939. <https://doi.org/10.1523/JNEUROSCI.5480-05.2006>.
- [212] M. Pekny, M. Nilsson, Astrocyte activation and reactive gliosis, *Glia* 50 (2005) 427–434. <https://doi.org/10.1002/glia.20207>.
- [213] N. Rosskothén-Kuhl, H. Hildebrandt, R. Birkenhäger, R.-B. Illing, Astrocyte Hypertrophy and Microglia Activation in the Rat Auditory Midbrain Is Induced by Electrical Intracochlear Stimulation, *Front. Cell. Neurosci.* 12 (2018) 43. <https://doi.org/10.3389/fncel.2018.00043>.
- [214] W.S. Carbonell, S.-I. Murase, A.F. Horwitz, J.W. Mandell, Migration of Perilesional Microglia after Focal Brain Injury and Modulation by CC Chemokine Receptor 5: An *In Situ* Time-Lapse Confocal Imaging Study, *J. Neurosci.* 25 (2005) 7040–7047. <https://doi.org/10.1523/JNEUROSCI.5171-04.2005>.

- [215] C.K. Donat, G. Scott, S.M. Gentleman, M. Sastre, Microglial Activation in Traumatic Brain Injury, *Front. Aging Neurosci.* 9 (2017) 208. <https://doi.org/10.3389/fnagi.2017.00208>.
- [216] Z. Gao, Q. Zhu, Y. Zhang, Y. Zhao, L. Cai, C.B. Shields, J. Cai, Reciprocal Modulation Between Microglia and Astrocyte in Reactive Gliosis Following the CNS Injury, *Mol Neurobiol* 48 (2013) 690–701. <https://doi.org/10.1007/s12035-013-8460-4>.
- [217] G. Lind, C.E. Linsmeier, J. Schouenborg, The density difference between tissue and neural probes is a key factor for glial scarring, *Sci Rep* 3 (2013) 2942. <https://doi.org/10.1038/srep02942>.
- [218] Y. Shinozaki, K. Shibata, K. Yoshida, E. Shigetomi, C. Gachet, K. Ikenaka, K.F. Tanaka, S. Koizumi, Transformation of Astrocytes to a Neuroprotective Phenotype by Microglia via P2Y1 Receptor Downregulation, *Cell Reports* 19 (2017) 1151–1164. <https://doi.org/10.1016/j.celrep.2017.04.047>.
- [219] Z.-L. Zhou, H. Xie, X.-B. Tian, H.-L. Xu, W. Li, S. Yao, H. Zhang, Microglial depletion impairs glial scar formation and aggravates inflammation partly by inhibiting STAT3 phosphorylation in astrocytes after spinal cord injury, *Neural Regen Res* 18 (2023) 1325. <https://doi.org/10.4103/1673-5374.357912>.
- [220] M.T. Fitch, C. Doller, C.K. Combs, G.E. Landreth, J. Silver, Cellular and Molecular Mechanisms of Glial Scarring and Progressive Cavitation: *In Vivo* and *In Vitro* Analysis of Inflammation-Induced Secondary Injury after CNS Trauma, *J. Neurosci.* 19 (1999) 8182–8198. <https://doi.org/10.1523/JNEUROSCI.19-19-08182.1999>.
- [221] A.P. Tran, P.M. Warren, J. Silver, New insights into glial scar formation after spinal cord injury, *Cell Tissue Res* 387 (2022) 319–336. <https://doi.org/10.1007/s00441-021-03477-w>.

- [222] Y. Xie, N. Martini, C. Hassler, R.D. Kirch, T. Stieglitz, A. Seifert, U.G. Hofmann, In vivo monitoring of glial scar proliferation on chronically implanted neural electrodes by fiber optical coherence tomography, *Front. Neuroeng.* 7 (2014). <https://doi.org/10.3389/fneng.2014.00034>.
- [223] A. Campbell, C. Wu, Chronically Implanted Intracranial Electrodes: Tissue Reaction and Electrical Changes, *Micromachines* 9 (2018) 430. <https://doi.org/10.3390/mi9090430>.
- [224] J. Zheng, H. Wu, X. Wang, G. Zhang, J. Lu, W. Xu, S. Xu, Y. Fang, A. Zhang, A. Shao, S. Chen, Z. Zhao, J. Zhang, J. Yu, Temporal dynamics of microglia-astrocyte interaction in neuroprotective glial scar formation after intracerebral hemorrhage, *Journal of Pharmaceutical Analysis* 13 (2023) 862–879. <https://doi.org/10.1016/j.jpha.2023.02.007>.
- [225] L. Buscemi, M. Price, P. Bezzi, L. Hirt, Spatio-temporal overview of neuroinflammation in an experimental mouse stroke model, *Sci Rep* 9 (2019) 507. <https://doi.org/10.1038/s41598-018-36598-4>.
- [226] Q. Yang, J. Zhou, Neuroinflammation in the central nervous system: Symphony of glial cells, *Glia* 67 (2019) 1017–1035. <https://doi.org/10.1002/glia.23571>.
- [227] C. Zhang, J. Kang, X. Zhang, Y. Zhang, N. Huang, B. Ning, Spatiotemporal dynamics of the cellular components involved in glial scar formation following spinal cord injury, *Biomedicine & Pharmacotherapy* 153 (2022) 113500. <https://doi.org/10.1016/j.biopha.2022.113500>.
- [228] A. Carnicer-Lombarte, S.-T. Chen, G.G. Malliaras, D.G. Barone, Foreign Body Reaction to Implanted Biomaterials and Its Impact in Nerve Neuroprosthetics, *Front. Bioeng. Biotechnol.* 9 (2021) 622524. <https://doi.org/10.3389/fbioe.2021.622524>.

- [229] A. Sharon, M.M. Jankowski, N. Shmoel, H. Erez, M.E. Spira, Inflammatory Foreign Body Response Induced by Neuro-Implants in Rat Cortices Depleted of Resident Microglia by a CSF1R Inhibitor and Its Implications, *Front. Neurosci.* 15 (2021) 646914. <https://doi.org/10.3389/fnins.2021.646914>.
- [230] H. Cui, X. Xie, S. Xu, L.L.H. Chan, Y. Hu, Electrochemical characteristics of microelectrode designed for electrical stimulation, *BioMed Eng OnLine* 18 (2019) 86. <https://doi.org/10.1186/s12938-019-0704-8>.
- [231] R.A. Green, P.B. Matteucci, C.W.D. Dodds, J. Palmer, W.F. Dueck, R.T. Hassarati, P.J. Byrnes-Preston, N.H. Lovell, G.J. Suaning, Laser patterning of platinum electrodes for safe neurostimulation, *J. Neural Eng.* 11 (2014) 056017. <https://doi.org/10.1088/1741-2560/11/5/056017>.
- [232] R.K. Shepherd, P.M. Carter, A.N. Dalrymple, Y.L. Enke, A.K. Wise, T. Nguyen, J. Firth, A. Thompson, J.B. Fallon, Platinum dissolution and tissue response following long-term electrical stimulation at high charge densities, *J. Neural Eng.* 18 (2021) 036021. <https://doi.org/10.1088/1741-2552/abe5ba>.
- [233] J. Venugopal, S. Low, A.T. Choon, T.S. Sampath Kumar, S. Ramakrishna, Mineralization of osteoblasts with electrospun collagen/hydroxyapatite nanofibers, *J Mater Sci: Mater Med* 19 (2008) 2039–2046. <https://doi.org/10.1007/s10856-007-3289-x>.
- [234] O.F.-A. Akinuoye, N. Ibrahim, A. Hamzah, Application of Electron Microscopy and Energy Dispersive X-Ray Spectroscopy in the Characterization of *Rhodococcus vanniellii*, *Journal of Advanced Microscopy Research* 6 (2011) 46–52. <https://doi.org/10.1166/jamr.2011.1055>.

- [235] T.L. Rose, L.S. Robblee, Electrical stimulation with Pt electrodes. VIII. Electrochemically safe charge injection limits with 0.2 ms pulses (neuronal application), *IEEE Trans. Biomed. Eng.* 37 (1990) 1118–1120. <https://doi.org/10.1109/10.61038>.
- [236] D.B. McCreery, W.F. Agnew, T.G.H. Yuen, L. Bullara, Charge density and charge per phase as cofactors in neural injury induced by electrical stimulation, *IEEE Transactions on Biomedical Engineering* 37 (1990) 996–1001. <https://doi.org/10.1109/10.102812>.
- [237] J.A. Fairfield, Nanostructured Materials for Neural Electrical Interfaces, *Advanced Functional Materials* 28 (2018) 1701145. <https://doi.org/10.1002/adfm.201701145>.
- [238] D. Harnack, C. Winter, W. Meissner, T. Reum, A. Kupsch, R. Morgenstern, The effects of electrode material, charge density and stimulation duration on the safety of high-frequency stimulation of the subthalamic nucleus in rats, *Journal of Neuroscience Methods* 138 (2004) 207–216. <https://doi.org/10.1016/j.jneumeth.2004.04.019>.
- [239] M.R. Abidian, J.M. Corey, D.R. Kipke, D.C. Martin, Conducting-Polymer Nanotubes Improve Electrical Properties, Mechanical Adhesion, Neural Attachment, and Neurite Outgrowth of Neural Electrodes, *Small* 6 (2010) 421–429. <https://doi.org/10.1002/sml.200901868>.
- [240] A.R. Harris, A.G. Paolini, G.G. Wallace, Effective Area and Charge Density of Iridium Oxide Neural Electrodes, *Electrochimica Acta* 230 (2017) 285–292. <https://doi.org/10.1016/j.electacta.2017.02.002>.
- [241] A.R. Harris, C. Newbold, P. Carter, R. Cowan, G.G. Wallace, Measuring the effective area and charge density of platinum electrodes for bionic devices, *J. Neural Eng.* 15 (2018) 046015. <https://doi.org/10.1088/1741-2552/aaba8b>.

- [242] Md.. K.U. Sikder, W. Tong, H. Pingle, P. Kingshott, K. Needham, M.N. Shivdasani, J.B. Fallon, P. Seligman, M.R. Ibbotson, S. Prawer, D.J. Garrett, Laminin coated diamond electrodes for neural stimulation, *Materials Science and Engineering: C* 118 (2021) 111454. <https://doi.org/10.1016/j.msec.2020.111454>.
- [243] A. Verkhratsky, C. Steinhäuser, Ion channels in glial cells, *Brain Research Reviews* 32 (2000) 380–412. [https://doi.org/10.1016/S0165-0173\(99\)00093-4](https://doi.org/10.1016/S0165-0173(99)00093-4).
- [244] K.L. Turner, H. Sontheimer, Cl^- and K^+ channels and their role in primary brain tumour biology, *Phil. Trans. R. Soc. B* 369 (2014) 20130095. <https://doi.org/10.1098/rstb.2013.0095>.
- [245] A. Gilmour, L. Poole-Warren, R.A. Green, An Improved in vitro Model of Cortical Tissue, *Front. Neurosci.* 13 (2019) 1349. <https://doi.org/10.3389/fnins.2019.01349>.
- [246] M.P. Lichtenstein, N.M. Carretero, E. Pérez, M. Pulido-Salgado, J. Moral-Vico, C. Solà, N. Casañ-Pastor, C. Suñol, Biosafety assessment of conducting nanostructured materials by using co-cultures of neurons and astrocytes, *NeuroToxicology* 68 (2018) 115–125. <https://doi.org/10.1016/j.neuro.2018.07.010>.
- [247] S.M. Potter, T.B. DeMarse, A new approach to neural cell culture for long-term studies, *Journal of Neuroscience Methods* 110 (2001) 17–24. [https://doi.org/10.1016/S0165-0270\(01\)00412-5](https://doi.org/10.1016/S0165-0270(01)00412-5).
- [248] R.T. Han, R.D. Kim, A.V. Molofsky, S.A. Liddelow, Astrocyte-immune cell interactions in physiology and pathology, *Immunity* 54 (2021) 211–224. <https://doi.org/10.1016/j.immuni.2021.01.013>.
- [249] M. Linnerbauer, M.A. Wheeler, F.J. Quintana, Astrocyte Crosstalk in CNS Inflammation, *Neuron* 108 (2020) 608–622. <https://doi.org/10.1016/j.neuron.2020.08.012>.

- [250] M. Ferguson, D. Sharma, D. Ross, F. Zhao, A Critical Review of Microelectrode Arrays and Strategies for Improving Neural Interfaces, *Advanced Healthcare Materials* 8 (2019) 1900558. <https://doi.org/10.1002/adhm.201900558>.
- [251] A.C. Patil, N.V. Thakor, Implantable neurotechnologies: a review of micro- and nanoelectrodes for neural recording, *Med Biol Eng Comput* 54 (2016) 23–44. <https://doi.org/10.1007/s11517-015-1430-4>.
- [252] K.D. Wise, A.M. Sodagar, Y. Yao, M.N. Gulari, G.E. Perlin, K. Najafi, Microelectrodes, Microelectronics, and Implantable Neural Microsystems, *Proceedings of the IEEE* 96 (2008) 1184–1202. <https://doi.org/10.1109/JPROC.2008.922564>.
- [253] X. Liu, D.B. McCreery, R.R. Carter, L.A. Bullara, T.G.H. Yuen, W.F. Agnew, Stability of the interface between neural tissue and chronically implanted intracortical microelectrodes, *IEEE Transactions on Rehabilitation Engineering* 7 (1999) 315–326. <https://doi.org/10.1109/86.788468>.
- [254] R.J. Vetter, J.C. Williams, J.F. Hetke, E.A. Nunamaker, D.R. Kipke, Chronic neural recording using silicon-substrate microelectrode arrays implanted in cerebral cortex, *IEEE Transactions on Biomedical Engineering* 51 (2004) 896–904. <https://doi.org/10.1109/TBME.2004.826680>.
- [255] J. Hoon Lee, H. Kim, J. Hun Kim, S.-H. Lee, Soft implantable microelectrodes for future medicine: prosthetics, neural signal recording and neuromodulation, *Lab on a Chip* 16 (2016) 959–976. <https://doi.org/10.1039/C5LC00842E>.
- [256] N. Nassir, A. Bankapur, B. Samara, A. Ali, A. Ahmed, I.M. Inuwa, M. Zarrei, S.A. Safizadeh Shabestari, A. AlBanna, J.L. Howe, B.K. Berdiev, S.W. Scherer, M. Woodbury-Smith, M. Uddin, Single-cell transcriptome identifies molecular subtype of autism

- spectrum disorder impacted by de novo loss-of-function variants regulating glial cells, *Hum Genomics* 15 (2021) 1–16. <https://doi.org/10.1186/s40246-021-00368-7>.
- [257] L. Gao, X. Pan, J.H. Zhang, Y. Xia, Glial cells: an important switch for the vascular function of the central nervous system, *Frontiers in Cellular Neuroscience* 17 (2023). <https://www.frontiersin.org/articles/10.3389/fncel.2023.1166770> (accessed January 2, 2024).
- [258] N. Schmid-Brunclik, C. Bürgi-Taboada, X. Antoniou, M. Gassmann, O.O. Ogunshola, Astrocyte responses to injury: VEGF simultaneously modulates cell death and proliferation, *American Journal of Physiology-Regulatory, Integrative and Comparative Physiology* 295 (2008) R864–R873. <https://doi.org/10.1152/ajpregu.00536.2007>.
- [259] M.K. Jha, M. Jo, J.-H. Kim, K. Suk, Microglia-Astrocyte Crosstalk: An Intimate Molecular Conversation, *Neuroscientist* 25 (2019) 227–240. <https://doi.org/10.1177/1073858418783959>.
- [260] F. Lotti, F. Ranieri, G. Vadalà, L. Zollo, G. Di Pino, Invasive Intraneural Interfaces: Foreign Body Reaction Issues, *Frontiers in Neuroscience* 11 (2017). <https://www.frontiersin.org/articles/10.3389/fnins.2017.00497> (accessed January 2, 2024).
- [261] O. Bouadi, T.L. Tay, More Than Cell Markers: Understanding Heterogeneous Glial Responses to Implantable Neural Devices, *Frontiers in Cellular Neuroscience* 15 (2021). <https://www.frontiersin.org/articles/10.3389/fncel.2021.658992> (accessed January 2, 2024).
- [262] K.M. Woeppel, X.T. Cui, Nanoparticle and Biomolecule Surface Modification Synergistically Increases Neural Electrode Recording Yield and Minimizes Inflammatory

- Host Response, *Advanced Healthcare Materials* 10 (2021) 2002150.
<https://doi.org/10.1002/adhm.202002150>.
- [263] E. Azemi, C.F. Lagenaur, X.T. Cui, The surface immobilization of the neural adhesion molecule L1 on neural probes and its effect on neuronal density and gliosis at the probe/tissue interface, *Biomaterials* 32 (2011) 681–692.
<https://doi.org/10.1016/j.biomaterials.2010.09.033>.
- [264] D. Kim, D. Park, T.H. Kim, J.J. Chung, Y. Jung, S.H. Kim, Substance P/Heparin-Conjugated PLCL Mitigate Acute Gliosis on Neural Implants and Improve Neuronal Regeneration via Recruitment of Neural Stem Cells, *Advanced Healthcare Materials* 10 (2021) 2100107. <https://doi.org/10.1002/adhm.202100107>.
- [265] N. Chen, B. Luo, I.H. Yang, N.V. Thakor, S. Ramakrishna, Biofunctionalized platforms towards long-term neural interface, *Current Opinion in Biomedical Engineering* 6 (2018) 81–91. <https://doi.org/10.1016/j.cobme.2018.03.002>.
- [266] M. Boulingre, R. Portillo-Lara, R. A. Green, Biohybrid neural interfaces: improving the biological integration of neural implants, *Chemical Communications* 59 (2023) 14745–14758. <https://doi.org/10.1039/D3CC05006H>.
- [267] N. Hoffmann, U. Mittnacht, H. Hartmann, Y. Baumer, J. Kjems, S. Oberhoffner, B. Schlosshauer, Neuronal and glial responses to siRNA-coated nerve guide implants in vitro, *Neuroscience Letters* 494 (2011) 14–18. <https://doi.org/10.1016/j.neulet.2011.02.043>.
- [268] Y. Zhong, G.C. McConnell, J.D. Ross, S.P. DeWeerth, R.V. Bellamkonda, A Novel Dexamethasone-releasing, Anti-inflammatory Coating for Neural Implants, in: *Conference Proceedings. 2nd International IEEE EMBS Conference on Neural Engineering, 2005.*, 2005: pp. 522–525. <https://doi.org/10.1109/CNE.2005.1419674>.

- [269] Z. Zhang, J. Nong, Y. Zhong, Antibacterial, anti-inflammatory and neuroprotective layer-by-layer coatings for neural implants, *J. Neural Eng.* 12 (2015) 046015. <https://doi.org/10.1088/1741-2560/12/4/046015>.
- [270] B. Liu, E. Kim, A. Meggo, S. Gandhi, H. Luo, S. Kallakuri, Y. Xu, J. Zhang, Enhanced biocompatibility of neural probes by integrating microstructures and delivering anti-inflammatory agents via microfluidic channels, *J. Neural Eng.* 14 (2017) 026008. <https://doi.org/10.1088/1741-2552/aa52dc>.
- [271] Y. Zhong, R.V. Bellamkonda, Dexamethasone-coated neural probes elicit attenuated inflammatory response and neuronal loss compared to uncoated neural probes, *Brain Research* 1148 (2007) 15–27. <https://doi.org/10.1016/j.brainres.2007.02.024>.
- [272] M. Asplund, C. Boehler, T. Stieglitz, Anti-inflammatory polymer electrodes for glial scar treatment: bringing the conceptual idea to future results, *Frontiers in Neuroengineering* 7 (2014). <https://www.frontiersin.org/articles/10.3389/fneng.2014.00009> (accessed January 2, 2024).
- [273] J. Shi, Y. Fang, Flexible and Implantable Microelectrodes for Chronically Stable Neural Interfaces, *Advanced Materials* 31 (2019) 1804895. <https://doi.org/10.1002/adma.201804895>.
- [274] H.C. Lee, F. Ejserholm, J. Gaire, S. Currin, J. Schouenborg, L. Wallman, M. Bengtsson, K. Park, K.J. Otto, Histological evaluation of flexible neural implants; flexibility limit for reducing the tissue response?, *J. Neural Eng.* 14 (2017) 036026. <https://doi.org/10.1088/1741-2552/aa68f0>.
- [275] P. Köhler, A. Wolff, F. Ejserholm, L. Wallman, J. Schouenborg, C.E. Linsmeier, Influence of Probe Flexibility and Gelatin Embedding on Neuronal Density and Glial Responses to

Brain Implants, PLOS ONE 10 (2015) e0119340.
<https://doi.org/10.1371/journal.pone.0119340>.

- [276] E. McGlynn, V. Nabaei, E. Ren, G. Galeote-Checa, R. Das, G. Curia, H. Heidari, The Future of Neuroscience: Flexible and Wireless Implantable Neural Electronics, *Advanced Science* 8 (2021) 2002693. <https://doi.org/10.1002/advs.202002693>.
- [277] M. Vomero, F. Ciarpella, E. Zucchini, M. Kirsch, L. Fadiga, T. Stieglitz, M. Asplund, On the longevity of flexible neural interfaces: Establishing biostability of polyimide-based intracortical implants, *Biomaterials* 281 (2022) 121372. <https://doi.org/10.1016/j.biomaterials.2022.121372>.
- [278] Z.J. Du, C.L. Kolarcik, T.D.Y. Kozai, S.D. Luebben, S.A. Sapp, X.S. Zheng, J.A. Nabity, X.T. Cui, Ultrasoft microwire neural electrodes improve chronic tissue integration, *Acta Biomaterialia* 53 (2017) 46–58. <https://doi.org/10.1016/j.actbio.2017.02.010>.
- [279] S.J. Hasan, B.H. Nelson, J.I. Valenzuela, H.S. Keirstead, S.E. Shull, D.W. Ethell, J.D. Steeves, Functional repair of transected spinal cord in embryonic chick, *Restor Neurol Neurosci* 2 (1991) 137–154. <https://doi.org/10.3233/RNN-1991-2303>.
- [280] J. Evers, K. Sridhar, J. Liegey, J. Brady, H. Jahns, M. Lowery, Stimulation-induced changes at the electrode–tissue interface and their influence on deep brain stimulation, *J. Neural Eng.* 19 (2022) 046004. <https://doi.org/10.1088/1741-2552/ac7ad6>.
- [281] J.E. Collazos-Castro, C. García-Rama, A. Alves-Sampaio, Glial progenitor cell migration promotes CNS axon growth on functionalized electroconducting microfibers, *Acta Biomaterialia* 35 (2016) 42–56. <https://doi.org/10.1016/j.actbio.2016.02.023>.
- [282] I. Cuenca-Ortolá, B. Martínez-Rojas, V. Moreno-Manzano, M. García Castelló, M. Monleón Pradas, C. Martínez-Ramos, J. Más Estellés, A Strategy for Magnetic and

- Electric Stimulation to Enhance Proliferation and Differentiation of NPCs Seeded over PLA Electrospun Membranes, *Biomedicines* 10 (2022) 2736.
<https://doi.org/10.3390/biomedicines10112736>.
- [283] A.R.R.H. Hamid, S. Maliawan, D.P.G.P. Samatra, N.M. Astawa, I.M. Bakta, I.M. Jawi, I.B.P. Manuaba, I.M.D. Sukrama, D.S. Perdanakusuma, Effect of immediate electrical stimulation in the distal segment of the nerve with Wallerian degeneration in rats with sciatic nerve injury, *Medical Journal of Indonesia* 31 (2022) 7–12.
<https://doi.org/10.13181/mji.oa.225870>.
- [284] C. McMakin, *Frequency Specific Microcurrent in Pain Management*, Elsevier Health Sciences, 2011.
- [285] X. Cheng, T. Li, H. Zhou, Q. Zhang, J. Tan, W. Gao, J. Wang, C. Li, Y.Y. Duan, Cortical electrical stimulation with varied low frequencies promotes functional recovery and brain remodeling in a rat model of ischemia, *Brain Research Bulletin* 89 (2012) 124–132.
<https://doi.org/10.1016/j.brainresbull.2012.07.009>.
- [286] K. van Kuyck, M. Welkenhuysen, L. Arckens, R. Sciot, B. Nuttin, Histological Alterations Induced by Electrode Implantation and Electrical Stimulation in the Human Brain: A Review, *Neuromodulation: Technology at the Neural Interface* 10 (2007) 244–261.
<https://doi.org/10.1111/j.1525-1403.2007.00114.x>.
- [287] P. Thevenaz, U.E. Ruttimann, M. Unser, A pyramid approach to subpixel registration based on intensity, *IEEE Trans. on Image Process.* 7 (1998) 27–41.
<https://doi.org/10.1109/83.650848>.

- [288] E.P.W. Jenkins, A. Finch, M. Gerigk, I.F. Triantis, C. Watts, G.G. Malliaras, Electrotherapies for Glioblastoma, *Advanced Science* 8 (2021) 2100978. <https://doi.org/10.1002/advs.202100978>.
- [289] M. Dihné, F. Block, H. Korr, R. Töpfer, Time course of glial proliferation and glial apoptosis following excitotoxic CNS injury, *Brain Research* 902 (2001) 178–189. [https://doi.org/10.1016/S0006-8993\(01\)02378-2](https://doi.org/10.1016/S0006-8993(01)02378-2).
- [290] J. Dreßler, U. Hanisch, E. Kuhlisch, K.D. Geiger, Neuronal and glial apoptosis in human traumatic brain injury, *Int J Legal Med* 121 (2007) 365–375. <https://doi.org/10.1007/s00414-006-0126-6>.
- [291] L. Yao, T. Shippy, Y. Li, Genetic analysis of the molecular regulation of electric fields-guided glia migration, *Sci Rep* 10 (2020) 16821. <https://doi.org/10.1038/s41598-020-74085-x>.
- [292] C. Yang, L. Wang, W. Weng, S. Wang, Y. Ma, Q. Mao, G. Gao, R. Chen, J. Feng, Steered migration and changed morphology of human astrocytes by an applied electric field, *Experimental Cell Research* 374 (2019) 282–289. <https://doi.org/10.1016/j.yexcr.2018.11.029>.
- [293] N.L. Chrobok, A. Jaouen, K.K. Fenrich, J.G.J.M. Bol, M.M.M. Wilhelmus, B. Drukarch, F. Debarbieux, A.-M. van Dam, Monocyte behaviour and tissue transglutaminase expression during experimental autoimmune encephalomyelitis in transgenic CX3CR1gfp/gfp mice, *Amino Acids* 49 (2017) 643–658. <https://doi.org/10.1007/s00726-016-2359-0>.
- [294] F.S.M. Tristão, M. Lazzarini, S. Martin, M. Amar, W. Stühmer, F. Kirchhoff, L.A.C. Gomes, L. Lanfumey, R.D. Prediger, J.E. Sepulveda, E.A. Del-Bel, R. Raisman-Vozari,

- CX3CR1 Disruption Differentially Influences Dopaminergic Neuron Degeneration in Parkinsonian Mice Depending on the Neurotoxin and Route of Administration, *Neurotox Res* 29 (2016) 364–380. <https://doi.org/10.1007/s12640-015-9557-5>.
- [295] A.L. Xavier, F.R.S. Lima, M. Nedergaard, J.R.L. Menezes, Ontogeny of CX3CR1-EGFP expressing cells unveil microglia as an integral component of the postnatal subventricular zone, *Frontiers in Cellular Neuroscience* 9 (2015). <https://www.frontiersin.org/articles/10.3389/fncel.2015.00037> (accessed January 29, 2024).
- [296] W.W. Pong, S.B. Higer, S.M. Gianino, R.J. Emmett, D.H. Gutmann, Reduced microglial CX3CR1 expression delays neurofibromatosis-1 glioma formation, *Annals of Neurology* 73 (2013) 303–308. <https://doi.org/10.1002/ana.23813>.
- [297] T. Ishijima, K. Nakajima, Inflammatory cytokines TNF α , IL-1 β , and IL-6 are induced in endotoxin- stimulated microglia through different signaling cascades, *Science Progress* 104 (2021) 00368504211054985. <https://doi.org/10.1177/00368504211054985>.
- [298] X. Lu, L. Ma, L. Ruan, Y. Kong, H. Mou, Z. Zhang, Z. Wang, J.M. Wang, Y. Le, Resveratrol differentially modulates inflammatory responses of microglia and astrocytes, *J Neuroinflammation* 7 (2010) 1–14. <https://doi.org/10.1186/1742-2094-7-46>.
- [299] H.S. Kwon, S.-H. Koh, Neuroinflammation in neurodegenerative disorders: the roles of microglia and astrocytes, *Transl Neurodegener* 9 (2020) 42. <https://doi.org/10.1186/s40035-020-00221-2>.
- [300] S.M. Sweitzer, R.W. Colburn, M. Rutkowski, J.A. DeLeo, Acute peripheral inflammation induces moderate glial activation and spinal IL-1 β expression that correlates with pain

- behavior in the rat¹Published on the World Wide Web on 17 March 1999.1, *Brain Research* 829 (1999) 209–221. [https://doi.org/10.1016/S0006-8993\(99\)01326-8](https://doi.org/10.1016/S0006-8993(99)01326-8).
- [301] T. Wang, Q. Sun, J. Yang, G. Wang, F. Zhao, Y. Chen, Y. Jin, Reactive astrocytes induced by 2-chloroethanol modulate microglia polarization through IL-1 β , TNF- α , and iNOS upregulation, *Food and Chemical Toxicology* 157 (2021) 112550. <https://doi.org/10.1016/j.fct.2021.112550>.
- [302] D. Boinagrov, S. Pangratz-Fuehrer, B. Suh, K. Mathieson, N. Naik, D. Palanker, Upper threshold of extracellular neural stimulation, *Journal of Neurophysiology* 108 (2012) 3233–3238. <https://doi.org/10.1152/jn.01058.2011>.
- [303] D.B. McCreery, W.F. Agnew, T.G.H. Yuen, L.A. Bullara, Relationship between stimulus amplitude, stimulus frequency and neural damage during electrical stimulation of sciatic nerve of cat, *Med. Biol. Eng. Comput.* 33 (1995) 426–429. <https://doi.org/10.1007/BF02510526>.
- [304] T. Tsoneva, G. Garcia-Molina, P. Desain, Neural dynamics during repetitive visual stimulation, *J. Neural Eng.* 12 (2015) 066017. <https://doi.org/10.1088/1741-2560/12/6/066017>.
- [305] J. Dowsett, C.S. Herrmann, Transcranial Alternating Current Stimulation with Sawtooth Waves: Simultaneous Stimulation and EEG Recording, *Front. Hum. Neurosci.* 10 (2016). <https://doi.org/10.3389/fnhum.2016.00135>.
- [306] D.M. Durand, A. Jensen, M. Bikson, Suppression of Neural Activity with High Frequency Stimulation, in: 2006 International Conference of the IEEE Engineering in Medicine and Biology Society, 2006: pp. 1624–1625. <https://doi.org/10.1109/IEMBS.2006.259396>.

- [307] A.L. Jensen, D.M. Durand, High frequency stimulation can block axonal conduction, *Experimental Neurology* 220 (2009) 57–70. <https://doi.org/10.1016/j.expneurol.2009.07.023>.
- [308] D.T. Brocker, W.M. Grill, Chapter 1 - Principles of electrical stimulation of neural tissue, in: A.M. Lozano, M. Hallett (Eds.), *Handbook of Clinical Neurology*, Elsevier, 2013: pp. 3–18. <https://doi.org/10.1016/B978-0-444-53497-2.00001-2>.
- [309] R.B. Keeton, S.A. Binder-Macleod, Low-Frequency Fatigue, *Physical Therapy* 86 (2006) 1146–1150. <https://doi.org/10.1093/ptj/86.8.1146>.
- [310] S.P. Hardy, T.B. Spalding, H. Liu, T.G. Nick, R.H. Pearson, A.V. Hayes, D.S. Stokic, The Effect of Transcutaneous Electrical Stimulation on Spinal Motor Neuron Excitability in People Without Known Neuromuscular Diseases: The Roles of Stimulus Intensity and Location, *Physical Therapy* 82 (2002) 354–363. <https://doi.org/10.1093/ptj/82.4.354>.
- [311] A.Y. Lai, K.S. Dhimi, C.D. Dibal, K.G. Todd, Neonatal rat microglia derived from different brain regions have distinct activation responses, *Neuron Glia Biology* 7 (2011) 5–16. <https://doi.org/10.1017/S1740925X12000154>.
- [312] T. Wyckhuys, R. Raedt, K. Vonck, W. Wadman, P. Boon, Comparison of hippocampal Deep Brain Stimulation with high (130Hz) and low frequency (5Hz) on afterdischarges in kindled rats, *Epilepsy Research* 88 (2010) 239–246. <https://doi.org/10.1016/j.eplepsyres.2009.11.014>.
- [313] M.-L. Welter, J.-L. Houeto, A.-M. Bonnet, P.-B. Bejjani, V. Mesnage, D. Dormont, S. Navarro, P. Cornu, Y. Agid, B. Pidoux, Effects of High-Frequency Stimulation on Subthalamic Neuronal Activity in Parkinsonian Patients, *Arch Neurol* 61 (2004) 89. <https://doi.org/10.1001/archneur.61.1.89>.

- [314] L. Garcia, J. Audin, G. D'Alessandro, B. Bioulac, C. Hammond, Dual Effect of High-Frequency Stimulation on Subthalamic Neuron Activity, *J. Neurosci.* 23 (2003) 8743–8751. <https://doi.org/10.1523/JNEUROSCI.23-25-08743.2003>.
- [315] J.-P. Lefaucheur, Methods of therapeutic cortical stimulation, *Neurophysiologie Clinique/Clinical Neurophysiology* 39 (2009) 1–14. <https://doi.org/10.1016/j.neucli.2008.11.001>.
- [316] S. van Heukelum, J. Kelderhuis, P. Janssen, G. van Luijtelaar, A. Lüttjohann, Timing of high-frequency cortical stimulation in a genetic absence model, *Neuroscience* 324 (2016) 191–201. <https://doi.org/10.1016/j.neuroscience.2016.02.070>.
- [317] Z. Song, B.A. Meyerson, B. Linderoth, High-Frequency (1 kHz) Spinal Cord Stimulation—Is Pulse Shape Crucial for the Efficacy? A Pilot Study, *Neuromodulation: Technology at the Neural Interface* 18 (2015) 714–720. <https://doi.org/10.1111/ner.12344>.
- [318] M. Brenner, A. Messing, GFAP Transgenic Mice, *Methods* 10 (1996) 351–364. <https://doi.org/10.1006/meth.1996.0113>.
- [319] M. Brenner, W.C. Kisseberth, Y. Su, F. Besnard, A. Messing, GFAP promoter directs astrocyte-specific expression in transgenic mice, *J. Neurosci.* 14 (1994) 1030–1037. <https://doi.org/10.1523/JNEUROSCI.14-03-01030.1994>.
- [320] L. Zhuo, B. Sun, C.-L. Zhang, A. Fine, S.-Y. Chiu, A. Messing, Live Astrocytes Visualized by Green Fluorescent Protein in Transgenic Mice, *Developmental Biology* 187 (1997) 36–42. <https://doi.org/10.1006/dbio.1997.8601>.
- [321] C. Nolte, M. Matyash, T. Pivneva, C.G. Schipke, C. Ohlemeyer, U.-K. Hanisch, F. Kirchhoff, H. Kettenmann, GFAP promoter-controlled EGFP-expressing transgenic mice:

- A tool to visualize astrocytes and astrogliosis in living brain tissue, *Glia* 33 (2001) 72–86.
[https://doi.org/10.1002/1098-1136\(20010101\)33:1<72::AID-GLIA1007>3.0.CO;2-A](https://doi.org/10.1002/1098-1136(20010101)33:1<72::AID-GLIA1007>3.0.CO;2-A).
- [322] C.G. Huber, H. Oberacher, Analysis of nucleic acids by on-line liquid chromatography–Mass spectrometry, *Mass Spectrometry Reviews* 20 (2001) 310–343.
<https://doi.org/10.1002/mas.10011>.
- [323] E. Largy, A. König, A. Ghosh, D. Ghosh, S. Benabou, F. Rosu, V. Gabelica, Mass Spectrometry of Nucleic Acid Noncovalent Complexes, *Chem. Rev.* 122 (2022) 7720–7839. <https://doi.org/10.1021/acs.chemrev.1c00386>.
- [324] E. Nordhoff, F. Kirpekar, P. Roepstorff, Mass spectrometry of nucleic acids, *Mass Spectrometry Reviews* 15 (1996) 67–138. [https://doi.org/10.1002/\(SICI\)1098-2787\(1996\)15:2<67::AID-MAS1>3.0.CO;2-8](https://doi.org/10.1002/(SICI)1098-2787(1996)15:2<67::AID-MAS1>3.0.CO;2-8).
- [325] J.H. Banoub, R.P. Newton, E. Esmans, D.F. Ewing, G. Mackenzie, Recent Developments in Mass Spectrometry for the Characterization of Nucleosides, Nucleotides, Oligonucleotides, and Nucleic Acids, *Chem. Rev.* 105 (2005) 1869–1916.
<https://doi.org/10.1021/cr030040w>.
- [326] C.L. Faingold, Electrical stimulation therapies for CNS disorders and pain are mediated by competition between different neuronal networks in the brain, *Medical Hypotheses* 71 (2008) 668–681. <https://doi.org/10.1016/j.mehy.2008.06.030>.
- [327] A.-L. Benabid, B. Wallace, J. Mitrofanis, C. Xia, B. Piallat, V. Fraix, A. Batir, P. Krack, P. Pollak, F. Berger, Therapeutic electrical stimulation of the central nervous system, *Comptes Rendus Biologies* 328 (2005) 177–186.
<https://doi.org/10.1016/j.crv.2004.10.011>.

- [328] E. Musk, Neuralink, An Integrated Brain-Machine Interface Platform With Thousands of Channels, *Journal of Medical Internet Research* 21 (2019) e16194. <https://doi.org/10.2196/16194>.
- [329] M.K. Nagai, C. Marquez-Chin, M.R. Popovic, Why Is Functional Electrical Stimulation Therapy Capable of Restoring Motor Function Following Severe Injury to the Central Nervous System?, in: M.H. Tuszynski (Ed.), *Translational Neuroscience: Fundamental Approaches for Neurological Disorders*, Springer US, Boston, MA, 2016: pp. 479–498. https://doi.org/10.1007/978-1-4899-7654-3_25.
- [330] S. Waldert, Invasive vs. Non-Invasive Neuronal Signals for Brain-Machine Interfaces: Will One Prevail?, *Frontiers in Neuroscience* 10 (2016). <https://www.frontiersin.org/articles/10.3389/fnins.2016.00295> (accessed January 30, 2024).
- [331] K. Joseph, M. Kirsch, M. Johnston, C. Münkler, T. Stieglitz, C.A. Haas, U.G. Hofmann, Transcriptional characterization of the glial response due to chronic neural implantation of flexible microprobes, *Biomaterials* 279 (2021) 121230. <https://doi.org/10.1016/j.biomaterials.2021.121230>.
- [332] D.G. Barone, A. Carnicer-Lombarte, P. Turlomousis, R.S. Hamilton, M. Prater, A.L. Rutz, I.B. Dimov, G.G. Malliaras, S.P. Lacour, A.A.B. Robertson, K. Franze, J.W. Fawcett, C.E. Bryant, Prevention of the foreign body response to implantable medical devices by inflammasome inhibition, *Proceedings of the National Academy of Sciences* 119 (2022) e2115857119. <https://doi.org/10.1073/pnas.2115857119>.
- [333] C.L. Frewin, C. Locke, L. Mariusso, E.J. Weeber, S.E. Sadow, Silicon carbide neural implants: In vivo neural tissue reaction, in: 2013 6th International IEEE/EMBS

- Conference on Neural Engineering (NER), 2013: pp. 661–664.
<https://doi.org/10.1109/NER.2013.6696021>.
- [334] D.Y. Lewitus, K.L. Smith, J. Landers, A.V. Neimark, J. Kohn, Bioactive agarose carbon-nanotube composites are capable of manipulating brain–implant interface, *Journal of Applied Polymer Science* 131 (2014). <https://doi.org/10.1002/app.40297>.
- [335] J.R. Eles, A.L. Vazquez, T.D.Y. Kozai, X.T. Cui, Meningeal inflammatory response and fibrous tissue remodeling around intracortical implants: An in vivo two-photon imaging study, *Biomaterials* 195 (2019) 111–123.
<https://doi.org/10.1016/j.biomaterials.2018.12.031>.
- [336] Y.-S. Chen, H.-J. Harn, T.-W. Chiou, The Role of Biomaterials in Implantation for Central Nervous System Injury, *Cell Transplant* 27 (2018) 407–422.
<https://doi.org/10.1177/0963689717732991>.
- [337] A.Ch. Lazanas, M.I. Prodromidis, Electrochemical Impedance Spectroscopy—A Tutorial, *ACS Meas. Sci. Au* 3 (2023) 162–193. <https://doi.org/10.1021/acsmesuresciau.2c00070>.
- [338] S.F. Cogan, P.R. Troyk, J. Ehrlich, C.M. Gasbarro, T.D. Plante, The influence of electrolyte composition on the in vitro charge-injection limits of activated iridium oxide (AIROF) stimulation electrodes, *J. Neural Eng.* 4 (2007) 79. <https://doi.org/10.1088/1741-2560/4/2/008>.
- [339] S. Venkatraman, J. Hendricks, Z.A. King, A.J. Sereno, S. Richardson-Burns, D. Martin, J.M. Carmena, In Vitro and In Vivo Evaluation of PEDOT Microelectrodes for Neural Stimulation and Recording, *IEEE Transactions on Neural Systems and Rehabilitation Engineering* 19 (2011) 307–316. <https://doi.org/10.1109/TNSRE.2011.2109399>.

- [340] S. Negi, R. Bhandari, L. Rieth, F. Solzbacher, In vitro comparison of sputtered iridium oxide and platinum-coated neural implantable microelectrode arrays, *Biomed. Mater.* 5 (2010) 015007. <https://doi.org/10.1088/1748-6041/5/1/015007>.
- [341] C. Henle, W. Meier, M. Schuettler, T. Boretius, T. Stieglitz, Electrical Characterization of Platinum, Stainless Steel and Platinum/Iridium as Electrode Materials for a New Neural Interface, in: O. Dössel, W.C. Schlegel (Eds.), *World Congress on Medical Physics and Biomedical Engineering*, September 7 - 12, 2009, Munich, Germany, Springer, Berlin, Heidelberg, 2009: pp. 100–103. https://doi.org/10.1007/978-3-642-03889-1_27.
- [342] I.R. Cassar, C. Yu, J. Sambangi, C.D. Lee, J.J. Whalen, A. Petrossians, W.M. Grill, Electrodeposited platinum-iridium coating improves in vivo recording performance of chronically implanted microelectrode arrays, *Biomaterials* 205 (2019) 120–132. <https://doi.org/10.1016/j.biomaterials.2019.03.017>.
- [343] A. Petrossians, J.J. Whalen, J.D. Weiland, F. Mansfeld, Surface modification of neural stimulating/recording electrodes with high surface area platinum-iridium alloy coatings, in: *2011 Annual International Conference of the IEEE Engineering in Medicine and Biology Society*, 2011: pp. 3001–3004. <https://doi.org/10.1109/IEMBS.2011.6090823>.
- [344] Q. Zeng, S. Yu, Z. Fan, Y. Huang, B. Song, T. Zhou, Nanocone-Array-Based Platinum-Iridium Oxide Neural Microelectrodes: Structure, Electrochemistry, Durability and Biocompatibility Study, *Nanomaterials* 12 (2022) 3445. <https://doi.org/10.3390/nano12193445>.
- [345] A. Ornoy, S. Yacobi, P. Yaffee, A simple method of culture of 11.5-day-old rat embryos in DMEM/F12 and 20% fetal bovine serum, *Journal of Anatomy* 203 (2003) 419–423. <https://doi.org/10.1046/j.1469-7580.2003.00225.x>.

- [346] C. Krizhanovskii, H. Kristinsson, A. Elksnis, X. Wang, H. Gavali, P. Bergsten, R. Scharfmann, N. Welsh, EndoC- β H1 cells display increased sensitivity to sodium palmitate when cultured in DMEM/F12 medium, *Islets* 9 (2017) e1296995. <https://doi.org/10.1080/19382014.2017.1296995>.
- [347] R. Pal, M. Hanwate, M. Jan, S. Totey, Phenotypic and functional comparison of optimum culture conditions for upscaling of bone marrow-derived mesenchymal stem cells, *Journal of Tissue Engineering and Regenerative Medicine* 3 (2009) 163–174. <https://doi.org/10.1002/term.143>.
- [348] K. Hemmrich, D. von Heimburg, K. Cierpka, S. Haydarlioglu, N. Pallua, Optimization of the differentiation of human preadipocytes in vitro, *Differentiation* 73 (2005) 28–35. <https://doi.org/10.1111/j.1432-0436.2005.07301003.x>.
- [349] U. Riekstina, R. Muceniece, I. Cakstina, I. Muiznieks, J. Ancans, Characterization of human skin-derived mesenchymal stem cell proliferation rate in different growth conditions, *Cytotechnology* 58 (2008) 153–162. <https://doi.org/10.1007/s10616-009-9183-2>.
- [350] M. Nikkhah, J.S. Strobl, E.M. Schmelz, M. Agah, Evaluation of the influence of growth medium composition on cell elasticity, *Journal of Biomechanics* 44 (2011) 762–766. <https://doi.org/10.1016/j.jbiomech.2010.11.002>.
- [351] P. Van Pham, N.C. Truong, P.T.-B. Le, T.D.-X. Tran, N.B. Vu, K.H.-T. Bui, N.K. Phan, Isolation and proliferation of umbilical cord tissue derived mesenchymal stem cells for clinical applications, *Cell Tissue Bank* 17 (2016) 289–302. <https://doi.org/10.1007/s10561-015-9541-6>.

- [352] R.C.C. Chang, C. Rota, R.E. Glover, R.P. Mason, J.-S. Hong, A novel effect of an opioid receptor antagonist, naloxone, on the production of reactive oxygen species by microglia: a study by electron paramagnetic resonance spectroscopy, *Brain Research* 854 (2000) 224–229. [https://doi.org/10.1016/S0006-8993\(99\)02267-2](https://doi.org/10.1016/S0006-8993(99)02267-2).
- [353] N. Elgrishi, K.J. Rountree, B.D. McCarthy, E.S. Rountree, T.T. Eisenhart, J.L. Dempsey, A Practical Beginner's Guide to Cyclic Voltammetry, *J. Chem. Educ.* 95 (2018) 197–206. <https://doi.org/10.1021/acs.jchemed.7b00361>.
- [354] Q. Zeng, K. Xia, B. Sun, Y. Yin, T. Wu, M.S. Humayun, Electrodeposited Iridium Oxide on Platinum Nanocones for Improving Neural Stimulation Microelectrodes, *Electrochimica Acta* 237 (2017) 152–159. <https://doi.org/10.1016/j.electacta.2017.03.213>.
- [355] Y. Park, S.H. Kim, S. Matalon, N.-H.L. Wang, E.I. Franses, Effect of phosphate salts concentrations, supporting electrolytes, and calcium phosphate salt precipitation on the pH of phosphate buffer solutions, *Fluid Phase Equilibria* 278 (2009) 76–84. <https://doi.org/10.1016/j.fluid.2009.01.005>.
- [356] S. Luo, Z. Liu, D. Liu, H. Zhang, L. Guo, M. Rong, M.G. Kong, Modeling study of the indirect treatment of phosphate buffered saline in surface air plasma, *J. Phys. D: Appl. Phys.* 54 (2020) 065203. <https://doi.org/10.1088/1361-6463/abc19c>.
- [357] A.A. Thorat, R. Suryanarayanan, Characterization of Phosphate Buffered Saline (PBS) in Frozen State and after Freeze-Drying, *Pharm Res* 36 (2019) 98. <https://doi.org/10.1007/s11095-019-2619-2>.
- [358] C. Boehler, S. Carli, L. Fadiga, T. Stieglitz, M. Asplund, Tutorial: guidelines for standardized performance tests for electrodes intended for neural interfaces and

- bioelectronics, *Nat Protoc* 15 (2020) 3557–3578. <https://doi.org/10.1038/s41596-020-0389-2>.
- [359] R.G. Ham, Clonal growth of mammalian cells in a chemically defined, synthetic medium*, *Proceedings of the National Academy of Sciences* 53 (1965) 288–293. <https://doi.org/10.1073/pnas.53.2.288>.
- [360] H.J. Morton, A survey of commercially available tissue culture media, *In Vitro* 6 (1970) 89–108. <https://doi.org/10.1007/BF02616112>.
- [361] C.-Y. Fang, C.-C. Wu, C.-L. Fang, W.-Y. Chen, C.-L. Chen, Long-term growth comparison studies of FBS and FBS alternatives in six head and neck cell lines, *PLOS ONE* 12 (2017) e0178960. <https://doi.org/10.1371/journal.pone.0178960>.
- [362] D.Y. Lee, S.Y. Lee, S.H. Yun, J.W. Jeong, J.H. Kim, H.W. Kim, J.S. Choi, G.-D. Kim, S.T. Joo, I. Choi, S.J. Hur, Review of the Current Research on Fetal Bovine Serum and the Development of Cultured Meat, *Food Science of Animal Resources* 42 (2022) 775–799. <https://doi.org/10.5851/kosfa.2022.e46>.
- [363] J.R. Vetsch, S.J. Paulsen, R. Müller, S. Hofmann, Effect of fetal bovine serum on mineralization in silk fibroin scaffolds, *Acta Biomaterialia* 13 (2015) 277–285. <https://doi.org/10.1016/j.actbio.2014.11.025>.
- [364] A.R. Harris, P. Carter, R. Cowan, G.G. Wallace, Impact of Protein Fouling on the Charge Injection Capacity, Impedance, and Effective Electrode Area of Platinum Electrodes for Bionic Devices, *ChemElectroChem* 8 (2021) 1078–1090. <https://doi.org/10.1002/celec.202001574>.

- [365] G.S. J. Peters M. Hendriks ,M., Estimation of the Electrical Conductivity of Human Tissue, *Electromagnetics* 21 (2001) 545–557. <https://doi.org/10.1080/027263401752246199>.
- [366] K.R. Jessen, Glial cells, *The International Journal of Biochemistry & Cell Biology* 36 (2004) 1861–1867. <https://doi.org/10.1016/j.biocel.2004.02.023>.
- [367] N. O. Laschuk, E. Bradley Easton, O. V. Zenkina, Reducing the resistance for the use of electrochemical impedance spectroscopy analysis in materials chemistry, *RSC Advances* 11 (2021) 27925–27936. <https://doi.org/10.1039/D1RA03785D>.
- [368] B. Bhattacharyya, Chapter 2 - Electrochemical Machining: Macro to Micro, in: B. Bhattacharyya (Ed.), *Electrochemical Micromachining for Nanofabrication, MEMS and Nanotechnology*, William Andrew Publishing, 2015: pp. 25–52. <https://doi.org/10.1016/B978-0-323-32737-4.00002-5>.
- [369] P. Kurzweil, Chapter 19 - Electrochemical Double-layer Capacitors, in: P.T. Moseley, J. Garche (Eds.), *Electrochemical Energy Storage for Renewable Sources and Grid Balancing*, Elsevier, Amsterdam, 2015: pp. 345–407. <https://doi.org/10.1016/B978-0-444-62616-5.00019-X>.
- [370] U. Rokkala, S. Bontha, M.R. Ramesh, V.K. Balla, A. Srinivasan, S.V. Kailas, Tailoring surface characteristics of bioabsorbable Mg-Zn-Dy alloy using friction stir processing for improved wettability and degradation behavior, *Journal of Materials Research and Technology* 12 (2021) 1530–1542. <https://doi.org/10.1016/j.jmrt.2021.03.057>.
- [371] P. Roach, D. Farrar, C.C. Perry, Interpretation of Protein Adsorption: Surface-Induced Conformational Changes, *J. Am. Chem. Soc.* 127 (2005) 8168–8173. <https://doi.org/10.1021/ja042898o>.

- [372] M. Moisel, M. a. F.L. de Mele, W.-D. Müller, Biomaterial Interface Investigated by Electrochemical Impedance Spectroscopy, *Advanced Engineering Materials* 10 (2008) B33–B46. <https://doi.org/10.1002/adem.200800184>.
- [373] S.E. Moulton, J.N. Barisci, A. Bath, R. Stella, G.G. Wallace, Investigation of Ig.G Adsorption and the Effect on Electrochemical Responses at Titanium Dioxide Electrode, *Langmuir* 21 (2005) 316–322. <https://doi.org/10.1021/la0487242>.
- [374] S. Devan, V.R. Subramanian, R.E. White, Transient Analysis of a Porous Electrode, *J. Electrochem. Soc.* 152 (2005) A947. <https://doi.org/10.1149/1.1884786>.
- [375] H. Vara, J.E. Collazos-Castro, Enhanced spinal cord microstimulation using conducting polymer-coated carbon microfibers, *Acta Biomaterialia* 90 (2019) 71–86. <https://doi.org/10.1016/j.actbio.2019.03.037>.
- [376] R.T. Leung, M.N. Shivdasani, D.A.X. Nayagam, R.K. Shepherd, In Vivo and In Vitro Comparison of the Charge Injection Capacity of Platinum Macroelectrodes, *IEEE Transactions on Biomedical Engineering* 62 (2015) 849–857. <https://doi.org/10.1109/TBME.2014.2366514>.
- [377] H. Mamata, F.A. Jolesz, S.E. Maier, Characterization of central nervous system structures by magnetic resonance diffusion anisotropy, *Neurochemistry International* 45 (2004) 553–560. <https://doi.org/10.1016/j.neuint.2003.11.014>.
- [378] H. McCann, G. Pisano, L. Beltrachini, Variation in Reported Human Head Tissue Electrical Conductivity Values, *Brain Topogr* 32 (2019) 825–858. <https://doi.org/10.1007/s10548-019-00710-2>.

- [379] M. Akhtari, D. Emin, B.M. Ellingson, D. Woodworth, A. Frew, G.W. Mathern, Measuring the local electrical conductivity of human brain tissue, *Journal of Applied Physics* 119 (2016) 064701. <https://doi.org/10.1063/1.4941556>.
- [380] J. Latikka, T. Kuurne, H. Eskola, Conductivity of living intracranial tissues, *Phys. Med. Biol.* 46 (2001) 1611. <https://doi.org/10.1088/0031-9155/46/6/302>.
- [381] M. Asplund, H. von Holst, O. Inganäs, Composite biomolecule/PEDOT materials for neural electrodes, *Biointerphases* 3 (2008) 83–93. <https://doi.org/10.1116/1.2998407>.
- [382] N. Rossetti, J. Hagler, P. Kateb, F. Cicoira, Neural and electromyography PEDOT electrodes for invasive stimulation and recording, *Journal of Materials Chemistry C* 9 (2021) 7243–7263. <https://doi.org/10.1039/D1TC00625H>.
- [383] Z. Zhang, G. Tian, X. Duan, H. Chen, D.-H. Kim Richie, Nanostructured PEDOT Coatings for Electrode–Neuron Integration, *ACS Appl. Bio Mater.* 4 (2021) 5556–5565. <https://doi.org/10.1021/acsabm.1c00375>.
- [384] E. Stewart, N.R. Kobayashi, M.J. Higgins, A.F. Quigley, S. Jamali, S.E. Moulton, R.M.I. Kapsa, G.G. Wallace, J.M. Crook, Electrical Stimulation Using Conductive Polymer Polypyrrole Promotes Differentiation of Human Neural Stem Cells: A Biocompatible Platform for Translational Neural Tissue Engineering, *Tissue Engineering Part C: Methods* 21 (2015) 385–393. <https://doi.org/10.1089/ten.tec.2014.0338>.
- [385] Y. Lu, T. Li, X. Zhao, M. Li, Y. Cao, H. Yang, Y.Y. Duan, Electrodeposited polypyrrole/carbon nanotubes composite films electrodes for neural interfaces, *Biomaterials* 31 (2010) 5169–5181. <https://doi.org/10.1016/j.biomaterials.2010.03.022>.
- [386] A. Kelly, N. Farid, K. Krukiewicz, N. Belisle, J. Groarke, E.M. Waters, A. Trotier, F. Laffir, M. Kilcoyne, G.M. O’Connor, M.J. Biggs, Laser-Induced Periodic Surface

- Structure Enhances Neuroelectrode Charge Transfer Capabilities and Modulates Astrocyte Function, *ACS Biomater. Sci. Eng.* 6 (2020) 1449–1461. <https://doi.org/10.1021/acsbiomaterials.9b01321>.
- [387] L.W. Tien, F. Wu, M.D. Tang-Schomer, E. Yoon, F.G. Omenetto, D.L. Kaplan, Silk as a Multifunctional Biomaterial Substrate for Reduced Glial Scarring around Brain-Penetrating Electrodes, *Adv. Funct. Mater.* 23 (2013) 3185–3193. <https://doi.org/10.1002/adfm.201203716>.
- [388] S. Rao, J. Winter, Adhesion molecule-modified biomaterials for neural tissue engineering, *Frontiers in Neuroengineering* 2 (2009). <https://www.frontiersin.org/articles/10.3389/neuro.16.006.2009> (accessed February 3, 2024).
- [389] X. Yuan, R. Chittajallu, S. Belachew, S. Anderson, C.J. McBain, V. Gallo, Expression of the green fluorescent protein in the oligodendrocyte lineage: A transgenic mouse for developmental and physiological studies, *Journal of Neuroscience Research* 70 (2002) 529–545. <https://doi.org/10.1002/jnr.10368>.
- [390] J.J. Vidal, Toward Direct Brain-Computer Communication, *Annu. Rev. Biophys. Bioeng.* 2 (1973) 157–180. <https://doi.org/10.1146/annurev.bb.02.060173.001105>.
- [391] S.M. Won, E. Song, J. Zhao, J. Li, J. Rivnay, J.A. Rogers, Recent Advances in Materials, Devices, and Systems for Neural Interfaces, *Advanced Materials* 30 (2018) 1800534. <https://doi.org/10.1002/adma.201800534>.
- [392] S.E. Mondello, M.R. Kasten, P.J. Horner, C.T. Moritz, Therapeutic intraspinal stimulation to generate activity and promote long-term recovery, *Front. Neurosci.* 8 (2014). <https://doi.org/10.3389/fnins.2014.00021>.

- [393] S.E. Mondello, L. Young, V. Dang, A.E. Fishedick, N.M. Tolley, T. Wang, M.A. Bravo, D. Lee, B. Tucker, M. Knoernschild, B.D. Pedigo, P.J. Horner, C.T. Moritz, Optogenetic spinal stimulation promotes new axonal growth and skilled forelimb recovery in rats with sub-chronic cervical spinal cord injury, *J. Neural Eng.* 20 (2023) 056005. <https://doi.org/10.1088/1741-2552/acec13>.
- [394] R.P. Carlyon, T. Goehring, Cochlear Implant Research and Development in the Twenty-first Century: A Critical Update, *JARO* 22 (2021) 481–508. <https://doi.org/10.1007/s10162-021-00811-5>.

Appendix: Supplemental to Chapter 3

This appendix presents figures supplemental to the data presented in Chapter 3.

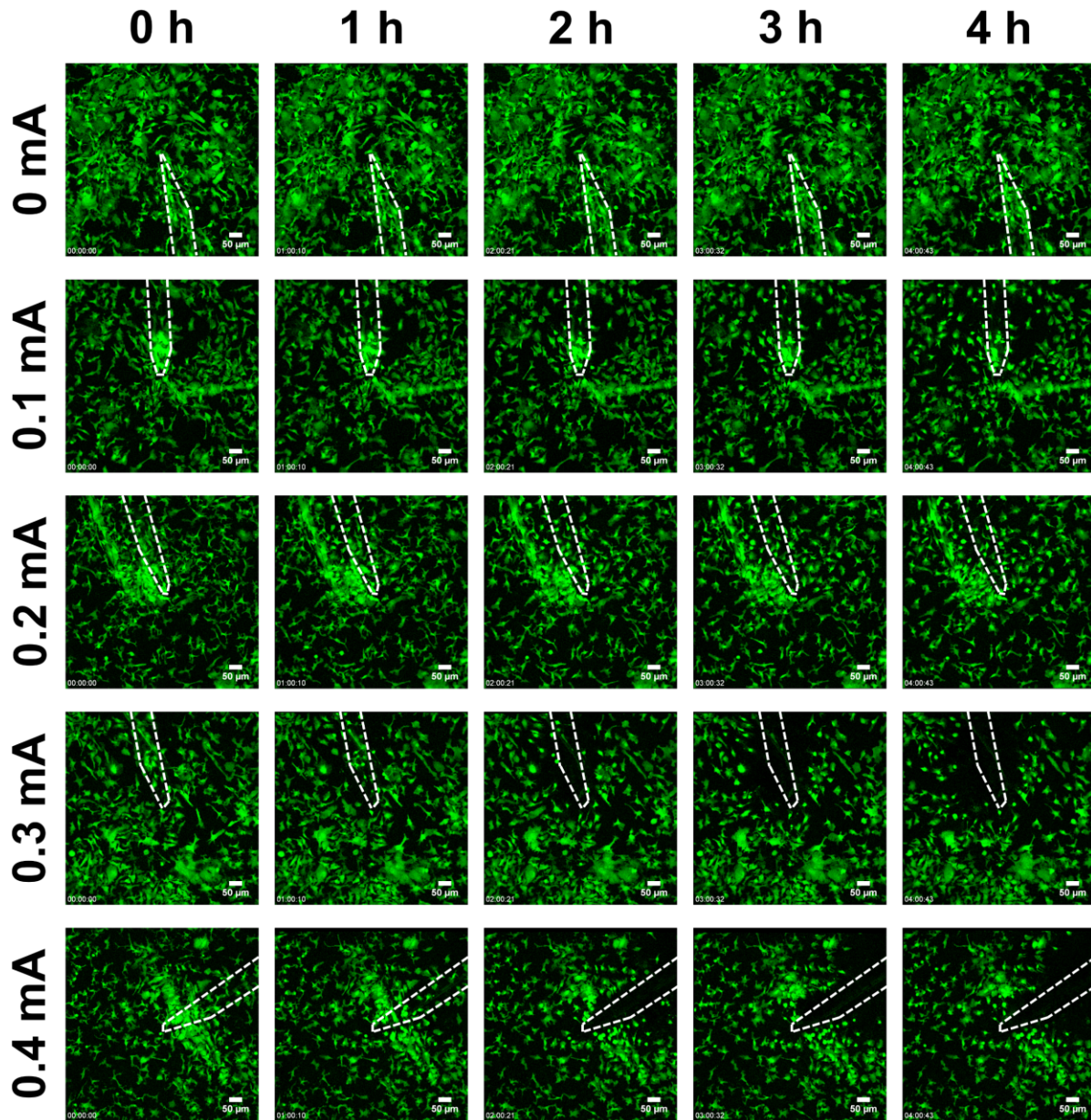


Figure S-1: Time-lapse image series of EGFP-positive microglia (current modification)

Microglia in mixed glial cell cultures were imaged on a confocal microscope while exposed to 4 h of electrical stimulation. The area around the electrode tip was imaged. Electrodes are marked by the white dashed outline in each image. Scale bars: 50 μm.

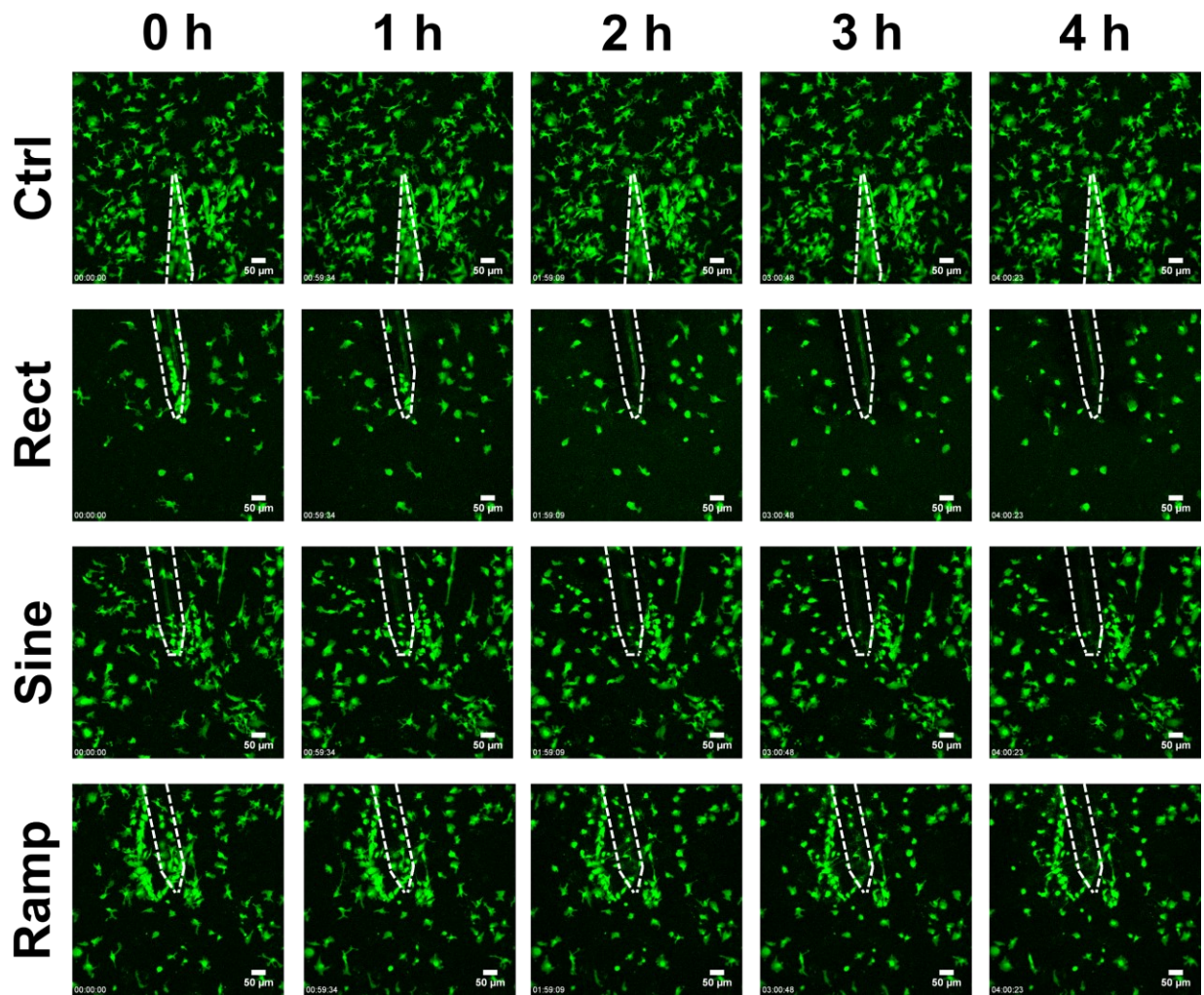


Figure S-2: Time-lapse image series of EGFP-positive microglia (waveform shape modification)

Microglia in mixed glial cell cultures were imaged on a confocal microscope while exposed to 4 h of electrical stimulation. The area around the electrode tip was imaged. Electrodes are marked by the white dashed outline in each image. Scale bars: 50 μm.

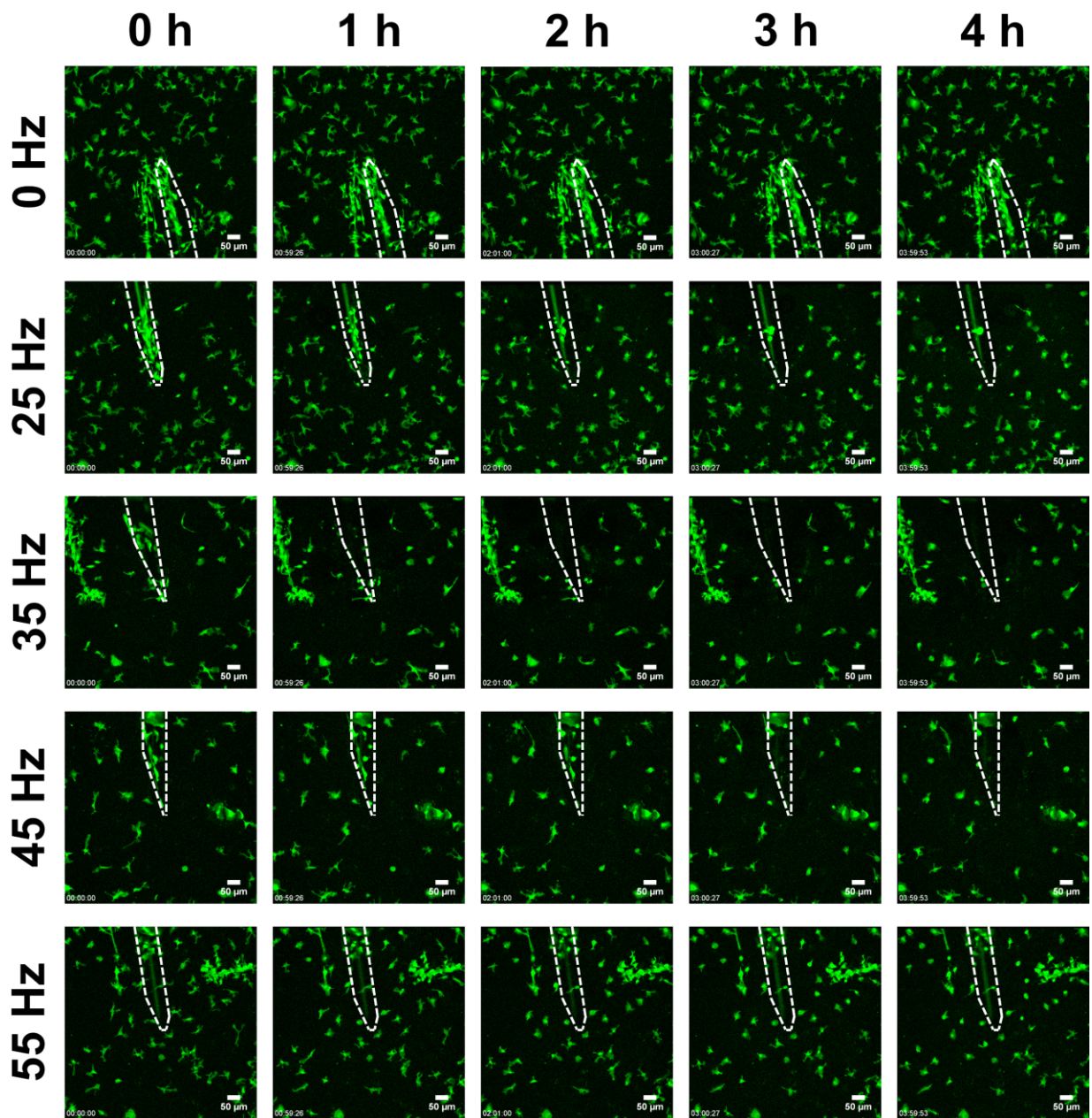


Figure S-3: Time-lapse image series of EGFP-positive microglia (frequency modification)

Microglia in mixed glial cell cultures were imaged on a confocal microscope while exposed to 4 h of electrical stimulation. The area around the electrode tip was imaged. Electrodes are marked by the white dashed outline in each image. Scale bars: 50 μm.